Springer Geography

Xiangzheng Deng
Burak Güneralp
Jinyan Zhan
Hongbo Su *Editors*

Land Use Impacts on Climate

Springer

Springer Geography

For further volumes:
http://www.springer.com/series/10180

The Springer Geography series seeks to publish a broad portfolio of scientific books, aiming at researchers, students, and everyone interested in geographical research. The series includes peer-reviewed monographs, edited volumes, textbooks, and conference proceedings. It covers the entire research area of geography including, but not limited to, Economic Geography, Physical Geography, Quantitative Geography, and Regional/Urban Planning.

Xiangzheng Deng · Burak Güneralp
Jinyan Zhan · Hongbo Su
Editors

Land Use Impacts on Climate

Springer

Editors
Xiangzheng Deng
Institute of Geographic Sciences
and Natural Resources Research
Chinese Academy of Sciences
Beijing
China

Burak Güneralp
Department of Geography
Texas A&M University
College Station, TX
USA

Jinyan Zhan
School of Environment
Beijing Normal University
Beijing
China

Hongbo Su
Department of Environmental Engineering
Texas A&M University-Kingsville
Kingsville, TX
USA

ISSN 2194-315X ISSN 2194-3168 (electronic)
ISBN 978-3-642-54875-8 ISBN 978-3-642-54876-5 (eBook)
DOI 10.1007/978-3-642-54876-5
Springer Heidelberg New York Dordrecht London

Library of Congress Control Number: 2014939640

Printed on acid-free paper

Springer is part of Springer Science+Business Media (www.springer.com)

Preface

Since the industrial revolution, climate changes caused by greenhouse gas emissions have attracted the attention globally from a diverse community including both politicians and scientists; however, the pending issues on the research of the climatic impact of land cover and land-use changes via terrestrial biogeophysical processes is far from resolved. The scientific community needs to provide comprehensive scientific support for global change adaptation. Land cover and land-use changes directly lead to change in the surface condition, thereby changing the surface albedo and surface roughness, and then affects surface heat balance and water cycles. In addition, the urban expansion causes aggravation of urban heat island effect. It is of significance to understand climatic impacts accompanied by biogeophysical processes induced by land-use changes, which is critical for food safety, extreme climate, biodiversity protection, and a series of problems. Land-use change, in turn, is occurring in the context of climate changes at a variety of scales.

Quantitative analysis for the impacts of land use and land cover changes on surface climate is one of the core scientific issues to understand the influence of human activities on global climate. This book first comprehensively analyzed the primary scientific issues about the impacts of land use and land cover changes on the surface climate in Chap. 1. Major models used in the study of land use impact on climate were introduced in Chap. 2, which lay a foundation for the subsequent researches in this book. While in Chap. 3, major methods of projecting the land use change were introduced, this would facilitate the study in the land use change impact.

From Chaps. 4 to 6, studies of climate effect of different types of land use change were introduced respectively. In Chap. 4, the climate effect due to the cultivated land change was simulated in typical areas, namely Northeast China and Northern China plain. Chapter 5 focuses on the grassland change. In Chap. 6, studies on the urban land change impact were introduced. Three case studies were made in different designated study areas, namely Beijing–Tianjin–Tangshan Metropolitan area, Jiangsu, and Wuhan Metropolitan. When it comes to the different areas worldwide, Chap. 7 proves that the methods and models showed

above can be applied to other countries in the world. Finally yet importantly, Chap. 8 explores the advancement in the models, data, and application for observing and estimating the land use impacts on surface climate, and points out further research needs and priorities, which hopefully will provide some references for related studies.

The authors claim full responsibility for any errors appearing in this work.

April 2014

Xiangzheng Deng
Burak Güneralp
Jinyan Zhan
Hongbo Su

Acknowledgments

The book was supported by the National Key Program for Developing Basic Science in China (Grant No. 2010CB950900). All the team members play an important role in the building of the land use and land cover database as well as the climate database. Also, a group of members provides a series of Simulation Platforms for land use dynamics and its impacts. In the whole process of the Program, several scientific meetings have been held in China and aboard. We appreciate the team leaders for their creative thoughts and advice.

Further, China National Natural Science Funds for Distinguished Young Scholar (Grant No. 71225005), the Key Project funded by the Chinese Academy of Sciences (Grant No. KZZD-EW-08) as well as Key Projects in the National Science and Technology Pillar Program (2013BAC03B03) also support this book through providing data and models.

During the preparation of this book, a number of scholars and experts gave us helpful advice. My special appreciation is to Profs. Jiyuan Liu and Jikun Huang, for the contribution of ideas, methodologies, and data.

Sincerely, we would like to express the depth of our gratitude to the editors Burak Güneralp, Hongbo Su, as well as all anonymous reviewers in *Advances in Meteorology* for their constructive comments, which helped us to improve the book.

Finally, we appreciate all the assistants in our group in Institute of Geographic Sciences and Natural Resources Research, Chinese Academy of Sciences. They have done a lot of work on map/table polishing, parameters revision, as well as text proofreading.

Contents

Chapter 1
Systematic Modeling of Land Use Impacts on Surface Climate

Xiangzheng Deng, Burak Güneralp and Hongbo Su

1.1 Introduction

LUCC, in which human activities play a dominant role, interacts with environment and has significant effects on ecosystems at local, regional and global scales, and consequently directly or indirectly exerts great influence on global climate changes (Foley et al. 2005; Pachauri and Reisinger 2007; Feddema et al. 2005). People have come to realize that global change always consists of a series of regional change with various processes and patterns according to more and more observations. On one hand, the initial regional change will gradually extend to inter-regional and even larger scales, which consequently influences global environment. Therefore, it is necessary to first take into account local and regional climatic effects of LUCC in this research. On the other hand, the impacts of LUCC on regional climate systems also vary greatly since there are the great differences in the physical, chemical and biological characteristics of land surface in different regions on the earth. For example, deforestation may lead to temperature increase in the tropic zone, while it may lead to surface temperature decrease in frigid zone (Bonan 2008). Consequently, in order to completely reflect the relationship between LUCC and climatic factors, it is necessary to: (1) make comparisons among various case studies in different regions and at multiple spatiotemporal scales; (2) analyze the spatiotemporal processes and land surface parameters of

X. Deng (✉)
Institute of Geographic Sciences and Natural Resources Research,
Chinese Academy of Sciences, Beijing 100101, China
e-mail: dengxz.ccap@igsnrr.ac.cn

B. Güneralp
Department of Geography, Texas A & M University,
College Station, TX, USA

H. Su
Department of Environmental Engineering, Texas A & M University,
Kingsville, TX, USA

X. Deng et al. (eds.), *Land Use Impacts on Climate*, Springer Geography
DOI: 10.1007/978-3-642-54876-5_1,

LUCC and the climate response. However, there have been very few relevant researches.

It has long been known that land use changes caused by human activities such as deforestation, and agriculture practices have some effects on climate (Foley et al. 2005; Pachauri and Reisinger 2007; Feddema et al. 2005; Bonan 2008; Kueppers and Snyder 2012). Land use changes influence climate by changing the properties of land surface which is not only the direct heat source of the troposphere, but also one of the main sources of atmospheric vapor water (Betts et al. 1996). Therefore, change of land surface parameters will directly affect land surface-atmosphere interaction and consequently alter thermodynamic and dynamic characteristics of the atmosphere, and finally lead to different climate processes and patterns. Land use activities have significantly changed regional land cover, thus leading to climate changes. For example, deforestation, afforestation, reclamation and urbanization, all influence the energy budget and Bowen ratio of land surface, the distribution of the precipitation among the soil water, runoff and evapotranspiration (Phillips et al. 2009; Pielke et al. 2007; Arora and Montenegro 2011). Human-induced land use activities also have important influence on regional climate system, e.g., temperature, evapotranspiration, precipitation, wind field, atmospheric pressure etc., especially temperature and precipitation (Pielke et al. 2007; Arora and Montenegro 2011; Degu et al. 2011). In addition, recent researches suggest that LUCC may affect the extremes in temperature and precipitation (Woldemichael et al. 2012).

LUCC affects local, regional and global climate system through various biogeochemical and biogeophysical processes (Arora and Montenegro 2011; Meiyappan and Jain 2012). For example, biogeochemical process can indirectly affect climate by altering the rate of the biogeochemical cycle and thereby changing the chemical composition of the atmosphere. Besides, it may also affect the climate through the absorption or emission of greenhouse gases (Friedlingstein and Prentice 2010). By contrast, biogeophysical process directly affects the physical parameters that determine absorption and disposition of energy at land surface (Arora and Montenegro 2011). For example, it influences albedo or reflective properties of land surface (Dirmeyer and Shukla 1994), alters absorption rate of solar radiation and hence influences energy availability at land surface (Georgescu et al. 2011). In addition, surface hydrology and vegetation transpiration characteristics also affect how received energy is distributed into latent and sensible heat fluxes (Feddema et al. 2005). Vegetation structure can affect surface roughness and thereby alter momentum and heat transport.

Owing to the limitation of knowledge and the lack of interdisciplinary cooperation, there is still insufficient understanding of the procedures mechanism of climate process and how LUCC influences regional climate and consequently influences global climate (Feddema et al. 2005). There are parallel studies of biogeochemical and biogeophysical effects of land use changes on climate in their

respective fields, and there are few researches on their joint effects on climate. However, there are still a lot of uncertainties in the current knowledge, and it is still very difficult to objectively assess the contribution of land use changes to climate change. For example, IPCC (Pachauri and Reisinger 2007) believed that the increase of CO_2 in the atmosphere will reinforce radiative forcing, 1/3 of which was contributed by land use changes, and consequently increase the temperature. So it is of great importance to objectively analyze the biogeochemical and biogeophysical effects of land use changes on surface climate (Foley et al. 2005). It is necessary to carry out further researches on the development of more accurate monitoring and modeling methods, which are essential to the understanding of these interactions and feedbacks (Bathiany et al. 2010). However, how to integrate biogeophysical and biogeochemical processes is the major challenge in current studies.

The impacts of land use changes on climate are the synthetic effects of biogeophysical process and biogeochemical process. But which of the two kinds of processes makes a greater contribution to climate change at regional scale, or which one plays a dominant role? What effects will the improvement of the regional climate model have on LUCC simulation? This chapter reviewed the history and methods of the relevant researches, and summarized the influence of LUCC on regional climate system and the simulation strategies according to the researches in recent decades. Finally, the application of regional climate models in the development and management of agricultural land and urban land are discussed.

1.2 Mechanism Research on the Influence of LUCC on Surface Climate

The research on the influence of land use changes on surface temperature and precipitation can be dated back to the 1970s. Land use changes can alter various physical characteristics of land surface, including parameters such as albedo (Dirmeyer and Shukla 1994), upward long-wave radiation and surface roughness and vegetation parameters such as vegetation coverage and leaf area index (LAI). All changes of these parameters perturb surface energy budget, water balance and atmospheric boundary layer (Lambert et al. 2011). So it can be said that changes in the parameters of land surface and vegetation is the fundamental reason for the effects of land use changes on the atmosphere (Brovkin et al. 1999). By the 1980s, researchers realized that land use influences the climate not only through the change in physical characteristics of the land surface, but also the amount of greenhouse emission. Thereafter, there were more and more researches on the effects of land use on carbon cycle. The influence of land use changes on the climate involves not only biogeophysical process, but also biogeochemical process.

1.2.1 Influence of Physical Characteristics on Climate

Charney (1975) first explored the relationship between the change of albedo and the drought in the Sahara region. Thereafter, there were a lot of researches on the influence on regional climate (e.g., temperature and precipitation), which is exerted by single parameter of physical characteristics of the land surface (e.g., albedo, roughness, leaf area index and soil moisture) (Shukla and Mintz 1982; Lambin and Geist 2006). The change in the underlying landscape alters the energy and moisture budgets of the land surface at regional scale, which in turn lead to the changes in the fluxes of heat, water, and dynamics of the near-surface atmosphere and influence the key thermodynamic and dynamic properties of the air, which is of great importance to air convection (Brovkin et al. 2013). The evidence to support this statement comes from the sensitivity studies that explore the impacts of change in characteristics of land surface (Wickham et al. 2012).

There is another considerable evidence of the significance of land surface processes generated through regional-scale perturbation experiments and researches on deforestation (Shukla et al. 1990), desertification (Salvati and Bajocco 2011) and land use changes. These researches all indicated LUCC contributed to the large and statistically significant change in temperature, rainfall and other variables at continental or regional scales.

First and foremost, some important researches on the sensitivity of climate to the change of land surface evapotranspiration were performed by Davin and Noblet-Ducoudré (2010), which provided significant evidence that the change of the land surface evapotranspiration can lead to great changes in temperature and precipitation. For example, deforestation will lead to the decrease of evapotranspiration, while the decrease of latent heat will increase the near-surface temperature and lead to higher sensible heat flux (Davin and de Noblet-Ducoudré 2010). There is a high transpiration rate in the tropic rainforest, with the decrease of transpiration rate due to the disappearance of the tropic rainforest may lead to regional warming and drought in the future (Defries et al. 2002). In addition, the change in evapotranspiration also influences water content in the atmosphere, and reduces the greenhouse effect and consequently reduces the temperature. While the decrease of cloud covers will increase the solar radiation, and consequently strengthen the temperature (Dessler 2010). Therefore, due to the large number of parameters, it is difficult to quantitatively compare the two feedbacks and there is great uncertainty (Pachauri and Reisinger 2007).

Land surface albedo is the fraction of solar energy (shortwave radiation) reflected from land surface into space. It represents the reflecting power of the land surface, and plays a key role in influencing the radiation balance and energy balance of the land surface (Lynch et al. 1999). The change of land surface albedo

directly alters the solar radiation absorbed by land surface, subsequently leads to the change in the long-wave radiation of land surface into space and sensible heat and latent heat, and finally influences the temperature (Chapin et al. 2005). Some of the key work demonstrating the sensitivity of climate to land surface albedo was performed by Charney et al. (1975). Without regard to the influence of advection process, the increase will lead to the decrease of the solar radiation absorbed by land surface, increase the land surface temperature, subsequently increase the long-wave radiation into the space and decrease the sensible heat and latent heat, and lead to the potential to decrease the temperature, and vice versa (Chapin et al. 2005). Lower land surface albedo indicates lower reflectivity and higher shortwave absorption of the land surface. Taking forest coverage as an example, its albedo is generally lower than that of the nudation and other vegetation types (Houldcroft et al. 2009). Historical deforestation in the middle-latitude zone led to the increase of the land surface albedo, which is especially remarkable after snowfall in the winter, and might have made northern hemisphere colder (Feddema et al. 2005).

Leaf area index is an important indicator that represents the canopy structure and productivity of the plant community. It directly influences the ability of plant to acquire and utilize solar energy and indirectly influence the canopy impedance ratio. Besides, being an important parameter of land surface albedo, it also directly influences the interaction between land surface and the atmosphere (Bonan and Pollard 1992). More recent studies have focused on the role of the leaf area index in influencing the climate. The relevant researches indicate that leaf area index is closely related with precipitation, temperature and specific humidity, etc. (Copeland et al. 1996).

The significance of roughness has also been well realized. Land surface roughness has impacts on the turbulent flow between land surface and the atmosphere and subsequently influences the local diffusion flux. If diffusion flux is higher, it will reduce the near-surface air temperature under the condition of no other feedback mechanisms (Bathiany et al. 2010). Deforestation will decrease land surface roughness and reduce the turbulent flow, and will consequently increase the temperature in theory. However, less turbulent flow will lead to the decrease of heat and moisture transfer, which will increase the temperature and moisture gradients between land surface and the atmosphere and in turn alleviate the warming effect. Davin and Noblet-Ducoudré (2010) analyzed the sensitivity to the roughness during the conversion of the forest to the grassland. Their result indicates that the change in roughness will make global temperature increase by 0.29 °C, and the increase will be even more obvious in the tropic zone.

1.2.2 Impacts on the Biogeochemical Process

The influence of the land use change on the biogeochemical process, especially the discharge or absorption of the greenhouse gases such as CO_2 in the atmosphere due to the land use change, can alter the concentration of the greenhouse gases in the atmosphere and consequently influence the climate. The historical accumulative carbon loss due to the land use change was estimated to be 180–200 PgC (House et al. 2002), and the land use change contributed to 10–30 % of the carbon discharge due to human activities. The deforestation, afforestation, forest restoration and agricultural activities are the major approaches through which the land use influences the carbon cycle. There are many researches on the influence of the land use change on the carbon cycle, most of which focused on the deforestation, especially the deforestation in the tropic rainforest. Since the 1850s, the global forest area decreased by 20 %, and the carbon emission due to the deforestation accounted for 90 % of the carbon emission caused by the land use change and 33 % of the man-made carbon emission (including the discharge from the fossil fuel burning and land use change).

The influence of the afforestation and forest restoration on the carbon cycle has also gradually become the hot issue in the relevant researches. Although the reforestation has not significantly influenced the terrestrial carbon sink at the global scale, it has played an important role in the carbon sink at the regional scale. For example, the man-made forests in China has stored over 0.45 Gt carbon since the 1970s (Fang et al. 2001). Some researches indicated the forest restoration played a key role in the carbon sink resulting from the land use (Pacala et al. 2001).

The productivity of the forest and decomposition of organic matters in the soil both influence the change of CO_2 in the atmosphere and the climate pattern, and consequently influence the terrestrial carbon sink). When the photosynthesis rate is bigger than the respiration rate, and discharge rate of the biogenic volatile organic compounds (BVOC), and the decomposition rate of organic carbon, the forest plays a role as the carbon sink (Heimann and Reichstein 2008). Besides, the deforestation will reduce the potential carbon sequestration (House et al. 2002). In addition, the higher temperature and higher CO_2 concentration will increase the NPP, which will lead to the negative feedback and make more CO_2 in the atmosphere sequestrated. The radiative forcing due to the carbon emission resulting and the accelerated respiration due to the higher temperature will lead the positive feedback, in which the organic matters will decompose more rapidly (Friedlingstein et al. 2006). For example, there is an extreme example in the climate-carbon cycle, i.e., the tropic rainforest in Amazon will gradually succeed into other vegetation if the temperature continuously increases and the precipitation continuously decreases.

The agricultural activities also have significant impacts on the carbon cycle. For example, the conversion of the natural vegetation to the cultivated land, loss of plant biomass and increased decomposition of organic matters in the soil, all make the agricultural activities become one of the major sources of CO_2 emission. By contrast, the utilization of the high yield variety and fertilizers, irrigation and no-till agriculture all contribute to the reduction of carbon loss and increase the absorption of carbon in the agricultural regions (Friedlingstein et al. 2006). For example, the no-till agriculture in the USA has increased the organic content in the soil, reaching 1.4 Gt carbon in the past 30 years. However, the increase of the organic matters in the soil can only last for 50–100 years, after that a new equilibrium of carbon cycle will be reached (Smith et al. 1997).

A lot of BVOC are generated by the plants and then released into the atmosphere. These compounds have significant influence on the physical and chemical characteristics of the atmosphere due to their great amount. Although the BVOC have no direct influence on the radiation balance of the atmosphere, they affect the longevity of the methane in the atmosphere and play an important role in the formulation of the ozone and secondary organic aerosols (SOAs). The SOAs can directly influence the climate since they can scatter or absorb the solar radiation and consequently decrease or increase the temperature (Spracklen et al. 2008). The overall influence of the SOAs on the climate system has not been accurately quantified so far, they may mainly play a role in decreasing the temperature (Chapin et al. 2005). The SOAs also have significant indirect impacts on the climate, i.e., they may act as the cloud condensation nuclei (CCN) in the formation of the clouds. In fact, the BVOCs released by the boreal forest has made the local CCN increased by 100 % (Spracklen et al. 2008), which in turn influences the number of water drops in the cloud and makes the albedo of the atmosphere increased by 3–8 %.

There will be an albedo difference ranging from -1.8 to -6.7 W/m^2 in the regions between 60–90°N since the albedo increases due to the indirect influence of BVOC. This means that owing to the feedback among BVOC released by the trees, SOA, CNN and land surface albedo, the boreal forest will make the local climate colder. The influence of BVOC on CCN is considered to be the most important in the boreal forest since the regional air pollution is slight (Spracklen et al. 2008). In addition, the net emission of carbon released due to the deforestation depends on the land use type converted from the forest or the temporal scale of the regeneration of the forest and the feedback mechanism mentioned above. According to the simulation which only takes into account the biogeochemical influence, the complete deforestation will make the global temperature increase by 0. 09 or 0.19 °C if the forests between 50–60°N and 0–10°S were completely felled (Chapin et al. 2005). This is because of the great amount of biomass in the tropic zone and depends on the total biomass of different forest types.

The impacts of LUCC on the regional temperature and precipitation are the synthetic effects of the processes mentioned above. There has been great progress in the research on the single process and their synthetic effects. Besides, the impacts of the land cover change happen at certain temporal and spatial scales. For example, the mesoscale land cover change influences the regional temperature through the land surface albedo in short and medium terms, while the geochemical process influences the change in temperature at larger temporal and spatial scales.

1.3 Simulation of the Effects of LUCC on the Regional Climate Model

1.3.1 Development from the Global Climate Models to the Regional Climate Models

The climate model consists of the set of equations that can be used to determine the characteristics and evolution of the components of the climate system according to the fundamental physical laws such as the law of conservation of energy and law of conservation of mass. Then the climate model is constructed by routinize the set of equations with the computer. The climate model can be used to not only simulate the current climate, but also simulate the climate change caused by the change in the boundary conditions (Kattenberg et al. 1996). Therefore, the climate model will serve as the most important test tool if the people wish to study the climate and its change with the experimental method.

The earliest researches on the regional climate effects generally used Global Climate Models (GCMs), and carried out the sensitivity test with the force-response method (Pielke et al. 1998), i.e., represent the land use changes with the changes of the land surface parameters (e.g., albedo, roughness and evapotranspiration). Generally, the control experiment is first carried out with the GCMs, and then the land surface parameters are changed to carry out the simulation and thereafter compare with the reference test so as to analyze the response of the climate to the land use changes (Himiyama and Bicik 2012). Thereafter, the method was applied to many researches on the response of climate to the change of the land surface parameters such as the evapotranspiration, roughness, stomatal conductance and leaf area index.

The GCMs have been widely used in the study of climate change, and a lot of effective work has been done in the simulation of influence of the LUCC on the global temperature and precipitation at large scale and the research on the climate effects of trace gases in the atmosphere, etc. (Salmun and Molod 2006). However,

it is difficult to simulate the regional climate at small scales precisely with the GCMs due to the limitation of the resolution. Besides, the resolution is very low in the GCMs (above 100–200 km), so they cannot be used to describe the complex terrain and land surface characteristics. Therefore, there is some bias and uncertainties in the simulation of the regional climate change with the GCMs (Brovkin et al. 2006), which influences the credibility of the simulation result.

Regional climate models were proposed during the late 1980s and the early 1990s and have become important tools in regional climate researches. Regional climate model can describe the detailed characteristics of the land surface with high resolution, and also can more reasonably simulate the regional forcing, such as terrain, rivers/lakes and urban buildings. Besides, they reflect the climate characteristics caused by strong regional forcing; consequently, they have been widely used in regional climate researches.

More attention has been paid to the response of regional and local climate to land use changes rather than that of global climate. However, the resolution of the current climate models, e.g., the global ocean-atmosphere-land system with high complexity and the Earth system model of the moderate complexity, is generally too low when the model is used at local and regional scales. In recent decades, high resolution regional climate models, e.g., RegCM2, RegCM3, RAMS, RIEMS, RegCM-NCC and IPCR-RegCM, have been widely used in the research on regional land use change. For example, these models have been applied to the desertification experiment, deforestation experiment in the tropic rainforest, vegetation restoration experiment, etc. Besides, some researchers analyze the impacts of land use change on regional temperature and precipitation, and the influence of land use changes on the fundamental regional climate characteristics at the national scale (Himiyama and Bicik 2012; Diffenbaugh 2009) by comparing the current land use data and the data of potential natural vegetation.

1.3.2 Research on the Integration of the Improved Land Surface Model and Regional Climate Model

Although some regional climate models have higher resolution (below 100 km), there are still a lot of great challenges in the simulation of the land surface processes. For example, it is still necessary to represent the land surface process which is very important to the climate at the small scales, although there is little evidence that the simulation with climate models can provide reliable information at small scales. Since the atmosphere and the land surface integrate into an inseparable whole system through the exchange of energy, dynamics and moisture, it is the key to the successful simulation with the regional model to construct a land

surface model that can accurately and precisely simulate the interaction between the atmosphere and the land surface.

By contrast with the regional climate model, the land surface model focuses more on the interaction between the atmosphere and the land surface, and can calculate the exchange of energy, dynamics and moisture between the land surface and the atmosphere. The scholars have gradually realized the importance of the land surface process in the climatology, geobiochemistry and weather forecasting, etc. since the 1970s. Since the middle 1980s, many researchers have studied the issue of deforestation in the tropical rain forest in the Amazon watershed and carried out a lot of sensitivity analysis (Malhi et al. 2009).With the development of the land surface process model, more biophysical processes of vegetation were introduced. The researches constructed complex parameterization schemes of the exchange of radiation, moisture, energy and dynamics above the vegetation, which can more realistically reflect the role of vegetation in the land surface process, especially the role of vegetation in the water budget and energy budget of the land surface.

Since the 1990s, the researches gradually considered the water-vapor absorption of vegetation and introduced the biochemical process that the vegetation absorbs CO_2 for photosynthesis into the land surface model according to the relationship between the photosynthesis and plant water. There have been many improved land surface models, e.g., the Land Surface Model (LSM), improved Simple Biosphere model (SiB2) (Sellers et al. 1996), Community Land Model (CLM) (Bonan et al. 2002). These improved land surface models have a better ability to simulate the carbon flux and daily and seasonal cycle of CO_2 concentration, and can be used to simulate the enhanced greenhouse effect due to the increase of CO_2 concentration in the atmosphere. The latest land surface models focus more on the biogeochemical process.

With the continuous development of the regional climate model, a great many of researchers have applied the coupled regional land surface model to the study of various physical processes and their impacts on the regional climate, energy budget and interactions between the land surface and the atmosphere. The relevant researches mainly focused on the schemes of the soil-vegetation-atmosphere interaction.

1.4 Application of Regional Climate Model

1.4.1 Agricultural Land Development and Management

The area of cultivated land has continuously increased so as to meet the demand of people for food all over the world, with 1,140 million hectares (Mha) forests converted into cultivated land during 1700–1992 in the whole world (Klein

Goldewijk et al. 2011). More attention has been paid to the influence of farmland management on climate, e.g., irrigation, no-till agriculture and crop rotation, among which the influence of irrigation received the most attention. The change in irrigation has been expected to influence local climate since it directly influences soil moisture, which will further affect land surface albedo, evaporation and variation in regional temperature and precipitation. The irrigation area has increased very rapidly during the past centuries. For example, global irrigation area was 8.0 Mha in 1800, it increased to 40 Mha in 1900 and further increased 2.7 Mha in 2000 (Kueppers et al. 2007). The global irrigation water accounts for 70 % of the water used by human beings (Douglas et al. 2009). The irrigation districts mainly include China, India, Pakistan, Thailand, North America and the Aral Sea watershed (Kueppers et al. 2007).

There have been very few quantitative studies of how the climate responds to irrigation. The simulation studies in many regions indicated that increased soil moisture due to irrigation will generally lead to significant decrease of local average and maximum temperature (T_{max}), while the change of the minimum temperatures (T_{min}) varies among regions (Kueppers et al. 2008). Irrigation will make the regional moisture in the atmosphere increase significantly, and consequently lead to regional precipitation increase under the appropriate weather conditions (Douglas et al. 2009). Besides, irrigation plays a role in reducing the difference between regional temperature and daily temperature (Oyama and Nobre 2004; Kueppers et al. 2008; Douglas et al. 2006; Lobell et al. 2009).

Irrigation affects surface climate mainly through the redistribution of latent heat and sensible heat. When the irrigation area increases, the latent heat will increase while the sensible heat will decrease. The increase of latent heat will further lead to the increase of cloud coverage and decrease of the net radiation of land surface. The researches have indicated that there are obvious seasonal variations of the temperature decrease due to the irrigation. The temperature will reduce significantly in the dry season and insignificantly in rainy season (Douglas et al. 2006; Lobell et al. 2009). Besides, there is obvious regional heterogeneity of the temperature decrease due to the irrigation (Lobell et al. 2009). The simulation researches indicated that the difference in the irrigation area will lead to the difference in soil moisture. The difference in the response of the cloud to the irrigation is the main reason for the difference in the regional climate. The cooling effect of irrigation in some regions (e.g., North America, northwest part of India, northeast part of China) is comparable to the warming effect in the magnitude, and consequently plays a role in alleviating the climate warming (Kueppers et al. 2007). However, according to the prediction of land use changes, the irrigation area in these regions will show a decreasing trend in the future decades, which will aggravate the climate warming.

1.4.2 Urbanization and Its Regional Climate Effect

Urbanization is an extreme way in which human activities alter the underlying surface properties and influence the local climate. The urban heat island effect due to urbanization is an extreme example of the influence of LUCC on regional climate. The urbanization has contributed to 50 % of the increase of land surface temperature in the USA since 1950 (Stone 2009). The city differs greatly from the natural land cover. The widespread impervious surface and the roof and wall of buildings, etc. in the cities, all influence the energy flux, circulation of water and other materials. They can reduce the evaporation from land surface, make it difficult to eliminate land surface heat, and consequently lead to the increase of land surface temperature (Li et al. 2011). Besides, man-made heat emission and decrease of vegetation coverage also contribute to the increase of land surface temperature. In some cities, local people have grown a lot of plants or painted the roofs write so as to reduce the reflectivity of the urban land surface and alleviate the urban heat island effect (Wong and Lau 2013).

Considerable progress has been made in the development of urban climate models which is able to predict/simulate meteorological conditions from regional to building scales. The results of current qualitative researches indicate that the lowest daily air temperature increases more than the highest daily air temperature, which leads to the decrease of daily temperature difference (Murata et al. 2012). Besides, the Bowen ratio and canopy temperature of cities will increase with the proportion of impervious surface (Ge et al. 2007). In addition, previous researches have mainly focused on the urban heat island effect of big cities.

1.5 Summary

This chapter reviews the advances in the researches on the influence of LUCC on surface climate, including how LUCC influences the surface climate, the relevant simulations and their improvement and the application in case studies, the main findings can be summarized as follows. A large number of researches have documented the important effects of LUCC on regional climate system. Besides, biogeophysical and biogeochemical effects of large-scale LUCC have also been studied. But the relevant researches on their mechanism have generally studied biogeophysical and biogeochemical effects separately. It is the main means of the research on the effects of land use changes on the climate to carry out numerical simulation with a series of climate models of different complexities. The regional climate models have higher resolution and can reflect the climatic characteristics caused by local forcing, and have been widely used in the research on some

representative land use changes, e.g., deforestation in the tropic zone, desertification, irrigation of the cultivated land and urbanization.

Although there have been many consentaneous conclusions in many aspects of the current researches, there is still great uncertainty in the simulation of LUCC effects on the regional climate. First, the climate system contains multi-scale dynamics and interactions between multiple weather systems. Second, there is great variation in the influence of land use changes in different regions of climate system. Therefore, in order to reduce the uncertainty in these relevant researches, on one hand, it is necessary to precisely examine and depict the parameters of LUCC and other parameters of land surface, which depends on the development of remote sensing techniques. On the other hand, it is still necessary to strengthen the research on land surface process. It not only requires mathematical–physical models that can effectively simulate the interaction between land surface and the atmosphere, but also needs to improve the observation techniques so as to understand the essence of land surface process and provide reasonable initial value parameters for mathematical–physical models.

Urbanization has significant influence on local climate, e.g., urban heat island effect due to the urbanization and the effects of urban aerosol on precipitation. However, since the area of the city is generally very small, it is difficult to parameterize the urban land surface due to its great complexity, and there have been no researches on the simulation of urbanization process in regional climate models, either. In fact, with the development of the society and economy, urban population will continually increase and urban area will further expand, and consequently the effects of urbanization on the climate will be more and more important. The assessment and prediction of the influence of urbanization will be one of the major directions in the relevant researches in the future.

As the intersection between the researches on land use changes and climate change, the researches on climate effects of future land use changes mainly focus on two important issues. Firstly, great efforts have been made to understand the climate effects of past and current LUCC, however, there have been very few researches for future LUCC. Secondly, how to predict land use changes in the future and assess its influence on future climate may become a hot issue in the relevant research fields.

References

Arora VK, Montenegro A (2011) Small temperature benefits provided by realistic afforestation efforts. Nat Geosci 4(8):514–518

Bathiany S, Claussen M, Brovkin V, Raddatz T, Gayler V (2010) Combined biogeophysical and biogeochemical effects of large-scale forest cover changes in the MPI earth system model. Biogeosci Discuss 7(1):387–428

Betts AK, Ball JH, Beljaars A, Miller MJ, Viterbo PA (1996) The land surface-atmosphere interaction: A review based on observational and global modeling perspectives. J Geophys Res Atmos (1984–2012) 101(D3):7209–7225

Bonan GB (2008) Forests and climate change: forcings, feedbacks, and the climate benefits of forests. Science 320(5882):1444–1449

Bonan GB, Pollard D (1992) Vegetation on global climate. Nature 359:22

Bonan GB, Oleson KW, Vertenstein M, Levis S, Zeng X, Dai Y, Dickinson RE, Yang Z-L (2002) The land surface climatology of the community land model coupled to the NCAR community climate model*. J Clim 15(22):3123–3149

Brovkin V, Ganopolski A, Claussen M, Kubatzki C, Petoukhov V (1999) Modelling climate response to historical land cover change. Glob Ecol Biogeogr 8(6):509–517

Brovkin V, Claussen M, Driesschaert E, Fichefet T, Kicklighter D, Loutre M, Matthews H, Ramankutty N, Schaeffer M, Sokolov A (2006) Biogeophysical effects of historical land cover changes simulated by six Earth system models of intermediate complexity. Clim Dyn 26(6):587–600

Brovkin V, Boysen L, Raddatz T, Gayler V, Loew A, Claussen M (2013) Evaluation of vegetation cover and land-surface albedo in MPI-ESM CMIP5 simulations. J Adv Model Earth Syst 5(1):48–57

Chapin F, Sturm M, Serreze M, Mcfadden J, Key J, Lloyd A, Mcguire A, Rupp T, Lynch A, Schimel J (2005). Role of land-surface changes in Arctic summer warming. Science 310(5748):657–660

Charney J, Stone PH, Quirk WJ (1975) Drought in the Sahara: a biogeophysical feedback mechanism. Science 187:434–435

Copeland JH, Pielke RA, Kittel TG (1996) Potential climatic impacts of vegetation change: a regional modeling study. J Geophys Res Atmos (1984–2012) 101(D3):7409–7418

Davin EL, de Noblet-Ducoudré N (2010) Climatic impact of global-scale deforestation: radiative versus nonradiative processes. J Clim 23(1):97–112

Defries RS, Bounoua L, Collatz GJ (2002) Human modification of the landscape and surface climate in the next fifty years. Glob Change Biol 8(5):438–458

Degu AM, Hossain F, Niyogi D, Pielke R, Shepherd JM, Voisin N, Chronis T (2011) The influence of large dams on surrounding climate and precipitation patterns. Geophys Res Lett 38(4):L04405, doi:10.1029/2010GL046482

Dessler A (2010) A determination of the cloud feedback from climate variations over the past decade. Science 330(6010):1523–1527

Diffenbaugh NS (2009) Influence of modern land cover on the climate of the United States. Clim Dyn 33(7–8):945–958

Dirmeyer PA, Shukla J (1994) Albedo as a modulator of climate response to tropical deforestation. J Geophys Res 99(D10):20863–20877

Douglas EM, Niyogi D, Frolking S, Yeluripati J, Pielke RA, Niyogi N, Vörösmarty C, Mohanty U (2006) Changes in moisture and energy fluxes due to agricultural land use and irrigation in the Indian Monsoon Belt. Geophys Res Lett 33(14):L14403, doi:10.1029/2006GL026550

Douglas E, Beltrán-Przekurat A, Niyogi D, Pielke Sr R, Vörösmarty C (2009) The impact of agricultural intensification and irrigation on land–atmosphere interactions and Indian monsoon precipitation—A mesoscale modeling perspective. Glob Planet Change 67(1):117–128

Fang J, Chen A, Peng C, Zhao S, Ci L (2001) Changes in forest biomass carbon storage in China between 1949 and 1998. Science 292(5525):2320–2322

Feddema JJ, Oleson KW, Bonan GB, Mearns LO, Buja LE, Meehl GA, Washington WM (2005) The importance of land-cover change in simulating future climates. Science 310(5754):1674–1678

Foley JA, Defries R, Asner GP, Barford C, Bonan G, Carpenter SR, Chapin FS, Coe MT, Daily GC, Gibbs HK (2005) Global consequences of land use. Science 309(5734):570–574

Friedlingstein P, Prentice I (2010) Carbon–climate feedbacks: a review of model and observation based estimates. Curr Opin Environ Sustain 2(4):251–257

Friedlingstein P, Cox P, Betts R, Bopp L, von Bloh W, Brovkin V, Cadule P, Doney S, Eby M, Fung I (2006). Climate-carbon cycle feedback analysis: Results from the C4MIP model intercomparison. J Clim 19(14):3337–3353

Ge J, Qi J, Lofgren BM, Moore N, Torbick N, Olson JM (2007) Impacts of land use/cover classification accuracy on regional climate simulations. J Geophys Res Atmos 112(D5):D05107, doi:10.1029/2006JD007404

Georgescu M, Lobell DB, Field CB (2011) Direct climate effects of perennial bioenergy crops in the United States. Proc Natl Acad Sci 108(11):4307–4312

Heimann M, Reichstein M (2008) Terrestrial ecosystem carbon dynamics and climate feedbacks. Nature 451(7176):289–292

Himiyama Y, Bicik I (2012) Land use changes in selected regions in the world. Hokkaido University of Education, Asahikawa

Houldcroft CJ, Grey WM, Barnsley M, Taylor CM, Los SO, North PR (2009) New vegetation albedo parameters and global fields of soil background albedo derived from MODIS for use in a climate model. J Hydrometeorol 10(1):183–198

House JI, Colin Prentice I, Le Quéré C (2002) Maximum impacts of future reforestation or deforestation on atmospheric CO_2. Glob Change Biol 8(11):1047–1052

Kattenberg A, Giorgi F, Grassl H, Meehl G, Mitchell J, Stouffer RT, Tokioka T Weaver A, Wigley T (1996) Climate models—projections of future climate. Climate Change 1995: the science of climate change. contribution of working group I to the second assessment report of the intergovernmental panel on climate change, pp 285–357

Klein Goldewijk K, Beusen A, van Drecht G, de Vos M (2011) The HYDE 3.1 spatially explicit database of human-induced global land-use change over the past 12,000 years. Glob Ecol Biogeogr 20(1):73–86

Kueppers LM, Snyder MA (2012) Influence of irrigated agriculture on diurnal surface energy and water fluxes, surface climate, and atmospheric circulation in California. Clim Dyn 38(5–6):1017–1029

Kueppers LM, Snyder MA, Sloan LC (2007) Irrigation cooling effect: regional climate forcing by land-use change. Geophys Res Lett 34(3):L03703

Kueppers LM, Snyder MA, Sloan LC, Cayan D, Jin J, Kanamaru H, Kanamitsu M, Miller NL, Tyree M, Du H (2008) Seasonal temperature responses to land-use change in the western United States. Glob Planet Change 60(3):250–264

Lambert FH, Webb MJ, Joshi MM (2011) The relationship between land-ocean surface temperature contrast and radiative forcing. J Clim 24(13):3239–3256

Lambin EF, Geist HJ (2006) Land use and land cover change: Local processes and global impacts. Springer, New York

Li J, Song C, Cao L, Zhu F, Meng X, Wu J (2011) Impacts of landscape structure on surface urban heat islands: a case study of Shanghai, China. Remote Sens Environ 115(12):3249–3263

Lobell D, Bala G, Mirin A, Phillips T, Maxwell R, Rotman D (2009) Regional differences in the influence of irrigation on climate. J Clim 22(8):2248–2255

Lynch A, Chapin Iii F, Hinzman L, Wu W, Lilly E, Vourlitis G, Kim E (1999) Surface energy balance on the arctic tundra: measurements and models. J Clim 12(8):2585–2606

Malhi Y, Aragão LE, Galbraith D, Huntingford C, Fisher R, Zelazowski P, Sitch S, Mcsweeney C, Meir P (2009) Exploring the likelihood and mechanism of a climate-change-induced dieback of the Amazon rainforest. Proc Natl Acad Sci 106(49):20610–20615

Meiyappan P, Jain AK (2012) Three distinct global estimates of historical land-cover change and land-use conversions for over 200 years. Front Earth Sci 6(2):122–139
Moss RH, Edmonds JA, Hibbard KA, Manning MR, Rose SK, van Vuuren DP, Carter TR, Emori S, Kainuma M, Kram T (2010) The next generation of scenarios for climate change research and assessment. Nature 463(7282):747–756
Murata A, Sasaki H, Hanafusa M, Kurihara K (2012) Estimation of urban heat island intensity using biases in surface air temperature simulated by a nonhydrostatic regional climate model. Theor Appl Climatol 122(1–2):351–361
Oyama MD, Nobre CA (2004) Climatic consequences of a large-scale desertification in northeast Brazil: a GCM simulation study. J Clim 17(16):3203–3213
Pacala SW, Hurtt GC, Baker D, Peylin P, Houghton RA, Birdsey RA, Heath L, Sundquist ET, Stallard R, Ciais P (2001) Consistent land-and atmosphere-based US carbon sink estimates. Science 292(5525):2316–2320
Pachauri R, Reisinger A (2007) IPCC fourth assessment report. IPCC, Geneva
Phillips OL, Aragão LE, Lewis SL, Fisher JB, Lloyd J, López-González G, Malhi Y, Monteagudo A, Peacock J, Quesada CA (2009) Drought sensitivity of the Amazon rainforest. Science 323(5919):1344–1347
Pielke RA, Avissar R, Raupach M, Dolman AJ, Zeng X, Denning AS (1998) Interactions between the atmosphere and terrestrial ecosystems: influence on weather and climate. Glob Change Biol 4(5):461–475
Pielke R, Adegoke J, Beltran-Przekurat A, Hiemstra C, Lin J, Nair U, Niyogi D, Nobis T (2007) An overview of regional land-use and land-cover impacts on rainfall. Tellus B 59(3):587–601
Ran Y, Li X, Lu L, Li Z (2012) Large-scale land cover mapping with the integration of multi-source information based on the Dempster-Shafer theory. Int J Geogr Inf Sci 26(1):169–191
Salmun H, Molod A (2006) Progress in modeling the impact of land cover change on the global climate. Prog Phys Geogr 30(6):737–749
Salvati L, Bajocco S (2011) Land sensitivity to desertification across Italy: past, present, and future. Appl Geogr 31(1):223–231
Sellers PJ, Tucker CJ, Collatz GJ, Los SO, Justice CO, Dazlich DA, Randall DA (1996) A revised land surface parameterization (SiB2) for atmospheric GCMs. Part II: the generation of global fields of terrestrial biophysical parameters from satellite data. J Clim 9(4):706–737
Sellers P, Dickinson R, Randall D, Betts A, Hall F, Berry J, Collatz G, Denning A, Mooney H, Nobre C (1997) Modeling the exchanges of energy, water, and carbon between continents and the atmosphere. Science 275(5299):502–509
Shukla J, Mintz Y (1982) Influence of land-surface evapotranspiration on the Earth's climate. Science 215(4539):1498–1501
Shukla J, Nobre C, Sellers P (1990) Amazon deforestation and climate change. Science (Washington) 247(4948):1322–1325
Singh RB, Nath R (2012) Remote sensing, GIS and micrometeorology for monitoring and predicting urban heat islands in Kolkata mega city. Ann NAGI 32(1):17–39
Smith P, Powlson D, Glendining M, Smith J (1997) Potential for carbon sequestration in European soils: preliminary estimates for five scenarios using results from long-term experiments. Glob Change Biol 3(1):67–79
Spracklen DV, Bonn B, Carslaw KS (2008) Boreal forests, aerosols and the impacts on clouds and climate. Philos Trans R Soc A Math Phys Eng Sci 366(1885):4613–4626
Stone Jr B (2009) Land use as climate change mitigation. Environ Sci Technol 43(24):9052–9056
Wickham JD, Wade TG, Riitters KH (2012) Comparison of cropland and forest surface temperatures across the conterminous United States. Agric For Meteorol 166:137–143

Woldemichael AT, Hossain F, Pielke Sr R, Beltrán-Przekurat A (2012) Understanding the impact of dam-triggered land use/land cover change on the modification of extreme precipitation. Water Resour Res 48(9):W09547

Wong JKW, Lau LS-K (2013) From the 'urban heat island'to the 'green island'? A preliminary investigation into the potential of retrofitting green roofs in Mongkok district of Hong Kong. Habitat Int 39:25–35

Chapter 2
Land Use Change Dynamics Model Compatible with Climate Models

Jinyan Zhan, Jiyuan Liu, Yingzhi Lin, Feng Wu and Enjun Ma

Land Use/Cover Change (LUCC) is an important part of the global environmental change, which has always been the scientific hot spot. There are two primary factors that contribute to climate change: land use change and greenhouse gas emission (Kalnay and Cai 2003). This chapter focuses on the Land Use Change Dynamics (LUCD) model which can be compatible with climatic models, including three sub-modules, namely economic module, vegetation change module, and agent-based module.

Firstly, the economic module is capable of estimating the demand of land use changes in economic activities and maximizing economic utility. In this sense, Computable General Equilibrium (CGE) modeling approach can include land as a production factor into the economic module. Second, vegetation change module provides the probability of vegetation change driven by climate change. The Agro-ecological Zone (AEZ) model is supposed as the optimal option for constructing the vegetation change module because it is naturally correlated with AEZs facilitating the coupling of economic module and vegetation change module. Third, the agent-based module identifies if the land use change demand and vegetation change can be realized and provides the land use change simulation results, which are the underlying surfaces needed by Regional Climate Models (RCMs). By importing the RCMs' simulation results of climate change and providing the simulation results of land use change for RCMs, the LUCD model would be compatible with RCMs.

J. Zhan (✉) · F. Wu
State Key Laboratory of Water Environment Simulation, School of Environment, Beijing Normal University, Beijing 100875, China
e-mail: zhanjy@bnu.edu.cn

J. Liu
Institute of Geographic and Natural Resources Research, Chinese Academy of Sciences, Beijing 100101, China

Y. Lin · E. Ma
School of Mathematics and Physics, China University of Geosciences (Wuhan), Wuhan 430074, China

X. Deng et al. (eds.), *Land Use Impacts on Climate*, Springer Geography

DOI: 10.1007/978-3-642-54876-5_2,

On the other hand, the climate model is an effective tool to study LUCC on surface climate, but how should it be applied to the research on the regional effects of LUCC? The framework of LUCD model compatible with RCMs is introduced in this chapter. Framework and modules of LUCD models are introduced in the first part. The Weather Research and Forecasting (WRF) Model, as a next-generation mesoscale numerical weather prediction system, is explained in detail in the second section.

The land use simulation model is an important tool to analyze the LUCC, which plays a key role in influencing the global climate. However, there have been few global LUCC simulation models, especially these that can be used to analyze the interaction among the socioeconomic development, climate change and LUCC. The Global Change Assessment Model (GCAM) and the GTAP-AEZ model take account of the influence of social economy and climate change at the global scale, but they may have some parameter errors due to the rough parameter setting. This study aims to compare the simulation results obtained with the GCAM model and GTAP-AEZ model and optimize their parameters according to the specific conditions of China, presented in the last section.

2.1 LUCD: Framework and Modules

LUCC is an important part of the global environmental change, which has always been the academic hot spot. Many simulation experiments have proven that the simulation results of RCMs are sensitive to underlying land use and land cover changes (Shepherd et al. 2010). While the interaction between land use change and climate change has been fully realized, most RCMs introduce LUCC data exogenously (Cai et al. 2010). Always, they apply the LUCC data of one year of history as underlying surfaces and keep them constant ignoring the interaction between LUCC and climate variations. This section provides a framework of LUCD model compatible with RCMs to introduce parameterized LUCC into regional climate change modeling endogenously. Several suggested models are introduced and some specific parameter processing approaches are explained in detail. This modeling framework helps to enhance the understanding of the coupling mechanism of land use system and climatic system, and strengthen the simulation capability of land system.

Land system is geographically complex, which is composed of natural factors, human land use activities, and other impact factors (GLP 2005). Land use change simulation is a prediction of when, where, why, and how land use pattern changes (Deng et al. 2010a, b). However, studies on land use change processes are often challenged by the complex and unexpected human activities and natural constraints. Land use change emerges from the interactions among various components of the coupled human–landscape system and feeds back to the subsequent development of these interactions (Le et al. 2008). Most land use change simulation models simulate successional pattern change of land use under the macro background of the regional population growth, economic development, social progress, changes in the natural environment, and other facts (Liu and Deng 2010).

On the whole, the land use change simulation models can be broadly divided into three major categories: empirical statistical model, agent-based model (ABM), and raster neighborhood relationship-based model (Liu et al. 2005a, b).

There are abundant empirical statistical models applied in land use change simulation. This kind of models can be broadly divided into two categories: econometric model that describes the process of land use change by establishing equations between land use and its influencing factors, and mechanism model identifying the relationship of land use change and its driving factors at grid levels. A typical example of the latter is the Conversion of Land Use and its Effect at Small regional extent (CLUE-S) model whose application in land use change simulation is currently in the ascendant (Veldkamp and Fresco 1996). The CLUE-S model is constructed to simulate land use change and its effects on environment at meso-micro scale. It has the capability of synchronously simulating the changes of multiple types and introduces the dynamic driving factors (such as population and economic growth) to improve the simulation accuracy.

Since the 1990s, along with the rapid development of complexity science, ABM began to be applied in land use change research. The Agent-based Models of Land Use and Cover Change (ABM/LUCC) was specially discussed by LUCC Report No.6, in which the development prospect of ABM in land use change simulation is highly valued (McConnell 2001). The ABM can be divided into two categories. One is simulation model of landscape scale mainly based on traditional spatial modeling techniques and the other depicts human decision-making processes and their interactions (Semboloni et al. 2004; Zhang et al. 2013). The latter mainly identifies the linkage between agents and environment by describing the interaction and affiliation of independent agents (Manson 2006). It is found that the agents would get more benefits under the scenario without climate changes in the long term, even though the total income is lower than that of under the scenario with climate changes. Studies showed that ABM is efficient in describing the interaction between macro individual and micro individual.

As a representative of raster neighborhood relationship-based model, CA model is widely used in land use change simulation, especially urban expansion. Syphard et al. (2005) analyzed the distinction of LUCC caused by urban expansion in areas with different slope with the CA model. One of the superiority of the CA model in land use change simulation is that it supports visualization of the simulation process. The structure of the CA model makes it difficult considering the impacts of land use policies. By combining ABM and Cellular Automata (CA) model, the simulation of land use change is characterized by multi-scale and becomes more effective in multi-objective decision making.

The existing models including CLUE-S model, ABM, and CA model are not compatible with RCMs. The CLUE-S model needs an input of the land use structure and ignores the influences of climate zone change on land use change. The ABM and CA model is good at urban expansion simulation but vegetation change driven by natural environment condition change. In this study, we developed a LUCD model in compatible with RCMs to describe the interdependencies and feedback mechanisms among social economics, ecosystem environment as

well as irrational decision making process. The LUCD model describes a combined and complex system composed of social economic, ecosystem components, and decision making process and consequences. It provides a consistent and comprehensive framework of land use change modeling and emphasis on how the models work together. By introducing Agro-ecological zone (AEZ) based on the simulation results of RCMs, the LUCD model is compatible with RCMs and constitutes an iterative simulation system of LUCC and climate changes.

2.1.1 Land Use Change Dynamics Model

2.1.1.1 Model Structure

LUCD model constitutes of three modules, namely economic module, vegetation change module, and agent-based module. The economic module calculates the land demand for all economic activities maximizing economic utility of land uses. The vegetation change module provides the probability of vegetation change driven by climate changes. And the agent-based module identifies that if the land demand and vegetation change can be realized and provides the land use change simulation results, which are the underlying surfaces needed by RCM. To feed the LUCD model results into RCMs, the land use system applied in the LUCD model should be consistent with the underlying surfaces used in RCMs (Fig. 2.1). By iteratively using the output of one model as the input of another, the LUCD model is compatible with RCMs. In Fig. 2.1, the dotted lines show the data transmission between the LUCD model and RCMs, while the solid lines stand for the flow of information in the LUCD model. The LUCD model provides the simulated land use for RCMs as underlying surface data, then RCMs can simulate the climate change resulted from the land use change. The results of climate change simulated by RCMs are further imported into the LUCD model, affecting land use change.

The economic module estimates the land use change demand driven by human activity. The current condition of land uses are introduced into this module as one of the limitations of economic activities as well as land use decisions. The equilibrium of markets determines the commodity supply and in turn influences the land use demand. Combining the land use demand, the limited amount of land as well as the current land use status, the land use change demand is obtained. The vegetation change module describes the possible vegetation change driven by climate change. The AEZ is the key concept that links the climate change and vegetation change and helps to couple human activity with climate change. The climate change leads to change of AEZs, which determines the growth of vegetation (Stehfest et al. 2007). Consequently, the climate change affects not only the evolution of natural vegetation but also the human activities including planting and breeding. By overlying the AEZs on the current vegetation pattern, the suitability of vegetation change can be evaluated. The agent-based module describes the procedure of land use decision coupled with the land use change demand and

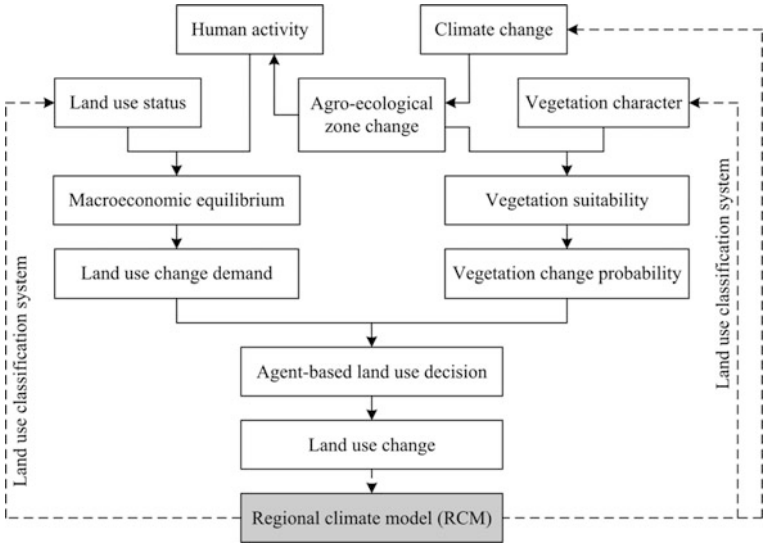

Fig. 2.1 Framework of feeding LUCD model results into RCMs simulation

vegetation change suitability using the agent-based simulation technology. This module identifies whether or not the theoretical land use change demand and the possible vegetation change estimated by the economic module and the vegetation change module can be realized. The output of this module, land use change, is the underlying surfaces that are needed by RCMs. By embedding the LUCD in RCMs, an iterative simulation system of land use change and climate change is constructed (Fig. 2.1).

2.1.1.2 Economic Module

The economic module should provide a comprehensive macroeconomic framework to describe market-oriented economies. CGE model is suggested to be appropriate for such a macroeconomic framework. For convenient application, the way that induces land into the economic module under a CGE modeling framework is proposed as well in this study (Fig. 2.2). Land is one of the three primary factors input in commodity production. And there are five components: producers, households, government, trade, and markets in CGE model. Producers decide demand of inputs including primary factors of land, labor, and capital, and supply of outputs (commodities) to maximize their profits. Households decide demand of commodities and supply of their endowments of labor and capital to maximize their economic utility. Government imposes taxes and expends them in public consumption and savings. The savings of government and households transform into investment according to reserve requirements, which is also an important component in demand. And we employ the small-country assumption that the

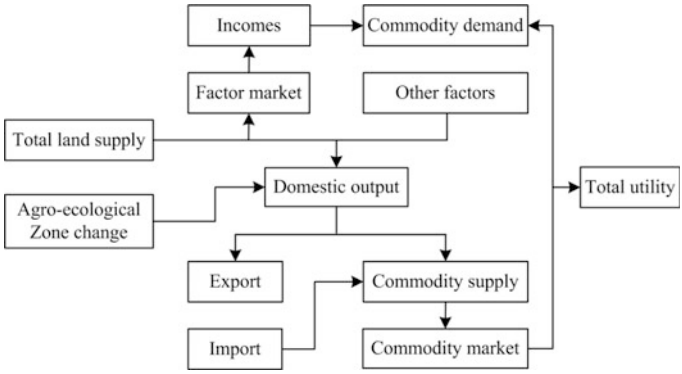

Fig. 2.2 Overview flow chart of economic module applying a CGE modeling framework

study area is too small to affect prices in international markets. Thus, import and export prices, which this country faces, are given for it in foreign currency terms. The demand and supply of commodities and primary factors are equilibrated in markets by price adjustment. With this module, we can compute land uses in various equilibriums to simulate what will happen in the future.

Though CGE models are good at describing the quantities and prices variation as others, we do not introduce land prices but land area in the economic module. This is because the land prices vary along with not only time but also location and productivity, etc. And as a macroeconomic model, CGE model do not support a diverse prices modeling framework. Thus, we summarize land uses in economic development as follows.

$$Y_{i,e} = b_{i,e} \prod\nolimits_h F_{h,i,e}^{\beta_{h,i,e}} \prod\nolimits_l Aec_{l,i,e}^{\zeta_{l,i,e}} \tag{2.1}$$

$$Aec_{l,i,e} = \frac{\zeta_{l,i,e} Y_{i,e}}{b_{i,e}} \tag{2.2}$$

where, i is the index of commodities; e is the index of AEZs; l is the index of land use type; h is the index of primary factors (labor and capital); $Y_{i,e}$ is the value added of the ith firm in the eth AEZ; $Aec_{l,i,e}$ is the input area of the lth land use type for ith commodity production in the eth AEZ; $F_{h,i,e}$ is the input of the hth factor by the ith firm in the eth AEZ; $b_{i,e}$ is the scaling parameter in production function, also called total factor productivity (TFP); $\zeta_{l,i,e}$ is the share parameter in production functions; and $\beta_{h,i,e}$ is the share parameter in production functions. Considering the value added is proportional to the input land area under the certain technique condition and primary factors input, the input area of each land use type is calculated by Eq. (2.2).

The input land area of each type of land use per unit of each commodity output is inversely correlated with primary factors input besides TFP. Consequently, the

share parameter, $\zeta_{l,i,e}$, is determined by the input of the hth factor by the ith firm in the eth AEZ, $F_{h,i,e}$.

$$\zeta_{l,i,e} = fl, e(Flabor, i, e, Fcaptial, i, e) \tag{2.3}$$

The land demand input in commodity production is determined by the economic system, because the economic links in the comprehensive macroeconomic framework provided by CGE model are tightly connected with each other. Each shock to economic system will influence the area demand of lands input in commodity production. For example, the growth in the rate of direct tax will lead to an increase in government revenues and a decrease in household income. Then, the structure differences of investments and consumptions between government and household determine the change of commodity demand structure. Under the market-clearing condition, the commodity production and supply structure should be altered. And finally, the area demand of lands input in commodity production will change.

As one of the economic models, the economic module assumes that the ultimate purpose of economic development is to increase the economic utility of household. Household's economic utility is dependent on the amount of consumption of commodity, which are purchased from producers.

$$Uec = \prod_i Xp_i^{\chi_i} \tag{2.4}$$

where, Uec is the economic utility; Xp_i is the amount of consumption of the ith commodity; and χ_i is the share parameter in the economic utility function.

The economic utility is indirectly restrained by the area of land used for economic development. In reality, the earnings from endowments of land are the component household's income which is the constraint of household consumption. And the input of land in production by producer determines the output and supply of commodity. Nevertheless, we only consider the constraint function of land in production in this module because the earnings from the endowment of land are not included when accounting income constraints. The economic development can be summarized as the following optimization problem:

$$\underset{\{Ueco,\, Uent\}}{\text{maximize}} \quad Uec = \prod_i Xp_i^{\chi_i} \tag{2.5}$$

subject to

$$Tland = \sum_e \sum_l \sum_i Aec_{l,i,e} \tag{2.6}$$

where, $Tland$ is the total land area which is exogenously defined. Equation (2.5) shows the objective function of economic utility to be maximized; and Eq. (2.6) is a total land area constraint equation meaning that total land areas used for commodity production must equal to the total land area used in economic activity on

the left-hand side of the equation. The simulated land use change demand at regional scale can be allocated to grids by using DLS model (Deng et al. 2010a, b), CLUE-S model (Verburg et al. 2002) and CA model (Lau and Kam 2005) etc.

2.1.1.3 Vegetation Change Module

The vegetation change module assesses the growth suitability of specific vegetation and provides the possibility of vegetation change. There are many models including Dynamic Global Vegetation Model, Holdridge Life Zone Model, and AEZ model that can be used to describe the vegetation change driven by climate change. In this study, we propose AEZ model as the optimal option because it is naturally correlated with AEZs facilitating the coupling of economic module and vegetation change module. We also illustrate how to estimate the possibility of vegetation change using AEZ model. The AEZ model is developed by Food and Agriculture Organization (FAO) of the United Nations with the collaboration of the International Institute for Applied Systems Analysis (IIASA) (Schmidhuber and Tubiello 2007). Climate, topography, and soil characteristics are three key inputs of the AEZ model. The model can estimate the climate limited vegetation productivity. Assuming that the estimated climate limited productivity of the vth type of vegetation in the pixel p in the tth year is $Y_{v,p,t}$, the possibility of vegetation change of the vth type of vegetation in the pixel p in the $(t + 1)$th year is

$$P_{v,p,t+1} = \frac{Y_{v,p,t+1} - Y_{v,p,t}}{Y_{v,\max}} \tag{2.7}$$

where, $Y_{v,max}$ is the maximum climate limited productivity of the vth type of vegetation; and $P_{v,p,t+1}$ is the possibility of vegetation change of the vth type of vegetation in the pixel p in the $(t + 1)$th year.

A positive $P_{v,p,t+1}$ implies that the vth type of vegetation in the pixel p will expand or be more thickly forested in the $(t + 1)$th year, while a negative $P_{v,p,t+1}$ means that the vth type of vegetation in the pixel p will be inclined to degrade in the $(t + 1)$th year. The possibility of vegetation change provides the comparison criterion of specific vegetation change of different pixel in different time. When comparing the superiority of different vegetation in the specific pixel and time, a superiority index, $S_{v,u,p,t}$, is proposed.

$$S_{v,u,p,t+1} = \frac{Y_{v,p,t+1} - Y_{v,p,t}}{Y_{u,p,t+1} - Y_{u,p,t}} \tag{2.8}$$

where, $S_{v,u,p,t+1}$ is the superiority index of the vth type of vegetation compared with the uth type of vegetation in the pixel p in the $(t + 1)$th year.

The superiority index cannot depict the dominance relations between two types of vegetation by itself. The application of this index should combine with the possibility of vegetation change. For instance, when $P_{v,p,t+1}$ is positive and

$S_{v,u,p,t+1}$ is larger than 1, the vth type of vegetation is more superior than the uth type of vegetation in the pixel p in the $(t + 1)$th year. A more exact mathematical formula for judging the dominance relations of multiple types of vegetation is proposed in the agent-based module.

2.1.1.4 Agent-based Module

Determination of land use change is partly characterized by non-rationality such as tradition and custom. The agent-based module identifies if the land use change demand simulated by economic module and the possible vegetation change assessed by vegetation change module can be realized under the background of irrational decisions. Agent-based modeling is able to simulate land use change by measuring the individual behavior and results of land use over time. Take the decision of land use change of a given household for instance. The dissimilarities between a given household h and all defined household groups in the population can be measured.

$$D_{h,g} = \sum_{s=1}^{S} w_s \left[\frac{\left(V_{h,s} - \bar{V}_{g,s}\right)^2}{\left|V_{h,s} + \bar{V}_{g,s}\right|} \right] \tag{2.9}$$

where, $D_{h,g}$ is the distance from household h ($h = 1, 2, \ldots, H$) to the household group g ($g = 1, 2, \ldots, G$). $V_{h,s}$ is the value of variable s ($s = 1, 2, \ldots, S$) representing the character of household h. $\bar{V}_{g,s}$ is the average value of variable s of households in household group g; w_s is the weight coefficient of the variable s in explaining the character of household and household group.

The household h is assigned into the most similar household group and makes the same land use change decision with the household group.

$$g' = \arg \ \min\left\{D_{h,1},\ D_{h,2},\ \cdots,\ D_{h,g},\ \cdots,\ D_{h,G}\right\} \tag{2.10}$$

where, g' is the most similar household group to household h. By establishing a case database of land use change decision, we can assign each household into one similar enough household group and deduce the land use decision. It helps correct the land use change results simulated of economic module based on ideas of optimization.

For the assessment result of vegetation change module, the agent-based module also provides a criterion to judge which kind of vegetation change will happen in a specific pixel.

$$L_{v,p} = \begin{cases} 1, & \begin{array}{r} \textit{if for } \forall u \neq v,\ P_{v,p,t+1} > 0 \textit{ and } S_{v,u,p,t+1} > 1 \textit{ or } \leq 0, \\ \textit{or } P_{v,p,t+1} \leq 0 \textit{ and } S_{v,u,p,t+1} > 0 \textit{ or } \leq 1; \end{array} \\ 0, & \begin{array}{r} \textit{if for } \forall u \neq v,\ P_{v,p,t+1} > 0 \textit{ and } S_{v,u,p,t+1} > 0 \textit{ or } \leq 1, \\ \textit{or } P_{v,p,t+1} \leq 0 \textit{ and } S_{v,u,p,t+1} > 1 \textit{ or } \leq 0. \end{array} \end{cases} \tag{2.11}$$

where, $L_{v,p} = 1$ denotes that the vth type of vegetation is the dominant vegetation in the pixel p and $L_{v,p} = 0$ denotes that the vth type of vegetation is not the dominant vegetation in the pixel p. This criterion defines that for any other vegetation type u, when $P_{v,p,t+1}$ is positive and $S_{v,u,p,t+1}$ is larger than 1 or no larger than 0, or $P_{v,p,t+1}$ is not positive and $S_{v,u,p,t+1}$ is smaller than 0 or no larger than 1, the vth type of vegetation is dominant vegetation in the pixel p in the $(t + 1)$th year; when $P_{v,p,t+1}$ is positive and $S_{v,u,p,t+1}$ is larger than 0 or no larger than 1, or $P_{v,p,t+1}$ is not positive and $S_{v,u,p,t+1}$ is larger than 1 or no larger than 0, the vth type of vegetation is not the dominant vegetation in the pixel p in the $(t + 1)$th year.

For a specific pixel, vegetation change will happen as long as the productivity of the new dominant vegetation exceeds that of the original dominant vegetation.

$$LV_{p,t+1} = v, \quad if\ for\ \forall u \neq v,\ RY_{v,p,t+1} > RY_{u,p,t+1} \tag{2.12}$$

$$RY_{v,p,t+1} = RY_{v,p,t} + \frac{RY_{v,p,t}}{RY_{p,t}} Y_{v,p,t+1} \tag{2.13}$$

$$RY_{p,0} = \sum\nolimits_{v} \frac{A_{v,p,0}}{A_p} Y_{v,p,0} \tag{2.14}$$

where, $LV_{p,t+1}$ denotes the new vegetation type that characterized the pixel p in the $(t + 1)$th year. $RY_{v,p,t+1}$ is the productivity of the vth type of vegetation in the pixel p in the $(t + 1)$th year. $RY_{p,t}$ is the total productivity of all the vegetation in the pixel p in the tth year; $\mathrm{RY_{p,0}}$is the total productivity of all the vegetation in the pixel p in the base year. A_p is area of pixel; $A_{v,p,0}$ is area the vth type of vegetation in the pixel p in the base year; and $Y_{v,p,0}$ is the productivity of the vth type of vegetation in the pixel p in the base year.

2.1.2 Concluding Remarks on LUCD Model

In this part, we introduced the LUCD model which is compatible with RCMs to provide endogenous underlying surface for climate modeling. This model is constituted by economic module, vegetation change module, and agent-based module. The economic module calculates the land use change demand driven by economic activities aiming at maximizing economic utility. The vegetation change module evaluates the probability of vegetation change driven by climate change. These two modules depict the land surface process under the condition of rational decision making and ideal circumstances. To couple the economic module and vegetation change module, the AEZ is introduced in the LUCD model. The agent-based module identifies if the land use change demand and vegetation change can be realized under the condition of irrational decision making and multiple vegetation competition. By introducing the simulation results of the LUCD model in

RCM and applying the simulation results of RCM in the LUCD model, a coupled simulation system of land surface system simulation can be established.

In addition to the modeling framework, several suggested models are introduced and some specific parameter processing approaches are explained in detail for the constitution of the LUCD model. For the economic module, a CGE modeling framework and the difference between land and other production factors in CGE model are introduced. The effects of climate change on human activities are also taken into consideration by establishing production function for each AEZ. The AEZ model is suggested for the vegetation change module and two indexes (possibility of vegetation change and superiority index) are supposed to determine the climate-induced vegetation change. For the agent-based module, an example of land use change decision making and the criterion of vegetation change is provided.

To ensure the output on LUCC of LUCD model easily feed into RCMs, the classification system of LUCC should be comparable with that needed by RCMs as underlying surface. The classification system determines the choice of driving factors that affect land use change, vegetation change as well as decision making processes in the LUCD model. And the specific parameter processing approaches provided in this study can also serve as valuable examples even if a new modeling approach is used in the LUCD model.

2.2 Weather Research and Forecasting Model

With the development of the climate models and land surface process models, the numerical simulation has become widely used to study the influence of LUCC on climate. The WRF Model is a next-generation mesoscale numerical weather prediction system designed to serve both atmospheric research and operational forecasting needs. It features two dynamical cores, a data assimilation system, and a software architecture allowing for parallel computation and system extensibility. The model serves a wide range of meteorological applications across scales ranging from meters to thousands of kilometers. The effort to develop WRF model began in the latter part of the 1990s and was a collaborative partnership principally among the National Center for Atmospheric Research (NCAR), the National Oceanic and Atmospheric Administration,[1] the Air Force Weather Agency (AFWA), the Naval Research Laboratory, the University of Oklahoma, and the Federal Aviation Administration (FAA).

[1] National Oceanic and Atmospheric Administration are represented by the National Centers for Environmental Prediction (NCEP) and the (then) Forecast Systems Laboratory (FSL).

WRF model allows researchers to produce simulations reflecting either real data (observations, analyses) or idealized atmospheric conditions. WRF model provides operationally forecasting, flexible and computationally efficient platform, offering advances in physics, numerics, and data assimilation contributed by many research community developers. WRF model is currently used at National Centers for Environmental Prediction (NCEP), the AFWA, and other centers.

2.2.1 Development of WRF Model

WRF model has a large worldwide community of users (over 20,000 in over 130 countries), and workshops and tutorials are held each year at NCAR. There are two dynamical core versions of WRF model, each with its own web page. The Advanced Research WRF (ARW) is supported to the community by the NCAR Mesoscale and Microscale Meteorology Division.[2] The WRF-NMM (NMM) is supported to the community by the Developmental Test bed Center (DTC).[3] The development of WRF model with ARW dynamic core is shown in Table 2.1.

The ARW model represents the latest developments following a particular modeling approach that uses time-splitting techniques to efficiently integrate the fully compressible nonhydrostatic equations of motion. The ARW is suitable for use in a broad range of applications across scales ranging from meters to thousands of kilometers. The main application includes idealized simulations (e.g., LES, convection, baroclinic waves), parameterization research, data assimilation research, forecast research, and real-time NWP. Besides, hurricane research, regional climate research, coupled-model application as well as teaching.

The Mesoscale and Microscale Meteorology Division of NCAR is currently maintaining and supporting a subset of the overall WRF code. The WRF modeling system software in the public domain is freely available for community use. The WRF modeling system consists of four important major programs, which are WRF Preprocessing System (WPS), WRF-DA, ARW solver, and the post-processing and visualization tools.

2.2.2 Application of WRF Model

WRF model is mainly applied to the weather and climate research when horizontal resolution is 1–10 km. It can also be applied to numerical simulation, physical parameterizations research, data assimilation, numerical ideal test and provide meteorological field for air quality model.

[2] For detailed information: http://www.mmm.ucar.edu/wrf/users.

[3] For detailed information: http://www.dtcenter.org/wrf-nmm/users.

Table 2.1 Development of WRF model with ARW dynamic core

Version	Release time	Note
WRF V1.0	2000.11	The first version was released
WRF V1.1.1	2001.11	The third version was released. WRF V1.1 was not changed much, except for two error revision
WRF V1.2	2002.4	The fourth version was officially released. Then V1.2.1 was released in May 22nd
WRF V1.3	2003.3	
WRF V2.0	2004.5	The nested versions was released, including single and double nested and 3-dimensional variational data assimilation system (3DVAR), and NMM was added and EM nesting was released
WRF V2.1	2005.8	EM becomes ARW
WRF V2.2	2006.11	WRF preprocessing system (WPS) was issued to replace the WRF standard initialization (WRF SI), and WPS was released
WRF V3.0	2008.4	WPS has been used, adding global ARW version
WRF V3.1	2009.4	
WRF V3.2	2010.4	
WRF V3.3	2011.4	4DVAR was updated
WRF3.4	2012.4	QNSE PBL method was added, as well as the Noah MP(multi-physics) land surface model, and variation of sea-ice albedo with T were allowed, thus, Noah and Noah MP were in new shared sea-ice module. Sfclay option 1 code was modified and cleaned up.
WRF3.5	2013.4	New land-surface models such as RUC LSM, PX LSM, and CLM4 land were included.

The key consideration of WRF model is to forecast the important weather process from the cloud scale to the synoptic scale, including pre-processing module WPS (WRF processing system) and main module ARW. WPS is not only the pre-processing part of mode data, but also the part that provides some initial boundary before the three-dimensional variation systems established. It is mainly responsible for the standard grid data preprocessing and terrain data preprocessing. WPS modules include three sub-modules: geogrid, ungrib, metgrid. Among them, main function of geogrid is to define and create land patterns. In the geogrid module, users can set the projection domain, range size, regional location, nesting, and other parameters. According to these custom settings, geogrid will interpolate topography, land use, soil type, and other data to the defined region network, the data format is NetCDF. Ungrib module's main function is converting standard grib files into ones that can be recognized by metgrid. Typically grib files have many different formats; the same meteorological elements may have different elements code. For these different formats, WPS provides the corresponding Vtable function pointer, such as AWIP, GFS, etc. Metgrid module is for meteorological data interpolation. It interpolates the meteorological of large area into calculated grid of

pattern (including the horizontal direction and the vertical direction), and provides initial and boundary condition file for the model.

In WRF model, the original land use data come from the global 24 types of land use and land cover classified by United States Geographical Survey land use systems (USGS). Each land use types have different roughness, albedo, and other parameters, affecting the flow of meteorological fields, precipitation, temperature, or temperature.

In WRF simulation, each grid point has a land cover type based on the land cover dataset being used for the model run. The properties (surface albedo, surface emissivity, moisture availability, surface roughness length) of each land cover type depend on the land surface model used in the WRF run. The land-surface model is the component that takes care of the processes involving land-surface interactions. For the WRF runs, the parameterization scheme of physical processes in the model should be set, USGS classification data set need to be used to specify land cover types and their properties.

The interactions between the atmosphere and other earth system components, which are important drivers of regional climate, are not well explained in most RCMs models. Although more and more of these interactions are now represented in GCMs, global models lack the spatial resolution to represent regional-scale processes and feedbacks. Biases in simulating regional precipitation, for example, can have far-reaching consequences in fully coupled models of the climate system, because water integrates across the physical, biological, and chemical components.

Therefore, WRF is strongly recommended to address a wide range of science questions specific to regional-scale processes, and forcing and response. Examples include interactive coupling of the RCM with sea ice and ocean models to represent air–sea interactions; chemistry and aerosol models, including dust, to represent chemistry–aerosol–cloud–radiation feedbacks; and marine and terrestrial ecosystem models to represent biogeochemical cycling processes. Additionally, developing more comprehensive treatments of land surface and hydrological processes, including river routing, subsurface flow, lake, land use, fires, and land ice, will enable a more dynamic representation of land–atmosphere feedbacks. It is noted that some development efforts are already underway in the framework of the Community Land Model (CLM) and Noah land surface model that have been implemented in WRF. Building data assimilation capabilities for the coupled model will enable the development of regional analyses of the Earth system; an example is an ocean and land data assimilation system. Finally, to facilitate model coupling, participants recommended accelerating the transition of WRF to the Earth System Modeling Framework (ESMF) (Tolstoy et al. 2004).

2.3 Global Models Combining Emission Scenarios with Land Use Changes

The land use simulation model is an important tool to analyze the LUCC, which plays a key role in influencing the global warming. However, there have been very few global LUCC simulation models, especially the models that can be used to analyze the interaction among the socioeconomic development, climate change, and LUCC. The Global Change Assessment Model (GCAM) and the GTAP-AEZ model are two models that take account of the influence of social economy and climate change at the global scale, but they may have some parameter errors due to the rough parameter setting. This study aims to compare the simulation results obtained with the GCAM model and GTAP-AEZ model and optimize their parameters according to the specific conditions of China. First, we simulated the land use structure in China in 2010 with the two models and compared the simulation results with the real one. Second, we calibrated these parameters of models according to the China's national conditions and implemented the simulation again. The result indicates the calibrated GCAM can provide more accurate simulation result of land use, which can provide significant reference information for the land use planning and policy formulation to mitigate the climate change in China.

2.3.1 Overview of Global LUCC Simulation Models

Humans have transformed significant portions of the Earth's land surface, 10–15 % of which is currently dominated by agricultural crop or urban-industrial areas, and 6–8 % is pasture (Vitousek et al. 1997).These land use changes have important implications for future climate changes, and consequently, great implications for subsequent land use changes (Deng et al. 2013; Nunes and Auge 1999; Turner 1994). Climate change and land use change are both global driving forces of environmental change, and the impact assessments generally show that interactions between them can lead to serious challenges to the provision of ecosystems services. Besides, in many cases it is impossible to determine the impacts of climate change without consideration of LUCC. LUCC is a widespread, significant, and accelerating process, and it has been one of the research cores of the international programmes, such as the International Geosphere-Biosphere Programme (IGBP) and the Global Environmental Change Human Dimensions Programme (IHDP) and is also one of the global environmental research focuses and cutting-edge issues (Liu and Deng 2010). LUCC is driven by human activities, and in many cases it also leads to changes that impact the humans, therefore, LUCC modeling is a critical way for formulating effective environmental policies and management strategies (Jiang et al. 2012). Understanding the role of land use change in the global environmental change requires the analysis of historical land

cover conversions and projection of possible future land use changes, both of which heavily rely on the land use simulation models. Besides, the land use simulation model also provides an essential approach for stakeholder to project and evaluate the potential consequences of policy decisions and other actions. As more scholars realized the importance of LUCC, the land use simulation model has become an important tool for the analysis of both the mechanism and the spatial distribution of LUCC in the past and future (Deng et al. 2012; Hu et al. 2004).

The land use simulation models include Markov model, logistic function model, regression model, econometric model, dynamic systems model, spatial simulation model, linear planning model, nonlinear mathematical planning model, mechanistic GIS model, CA model, and so on (Flamenco-Sandoval et al. 2007). All of these models may help to explore the combined effects of social policies, individual behavior, and other drivers of the land use change, however, most of them have some drawbacks. For example, the Markov model has been widely used to simulate the land use change, but it involves no spatial factors, so the land use change cannot be spatially explicitly reflected. The CLUE-S model can comprehensively analyze the regional LUCC process and driving force, but it can only be used in the spatial allocation so far, while the nonspatial changes must be estimated with other methods (Deng et al. 2008). Therefore, although some models can be used to simulate land use change, there are still some serious drawbacks (Liu and Deng 2010; Cai et al. 2004). Moreover, there were few global models to simulate the LUCC, especially in the study of the interaction mechanism among the social economy, climate change, and LUCC. In some sense, the GTAP-AEZ model and the Global Change Assessment Model (GCAM) are more useful in the land use simulation, which can simulate the land use change of each agricultural ecological zone (AEZ), combined with the influences of social economy and climate change at global scale (Sands and Leimbach 2003; Lee 2004; Burniaux and Lee 2003). However, the parameters of these models are rough and the simulation accuracy needs to be improved.

In the preparation for the fifth Assessment Report of the Intergovernmental Panel on Climate Change (IPCC AR5), the international community is developing new advanced Earth System Models (ESMs) to address the combined effects of human activities (e.g., land use and greenhouse gas emissions) on the carbon-climate system. Besides, the four Representative Concentration Pathways (RCPs) scenarios of the future (2005–2100) have been provided by the four Integrated Assessment Model (IAM) teams, which are used as input to the ESMs for the future carbon-climate projection (Moss et al. 2008; Moss et al. 2010). This study aims to compare the simulation results of land use change obtained from the GCAM and GTAP-AEZ model and improve the simulation accuracy through optimizing the input parameters of the models, and the calibrated GCAM can be used to provide more scientific reference information of land use change for the land use planning and policy formulation to mitigate the climate change in China.

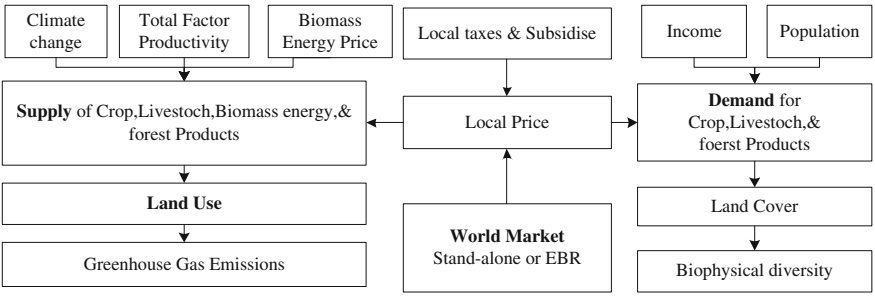

Fig. 2.3 Land use allocation framework of GCAM

2.3.2 Key Methods and Models to Combine Emission Scenarios with Land Use Changes

2.3.2.1 GCAM Model

GCAM is a dynamic recursive model of land use and land cover, economy, agriculture, and energy, which fully integrates the energy and agriculture systems with economic equilibrium in the energy and agriculture markets (Wise et al. 2009). GCAM consists of four modules, i.e., Edmonds-Reilly-Barnes model (ERB) (Edmonds et al. 1997), Agriculture and Land use simulation model (AgLU) (Sands and Leimbach 2003; Thomson et al. 2005), Model for the Assessment of Greenhouse gas Induced Climate Change (MAGICC) (Wigley and Raper 1992), and Regional Climate Change Scenario Generator (SCENGEN) (Hulme et al. 1995). The inputs of GCAM include capital, labor, initial land use allocation, all of which need to be provided by researchers.

The land allocation diagram (Fig. 2.3) shows how land is allocated among alternative land uses types, selection of land use is based on maximizing economic return at a region, profit per hectare is equal to revenue (yield per hectare times price received) less production cost (yield per hectare times nonland cost per unit of output). This relationship is shown in Eq. (2.15)

$$\pi r_{i,l,m,p} = y_{i,l,m,p} \cdot \left(P_{i,l,m} - G_{i,l,m}\right) \tag{2.15}$$

where $\pi r_{i,l,m,p}$ is the economic return of the land as a profit rate (\$/ha-yr), $y_{i,l,m,p}$ is yield per hectare for land use i in region j at location p (calories/ha). $P_{i,l,m}$ is the market price for the product produced by land use i (units \$/yield units: calories or m^3). $G_{i,l,m}$ is the non-land cost per unit of output in land use (units are \$/yield units: calories or m^3), i is an index for land use type. l is the region index. p is an index for geographical location within a region.

While calculating profit rate πr of forest products is different somewhat because of the time lag between planting and harvest. The profit rate expression for forest

products includes a term that discounts future earnings into the present; this forward price is denoted by $\bar{P}_{i,l,m}$.

$$\pi r_{i,lm,p} = \frac{r}{(1+r)^{45}-1} \cdot \left(\overline{P}_{i,l,m} - G_{i,l,m}\right) \tag{2.16}$$

where r is the interest rate ($/$ that is unitless).

In order to determine the share of land allocated to each land use type, land use shares should be calculated numerically, by summing over the land distributions implied in Eqs. (2.15) and (2.16). We use instead a reduced-form expression for land shares that effectively sums over the index p in Eqs. (2.15) and (2.16) based on maximizing profit rates, which is at the core of finding land shares that provide the yields leading to maximum profits.

With the specific assumptions on the functional form of the yield distribution, the share of land allocated to use i is given by a logit share equation:

$$S_{i,l,m} = \frac{\overline{\pi} r_{i,l,m}^{\frac{1}{\lambda}}}{\sum_{p} \overline{\pi} r_{i,l,m,p}^{\frac{1}{\lambda}}} \tag{2.17}$$

where λ is a positive parameter that determines the rate that land shares change in response to a change in profit rate. $\bar{\pi} r_{i,l,m}$ is the average profit rate using land use type i, which is the profit rate evaluated at an average or intrinsic yield, $\bar{y}_i$

Land use for a specific purpose is calculated based on this logit-based share of total land:

$$Landuse_{i,l,m} = S_{i,l,m} \cdot Totalland_l \tag{2.18}$$

2.3.2.2 GTAP-AEZ Model

The GTAP-AEZ model is based on the GTAP-E model, which allows for substitution between capital and energy, and between various fuels in sectoral production. Sectors may substitute energy for capital when the rise of energy price is more than that of the capital rental (Fig. 2.4). The inter-fuel substitution comprises of three sub-nestings: (a) electricity versus non-electricity composite; (b) coal versus non-coal composite; and (c) among oil, gas, and petroleum products. For example, sectors may substitute coal for non-coal fuel (a composite of oil, gas, and petroleum products) when coal is more expensive than non-coal fuels.

Based on the RCP 4.5 scenario, potential future economic activities are assumed. Using this land use model, equilibrium solutions are then found. The inputs used for the production are capital, labor, land, and other intermediate inputs. In the GTAP-AEZ model, we recognize a unique production function for

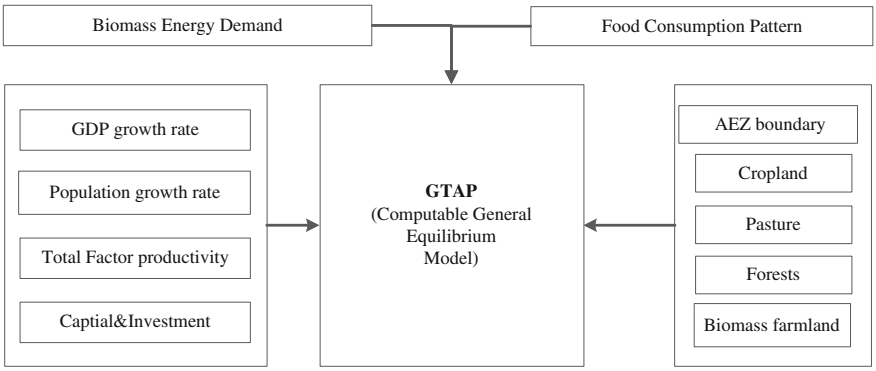

Fig. 2.4 Framework of the GTAP-AEZ model The GTAP-E model is a multisector, multi-region, and recursive dynamic CGE model that extends the standard GTAP model through including the international capital mobility, endogenous capital accumulation, and the adaptive expectations of investment. This model is distinguished for its disequilibrium mechanism of determining the regional supply of investments. This disequilibrium mechanism includes the adjustment of the expected rate of return toward an actual return rate within each region and adjustment of the regional expected return rate toward the global return rate. These lagged adjustment mechanisms, as well as the mechanism of determining the composition of capital and allocation of wealth are parameterized according to the econometric estimation documented by Golub (Golub 2006). In the analysis of the equilibrium of land use, it is assumed that the land is distributed among sectors for the maximization of profits in each period with similar capital and labor, although the land use does not change rapidly

each of the land-using sectors located in a specific AEZ. For example, the paddy rice sector located in AEZ 1 has a different production function from the paddy rice sector located in AEZ 6. This is to identify the difference in the productivity of land of different climate characteristics. Nevertheless, all the paddy rice sectors located in the AEZ6 produce homogenous output to meet market demand.

We assume that transition of land in a specific AEZ can occur only between sectors whose land is appropriate for their use. This is a new concept beyond the standard GTAP model, in which land is assumed to be transformable between uses of crop growing, livestock breeding, or timber plantation, regardless of climatic or soil constraints. Facts show that most plants can only grow on land that is under certain temperature, moisture, soil type, land form, etc. We believe that the introduction of the agro-ecological zoning (AEZ) renders a sound presentation of sector competition for land.

We split the total sector land rent into 18 AEZs according to the AEZ-specific production shares derived from the data provided by the Center for Sustainability and the Global Environment (SAGE) (Lee 2004) as follows.

$$L_{ca} = L_c * [\sum_{i \in SAGECROPS=c} Pi * \frac{Q_{ia}}{H_{ia}} * H_{ia} / \sum_{a \in AEZS} \sum_{i \in SAGEROPS=c} Pi * \frac{Q_{ia}}{H_{ia}} * H_{ia}]$$
$$c \in LANDUSE; i \in SAGECROPS; a \in AEZS. \quad (2.19)$$

where L_{ca} is the land rent accrued to the land use sector c in AEZ a; L_c is the land rent of the land use sector c, with no AEZ distinction; P_i is the per-ton price of SAGE's land use type i; Q_{ia} is the production (ton) of SAGE's land use type i in AEZ a; and H_{ia} is the harvest area of SAGE's land use type i in AEZ a. The $\sum_{i \in SAGECROPS}$ operator means to aggregate over the disaggregated land use type i to the corresponding aggregated land use sector c. Note that we assume the per-ton land production price P_i is homogenous across the AEZs.

2.3.3 Scenarios

The Integrated Assessment Models (IAMs) explored a range of technological, socioeconomic, and policy futures that could lead to particular concentration pathways and magnitudes of climate change, which is represented by the RCPs. The RCPs include four different scenarios (Table 2.2), i.e., one mitigation scenario leading to a very low forcing level (RCP2.6), two medium stabilization scenarios (RCP4.5/RCP6), and one very high baseline emission scenarios (RCP8.5), all of which could be obtained with different combinations of economic, technological, demographic, policy, and institutional futures. The development of the RCPs in the first phase allows climate modelers to proceed with experiments in parallel to the development of emission and socioeconomic scenarios, expediting the overall scenario development process (Moss et al. 2010). Coupled carbon-cycle climate models can then as well calculate associated emission levels (which can be compared to the original emissions of the IAMs) (Hibbard et al. 2007).

Two important characteristics of RCPs are reflected in their names. The word "representative" indicates that each of the RCPs represents a large set of scenarios in the literatures. In fact, as a set, the RCPs should be compatible with the full range of emissions scenarios available in the current scientific literatures, with and without the climate policy. The words "concentration pathway" means to emphasize that these RCPs are internally consistent sets of projections of the components of radiative forcing that are used in subsequent phases rather than the final new and fully integrated scenarios, i.e., they are not a complete package of socioeconomic, emission, and climate projections. The use of the word "concentration" instead of "emissions" also emphasizes that concentrations are used as the primary product of the RCPs and designed as inputs for climate models (Wu et al. 2013).

Table 2.2 Description of RCPs

RCPs	Description	Publication-IA Model
CP8.5	Rising radiative forcing pathway leading to 8.5 W/m^2 in 2100	MESSAGE (Riahi et al. 2007)
RCP6	Stabilization without overshoot pathway to 6 W/m^2 at stabilization	AIM (Y. Hijioka 2008)
RCP4.5	Stabilization without overshoot pathway 4.5 W/m^2 at stabilization after 2100	GCAM (Smith and Wigley 2006)
RCP2.6	Peak in radiative forcing at ~3 W/m^2 before 2100 and decline	IMAGE (Van Vuuren et al. 2006)

The RCP4.5 scenario is a stabilization scenario in which the total radiative forcing is stabilized shortly after 2100, without overshooting the long-run radiative forcing target level (Liu et al. 2005a, b). RCP4.5 includes long-term, global emissions of greenhouse gases, short-lived species, and land use-land cover in a global economic framework which stabilizes the radiative forcing at 4.5 Watts per square meter (W/m^2), approximately 650 ppm CO_2-equivalent in the year 2100 without ever exceeding that value. The defining characteristics of this scenario are enumerated in Moss' papers (Moss et al. 2008; Moss et al. 2010). RCP 4.5 was updated from earlier GCAM scenarios to incorporate the historical emissions and land cover information and follows a cost-minimizing pathway to reach the target radiative forcing. The necessity to limit emissions in order to reach this target leads to the changes in the energy system, including shifts to electricity, lower emissions energy technologies and the deployment of carbon capture and geologic storage technology. In addition, the RCP4.5 emission price is also applicable to the land use emissions. The simulated future emissions and land use were downscaled from the regional scale to the grid scale to facilitate the transfer to climate models. While there are many alternative pathways to achieve a radiative forcing level of 4.5 W/m^2, the application of the RCP4.5 provides a common platform for climate models to explore the response of the climate system to stabilizing the anthropogenic components of radiative forcing. Therefore, the RCP4.5 scenario is used in this study, under which the land use change is simulated with GCAM. Besides, the GTAP-AEZ model, which is similar to GCAM, is also used to analyze the land use structure in AEZs, and the results obtained with the two models were finally compared.

2.3.4 Results and Analysis

The results indicate that the land use area in different AEZs, which are obtained with the GCAM model and the GTAP-AEZ model, are generally consistent. The pasture land areas simulated with the two models differ most greatly, but are still generally consistent in different AEZs. Besides, the results obtained with the GTAP-AEZ model and the GCAM model both show that the grassland is approximately equally

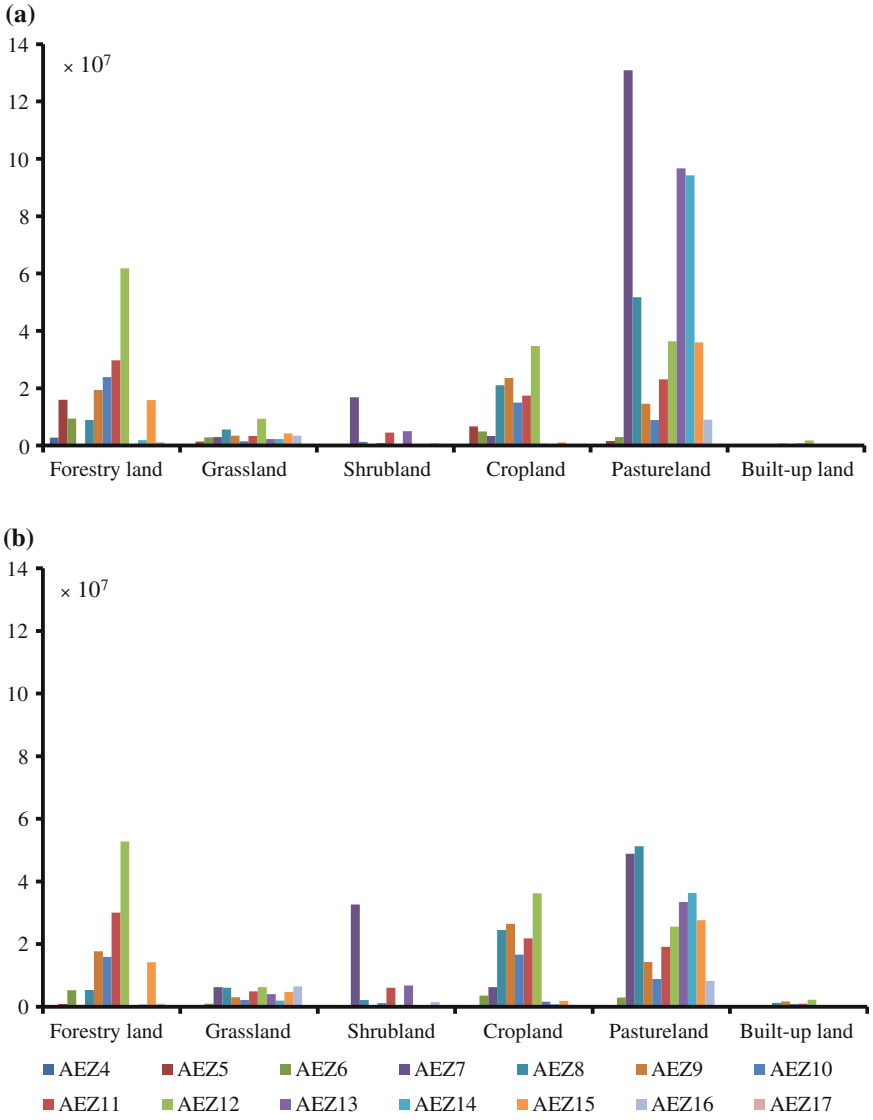

Fig. 2.5 Simulated land use area in 14 AEZs in 2010 using the GCAM model (**a**) and GTAP-AEZ model (**b**) (hectare)

distributed in different AEZs, but the grassland area in different AEZs differs a bit more greatly in the result obtained with the GCAM model. In addition, the results obtained with the two models show that the forestland is mainly located in AEZ9-AEZ12, while the shrubland and cropland are mainly in AEZ7-AEZ13. What's more, the built-up land, the area of which is the smallest, is generally distributed in AEZ10 (Fig. 2.5). Comparing the results obtained with the two models, we found

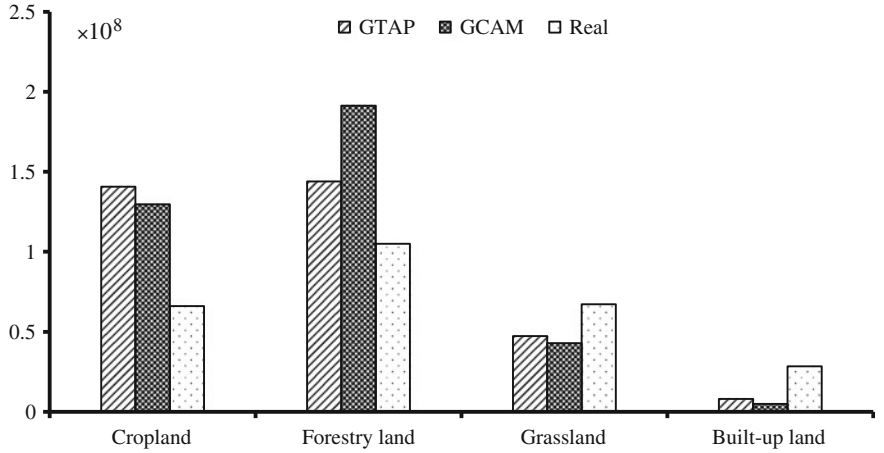

Fig. 2.6 The comparison of land use area between simulated and real in 2008 (hectare)

Table 2.3 The adjustment of GCAM input parameters (%) in 2010

Input parameters	Previous parameters	Adjusted parameters
GDP growth	10	10.4
Labor growth	0.4	0.4
Capital growth	12.6	12.8
TFP growth	0.9	1.1
Population growth rate	0.8	0.5

that the distribution of different land use types among AEZs is approximately consistent, but with some difference between them.

There is still some difference between the real land use area and that obtained with the two models, and the simulation result with the GTAP-AEZ model is better than that with the GCAM model (Fig. 2.6). The results show that the area of cropland and forestry land simulated with the GCAM model and the GCAM model are far higher than the real one, which is 2.13 and 1.96 times larger than the real one, respectively. However, the areas of grassland and built-up land simulated with the two models are both lower than real values. This indicates there is still some inaccuracy in data of the land use structure, industry structure, and social economic situation of China in the global simulation. For example, the forest land should be divided into economic forest lands and ecological forest lands, but not distinguished in this study, leading to the significant difference between the simulated and real areas for the forest land.

There is an extremely complex socioeconomic structure and land use structure in China, both of which have changed greatly due to the rapid economic

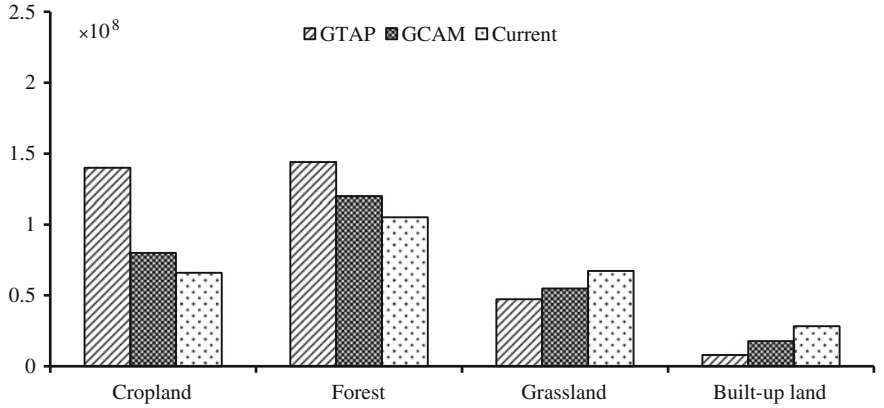

Fig. 2.7 The comparison of land use area in China in 2010 simulated with the calibrated GCAM model and the GTAP model and the real values (hectare)

development of China and consequently made it very difficult to accurately simulate the land use change in China using models with static data. For instance, the estate price in China has fluctuated prominently during the past decades, but a static estate price is first used in the GCAM model in this study, which makes it obviously difficult to simulate the constantly changing industrial structure in China. Therefore, it is necessary to calibrate the models before simulating the land use change.

In order to more accurately simulate the change of the land use structure in China according to the reality and improve the precision of future scenario simulation, we calibrated the parameters of the GCAM model and the GTAP-AEZ model (Table 2.3). The influence of policy intervention is included in the models according to the specific national condition of China, and other parameters were also calibrated. In this study, the price of agricultural products is set to increase by 1.5 % every year, TFP will increase by 0.1 %, and the annual population growth rate will decrease from 0.8 to 0.5 %. The results indicate that the land use structure simulated with the calibrated GCAM model becomes much more accurate than before and has more closely approached to the reality. Besides, the simulation accuracy with the calibrated GCAM model is much higher than that with the calibrated GTAP-AEZ model (Fig. 2.7).

2.3.5 Concluding Remarks on Combining Emission Scenarios with Land Use Changes

This study simulated the LUCC in China under the RCP 4.5 scenario with GCAM and GTAP-AEZ, and compared the simulated and real land use structures. The simulation results obtained with GCAM and GTAP-AEZ are generally consistent,

but also with some difference, and the land use structure simulated with GTAP-AEZ is more close to the real conditions in some AEZs than that obtained with GCAM. For example, the consistence between the forest land area simulated with GCAM and the real one reached more than 80 %, while that with GTAP-AEZ reached only 37 %. Overall, GCAM involves the driving factors of the rapid economic development, which makes the simulation more close to the reality. However, neither of the two models takes account of the impacts of policies on socioeconomic development, which also has great influence on the land use change. Therefore, it is necessary to calibrate the models through optimizing the model input parameters. When the models are calibrated through adjusting these socio-economic parameters according to the specific conditions, the overall simulation accuracy of GCAM reached 82 % and that of GTAP-AEZ also reached 60 %. So that it is possible and necessary to improve the simulation accuracy through calibrating input parameters of the models according to the specific conditions.

In recent decades, more and more land use simulation models have been developed, but it is still a hard task to implement the calibration of input parameters for these models. In the study, the land use structure of China in 2010 is simulated with GCAM and GTAP-AEZ under the RCP 4.5 scenario, both of which were further calibrated through adjusting the input parameters, focusing on comparing the accuracy of the results simulated by two models. The result indicates the simulated areas of cropland and forest land with both two models are higher than the real one, while the simulated areas of grassland and built-up land were lower than the real values, and the accuracy is greatly improved after the calibration.

2.4 Summary

The framework of LUCD model compatible with RCMs was introduced, which has been divided into three sub-modules. The modeling approaches of three modules of the LUCD model should be accordant with specific RCM, so that we make the LUCC classification flexible in the LUCD model. However, due to the uncertainties of climate change, economic development, and other factors, it is very difficult to accurately simulate the long-term land use change in the future. Therefore, it is necessary to study more deeply on how to optimize the parameters according to the specific conditions in the future.

Finally, we introduced the Global Change Assessment Model (GCAM) and the GTAP-AEZ model which can take account of the influence of social economy and climate change at the global scale. We simulated the land use structure of China in 2010 with the two models and compared the results with the real one. Also, we calibrated these parameters of models according to the China's national conditions and implemented the simulation again. The result indicates that the calibrated

GCAM can provide more accurate result of land use, which can provide significant reference information for the land use planning and policy formulation to mitigate and adapt the climate change in China.

References

Burniaux JM, Lee HL (2003) Modelling land use changes in GTAP[C]. In: Sixth annual conference on global economic analysis. The Hague, The Netherlands

Cai Y, Liu Y, Yu ZR, Verburg PH (2004) Progress in spatial simulation of land use change—CLUE-S model and its application. Prog Geogr 23(4): 63–71 (in Chinese)

Cai Y, Tan L, Cheng H, An Z, Edwards RL, Kelly MJ et al (2010) The variation of summer monsoon precipitation in central China since the last deglaciation. Earth and Planet Sci Lett 291(1): 21–31

Deng X, Su H, Zhan J (2008) Integration of multiple data sources to simulate the dynamics of land systems. Sensors 8(2):620–634

Deng X, Jiang QO, Su H, Wu F (2010a) Trace forest conversions in Northeast China with a 1-km area percentage data model. J Appl Remote Sens 4(041893): 041893

Deng X, Jiang QO, Zhan J, He S, Lin Y. (2010b). Simulation on the dynamics of forest area changes in Northeast China. J Geog Sci 20(4):495–509

Deng X, Yin F, Lin Y, Jin Q, Qu R (2012) Equilibrium analyses on structural changes of land uses in Jiangxi province. J Food Agric Environ10(1):846–852

Deng X, Zhao C, Yan H (2013) Systematic modeling of impacts of land use and land cover changes on regional climate: a review. Adv Meteorol

Edmonds J, Wise M, Pitcher H, Richels R, Wigley T, Maccracken C (1997) An integrated assessment of climate change and the accelerated introduction of advanced energy technologies-an application of MiniCAM 1.0. Mitig Adapt Strat Glob Change 1(4):311–339

Flamenco-Sandoval A, Martínez Ramos M, Masera OR (2007) Assessing implications of land-use and land-cover change dynamics for conservation of a highly diverse tropical rain forest. Biolo Conserv 138(1):131–145

GLP (2005) GLP Science plan and implementation strategy. (IGBP Report No. 53/ IHDP Report No 19), pp 64

Golub A (2006) Projecting the global economy to 2025: A dynamic general equilibrium approach. Ph.D. Dissertation, Purdue University

Hibbard KA, Meehl GA, Cox PM, Friedlingstein P (2007) A strategy for climate change stabilization experiments. Eos Trans Ame Geophys Union 88(20):217–221

Hijioka YMY, Nishimoto H, Masui T, Kainuma M (2008) Global GHG emission scenarios under GHG concentration stabilization targets. Glob Environ Eng 13:97–108

Hu Y, Liu Y, Deng X (2004) Relativity analysis on land use and land cover change and optimal allocation of land resources. Prog Geogr 23(2):51–57

Hulme M, Jiang T, Wigley T (1995) SCENGEN: a climate change scenario generator. Software user manual, version 1.0. Climate research unit. University of East Anglia, Norwich

Jiang QO, Deng X, Yan H, Liu D, Qu R. (2012). Identification of food security in the mountainous Guyuan Prefecture of China by exploring changes of food production. J Food Agricul Environ 10(1):210–216

Kalnay E, Cai M (2003) Impact of urbanization and land-use change on climate.Nature 423(6939):528–531

Lau KH, Kam BH (2005) A cellular automata model for urban land-use simulation. Environ Plann Plann Des 32(2):247–263

Le QB, Park SJ, Vlek PL, Cremers AB (2008). Land-Use Dynamic Simulator (LUDAS): A multi-agent system model for simulating spatio-temporal dynamics of coupled human–landscape system. I. Structure and theoretical specification. Ecolo Informa 3(2):135–153

Lee HL (2004) Incorporating agro-ecologically zoned land use data and land-based greenhouse gases emissions into the GTAP framework. Centre for global trade analysis. Purdue University

Liu J, Deng X (2010) Progress of the research methodologies on the temporal and spatial process of LUCC. Chin Sci Bull 55(14):1354–1362

Liu J, Tian H, Liu M, Zhuang D, Melillo JM, Zhang Z (2005a) China's changing landscape during the 1990s: Large-scale land transformations estimated with satellite data. Geophys Res Lett 32(2):173

Liu J, Zhan J, Deng X (2005b) Spatio-temporal patterns and driving forces of urban land expansion in China during the economic reform era. AMBIO J Hum Environ 34(6):450–455

Manson S (2006) Land use in the southern Yucatan peninsular region of Mexico: scenarios of population and institutional change. Comput Environ Urban Syst 30(3):230–253

McConnell WJ, Parker D, Berger T, Manson S (2001) Agent-based models of land-use and land-cover change. LUCC International Project Office, Belgium

Moss RH, Babiker M, Brinkman S, Calvo E, Carter T, Edmonds JA et al (2008) Pacific northwest national laboratory (PNNL). Richland, WA (US)

Moss RH, Edmonds JA, Hibbard KA, Manning MR, Rose SK, Van Vuuren DP et al (2010) The next generation of scenarios for climate change research and assessment. Nature 463(7282):747–756

Nunes C, Auge' JI (eds) (1999) Landuse and landcover (LUCC) implementation strategy. IGBP Report 48, IHDP Report 10, Stockholm

Riahi K, Grübler A, Nakicenovic N (2007) Scenarios of long-term socio-economic and environmental development under climate stabilization. Technol Forecast Soc Change 74(7): 887–935

Sands RD, Leimbach M (2003) Modeling agriculture and land use in an integrated assessment framework. Clim Change 56(1–2):185–210

Schmidhuber J, Tubiello FN (2007) Global food security under climate change. Proc Nat Acad Sci 104(50):19703–19708

Semboloni F, Assfalg J, Armeni S, Gianassi, R, Marsoni F (2004) CityDev, an interactive multi-agents urban model on the web. Comput Environ Urban Syst 28(1):45–64

Shepherd JM, Carter M, Manyin M, Messen D, Burian S (2010) The impact of urbanization on current and future coastal precipitation: a case study for Houston. Environ Plann Plann Des 37(2): 284–304

Smith SJ, Wigley T (2006) Multi-gas forcing stabilization with MiniCAM. Energy J 6(3):373–392

Stehfest E, Heistermann M, Priess JA, Ojima DS, Alcamo J (2007) Simulation of global crop production with the ecosystem model dayCent. Ecolo Model 209(2):203–219

Syphard AD, Clarke, K. C., & Franklin, J (2005) Using a cellular automaton model to forecast the effects of urban growth on habitat pattern in southern California. Ecological Complex 2(2)185–203

Thomson AM, Brown RA, Rosenberg NJ, Izaurralde RC, Benson V (2005) Climate change impacts for the conterminous USA: an integrated assessment. Climate change impacts for the conterminous USA. Springer, Berlin, pp 43–65

Tolstoy E, Irwin M, Helmi A, Battaglia G, Jablonka P, Hil, V et al (2004) Two distinct ancient components in the sculptor dwarf spheroidal galaxy: first results from the dwarf abundances and radial velocities team. Astrophys J Lett 617(2), L119

Turner B (1994) Local faces, global flows: the role of land use and land cover in global environmental change. Land Degrada Dev 5(2):71–78

Van Vuuren D, Eickhout B, Lucas PL, Den Elzen M (2006) Long-term multi-gas scenarios to stabilise radiative forcing–exploring costs and benefits within an integrated assessment framework. Eenergy J 27:201–233

Veldkamp A, Fresco L (1996) CLUE: a conceptual model to study the conversion of land use and its effects. Ecolo Model 85(2):253–270

Verburg PH, Soepboer W, Veldkamp A, Limpiada R, Espaldon V, Mastura SS (2002) Modeling the spatial dynamics of regional land use: the CLUE-S model. Environl Manage 30(3):391–405

Vitousek PM, Mooney HA, Lubchenco J, Melillo JM (1997) Human domination of Earth's ecosystems. Science 277(5325):494–499

Wigley T, Raper S (1992) Implications for climate and sea level of revised IPCC emissions scenarios. Nature 357(6376):293–300

Wise M, Calvin K, Thomson A, Clarke L, Bond-Lamberty B, Sands R et al (2009) Implications of limiting CO2 concentrations for land use and energy. Science 324(5931):1183–1186

Wu F, Deng X, Yin F, Yuan Y (2013) Projected changes of grassland productivity along the representative concentration pathways during 2010–2050 in China. Adv Meteorol 2013, Article ID 812723, 9 pages, doi: 10.1155/2013/812723

Zhang T, Zhan J, Huang J, Yu R, Shi C (2013) An agent-based reasoning of impacts of regional climate changes on land use changes in the three-river headwaters region of China. Adv Meteorol 2013, Article ID 248194, 9 pages, doi: 10.1155/2013/248194

Chapter 3
Spatially Explicit Land-Use and Land-Cover Scenarios for China

Feng Wu, Qun'ou Jiang, Yongwei Yuan, Qian Xu and Xing Li

In climate modeling, land use data is applied as underlying surfaces and definitively determines the simulation results of regional climate. Researches show that Land Use and Cover Change (LUCC) not only affects the terrestrial ecosystem biodiversity, energy balance, water cycle, but also exerts influence on climate and social economy (Berg et al. 2010; Liu and Diamond 2005). Besides, LUCC is a significant performance of material and energy interactions between human and global environment. It not only affects the geographical distribution of terrestrial ecosystem patterns and productivity, but also objectively reflects how human influence biogeochemical cycles and the structure and function of ecosystem (Jiang et al. 2013).

Some achievements have been made in the researches on LUCC, but it still far from being able to meet the need to alleviate and adapt to global environmental change. Meanwhile, LUCC contributes to climate change and variability at global, regional and local scales (Hibbard et al. 2010). With the progress of researches on climatic modeling over the past decades, it has been widely recognized that there is an urgent need to accurately characterize land surface as boundary conditions in climate modeling (Hibbard et al. 2010; Sertel et al. 2010). Land cover datasets, which are often derived from the remote sensing images, have been widely used to describe underlying surface conditions in climate models. But the accuracy of these datasets is still not high enough to meet the requirement of high resolution climate simulation.

F. Wu (✉)
State Key Laboratory of Water Environment Simulation, School of Environment, Beijing Normal University, Beijing 100875, China
e-mail: wuf.dls@gmail.com

Q. Jiang
School of Soil and Water Conservation, Beijing Forestry University, Beijing 100038, China

Y. Yuan
Faculty of Resources and Environmental Science, Hubei University, Wuhan 430062, China

Q. Xu · X. Li
School of Mathematics and Physics, China University of Geosciences (Wuhan), Wuhan 430074, China

X. Deng et al. (eds.), *Land Use Impacts on Climate*, Springer Geography
DOI: 10.1007/978-3-642-54876-5_3,

In the Sect. 3.1 of this chapter, we choose China as the study area, and explore possible land use change trends based on the AgLU module and ERB module of global change assessment model (GCAM model). In the second section, scenarios of future LUCC in China are simulated. This study predicts the future structure of land use/cover on the basis of GCAM and econometric model with the socio-economic factors as the driving forces. The future spatial pattern of land use/cover in China is simulated with the Dynamics of Land System (DLS) under the Business as Usual (BAU) scenario, Rapid Economic Growth (REG) scenario and Cooperate Environmental Sustainability scenario (CES). Last but not least, LUCC data is reclassified to simulate regional impacts of LUCC on climate in the third section. We combined land cover data with land use data to generate high accuracy underlying surface information that can be applied in climatic simulation.

3.1 Possible Trends of Land Use Changes in China

LUCC is one of the core research focuses of International Geosphere-Biosphere Programme (IGBP) and the International Human Dimension Programme (IHDP) on Global Environmental Change.

Scholars conducted a lot of studies on LUCC to reveal the relationship of land, environment, population and social development. In this study, we aim to investigate how LUCC affect CO_2 emissions and tried to reveal the influential mechanism of LUCC to CO_2 emissions. To achieve this goal, we simulate land use changes with AgLU module of GCAM model, and then project CO_2 emissions with ERB module based on the simulated land use change. The comparison of scenarios' results indicated that CES scenario reflects sustainable development and is more suitable for development in China. Scenario-based analysis provide more suitable development route of China towards sustainable development based on future structural change of land uses.

3.1.1 Data

3.1.1.1 Land Use Data

We use TM/ETM+ images from 1990 to 2010 as data source, which are provided by the Resources and Environment Data Center, Chinese Academy of Sciences (CAS) (Liu et al. 2003). The Landsat TM/ETM+ data are further grouped into six aggregated classes of land cover, we use the five types land use: cultivated land, forest land, grassland, bare land and built-up areas including urban areas. Cultivated land includes paddy and dry farming land. Forest land includes timberland, shrub and others (e.g., orchards). Grassland includes dense, moderate and sparse grassland. Bare land includes sandy land, Gobi, Salina, wetland, bare soil, bare rock and others (such as alpine desert and tundra). Built-up land includes urban areas, rural settlements and others (such as roads and airports).

3.1.1.2 Socio-Economic Data

Socio-economic data include total population, population density and growth rate of per capita income, proportion of agricultural population, urbanization ratio, GDP and price index of oil, gas, coal, and hydropower from 1990 to 2010. Among them, population, GDP, population density, proportion of agricultural population and urbanization ratio are derived from the Statistical Yearbook of China and the provincial statistical data. Price index of natural gas, coal, and hydropower are mainly extracted from the Energy Statistics Yearbook. Average household income growth ratio, which reaches about 11.24 % from 1990 to 2010, is obtained by looking for literatures and other relevant materials.. Population, average income growth ratio and commodity market prices are the main parameters of AgLU module and the relevant specific data will be used in the section of scenario design.

3.1.2 Methods

3.1.2.1 GCAM Model

GCAM model is an integrated assessment model that focuses on energy and agriculture sectors. It is a partial-equilibrium model that designed to examine long-term, large-scale changes in global and regional energy system where the characteristics of existing capital stocks are not the dominant factor in determining the dynamics of energy system. The markets in GCAM are defined for oil, gas, coal, biomass, carbon, and agricultural products. The goal of land use allocation is achieved through AgLU module that drove by factors of population, labor productivity growth and the price of resources in the market. Besides, through incorporation of the ERB module, emissions of greenhouse gases can be calculated (Brenkert et al. 2003).

3.1.2.2 Land Allocation

Land allocation diagram shows how land is allocated among alternative land uses. Determination of land use is based on maximizing economic return at each location. Per hectare profit is equal to revenue (per hectare yield multiply price received) subtract production cost (per hectare yield times per unit of output non-land cost). This relationship is shown in Eq. (3.1).

$$\pi r_{i,l,m,p} = y_{i,l,m,p} \cdot \left(P_{i,l,m} - G_{i,l,m}\right) \tag{3.1}$$

where $\pi r_{i,l,m,p}$ is the economic return of the land as a profit rate (\$/ha·yr); $y_{i,l,m,p}$ is yield per hectare for land use i in region j at location p (calories/ha); $P_{i,l,m}$ is the market price for the product produced by land use i (\$/calories or \$/m^3). $G_{i,l,m}$ is

the non-land cost per unit of output in land use (\$/calories or \$/m^3). i is an index for land use type. l is the region index. p is an index for geographical location within a region.

Profit rate (πr) calculation for forest products is somewhat different because of the time lag between planting and harvest. Profit rate expression for forest products includes a term that allocates future earnings into the present and distributes those earnings over 45 years; this forward price is denoted by $\overline{P}_{i,l,m}$,

$$\pi r_{i,lm,p} = \frac{r}{(1+r)^{45}-1} \cdot \left(\overline{P}_{i,l,m} - G_{i,l,m}\right) \tag{3.2}$$

where r is the interest rate (unitless).

To determine the share of land allocated to each land use type, land use shares would, in general, be calculated numerically by summing the land distributions implied in Eqs. (3.1) and (3.2). In integrated modeling context, however, we wish to work on large regional scales. We use instead a reduced-form expression for land shares that effectively sums up the index p in Eqs. (3.1) and (3.2) based on maximizing profit rate which is the core of finding land shares that provide the yields leading to maximum profits.

With specific assumptions on the functional form of yield distribution, the share of land allocated to use i is given by a logit share equation as follows.

$$S_{i,l,m} = \frac{\overline{\pi} r_{i,l,m}^{\frac{1}{\lambda}}}{\sum_{p} \overline{\pi} r_{i,l,m,p}^{\frac{1}{\lambda}}} \tag{3.3}$$

where λ is a positive parameter that determines the rate that land shares change in response to a change in profit rate. $\overline{\pi} r_{i,l,m}$ is the average profit rate using land i, which is the profit rate evaluated at an average or intrinsic yield, $\overline{y}_i$, for land use i.

Land use for a specific purpose is calculated based on this logit-based share of total land:

$$\text{Land use}_{i,l,m} = S_{i,l,m} \cdot \text{Total land}_l \tag{3.4}$$

3.1.2.3 CO_2 Emissions

Carbon emissions are accounted for in two separate categories, those from industry and fossil fuel use and those as net land-use emissions. Land-use emissions have different implications for carbon-cycle than industrial emissions, which are the sum of emissions from fossil-fuel and cement production.

CO_2 Emissions from the AgLU Module

Carbon emissions from land-use change are calculated as the difference in carbon stock between periods. Land use changes over time in response to changing demands, income, agricultural technologies, and prices of agricultural products. Each regional land-use category is assigned a carbon density for soils and above ground plant material. Changes in land use are translated directly to changes in carbon stocks. The net carbon emissions equal to the product of area of land use changes multiply carbon densities for each land-use change class.

For crops, pasture, forests, and bare land, the carbon emissions from above ground are calculated as follows:

$$EmLC_{i,l,m} = \sum_{l=1}^{nr} \left(CLdens_{l,i} \cdot \frac{\text{Land use}_{i,l,m} - \text{Land use}_{i,l,m-1}}{N \text{ step}} \right) \tag{3.5}$$

where i is an index for land use: crops, pasture, forests, and bare land.

Carbon emissions from soils are based not only on land use changes, but also on decomposition of carbon according to decay rates. Thus, 60 % of soil carbon is assumed to decay when land use change occurs during the simulated time period ($Pd_0 = 0.6$); 30 % of the soil carbon is assumed to only decay in the next time period ($Pd_{-1} = 0.3$), and 10 % of the soil carbon is assumed to decay during the second time period-30 years-after the land use change occurs ($Pd_{-2} = 0.1$).

$$EmSC_{i,m} = \sum_{l=1}^{nr} \left[\sum_{m=m-2}^{m} \left(CSdens_{l,i} \cdot Pd_m \cdot \frac{\text{Land use}_m - \text{Land use}_{m-1}}{N \text{ step}} \right) \right] \tag{3.6}$$

CO_2 Emissions from ERB Module

Carbon dioxide emissions from fossil fuel use in the ERB module are calculated under the condition that global fuel demands have been determined. Emissions are equal to carbon emission coefficient times the amount of fuel used. Energy transformations (such as synthetic fuels, electricity generation, and hydrogen production) are associated to the region where the transformation occurs.

For conventional oil, gas, coal, and biomass, emissions are calculated as follows. If $RemFrac_{2,l}$ parameter is not equal to zero, carbon removal through scrubbing technology are taken into consideration. Emissions from direct biomass burning are set to zero in most scenarios.

$$\begin{aligned} EmSC_i = & CO_i \cdot \Big[FFcons \cdot \left(1 - SedFil_{i,l}\right) - RemFrac_{2,l} \\ & \cdot \left(ESU_{ui,l,m} gu_{ui,l,m} gij_i + ESH_{hi,l,m} gh_{hi,l,m} gij_i\right) biggr \Big] \end{aligned} \tag{3.7}$$

where CO_i is the emission coefficient of oil, gas, coal or biomass; $SedFil_{i,l}$ is the fraction of feedstock that is not combusted; $RemFrac_{2,l}$ is the fraction of emissions that can be scrubbed during electricity and/or hydrogen generation; $ESU_{ui,l,m}$ is the energy (in Joules) that needs to be combusted as secondary energy (electricity) to meet demand and that needs to be converted to primary energy for emission calculations by multiplying with the conversion coefficients $gu_{ui,l,m}$ and gij_i; $ESH_{hi,l,m}$ is the energy (in Joules) that needs to be combusted as secondary energy (hydrogen) to meet demand and that needs to be converted to primary energy for emission calculations by multiplying with the conversion coefficients $gh_{hi,l,m}$ and gij_i. $gh_{hi,l,m}$ is the transformation efficiency when electricity and hydrogen is produced. gij_i is the transformation efficiency from primary to secondary fuel conversion. *FFcons* equals to primary fuel demanded for transformation into secondary fuel supply.

For each of the end-use sectors emissions are based on fuel mode demands, attributing shale oil production emissions and flared emissions to the industrial sector.

$$EmSC_k = \sum_j CO_j \cdot Fjk_{j,k,l,m} \cdot \left(1 - SedFil_{j,l}\right) \tag{3.8}$$

where CO_j is the emission coefficient of oil, gas, coal or biomass; $SedFil_{j,l}$ is the fraction of the feedstock that is not combusted; $Fjk_{j,k,l,m}$ is the primary fuel demands.

3.1.3 Scenarios

3.1.3.1 Socio-economic Analysis on China

With a rapid development of economy in China in the past 30 years, GDP has a great increase from 364.52 billion Yuan at the beginning of reform and opening up to 34.05 trillion Yuan in 2009, with an average annual GDP growth rate of 9.6 %. This growth rate is significantly higher than those of most other countries worldwide. Meanwhile, China is rapidly industrialized and urbanized. Urbanization level in China rose from 18 % in 1978 to 46.6 % in 2009, and it will reach 65 % by 2030. Urban population growth will not only directly bring about the increase of consumer demand, but also put forward more requirements for urban infrastructure investment. Industrialization and urbanization will certainly exacerbate some structural contradictions, which will raise the cost of labor, land, natural resources and social undertakings. However, industrialization and urbanization is still the main internal driver for economic growth for a long time in China.

China's population growth has stepped into the phase with the character of "low birthrate, low death rate and low growth" since the early twenty-first century. Some

studies have shown that total population will reach the peak around 2030, and then begin to gradually decline and thus enter a negative growth phase. After 2015, China's working-age population will decline and labor supply in China will gradually decline in the next 20 years.

According to statistics report released by National Bureau of Statistics, the proportion of the added value of first, second and tertiary industry to GDP was 10.2 %, 46.9 %, and 42.9 % in 2001. In comparison to 1990, the proportion of primary industry decreased by 16.9 %, while the secondary industry and tertiary industry increased by 5.6 % and 11.4 % respectively. Overall, China's industrial structure changes in the past 20 years sustained the main changing characteristics since the 1970s. In other words, the proportion of primary industry declined, the secondary industry consolidated its position, and the tertiary industry significantly increased. In addition, the industrial structure will be further optimized in the future.

With the continuous development of global economy, the demand for resources and energies will continue to grow. Supply-demand balance of resources and energy determines the price of energies and resources, such as oil, natural gas, and coal. According to China Statistical Yearbook, in 2009, China's total energy production was 2.75 billion tons; however, the consumption has reached 3.07 billion tons. There was an obvious gap between consumption and demand. Meanwhile, coal and oil accounted for a large share in China's total energy production, and the percentage of coal and oil was 70.4 and 17.9 % correspondingly. While the hydro-power, nuclear power and wind power is relatively slow growing and only accounts for 7.8 % of total energy production. However, with the constraints of resources and energy, the impacts of resources and energy on human social-economic development will become more and more obvious. According to the forecasts of International Energy Agency and the U.S. Department of Energy, despite global demand for energy resources continuously grew between 2005 and 2030, the overall supply and demand will be close to equilibrium in the future.

3.1.3.2 Scenarios Design

According to the characteristics of social-economic development in the past 30 years in China, we design three social-economic development scenarios, i.e. BAU, REG and CES. BAU scenario is designed according to the economic development process and the structural characteristics in China combining the factors with most possible changes such as population, factor endowments and technological advances. This scenario reflects likely changing trends of social-economic development, and also provides a reference which can be compared with other scenarios. REG scenario is designed to explore land use changes under accelerating social-economic development. CES scenario is designed to simulate the possible trends of land use changes under the effect of increasing environmental pressure.

BAU Scenario

In a long term, investment and improvement in productivity and changes in labor supply determine the overall economic growth situation. Labor supply depends on the total amount and age structure of population. Population age structure and changes of total labor numbers have significant effects on the labor force immigration. Population growth is impacted by several factors, such as family planning policy, improvement of people's living standards, lifestyle changes, among which national population policy is the major influencing factor. In this study, population growth is exogenous variable, and population forecast is from the Institute of Population and Labor Economics. According to this forecast, China's population will peak in 2037 with approximate 1.47 billion, while the peak of working-age population will occur in 2017–2027 with about 10 million. According to the proportion of labor forces to the working-age population labor in 2006, the total labor resources in the whole country will be about 820 million at the moment when the working-age population is in the peak, and it will increase by 40 million in comparison to 2006.

Productivity improvement is mainly reflected as the changes of total factor productivity (TFP) in the model. Through studies on TFP in the past 30 years, we found that there are amounts of factors affecting TFP in China, such as institutional reform, human capital spillover effect, technological capital, market reform, urbanization, foreign investment effect, foreign trade effect, infrastructure and administrative costs, and final consumption rate. Although previous quantitative research produced different results, most of the studies show that the average annual growth rate of TFP in China is between 2 and 4 %. In a long run, some significant factors of promoting TFP growth will continue to play an important role, for example, reform will be further deepened, urbanization will be steadily pushed forward, rural labor force will continue to be migrated, and human capital will be accumulated. Therefore, in BAU scenario, model assumes that the average annual growth rate of TFP continues to follow the development ratio in the past during 2008–2050, and remain at the level of about 2 %.

China's demand for energy has surged to fuel its rapidly expanding industrial and commercial sectors as well as households experiencing rising living standards. Previous studies indicated that average energy consumption has risen by 5.2 % since 1978, while during 2001–2007, the primary energy consumption has soared through an average annual increase of 9.8 %, and the GDP has increased by 10.2 % in the same period (Liu et al. 2011). Previous studies also showed that from 1999 to 2008, the average growth rate of coal production in China was 11.37 %, which was almost twice as much as that of 5.81 % from 1982 to 1996. In 2008, coal production in China rose to 2716 million tons (40 % of global coal production) (Lin and Liu 2010). Moreover, integrated modeling that considering the factors of population growth, economic growth and industrial structure changes, technological advance, environmental impact and energy security estimated that in 2050 primary energy demand will reach 3,440–4,150 Mtce. The structure of energy get improved significantly, and the proportion of coal in primary energy

Table 3.1 The growth rate (%) of economic factors under BAU scenario in 2008–2100

	2008–2010	2011–2015	2016–2020	2021–2025	2026–2030	2031–2040	2041–2050	2051–2075	2076–2100
GDP growth	8.7	7.9	7.0	6.6	5.9	5.6	5.5	4.6	3.9
Labor growth	0.4	0.5	0.0	0.0	−0.3	−0.3	−0.4	−0.6	−0.9
Capital growth	12.6	9.4	8.4	7.8	6.7	6.2	5.9	5.4	4.8
TFP growth	0.9	2.0	2.0	1.9	2.0	1.9	1.9	1.9	1.8

consumption from 60 % in 1990 (excluding biomass 76.2 %) declined to 47.7 % in 2050 (51.9 %), while oil and gas from 14.8 % (18.7 %) increased to 26.3 % (28.6 %). Primary energy supply capacity would increase from 1,302 Mtce in 1990 to 2,980–3,740 Mtce in 2050, which coal 2,500–2,700 Mtce, crude 100–200 Mt, natural gas 120 billion cubic meters to 1,400 cubic meters.

Under BAU scenario, urbanization and industrialization will continue to be pushed forward, the level of urbanization will increase 0.35–0.55 % per year, and it will be expected to be 52 % in 2015, 65 % in 2030, and up to around 70 % in 2050. Taking into account of the international economic environment and changes of comparative advantage in China, export growth rate will gradually reduce under this scenario. Trade surplus will continue to exist in a long time with a gradually declining trend, and the balance between import and export will be achieved by 2050 and rise steadily during 2050–2100 (Table 3.1).

Control Scenario One: REG Scenario

Under REG scenario, reforms will be putted forward quickly and smoothly, the role of market in the allocation of resources will be enhanced obviously, structural adjustment will be vigorously promoted, and the economic growth pattern will make rapid progress. The specific settings are as follows: (i) price of all kinds of resources will be straightened out, there will be a more rational allocation for resources, and resource use efficiency will be improved. The external cost of economic activities will be internalized by the means of taxation and energy. (ii) Public expenditure structure of government will be adjusted and the proportion of the expenditure on education, medicine, scientific research and social welfare will be increased. Many studies have found that the low proportion of government spending on public services is one of the significant reasons to a lower consumer will. Therefore, adjusting the structure of government expenditure is helpful to promote the coordinated development of consumption and investment. (iii) Barriers of labor force immigration are eliminated, and the process of urbanization is accelerated. Urbanization is the significant drivers to promote the optimal allocation of resources, economic growth and industrial structure adjustment. (iv) Development of support service is intensified and industrial structure is further upgraded. In this model, the accelerated development of services is reflected by the higher TFP growth and lower tax levels (Table 3.2).

Table 3.2 The growth rate (%) of economic factors under the REG scenario in 2008–2100

	2008–2010	2011–2015	2016–2020	2021–2025	2026–2030	2031–2040	2041–2050	2051–2075	2076–2100
GDP growth	8.7	8.4	7.2	6.6	5.8	5.7	5.6	4.9	4.3
Labor growth	0.4	0.5	0	0	−0.3	−0.4	−0.4	−0.8	−1.2
Capital growth	12.6	9.2	7.5	6.8	5.5	4.6	3.9	2.9	2.1
TFP growth	0.9	2.7	2.7	2.6	2.6	2.6	2.5	1.9	1.8

Table 3.3 The growth rate (%) of economic factors under the CES scenario in 2008–2100

	2008–2010	2011–2015	2016–2020	2021–2025	2026–2030	2031–2040	2041–2050	2051–2075	2076–2100
GDP growth	8.7	7.0	5.7	5.1	4.3	3.5	2.8	2.6	2.3
Labor growth	0.4	0.5	0.0	0.0	−0.3	−0.3	−0.4	−0.5	−0.8
Capital growth	12.6	9.2	6.9	6.1	4.9	4.2	3.4	2.5	1.8
TFP growth	0.9	1.3	1.6	1.4	1.5	1.3	1.2	1.1	0.9

Control Scenario Two: CES Scenario

CES scenario mainly considers the following aspects of changes: (i) Slow urbanization. Slow urbanization restricts not only the smooth and effective immigration of labor force, but also the upgrading of consumption structure and industrial structure optimization. (ii) Slow recovery of world economy, serious trade protection and slow export growth. Exports are the significant motive force of economic growth, and the annual growth rate of China's exports has been over 20 % since 2000. The proportion of exports to GDP has also gradually increased from about 23.3 % in 2000 to 36.9 % in 2008, with an increase of 13.6 % during 8 years. In the situation of slow economic growth, industrial structure adjustment and optimization will also be difficult. (iii) Higher international energy prices and restricted energy imports. In recent years, with the rapid economic development, the dependence on some kinds of resources especially crude oil and iron ore was also rising. In 2007, China produced 186 million tons of crude oil and imported 211 million tons, obviously, the imports have exceeded domestic production. Once the international energy and resource prices rise, energy imports are restricted, which will be a greater constraint to economic development. (iv) Slow progress in system reform and slow technological innovation and efficiency improvement. Low innovation ratio may cause slow efficiency improvement, and result in slow conversion of development patterns and slow growth rate. Under this scenario, the TFP value is lower than that under BAU scenario by 0.4 % (Table 3.3).

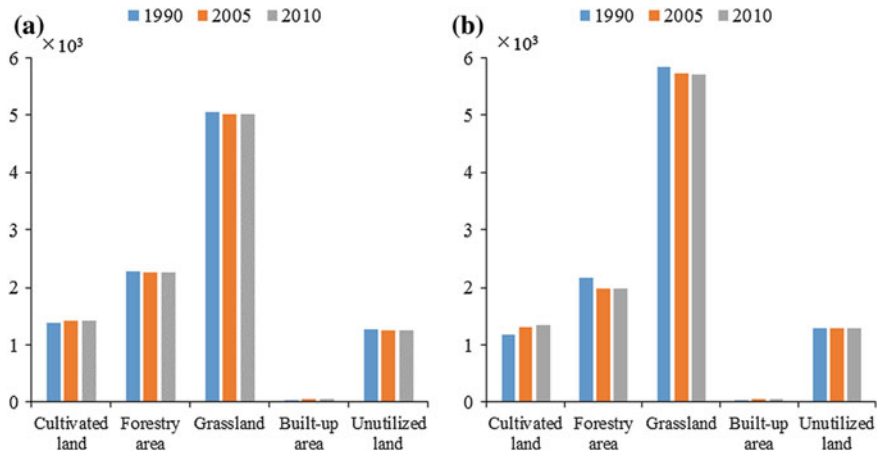

Fig. 3.1 Comparison of simulated land use and real land use; **a** the real land use area in 1990, 2005 and 2010; **b** simulated land use area in 1990, 2005 and 2010 (1,000 km^2)

Table 3.4 Simulation accuracy (%) of land use allocation

	Cultivated land	Unutilized land	Forestry area	Grassland	Built-up area	Average error	Total average error
1990	−14.63	−5.06	15.61	−12.72	1.74	9.95	8.67
2005	−7.50	3.23	−12.35	14.03	−2.85	7.99	
2010	−5.21	2.93	−12.56	13.75	5.92	8.07	

3.1.4 Land Use Changes Under Different Scenarios

3.1.4.1 Accuracy Analysis of Land Use Simulation

GCAM model is applied to simulate structure and amount of land use types in 1990, 2005 and 2010. We analyze land use simulation accuracy according to the comparison of simulated land use and real land use in 1990, 2005 and 2010 (Fig. 3.1, Table 3.4).

As seen from the comparison of simulation results and real land use in 1990, 2005 and 2010 in Fig. 3.1, we found that the simulation results is similar to the real land use change. Cultivated land increases due to population growth and domestic demand expansion. A larger demand for timber because of social and economic development, so that forestry area shows a downward trend overall, but the decreasing ratio is declining. As for the grassland, overgrazing has caused serious area shrinking. In the past decades, with rapid economic development, urbanization is rising all the way and it brings about the built-up area keeping expanding in recent years. We are unconcerned about desert, Gobi and other land that is difficult

to reclaim in this study. We also assumed no change in GCAM model. Besides, according to the accuracy analysis in Table 3.4, the total average error is about 8.67 %. The good accuracy of simulation indicates that the model is suitable to simulate land use change trends of China.

3.1.4.2 Simulation of Land Use Change Under Three Scenarios

Land Use Change Under BAU Scenario

Under BAU scenario, we use GCAM model to simulate the trends of land use changes that drove by inertial socio-economic growth (Fig. 3.2).

As shown in Fig. 3.2, under BAU scenario, cultivated land increases first and then decreases. The total forestry area is relatively stable, while the managed forestry area shows a downward trend during 1990–2005, then increases gradually after 2005, and stabilizes in 2080. The unexplored forestry area reduces before 2080, and then steps into a stage of steady increase. Due to expansion of the range of human activities, the managed grassland goes up until 2065, and then is in a steady stage during 2065–2095. As for the unexplored grassland, it declines from 1990 to 2050, and tend to be stable after then. The total grassland also decreases first and then in a stable condition. Urban area under BAU scenario has no significant expansion, but it will still increase steadily, and the extent is relative small. Because of the current rapid development, more food demand requires more cultivated land, thus cultivated land increases rapidly, and it will reach the maximum before the middle of twenty-first century. With the technological development, agricultural productivity increases gradually, and the decreasing dependence on cultivated land needs less cultivated land, so that cultivated land decreases all the way since the middle of twenty-first century, and the rate of declining will gradually increase first and then gradually decrease.

Land Use Change Under REG Scenario

In REG scenario, under the drive of socio-economic and simulation results with GCAM model, we obtained the land use change trends (Fig. 3.3).

The simulation results of land use under REG scenario show that the obvious land use characteristics is that urban area increased significantly due to rapid urbanization. Cultivated land still increases first during 2010–2035 and then decreases after then. Accelerated economic development promotes the rising demand for timber, As shown in Fig. 3.3, the total forestry area decreases significantly, and the explored forestry area increases all the way. Rapid economic development accelerates the scarcity of resources; moreover, the demand gap will be widened under REG scenario. The total area of grassland is in a downward trend, and the unexplored grassland reduces all the way, while the explored

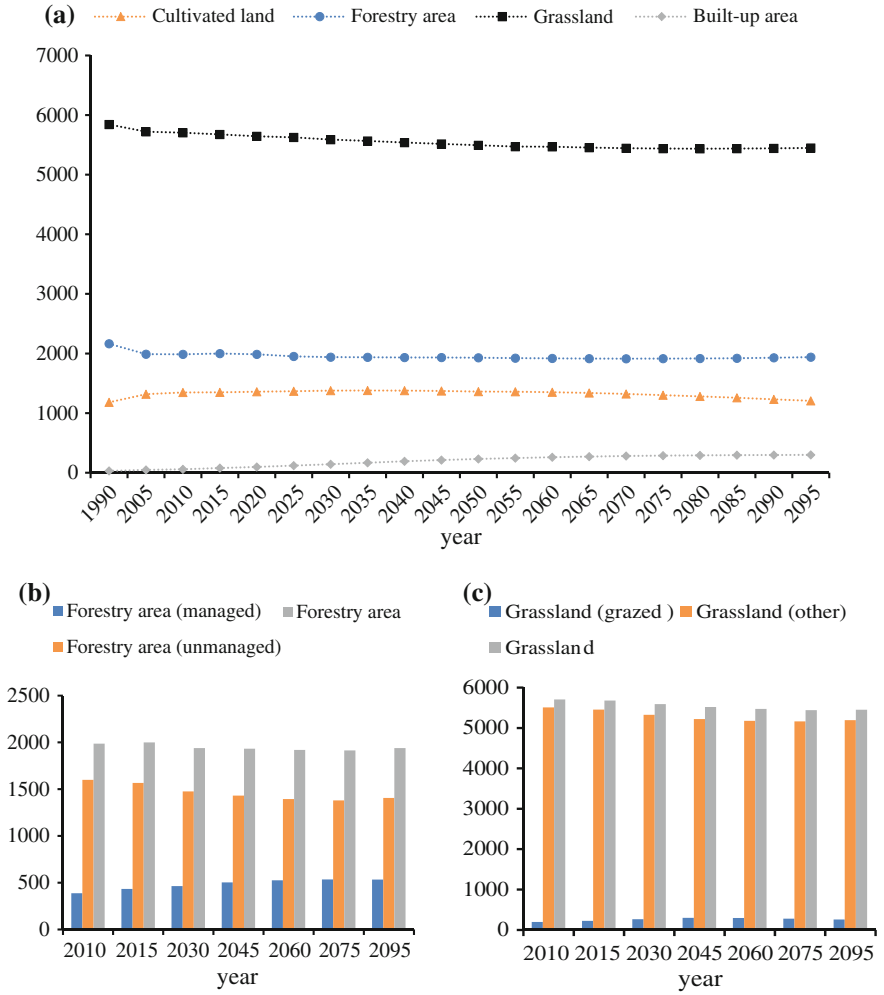

Fig. 3.2 Land use change trends of China under BAU scenario during 1990–2095; **a** Land use change trends of cultivated land, forest land, grassland and built-up land; **b** trends of managed and unmanaged forest land; **c** trends of grazed and other grassland (1,000 km^2)

grassland grows obviously. Under this scenario, it can be seen that explored grassland has been seriously damaged due to overgrazing.

Land Use Change Under CES Scenario

Under CES scenario, the speed of socio-economic development slowed down. Driven by socio-economic factors, simulation results of land use change trends are obtained with GCAM model (Fig. 3.4).

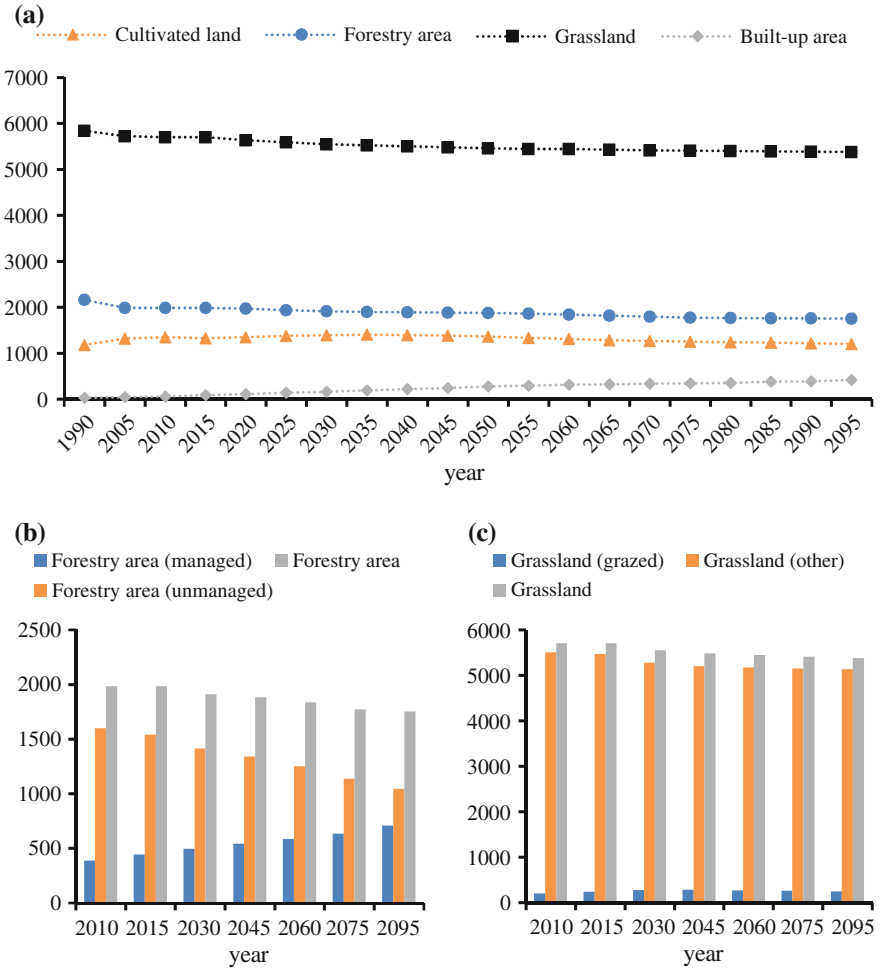

Fig. 3.3 Land use change trends of China under REG scenario during 1990–2095; **a** Land use change trends of cultivated land, forest land, grassland and built-up land; **b** trends of managed and unmanaged forest land; **c** trends of grazed and other grassland (1,000 km^2)

According to Fig. 3.4, cultivated area increases from 1990 to 2035 and decreases after then under CES scenario. As for the forestry area, the implementation of conservation measures has protected the forestry area excellently, so the forestry area increases all the way from 2005 to 2050, although it decreases during 1990–2005. After 2050, it will make small range of reduction. The unmanaged forestry area has been reduced all the time, while it will rise after 2070. The total forestry area decreases first and then increases due to the implementation of environmental conservation strategy. Grassland decreases during 1990–2030 and then increases after 2030. According to Fig. 3.4, unexplored

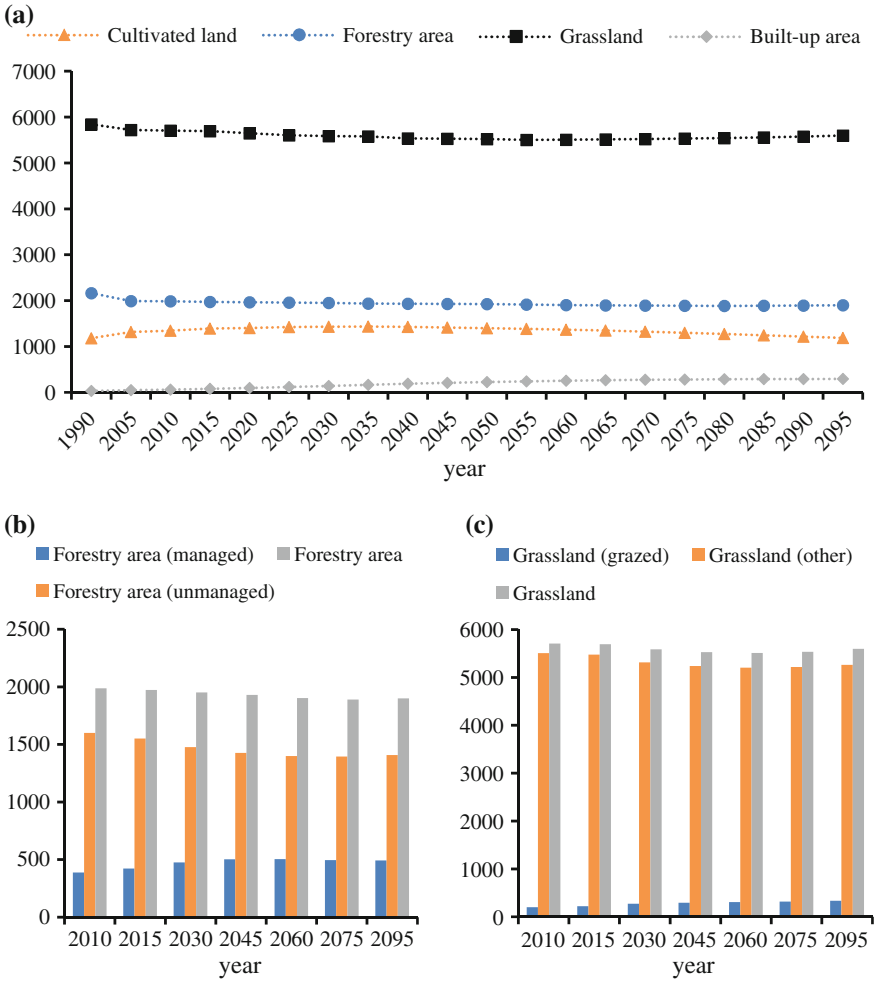

Fig. 3.4 Land use change trends of China under CES scenario during 1990–2095; **a** Land use change trends of cultivated land, forest land, grassland and built-up land; **b** trends of managed and unmanaged forest land; **c** trends of grazed and other grassland (1,000 km^2)

grassland has been in a downward trend during 1990–2065, and then become stable after 2065, while the explored grassland increases obviously. Therefore, CES scenario has positive effect on the protection of environment, and it is consistent with the model of sustainable development and low-carbon economic development. Apparently, urbanization still plays an irreplaceable positive role in the process of social-economic development, and the built-up area also has an increasing trend under CES scenario.

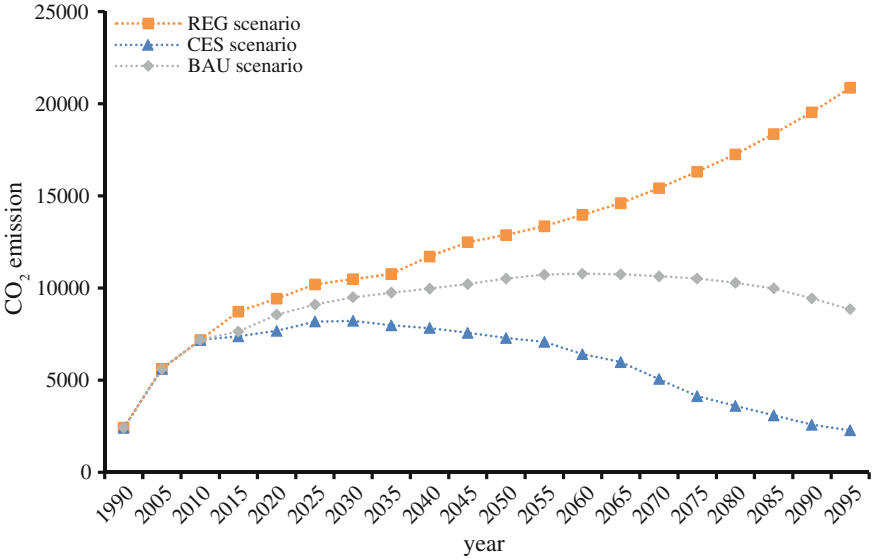

Fig. 3.5 CO_2 emissions under three scenarios during 1990–2095

3.1.5 CO_2 Emissions from Land Use Change

As shown in Fig. 3.5, under BAU scenario, CO_2 emissions will have a certain amount of increase in the coming decades and begin to drop down around 2065 although it will be extremely slow. CO_2 emissions will continue to accumulate over the next 50 years, and CO_2 emissions are maintained at the relative high level for a long time under BAU scenario. Therefore, although it will not cause the serious pressure on environment under BAU scenario, the negative effect is still profound, and it is not suitable for current environment. Under REG scenario, CO_2 emissions are at a higher level compared to the other two scenarios. CO_2 emissions have rising trends all the time. The greenhouse effect is serious currently, so controlling CO_2 emission is the primary objective of developing low carbon economy around the world. It can be seen from the simulation results under REG scenario, it is contrary to the strategic goal of sustainable development although rapid economic development can be obtained. Therefore, REG scenario can't meet the requirements of social development. Differently, under CES scenario, CO_2 emissions are beginning to show a downward trend in 2030, and have maintained at a low level after 2070, which is close to the level in 1990s. This scenario is beneficial to protect environment, and relieve environmental pressures in line with the strategic objectives of sustainable development. Moreover, it ensures the steady development of social economy as well. Therefore, this scenario achieves double win, not only protects environment, but also promotes economic development. Thus, CES scenario is the most suitable scenario in this study.

3.1.6 Concluding Remarks on the Tendency of Land Use Changes in China

In this study, three scenario, i.e. BAU scenario, REG scenario and CES scenario are designed. We use the GCAM model to simulate land use change from 2015 to 2095 and estimate the impact of land use change on CO_2 emissions that drove by social economy factors, then find which kind of land use change can adapt to climate change. The main conclusions are presented as follows.

BAU scenario kept the development trend in the past decades, and there is still a relatively high speed of economic development. However, it needs time to digest and absorb the great achievements brought by rapid economic development in the coming period in order to make all the aspects adapt to the development requirement, such as the promotion of environmental protection technology, the rationalization of emission standard, and the further narrowing of urban and rural gaps. When the whole society adapts to the economic development achievements, the bubble economy cannot be formed and the future economy will show more steady improvement. Simulation results indicate that CO_2 emissions will be at an extreme high level for a long time in China under BAU scenario. Government should take the appropriate measures or polies at different stages to meet the real requirements of social-economic development. Therefore, baseline scenario is not suitable for controlling future CO_2 emission.

Under REG scenario, the rapid growth of GDP and population brings about the increasing pressure on environment. The adjustment of industrial structure especially the rising proportion of secondary industry will lead to the growing of energy consumption and demand. For example, the total amount of exploitation and import of oil, natural gas and coal is obviously increasing. Besides, the rapid urbanization will consume more energy and resources. According to the simulation results of this scenario, CO_2 emissions will rise sharply and stay at an extreme high level, and it will not meet the sustainable development and low-carbon economic development model. Moreover, this scenario will lead to serious environmental crisis. Therefore, it is undesirable.

CES scenario focuses on the purpose of environment protection, and controls the growth rate of GDP and population. The setting for urbanization level is consistent with the one under BAU scenario in order to avoid further pressure on environment. The adjustment of industrial structure is to vigorously develop the tertiary industry reduce the proportion of the first industry, and control the development of the secondary industry. Under this scenario, the industrial structure optimization can be sped up, and CO_2 emission can be effectively controlled. Therefore, this scenario is more suitable for China.

This study is closely related with socio-economic factors and climate change through taking land use change as the core influencing factor of climate change and the socioeconomic development as the driving force, and the results of this study are of great practical significance and far-reaching research value. However, there are still some shortcomings in this study. Firstly, there are various factors of

the socioeconomic development, which were not taken into account in the scenario design. Therefore, it is necessary to implement more detailed analysis of socioeconomic drivers of land use change in the future study. In addition, the impacts of socioeconomic factors on the land use change are represented in approach parameterization, which have some limitations since they failed to thoroughly reveal how socioeconomic development influences land use change. Meanwhile, only three scenarios, which can set general direction of socioeconomic development, were designed in this study, but they cannot provide more specific details. In this aspect, more scenarios should be designed in the future research so as to fully reveal the best land use change to adapt to the climate change, e.g., more specific scenarios of the same type can be designed under the CES scenarios.

3.2 Scenarios of LUCC in China

The core part of researches on LUCC includes driving force, driving mechanism, their effects and model simulation of LUCC. In the past decades, scholars of different fields have paid great attention to LUCC, mainly focusing on the spatiotemporal change, driving mechanism, eco-environmental impacts and simulation of LUCC (Hasselmann et al. 2010). The research on the spatiotemporal analysis of LUCC mainly focuses on the change in quantity and spatial pattern (Patarasuk and Binford 2012). While the research on driving mechanism of LUCC makes great contribution to revealing basic processes of LUCC and its driving factors, further predicting future changes and formulating their corresponding policies. Currently, there have been various models to reveal the mechanism, explore their driving factors and simulate dynamic process of LUCC (Liu et al. 2008; Munroe and Müller 2007).

Previous models for forecasting LUCC in the future mainly covered empirical statistical models, agent-based models, methods based on relationships of adjacent grids in a dynamic simulation of land system (Zhao et al. 2011). The empirical statistical models can extract those major driving factors of LUCC and explore the reasons through its spatiotemporal processes. The Conversion of Land Use and Effects (CLUE) model and Conversion of Land Use and Effects at Small Region Extent (CLUE-S) model are two representative empirical statistical models (Veldkamp and Fresco 1996). However, there is generally a very large spatial scale and low resolution used in the simulation with the CLUE model, while the CLUE-S is mainly applied in dynamic simulation of regional land use at small scales (Verburg et al. 1999). The simulation of the structural change of land use with the Agent-based Model (ABM) has many advantages, but it generally concentrates on small study area. The Cellular Automaton (CA) simulates the processes of cellular evolution rules, but it requires a variety of spatial statistical methods to assist in this detection (White and Engelen 2000). Many scholars have tried to explore land use change through other methods and models, such as land-use dynamic degree model (Liu et al. 2003), identification model of driving forces (Geist and Lambin 2002),

and DLS model. The DLS model is capable of simulating the spatial dynamics of LUCC, and case studies indicate that it is an effective tool to simulate the process of land use change (Yin et al. 2010; Deng et al. 2008).

One of major issues is to settle temporal data of current research on driving force of LUCC which is only from simple perspectives. Therefore, it is significant to obtain the long-term temporal data of LUCC parameters. For that purpose, this study simulates structural changes of land use in China with the GCAM through an econometric model with socioeconomic factors as the driving forces. Thereby an econometric model is set up to forecast the built-up area change, and the changing trend of land use is simulated based on different scenarios of socioeconomic development. Thereafter the DLS model is used to forecast the future spatial pattern of LUCC in China.

3.2.1 Scenario Design and Downscaling Simulation Method

3.2.1.1 Scenario Design

In this study, three scenarios were designed according to characters of historical socioeconomic development of China, including the BAU scenario, REG scenario and CES scenario. The BAU scenario mainly reflects future changing trends of population and economy, which provides the baseline trend of land use change. Based on the BAU scenario, the REG scenario and CES scenario were designed according to main risks and adjusted direction of China's medium and long-term development plan. It is assumed that under the BAU scenario urbanization and industrialization will continue, the TFP that is on behalf of scientific and technological progress will develop by following the historical development trend, and China's population will peak in 2030s, but the population growth rate will gradually reduce. The REG scenario assumes that the industrial structure adjustment would be smoothly carried out, resource allocation and industrial structure would be more reasonable, while the speed of economic growth will keep steady. Under the CES scenario, the population growth rate is lower than it is under the BAU scenarios, the urbanization rate is relatively lower and GDP would increase with a lower rate (Table 3.5).

3.2.1.2 Data

Input data used in this study include the baseline structure land use/cover data and historical socio-economic data for both GCAM model and econometric model, and the baseline land use/cover data and some driving factors data for DLS model.

The baseline data of land use/cover change are derived from the dataset of National Basic Research Program of China. With these spatial distribution data, the initial land use allocation data in 2000 used by GCAM model could also be

Table 3.5 Projected change rates of GDP (%) and population (POP, ‰) in China, 2011–2100

	Scenarios	2011–2015	2016–2020	2021–2025	2026–2030	2031–2040	2041–2050	2051–2075	2076–2100
GDP	BAU	7.90	7.00	6.60	5.90	5.60	5.50	3.90	2.40
	REG	8.30	7.35	6.93	6.20	5.88	5.78	4.10	2.52
	CES	7.51	6.65	6.27	5.61	5.32	5.23	3.71	2.28
POP	BAU	6.24	4.10	1.67	−0.14	−1.04	−3.99	−5.54	−5.12
	REG	6.55	4.30	1.75	−0.13	−0.99	−3.79	−5.26	−4.87
	CES	5.93	3.89	1.59	-0.15	−1.10	−4.19	−5.82	−5.38

Note The data come from researches by Deng et al. (2008), Lutz and Samir (2010), and Samir et al. (2010). The change rates of GDP are expanded to 2100 according to historical changing trend. Under the CES scenario, the rates of population growth rate and GDP increase are 5 % lower than that under the BAU scenario, while they are 5 % higher under the REG scenario than the BAU scenario

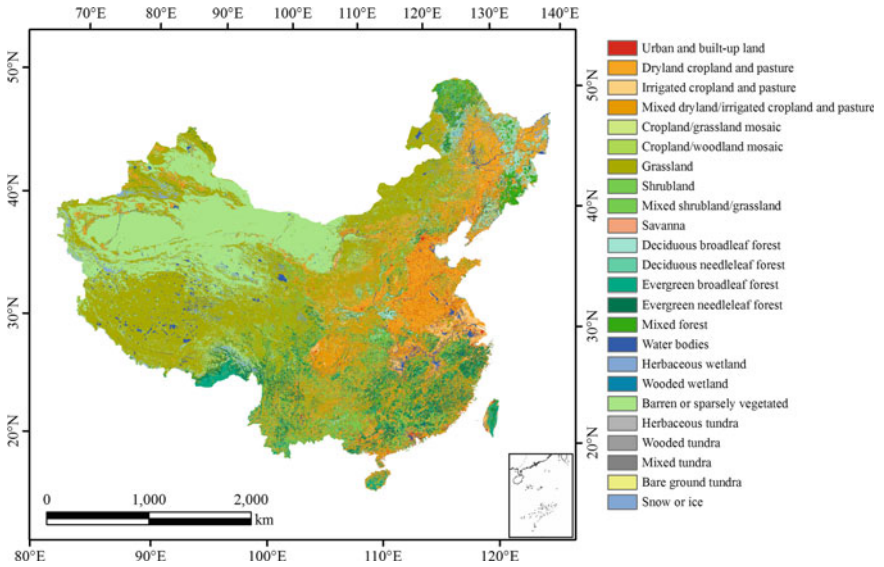

Fig. 3.6 Land use/cover data with USGS classification system in 2000 in China

obtained. The dataset is originally established with a 1 × 1 km grid scale using the land use/cover classification system of the United States Geological Survey (USGS) based on the remote sensing image and ground information of 2000 (Fig. 3.6). The socio-economic data include the population, population density and growth rate of per capita income, the proportion of agricultural population, urbanization ratio, GDP and price index of oil, gas, coal and hydropower. As essential input parameters, they are used in the GCAM model.

The input variables of driving factors in DLS model include natural environment data and social economic data. The natural environment data include basic geographic information data set of climate, location, terrain, soil property. The meteorological data used in this study, including near-surface temperature and precipitation, were all from meteorological stations of China Meteorological Administration, which were interpolated into 1 km resolution grid data with the Kriging interpolation algorithm, and got annual average value between 1998 and 2002. Location data include grid distance data and neighborhood land use/cover structure data. Among them, the grid distance data are the distance data of each grid center to the nearest road (including highway, state roads, provincial roads, county roads, and other roads), and provincial capital city, cities, water body and their ports, which were extracted and calculated based on 1:250000 basic geographical information data. The data neighborhood of land use/cover structure were calculated as the area percentage of the same land use/cover type with the target grid in rectangular ranges of 11 × 11 grids surrounding the target grid. Terrain data include slope, aspect, plain area ratio, altitude, topography and other data. Slope and elevation data were extracted based on 1:250,000 digital elevation

models. The soil attribute dataset were from 1:10,000,00 soil database built up in the second general survey of soil in China, and interpolated with the Kriging interpolation algorithm. This dataset includes data of loam proportion, organic content, Nitrogen content, phosphorus content, potassium content, the content of rapid available phosphorus, the content of rapid available potassium, pH value.

3.2.1.3 Models

The Agriculture and Land Use (AgLU) module of GCAM and simulated land use change trend data under three scenarios in the future were used to complete the structure land use simulation. AgLU module is a dynamic partial equilibrium economic model, at the core of the AgLU model is a mechanism that allocates land among cropland, grassland, forestry area, and other land and the economic return from each land use type in each region is maximized. The three primary drivers of land use change are population growth, income growth, and autonomous increases in future crop yields.

As there is no simulation function for built-up area in the GCAM model, an econometric model is set up to simulate the built-up area. In order to optimize the simulation results, the coefficients in the econometric model were calibrated according to the variation of population, GDP and urbanization ratio year by year.

The major driving factors in GCAM model are GDP and population with no urbanization ratio involved in, thus, urbanization ratio variable should be added. American urban geographer Northam has researched the process of urbanization in various countries in the world (Northam 1971). His studies indicated that the process of urbanization was expressed as an S. Therefore, the equation is built as follows:

$$y = 1/(1 + \partial \cdot e^{-\beta t}) \tag{3.9}$$

where y represented the urbanization ratio, t represented time, ∂ and β are parameters. It could be deformed as follows:

$$\ln(1/y - 1) = \ln \partial - \beta t \quad (\text{or } y_1 = a_0 + a_1 t) \tag{3.10}$$

The urbanization ratio over the years is obtained from statistical yearbook, and according to which the parameters ∂ and β in the formula are obtained from the simulation. Hence, the calculated equation of urbanization is worked out as follows:

$$y = 1/(1 + 4.5748e^{-0.04t}) \tag{3.11}$$

Afterwards, the impact on built-up area of population, GDP and urbanization ratio, as socio-economic indicators, are estimated by econometric model as follows:

$$Y_t = a_0 + a_1 X_{1t} + a_2 X_{2t} + a_3 X_{3t} + \varepsilon_t \tag{3.12}$$

where Y_t stands for the area of built-up area, X_{1t} represents population, X_{2t} is GDP, X_{3t} is urbanization ratio, α_0 is intercept. ε_t is random error term, which is a random variable independent with other explaining variables, and assumed it satisfied normal distribution with zero expectation and homoscedasticity.

DLS model presumes that the change of land use pattern is affected by both the historic land use pattern and the driving factors within the pixel and adjacent pixels (Yin et al. 2010). DLS model includes three modules: driving force analysis module, scenario analysis module and spatial allocation module.

DLS model analyzes balance between supply and demand of land resources at the grid scale through spatial allocation module, which can be used to realize the spatial allocation of structural data of land use so as to simulate LUCC under different scenarios (Yin et al. 2010; Deng et al. 2008). DLS model provides response function about land system structural changes. In addition, based on evaluation of the suitability of land use type distribution, DLS will express spatial dominant of possible scenarios on regional change of land system structure by estimating the response function. DLS expresses the difficulty level of conversion from one land type to other land types through defining transformation rule. Spatial allocation module calculates the number of grids to allocate. As for the grids needing distribution, the model would calculate the distribution probability of the different land use/cover types and allocate those.

3.2.2 Simulation of the Pattern of LUCC in China

3.2.2.1 Simulation Scheme

The simulation scheme is as follows. The structural data of LUCC were simulated on the basis of GCAM combined with the econometric model. Based on the correspondence table of USGS classification and GCAM classification (Table 3.6), we allocated the land area in the structural data of LUCC with the original area percentage of each land use/cover type in last year as the weight. So the data of demand for each land use/cover type of USGS classification in each year during 2010–2100 are obtained.

$$ld_{i,t+1} = \frac{ld_{k,j,t}}{\sum ld_{k,j,t}} \times ldg_{j,t} \tag{3.13}$$

Table 3.6 Mapping table of land use/cover types of USGS and GCAM classification systems

ID	USGS_Code	USGS_Name	GCAM_Code
1	100	Urban and built-up land	50
2	211	Dryland cropland and pasture	10
3	212	Irrigated cropland and pasture	10
4	213	Mixed dryland/irrigated cropland and pasture	10
5	280	Cropland/grassland mosaic	10
6	290	Cropland/woodland mosaic	10
7	311	Grassland	30
8	321	Shrubland	20
9	330	Mixed shrubland/grassland	30
10	332	Savanna	30
11	411	Deciduous broadleaf forest	20
12	412	Deciduous needleleaf forest	20
13	421	Evergreen broadleaf forest	20
14	422	Evergreen needleleaf forest	20
15	430	Mixed forest	20
16	500	Water bodies	40
17	620	Herbaceous wetland	40
18	610	Wooded wetland	40
19	770	Barren or sparsely vegetated	30
20	820	Herbaceous tundra	30
21	810	Wooded tundra	30
22	850	Mixed tundra	30
23	830	Bare ground tundra	30
24	900	Snow or ice	40

Note in the column "GCAM_Code", 10 represents Cropland; 20 represents Forestry area represents 30, Grassland represents 40 represents Water area; 50 represents Built-up area

where $ld_{i,t+1}$ is the predicted area of the ith land use/cover type of USGS classification in year $t + 1$. $ldg_{j,t}$ is the predicted area of the ith land use/cover type of USGS classification in year t. $ld_{k,j,t}$ is the predicted area of the kth land use/cover type of USGS classification, which corresponds to the jth land use/cover type of GCAM classification in year t.

3.2.2.2 Simulation Results

In the future, the land use/cover in China will be continually changed by human activities and climate changes, and their spatial pattern will change dynamically as well.

(i) The simulated changes of LUCC. In the study, we simulated the changes of LUCC in China in the future using GCAM model combined with the econometric model under the three scenarios (Fig. 3.7). The simulated results show the changing trends of different land use/cover in three different scenarios.

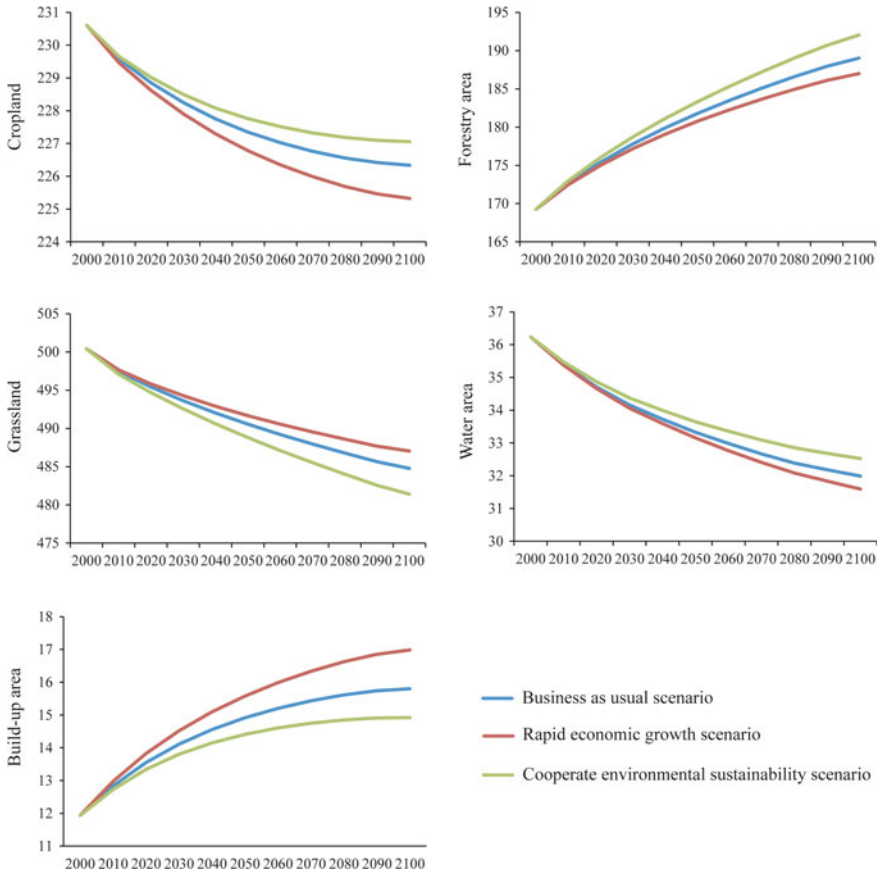

Fig. 3.7 Simulated changes of LUCC area (measured in million ha) in China, 2010–2100

On the whole, built-up area, forestry area will show an increasing trend under the three scenarios. On the contrary, cropland, grassland and water area will show a decreasing trend under the three scenarios. However, grassland and forestry area change at the fastest rate under CES scenario, at the lowest rate under REG scenario, while other types change at the lowest rate in CES scenario and fastest rate in REG.

Statistical analysis of the simulation result indicated that land cover will change as follows. The area of built-up area will increase most rapidly during 2000–2010, with the 10-year increasing rate reaching 3.86, 5.05 and 2.98 % under the BAU scenario, REG scenario and CES scenario, respectively. The built-up area will increase rapidly during 2010–2060 under the BAU scenario and CES scenario with the 10-year increasing rate as 0.54 and 0.44 million ha, respectively. Whereas, the 10-year increasing rate tends to slow down during the latter time period of 2060–2100 with the 10-year increasing rate only as

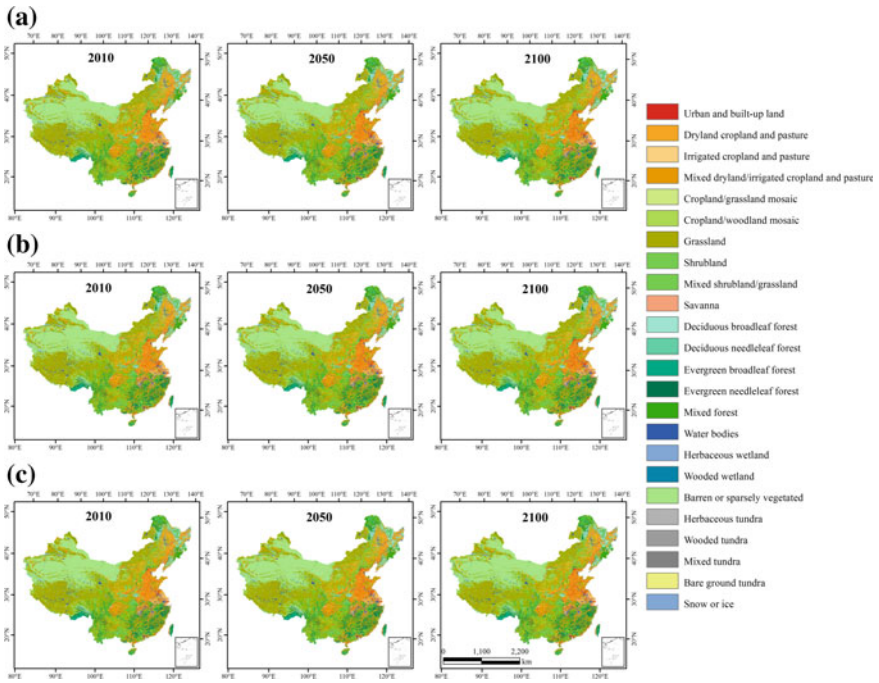

Fig. 3.8 Simulated spatial pattern of LUCC in China in 2010, 2050 and 2100 under the Business as Usual scenario (**a**), Rapid Economic Growth scenario (**b**) and Cooperate Environmental Sustainability scenario (**c**)

0.15 and 0.08 million ha, respectively. Under the REG scenario the increasing trend of built-up area tends to be rapid on the whole during 2010–2100, with the 10-year increasing rate reaching 0.5 million ha and the total area of built-up area reaching 5.05 million ha. By contrast, cropland and water area both show a decreasing trend under all the three scenarios, especially the REG scenario, under which their 10-year decreasing rates reach 0.23 and 1.28 %, respectively. Under the BAU scenario and CES scenario, the change of these two land cover types tends to slow down, with their 10-year decreasing rates reaching 0.19 and 0.15 %, 1.17 and 1.03 %, respectively. The increase of forestry area reaches to 19.77, 17.74 and 22.79 million ha under the BAU scenario, REG scenario and CES scenario, respectively. While, the changes of grassland under the BAU scenario, REG scenario and CES scenario show a decreasing trend with the rates of 3.12, 2.67 and 3.80 %, respectively.

(ii) The spatial pattern of land use/cover change. The simulation results indicated that the spatial patterns of land cover in China under the three scenarios are consistent on the whole, but with some regional difference (Fig. 3.8). The spatial pattern of land cover in China in the future is as

follows. The urban and built-up land has special requirement for location, the spatial pattern of the built-up land in the future will show significant regional differentiation under the joint influence of natural factors, socio-economic factors, topographic conditions, etc. In the eastern part of China, the urban and built-up land will continue to gather in the three major plain regions (i.e., Northeast China Plain, North China Plain and Middle-Lower Yangtze Plain), Yangtze River Delta and Pearl River Delta, it will show an expanding trend on the original basis. In the western part of China, the urban and built-up land will mainly concentrate in the regions such as Sichuan Basin, Guanzhong Basin, Hetao Plain, Hexi Corridor, oases in Xinjiang Province. While with the implementation of policies to exploit the land resources on the low hill and gentle slope, the land in hills with gentle slope, mountains and plateaus may also become urban and built-up in the future.

The cropland, including dryland cropland and pasture, irrigated cropland and pasture, mixed dryland/irrigated cropland and pasture, cropland/grassland mosaic and cropland/woodland mosaic, will still be contiguously distributed in the three major plain regions (i.e., Northeast China Plain, North China Plain and Middle-Lower Yangtze Plain), Sichuan Basin, Hexi Corridor, oases in Xinjiang Province, etc. Besides, it will also gather in some alluvial plains and regions of the low hill and gentle slope. In addition, in the marginal areas between cropland, grassland and forest land, there may be some farming-grazing or farming-forestry ecotones, which include various land cover types.

Grassland is mainly located in Inner Mongolia, Qinghai-Tibet Plateau in the western part of China. While in the eastern part of China, grassland will be mainly distributed in the regions of the low hill and gentle slope, and it will generally be mixed with cropland or forest land. There will be great regional heterogeneity of the distribution of land cover types that mainly include the forest land, such as shrubland, mixed shrubland/grassland, deciduous broadleaf forest, deciduous needleleaf forest, evergreen broadleaf forest, evergreen needleleaf forest and mixed forest. In the northern part of China, the forest land will be mainly located in Northeast China, e.g., Greater Khingan Mountains, Lesser Khingan Mountains, Changbai Mountains and Liaodong Basin. While in the southeast part (e.g., Lingnan area, Taiwan), southwest part (e.g., the Yunnan-Guizhou Plateau, Sichuan Basin and Guangxin Province), the forest land will be mainly distributed in the regions of hills and mountains.

Some land use/cover types, including water bodies, herbaceous wetland and wooded wetland, will still remain in the original regions, but will show an shrinking trend on the whole on the original basis; In spatial pattern, there will be more of these land use/cover types in the eastern part and less in the western part, more in the southern part and less in the northern part. Savanna, herbaceous tundra, wooded tundra and bare ground tundra will be located in the Alpine regions of Himalaya Mountains. There is no mixed tundra in China.

Snow or ice will be mainly distributed in the regions above the snow line in the high mountains (Tianshan Mountains, Qilian Mountains, Kunlun Mountains and Himalaya Mountains) in the southwest and northwest part of China. Barren or

sparsely vegetated land will mainly gather in the arid desert areas centering on Taklimakan Desert in Tarim Basin, Qaidam Basin, etc. In the northwest part of China, including the Alpine arid regions in Qinghai-Tibet Plateau, middle part of Inner Mongolia, northwest part of Gansu Province, etc.

3.2.3 Concluding Remarks on Scenarios of the Future LUCC

In this study, three scenarios of the future LUCC in China are designed on the basis of the trends of future socioeconomic development and national policies (e.g., Grain for Green). The simulation results showed that spatial pattern of land use/cover in China under the three scenarios is consistent on the whole, but with some regional difference. The simulation results based on different scenarios reflect spatial pattern of land use/cover of China in the future to some extent, which have important policy implications and scientific supporting on land use planning and sustainable development of the society and can provide the input underlying surface data for the climate models.

There are still some uncertainties in the results of scenario simulation of future land use/cover change due to those uncertain driving factors since the land system is a complex system that is closely associated with human activities and natural conditions. Moreover, this study uses the land use/cover classification system correspondence from the GCAM model with five categories of classification into USGS with 24 categories, which also lead to the risk of uncertainties. Therefore, the simulation results cannot represent actual change of area of different land use/cover types and their spatial pattern, but they can still make good sense in reasonable confidence interval to a certain extent due to the robustness of the model.

3.3 Reclassified LUCC for the Simulation of Regionalized Impacts

The temporal land cover datasets have been widely used in numerous climate simulation projects. Most attention has been paid to effects of the accuracy of the land cover data on the climate simulation. The accuracy of temporal land use data from CAS is higher than 90 %, but the high-precision land cover data is absent. We overlaid the land cover maps of the IGBP, Global Land Cover2000 (GLC), University of Maryland Data (UMD) and Data Center for West China (WESTDC), and the grids with agreement of classification were selected as the sample grids. We can combine the land cover data with the land use data to generate land cover data of high accuracy for the climate simulation. By comparing results obtained with different decision tree classifiers with the WEKA toolkit for data mining, this

study find that the C4.5 algorithm is suitable for converting land use data to land cover data of IGBP classification. We reset the decision rules with Net Primary Productivity (NPP) and Normalized Difference Vegetation Index (NDVI) as the indicators. The dataset with the accuracy of 88.96 % is divided into 66 % training data and 34 % testing data. The validated accuracy of the classified land cover data is 83.14 % by comparing with the Terrestrial Ecosystem Monitoring Sites (TEMS) and high resolution images. Therefore, we may produce the temporal land cover data using this method, which can meet the accuracy requirement of climate simulation and that can be the parameters of dynamical downscaling in regional climate simulation.

Many land cover data of China have been produced in recent years with the remote sensing data. The previous study showed that the result of the precipitation study would be greatly influenced if the accuracy of land cover data is under 80 %, and the result may be worse as the accuracy continue to decrease (Ge et al. 2007). Unfortunately, neither the overall nor class-specific accuracy of most datasets can meet the common requirements of the regional climate modeling. Therefore, it is necessary to produce the land cover dataset with high accuracy for the climate simulation based the existing land use dataset, land cover datasets and some ancillary datasets. These available data with a high level of uncertainty may be improved by the combining the different data sources so as to meet the requirement of climate simulation.

The researches on the climate modeling vary substantially in the spatial and temporal scales. So the temporal land cover datasets are essential to the development of a cohesive climate model. The CAS has constructed a land use dataset that includes the data of 1988, 1995, 2000 and 2005 (Liu et al. 2003). However, there are still no comparisons of land cover datasets at the regional scale, especially in China where the land use is changing drastically due to rapid economic development and anthropogenic disturbance. Many studies have indicated that the disagreement among the land cover datasets primarily resulted from the differences of sensors, spatial resolutions, algorithms, and classification schemes (Kaptué Tchuenté et al. 2011); Among them, the difference in the classification schemes is considered to be the key reason for disagreement of the land cover datasets and the main obstacle to comparing different land cover datasets. Therefore, it can make great contribution to climate change research if we can take advantage of the long-term land use datasets from the CAS, and use an appropriate method to convert them to the International Geosphere Biosphere Programme (IGBP) land classification scheme. It consists of seventeen categories (Table 3.7) and is widely accepted and used in the simulation of climate changes (Gao and Jia 2012).

The decision tree is one of the most powerful classification algorithms to classify land cover type of remote sensing image (Simard et al. 2010). The decision tree technique is more suitable for the analysis of categorical outcomes. Besides, it is easy to interpret, computationally inexpensive and capable of dealing with noisy data. Furthermore, its prediction model is more understandable to the users. The decision tree classifiers include the C4.5/C5.0/J48, NBTree, SimpleCart, REPTree, BFTree, etc., among which the C4.5/C5.0/J48 classifier is the most

Table 3.7 Types and descriptions of IGBP land cover classification scheme

Code	Type	Descriptions
1	Evergreen needleleaved forest	Land is dominated by trees with a per cent canopy cover >60 % and height >2 m. Almost all trees remain green all year. Canopy is never without green foliage
2	Evergreen broadleaved forest	Land is dominated by trees with a per cent canopy cover >60 % and height >5 m. Almost all trees remain green all year Canopy is never without green foliage
3	Deciduous needleleaved forest	Land is dominated by trees with a per cent canopy cover >60 % and height >2 m. Consists of seasonal Needleleaved tree communities with an annual cycle of leaf-on and leaf-off periods
4	Deciduous broadleaved forest	Land is dominated by trees with a per cent canopy cover >60 % and height >2 m. Consists of seasonal Broadleaved tree communities with an annual cycle of leaf-on and leaf-off periods
5	Mixed forests	Land is dominated by trees with a per cent canopy cover >60 % and height >2 m. Consist of tree communities with interspersed mixtures or mosaics of other four forest cover types. None of forest types >60 % of landscape
6	Closed shrublands	Land with woody vegetation less than 2 m tall and with shrub-canopycover >60 %. The shrub foliage can be, either evergreen or deciduous
7	Open shrublands	Lands with woody vegetation less than 2 m tall and with shrub canopy cover between 10–60 %. The shrub foliage can be either evergreen or deciduous
8	Woody savannas	Land with herbaceous and other understorey systems and with forest canopy between 30 and 60 %. The forest cover height exceeds 2 m
9	Savannas	Land with herbaceous and other understorey systemsand with forest canopy between 10 and 30 %. The forest cover height exceeds 2 m
10	Grasslands	Land with herbaceous types of cover. Tree and shrub cover is less than 10 %
11	Permanent wetlands	Land with a permanent mixture of water and herbaceous or woody vegetation that cover extensive areas. The vegetation can be present In either salt, brackish or fresh water
12	Croplands	Land is covered with temporary crops followed by harvest and a bare soil period (e.g. single and multiple cropping systems). Note that perennial woody crops will be classified as the appropriate forest or shrubs land cover type
13	Urban and built-up	Land covered by buildings and other man-made structures. Note that this class will not be mapped from the AVHRR imagery but will be developed from populated places layer that is part of Digital Chart of the World
14	Cropland/natural vegetation mosaic	Land with a mosaic of croplands, forest, shrublands, and grasslands in which no one component comprises more than 60 % of the landscape
15	Snow and ice	Lands under snow and/or ice cover throughout the year

(continued)

Table 3.7 (continued)

Code	Type	Descriptions
16	Barren or sparsely vegetated	Land of exposed soil, sand, rocks or snow and never has more than 10 % vegetated cover during any time of the year.
17	Water bodies	Oceans, seas, lakes, reservoirs, and rivers. Can be either fresh or salt water.

popular and powerful one (Ghose et al. 2010). The C4.5 classifier is selected in this study according to the accuracy assessment to identify the vegetation disaggregation classification in the farming-pastoral ecotone of north China.

The ecotones are recognized as one of the most important objects of the ecological research, since they are unstable and very sensitive to the surrounding environment. Besides, ecotones are more suitable for the study of the land cover mapping for the climate simulation. The farming-pastoral ecotone has received a lot of attention from academic community due to its largest area, longest span and typical characteristics. It involves nine provinces and 106 counties, with a total area of 654, 564 km^2 (Liu et al. 2007). The total population in this area is 3.14×10^7, with the average population density of 47.9 persons per square kilometer. The land use has changed drastically throughout farming-pastoral ecotone of North China after the widespread and profound economic reform that was initiated in the early 1980s (Dong and Xu 2009), and the current ratio of the cropland, forest land and grassland is 1.0: 1.17: 3.67 (Fig. 3.9). The temperature rise has been more and more obvious in the past 50 years, with an average increase rate of 0.4 °C/10a (Friedl et al. 2002).

3.3.1 Data Preparation

This study presents an inference rule of spatial data mining to distinguish forest types based on the consistent grids in the data of the IGBP Data and Information System (IGBPDIS, Bartholomé and Belward 2005),[1] GLC (GLC2000, Ran et al. 2012),[2] multi-source Integrated Chinese Land Cover (WESTDC, Liu et al. 2005)[3] and UMD[4] land cover data in 2000. The classification rule is first rectified so as to improve accuracy in 2000. Then the land use data of 1988, 1995 and 2005 were converted to the land cover data according to this inference rule.

In this study, we also used the land use database developed by the CAS. The data are available during four periods, i.e., year 1988, year 1995, year 2000 and

[1] For more imformation: http://edcdaac.usgs.gov/modis/mod12q1v4.asp.

[2] For more imformation: (http://www.gem.jrc.it/glc2000).

[3] For more imformation: (http://westdc.westgis.ac.cn).

[4] For more imformation: (http://www.landcover.org).

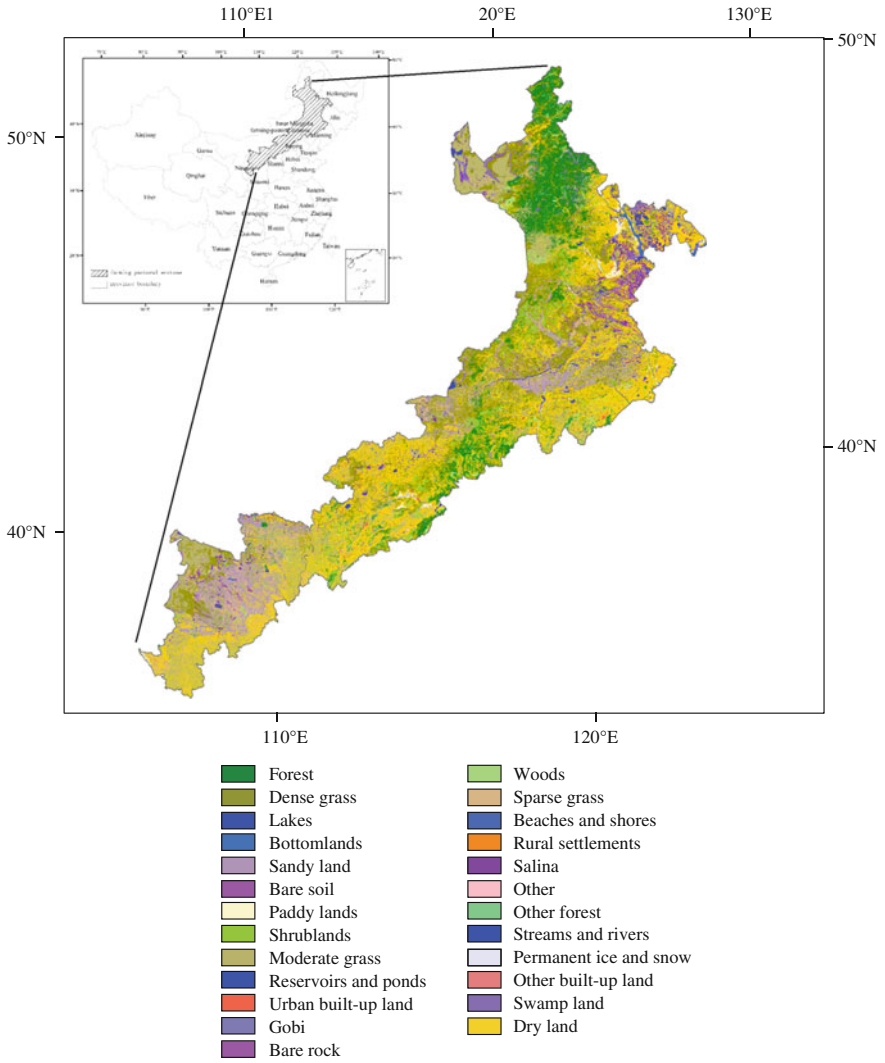

Fig. 3.9 The location and 2000 year's land use map of farming-pastoral ecotone in North China

year 2005, which are limitedly applied for a hierarchical classification system of 25 land cover classes. The data team also spent considerable time validating the precision of the interpretation of TM images and land cover classification by extensive field surveys (ground validation). The validation result indicated that the average precision of the interpretation reached 95 %. The 1*1 km land use map of China is derived from 1:100,000 land use database. It includes two kinds of data, one was geocoded with the greatest-area method (i.e., if a cell has more than one possible code or it contains two or more polygons, the code of the polygon with the

greatest area in the cell is used). The other was geocoded with area percentage grid method, in which each cell can be divided into 25 layers to record the area of each type (Liu et al. 2003). Besides, the vegetation map can provide the reference information of vegetation since the change of forest categories is slight in the short term. The vegetation map of China reflects detailed information on the distribution of vegetation and includes horizontal and vertical zones of 11 vegetation groups, 54 vegetation types, 135 biome units and 796 sub-biome units (DeFries and Townshend 1994).

The mapping of land cover data in 2000 based on the data mining is a benchmark of the long term land cover dataset. It is necessary to collect the ancillary data due to the absence of other data series. Data of physical geography include information on terrain slope, information on vegetation property variability and so on. Information on the terrain slope and the plain area proportion are derived from DEM data covering the entire China at the scale of 1:250,000. These data are provided by the Data Center for Resources and Environmental Sciences, CAS. The meteorological data, including the annual temperature and annual precipitation, are acquired from China Meteorological Bureau. The NDVI dataset come from the Pathfinder dataset of Earth Resources Observation System (EROS), it is extracted from the NOAA/AVHRR-NDVI images. The spatial resolution of images is 1 km $\times$ 1 km, and their temporal resolution is 15 days. In order to guarantee the data quality, all the data have all been preprocessed with the internationally accepted reliable approach (Chen et al. 2004). Besides, in order to eliminate the noise caused by the cloud pollution and the atmospheric influence, we also smooth the time-series NDVI data with the Savitzky-Golay smoothing filtering method (Ahlqvist 2008). The NPP data during 1985–1999 come from the remote sensing data of NOAA/AVHRR, and that during 2000–2010 come from the NPP product of MODIS.

3.3.2 Methodology

The working procedure of the classification is as follows. First, based on the definition of mosaics type, we produce the Cropland/Natural vegetation mosaics data by using the grid area percentage dataset in CAS land use system. Then other types of land use except for forest and woods are achieved by utilizing grid maximum area mapping with two sub-classification definition between the CAS and IGBP. Thereafter, we check out and determined the grids whose type were consistent with the forest and woods among the WESTDC, UMD, GLC and IGBPDIS land cover data, at the same time we identify the boundary of the forest and woods, which are consistent with CAS land use, generate them into the sample data. Finally, we realize the conversion of forest types of IGBP scheme with the C4.5 classifier (Fig. 3.10).

The land use types are first transformed into the land cover types. It is easy to transforming some land use types, e.g., 3 classes of developed and mosaic lands,

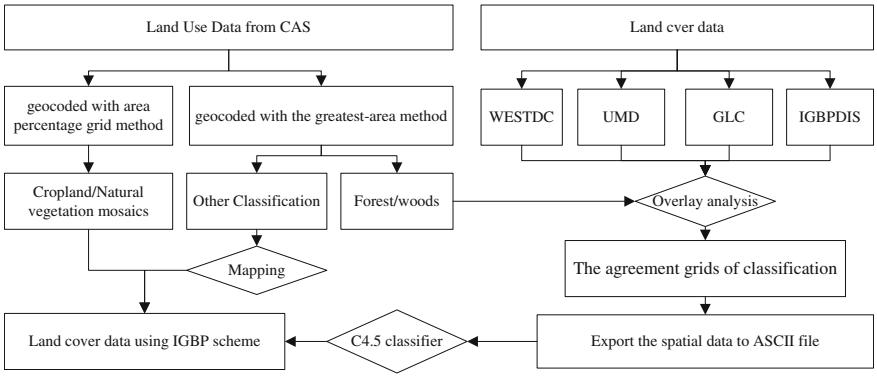

Fig. 3.10 The work flow of mapping based on multi-source spatial data mining approach Sect. 3.3.2.1 Mapping the land use types to determinate the land cover classification

2 classes of artificial lands, 1 class of water among the IGBP land cover classification.

It only needs to transform from many to one or one to one (Table 3.8). For example, the Paddy land and Dry land in the land use map of CAS are explicit and correspond to the cropland class definition in the IGBP, so it only needs to aggregate them into cropland with the binary grid. It is more feasible to judge the land cover classification of Cropland/Natural Vegetation Mosaic with the area percentage grid data of Paddy lands, Dry lands, Forest, Shrub lands, among which no single type comprises more than 60 % of the landscape. The land cover of Cropland/Natural Vegetation Mosaic is mainly located in the Inner Mongolia, Liaoning, Hebei, Shaanxi, Shanxi, provinces, with a total area of about 730,00 km^2 in 2000 (Fig. 3.11). The 8 classes of land cover types including the IGBP10-IGBP17 were transformed, which account for nearly half of the total land area. In addition, there is a little savanna in China, which is convenient to judge based on the temperature and land use type. However, the 8 classes of vegetation (forest, shrubs, and herbaceous vegetation) and the leaf attributes (evergreen and deciduous), and the leaf types (broadleaved and coniferous) are difficult to determine because we lack of vegetation information.

3.3.2.1 Selecting the Spatial Agreement Samples of Vegetation for Data Mining

The closed forest and other forest classes are arbor forest classes in land use classifications of CAS. They do not concretely specify the forest type information. However, this provides an accurate boundary for the forest; therefore, we need an inference rule to transform between forest in land use classification system and IGBP forest categories: evergreen needle-leaf forest, evergreen Broadleaved

Table 3.8 Contrast the CAS land use classification and IGBP land cover scheme

	Paddy land	Dryland	Stream and Rivers	Lakes	Reservoirs and pond	Permanent ice and snow	Beach and shores	Bottomland	Dense grass	Moderate grass
IGBP12	+	+	−	−	−	−	−	−	−	−
IGBP15	−	−	−	−	−	+	−	−	−	−
IGBP17	−	−	+	+	+	−	+	+	−	−
IGBP10	−	−	−	−	−	−	−	−	+	+

	Urban Built-up	Rural settlment	Other built-up	Sandy Land	Gobi	Salina	Swamp land	Bare soil	Bare rock	Other
IGBP11	−	−	−	−	−	−	+	−	−	−
IGBP13	+	+	+	−	−	−	−	−	−	−
IGBP16	−	−	−	+	+	+	−	+	+	+

Note + stands for match

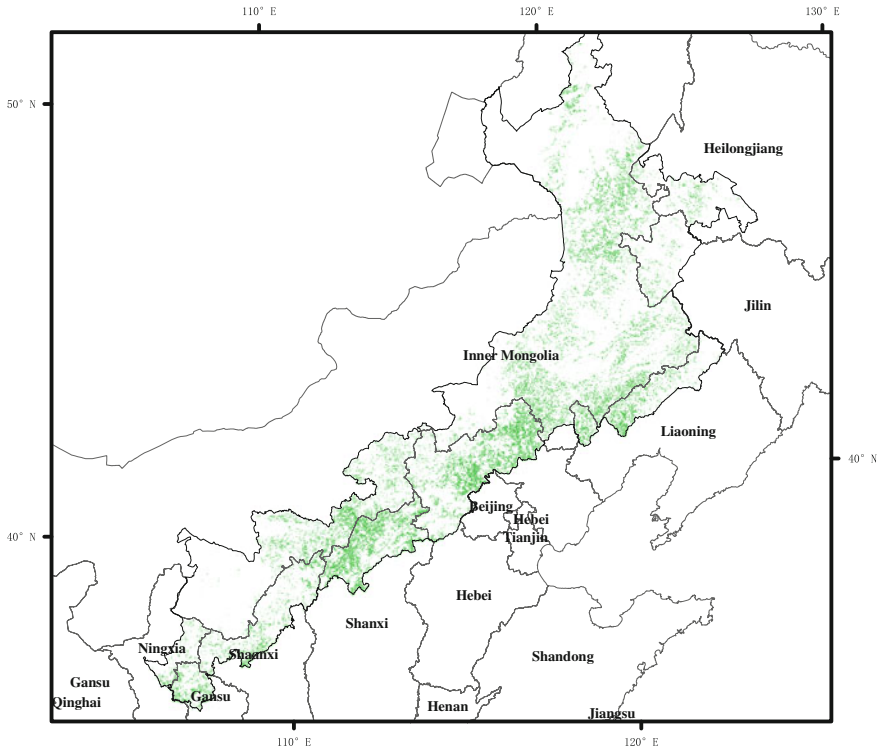

Fig. 3.11 The distribution of Cropland/Natural vegetation mosaics in 1 km grid all over North China

forest, deciduous needle-leaf forest, deciduous Broadleaved forest and mixed forest based on the ancillary data in 2000.

The degree of overlap between any two land cover classes based on the feature definitions of the classification schemes is used to select sample grids among the IGBPDIS, WESTDC, UMD and GLC data (Ahlqvist 2008). The degree of agreement for each grid is determined by the overlap metric, which indicates the feature-based similarity among different land cover products. If the classes of two products are identical or mostly overlapped for a given grid, then the grid will be assigned a value of 1, which indicates that the two classes of different classification schemes completely agree with each other. Otherwise, the grid will be assigned a value of 0. Finally, agreement and disagreement maps will be created over the entire region, which highlight areas that have a high confidence of classification (Fig. 3.12). In other words, the sample grids could be selected from the agreement degree maps.

In this study, the method improves the classification results by further applying the data mining technique and using ancillary information. The detailed DEM data, NDVI, NPP and meteorological data were utilized as ancillary information to separate those vegetation classes, the ecological characteristics of are very different. The vegetation types are closely related to physiographic factors and

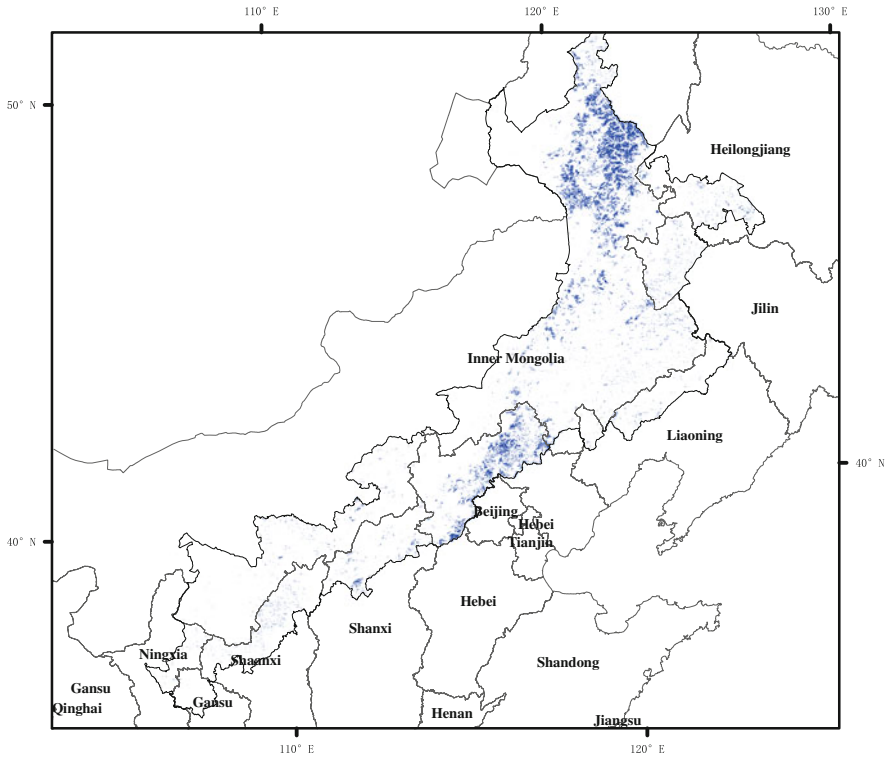

Fig. 3.12 The agreement grids of classification among GLC, UMD, IGBPDIS and WESTDC

meteorological conditions. The topography at every grid could be described by landform classes (e.g. hill, slope, depression et al.) by processing the raw elevation data, and the meteorological data of observation could be interpolated to 1 km grid cell. Therefore, these datasets could be expressed with the 1 km grid data. The additional information sources were used to refine result of the C4.5 classifier. We overlapped land cover maps and these ancillary data, and sampled the dataset for ASCII text format with the ArcInfo WorkStation toolkit. Thereafter the dataset for the training and testing the classifier of data mining in the WEKA toolkit is constructed.

3.3.2.2 Constructing the Classification Method to Identify Vegetation Types

Many classification methods have been proposed by researchers in the fields of machine learning, pattern recognition and statistics. In this study, we focuses on the classification methods to convert forest and grassland classification to the IGBP land cover scheme. In this case, the hidden and valuable knowledge

discovered in related ancillary databases is summarized in the decision tree structure. This classification with the technique of decision tree can be performed without complicated computation, and this method can be used for both the continuous and categorical variables. We find that the C4.5 classifier achieved the highest accuracy among these methods for the land cover identification. The classifier is developed on the basis of the decision tree learning, which is a heuristic, one-step look ahead (hill climbing), non-backtracking search through the space of all possible decision trees.

The specific principles of this classifier are as follows. First, the initial sample data were recursively partitioned into sub-groups. Then gain values of all the attributes of sample data are calculated, according to the numerical value of which attributes to select classification. Next, the attribute with the largest gain value is used in logical test, and each test forms a branch, and subsets of samples (training data) satisfying outcomes at those child nodes are moved to their corresponding child nodes. Thereafter, this process runs recursively on each child node until the needed leaf nodes are obtained. Finally, the decision tree is modified according to relevant empirical knowledge. The C4.5 classifier is one of the decision tree families that can produce both decision tree and rule-sets; The C4.5 classifier uses two heuristic criteria to rank proper tests, i.e., the information gain that uses the attribute selection measure, which minimizes the total entropy of subset, and default gain ratio that divides the information gain provided by the test outcomes. Note that the information gain algorithm is described as the Gain function (A) as follows:

i. The attribute with the highest information gain is selected.
ii. S contains Situples of the class Ci ($i = 1, \ldots, m$). m means the number of classification.
iii. The information measure or expected information is required to classify any arbitrary tuple:

$$I(S_1, \ldots, S_m) = -\sum_{i=1}^{m} \frac{S_{\mathrm{i}}}{\mathrm{S}} \log_2 \frac{S_i}{S} \tag{3.14}$$

iv. Entropy of attribute A with values $\{a_1, a_2, \ldots, a_v\}$ is calculated.

$$E(A) = \sum_{j=1}^{v} \frac{S_{1\mathrm{j}} + \ldots + S_{mj}}{S} I(S_{1j}, \ldots, S_{mj}) \tag{3.15}$$

v. The information gain means how much can be gained by branching on the attribute A:

Table 3.9 The attribute Gain Ratio value for constructing decision tree

Name	Gain ratio	Rank	Description
X	0.03	8	Rectangular coordination of Longitude
Y	0.22	2	Rectangular coordination of latitude
PA	0.12	6	0.1mmannual precipitation
TA	0.20	3	0.1 °C annual accumulated temperature
DEM	0.15	4	Elevation
LFM	0.11	7	Landform type
NDVI-3	0.22	2	Normalized differential vegetation index in March
NDVI-12	0.27	1	Normalized differential vegetation index in December
NPP	0.14	5	Net primary productivity (g C/m^2/year)

$$\text{Gain}(A) = I(S_1, S_2, \ldots, S_m) - E(A) \tag{3.16}$$

The attribute A contains the DEM, longitude, latitude, annual temperature, annual precipitation, NPP, NDVI and other ancillary spatial data. We calculate the gain ratio to select the attributes that can generate the ancillary information of classification (Table 3.9). There are about 35,396 sample cells of the closed forest and other forest. The gain ratio for training dataset is calculated, the biggest value of which is 0.27, indicating that NDVI-12 is the most suitable to be the attribute for the forest categories. The forest is further divided into two sub-categories according to the NDVI-12 and NDVI-3, i.e., the forest with the NDVI-12 reaching 0.53 and NDVI-3 reaching 0.39 is categorize into the evergreen forest, while the forest with the NDVI-12 below 0.53 and NDVI-3 reaching below is categorized into the deciduous forest. Although the gain ratio of DEM and temperature is higher than that of the NPP, it is difficult to distinguish the forest type according to them. Therefore, we distinguish Broadleaved, Needleleaved and mixed forest according to the NPP. Broadleaved forest is more than 445, and that of Needleleaved forest is less than 297, and the forests with the middle NPP value is categorized into the mixed forest.

The accuracy of different classifiers is compared with the WEKA toolkit. We reset the decision tree rule using the NPP and NDVI according to the aforementioned information. The WEKA toolkit is a collection of machine learning algorithms for data mining tasks. It contains tools for data pre-processing, classification, regression, clustering, association rules and visualization. It is also very suitable for developing new machine learning schemes.

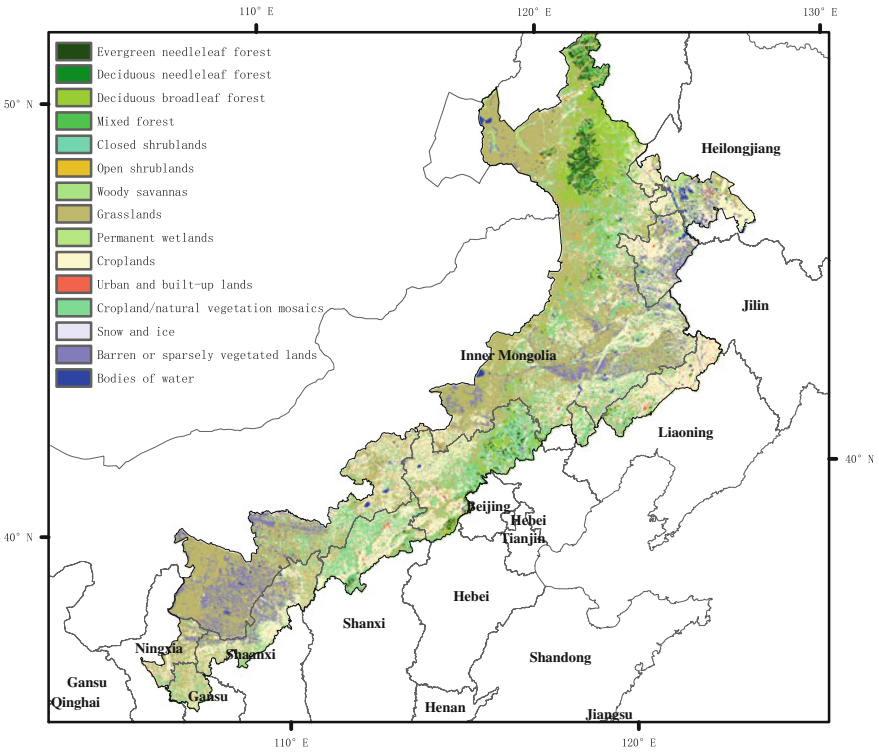

Fig. 3.13 The transformed land cover map over farming-pastoral ecotone in 2000

3.3.3 Results and Discussion

3.3.3.1 Evaluating the Accuracy of the Land Cover Classification

Using the method mentioned above, a Serving Climate Simulation Land Cover (SCSLC) map is generated with a decision rule based on multi-source spatial data mining in the farming-pastoral ecotone of North China (Fig. 3.13). To analyze the characteristics of this map, we compare the area of each land cover class in this map with other three popular land cover maps, i.e., the WESTDC map, UMD map and GLC map. The overall areas of each land cover class in the four maps were shown according to the same classification (Table 3.10). It is notable that the SCSLC map using the C4.5 classifier is similar to the WESTDC map, but there is remarkable increase in the cropland/natural vegetation mosaics and the corresponding decrease in grassland. We also find that the accuracy of the GLC map and UMD map is lower than that of the SCSLC and WESTDC. The GLC map ignores the urban and Built-up land and the UMD ignores the Water Bodies in the farming-pastoral ecotone of North China, but two kinds of land cover types are vital to the climate simulation.

Table 3.10 Comparison of different classification among the IGBPDIS, SCSLC, WESTDC and UMD products (km^2)

Class name	WESTDC	SCSLC	GLC	UMD
Evergreen needleleaved forest	13,174	11,532	19,250	9,075
Deciduous needleleaved forest	312	4,309	25,702	10,819
Deciduous broadleaved forest	36,330	32,120	33,971	67,687
Mixed forests	6,680	3,434	123	3,529
Closed shrublands	7,219	4,878	16,212	24,049
Open shrublands	4,198	4,945		184,674
Grasslands	267,639	234,562	325,539	265,344
Permanent wetlands	18,731	18,284	10,055	
Croplands	195,069	161,682	163,214	7,038
Urban and built-up	10,274	9,059		5,182
Cropland/natural vegetation mosaic	7,419	84,276		
Barren or sparsely vegetated	47,482	46,324	29,255	48,860
Water bodies	11,739	10,861	2,945	9

Table 3.11 The confusion matrix for the vegetation classification from land use type to land covers scheme

Class	EN	DN	DB	MF	CS	OS	Classified total	Number correct	Accuracy	
									Producer's	User's
EN	87,920	452	121	389			9,754	8,792	90.14	90.86
DN	990	5,346	327	213			5,985	5,346	89.32	84.62
DB	720	72	4,783	412			5,339	4,783	89.59	87.70
MF	7,130	448	223	4,956			6,340	4,956	78.17	83.02
CS					3,268	123	3,391	3,268	96.37	89.95
OS					365	4,222	4,587	4,222	92.04	97.17
Reference total	96,760	6,318	5,454	5,970	3,633	4,345	35,396	31,367		
Overall classification accuracy = 88.62 %								Overall kappa statistics = 0.86		

EN evergreen nedleleaved forest, *DN* deciduous needleleaved forest, *DB* deciduous broadleaved forest, *MF* mixed forests, *CS* closed shrublands, *OS* open shrublands

Throughout the classification process, the accuracy of the classification maps is assessed by a set of 35,396 sample points selected with the stratified random sampling method; these sampling points were randomly selected for each of the classes in the first generated classification map in this research. For each map, a confusion matrix is created and the accuracy is measured. The use of measurements such as the overall accuracy, Kappa statistics, producer's accuracy and user's accuracy have been quite common and have been explained in detail in numerous publications. The confusion matrix is constructed with the land cover data using the decision rule and the large scale land cover mapping with the integration of multi-source information, which is recognized as the real data. The result indicates that an overall accuracy of 88.69 % is achieved, which suggests that it gained about a 17.69 % increase in accuracy in comparison to the WESTDC map (Table 3.11).

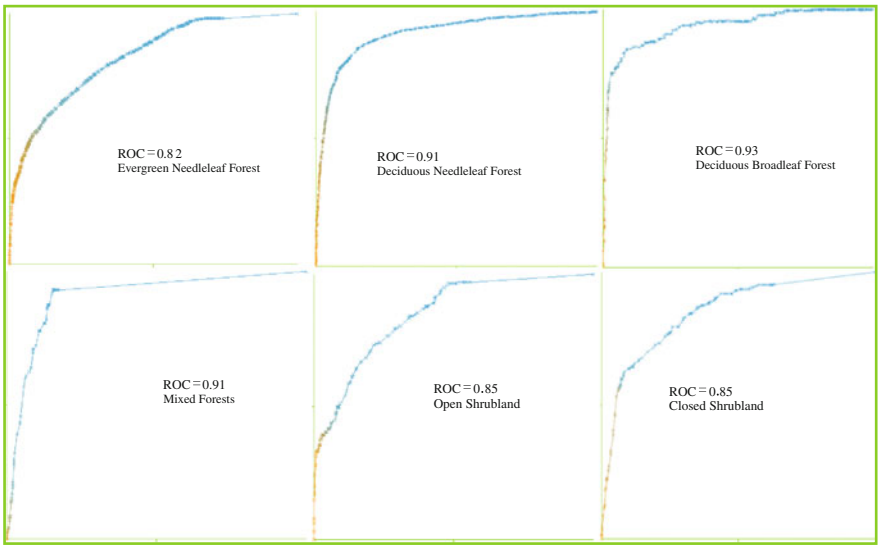

Fig. 3.14 The ROC curve value of different vegetation class rule

In addition, we draw the Receiver Operating Characteristic (ROC) curve of each forest classification decision rule using the WEKA. The true positive rate (sensitivity) is plotted in the false positive rate (1-Specificity) function for different cut-off points in the ROC curve. Each point in the ROC curve represents a sensitivity/specificity pair corresponding to a particular decision threshold. A test with the perfect discrimination (no overlap in two distributions) is carried out on the ROC curve that passes through the upper left corner (100 % sensitivity, 100 % specificity). The closer to the upper left corner the ROC curve is, the higher the overall accuracy of the test is. The area under ROC curve (AUC) for evergreen needleleaved forest, deciduous needleleaved forest, deciduous broadleaved forest, mixed forest, open shrub land and closed shrub land are 0.82, 0.91, 0.93, 0.91, 0.85 and 0.85, respectively (Fig. 3.14). The biggest value of AUC is assigned to the evergreen Broadleaved forest, indicating that the result gained by the evergreen broadleaved forest should be better than other four models.

3.3.3.2 Validation with the Ground Reference Data

It is difficult to carry out the validation of the large-scale map for all land cover types in all regions due to lack of reference data that can represent the 'true' land cover. Gong performed the validation of a global land cover map using the ground-truth sample land cover data from the global flux site (Gong 2009). In this study, the accuracy of the input land use data is high and has been validated in 2000. So we only need to validate the accuracy of the forest type and grassland type. The

Table 3.12 The ground sample sites for validation over the farming-pastoral ecotone of North China

Longitude (°E)	Latitude (°N)	Station	Land cover types
123.01	51.78	Huzhong	Temperate coniferous forests
121.56	50.83	DaXinAnLing	Cold coniferous forests
127.53	45.38	MaoErShan	Temperate deciduous forest
127.09	42.40	ChangBaiShan	Temperate mixed forest
119.94	49.33	HuLunBeiEr	Temperate meadow steppe
116.32	44.13	XiLinGeLe	Temperate grassland
117.45	43.50	XiLinHaoTe	Leymuschinensis steppe
115.99	41.27	Google earth	Evergreen needleleaved forest
115.61	40.60	Google earth	Temperate mixed forest
111.72	40.61	ShaErQin	Grassland
124.91	41.82	QinYuan	Deciduous broad-leaved forest

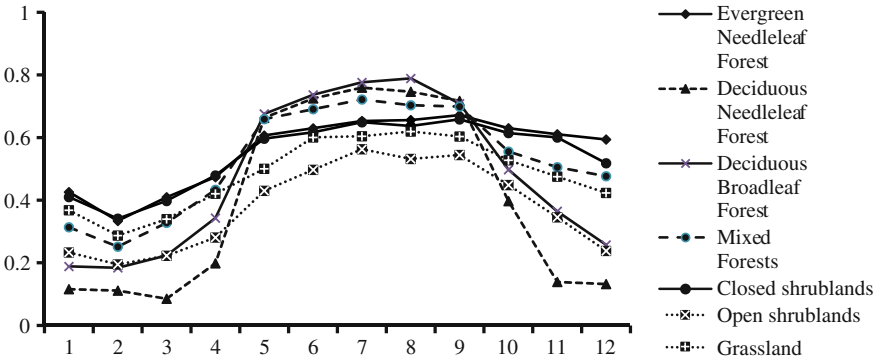

Fig. 3.15 The NDVI characteristics of different vegetation types

ground reference data, which come from multiple sources such as field investigations, TEMS and 2 samples from high-resolution images obtained via Google Earth, are used to validate land cover products (Table 3.12). The results show that overall accuracy of the SCSLC map is 83.14 % which is much higher than that of the GLC land cover map (68 %) and the UMD land cover map (52 %).

In addition, the temporal characteristics are also very important to the validation of the information of the vegetation type. We compare the temporal NDVI value of the transformed land cover data to analyze characteristics of different forest types. We evaluate the dataset according to phenological traits of vegetation which are closely related to the temperature as well as the elevation. Vegetation dynamics presents some important short-term and long-term ecological processes. The continuous temporal observations of the land surface parameters with the satellite can reveal their seasonal and annual development. In this study, we use vegetation indices of classified forests to characterize the state and dynamics of vegetation. In most cases, different types of vegetation have different phonological

patterns. The NDVI value of the deciduous broadleaved forest is the highest in those four types of vegetation, and that of open shrublands is the lowest. The statistical curve from the classified land cover maps shows that the evergreen land cover had no remarkable change during the study period. However, the deciduous forest has a single peak in the sliding curve of NDVI in a year (Fig. 3.15). The possible reason is that the deciduous broadleaved forests are mainly located in the temperate zone, while the needleleaved forests are mainly in a cold-temperate zone or on mountains in a temperate zone.

3.3.4 Concluding Remarks on the Reclassified LUCC

In this chapter, this study aims to improve vegetation classification accuracy of the land cover in North China by employing the technique of data mining different satellite-derived land cover data of China, higher-precision land use data and other ancillary spatial data. By computing the gain value of attributes for the vegetation classification, the results showed that special monthly NDVI information is the most important, and temperature is more sensitive than precipitation to the local land cover changes. Vegetation classification method identifies the classes including closed forest, shrubland and grassland with their exclusive spectral feature parameters.

The accuracy of land cover classification is assessed by comparing the classification results with some reference data that is proved with actual land cover. In this study, we find the accuracy of the C4.5 classifier is 88.96 %, which is higher than others, including NBTree, SimpleCart, REPTree and BFTree. Besides, we calculate the confusion matrix and ROC value of vegetation classification. The kappa factor is 0.87 and the ROC value almost reach 0.90 in a lump sum, but the ROC value of the deciduous broadleaved forest is only 0.74. The validation all over China show that the overall accuracy of the land cover map is 83.14 %, which is over 80 % and higher than that of other land cover maps matching requirement of climate simulation work. Therefore, the results indicate provable improvement of modeling accuracy for simulation of the land surface processes over China and which can be introduced as parameters of dynamical downscaling into other regional climate simulation.

To summarize, the developed classifier in this study can rapidly convert the high resolution CAS land use types into the land cover types for climate simulation work at regional climate models. Moreover, time-series NDVI and NPP data retrieved from the remote sensing data can fast generate high resolution time-series vegetation data and automatically recognize dynamic parameters input of the regional climate model, which can also efficiently improve the accuracy of regional climate simulation model. In addition, the results may provide supports to other land surface scientific researches.

3.4 Summary

In this chapter, specific simulations of land use changes were introduced. In the first section, we assess the possible trends of land use change that drove by social and economic development in order to better mitigate climatic change, especially CO_2 emissions. We use AGLU module of GCAM model to assess corresponding land use structural changes, and then use land use change to obtain the CO_2 emissions under each scenario. By setting three different socio-economic development scenarios,, we can choose the optimized scenario of reducing CO_2 emissions, which provides a theoretical basis of land use planning to climate change mitigation.

In the second section, we predict the future structure of land use/cover with the aid of GCAM and an econometric model. Spatial allocation of future land use/cover in China is simulated with the DLS under three scenarios, i.e., BAU scenario, REG scenario and CES. The simulation results show that land use/cover in China will change continually due to human activities and climate change, and the spatial pattern of land use/cover will also change as time goes by. Besides, the spatial pattern of land cover in China under these three scenarios is consistent on the whole, but with some regional variance. Built-up area will increase rapidly under all three scenarios, however, most of the other land cover types will show a decreasing trend to different degrees under different scenarios.

To date, high-precision land cover data to support climatic modeling in China is absent. To this end, in the third section of this chapter, we first overlay the land cover maps of the IGBPDIS, GLC, UMD and WESTDC, and select the grids with agreement of classification as the sample grids. We then combine the land cover data from CAS with the land use data to generate land cover data of high accuracy for climate simulation. The produced temporal land cover data using this method can meet the accuracy requirement of climate simulation and can be applied as the parameters of dynamical downscaling in regional climate simulation.

References

Ahlqvist O (2008) Extending post-classification change detection using semantic similarity metrics to overcome class heterogeneity: a study of 1992 and 2001 US National Land Cover Database changes. Remote Sens Environ 112(3):1226–1241

Bartholomé E, Belward A (2005) GLC2000: a new approach to global land cover mapping from earth observation data. Int J Remote Sens 26(9):1959–1977

Berg A, Papageorgiou C, Pattillo CA, Spatafora N (2010) The end of an era? the medium-and long-term effects of the global crisis on growth in low-income countries. IMF Working Papers, pp 1–29

Brenkert AL, Smith A, Kim SH, Pitcher HM (2003) Model documentation for the MiniCAM. Pacific Northwest National Laboratory, Richland, WA

Chen J, Jönsson P, Tamura M, Gu Z, Matsushita B, Eklundh L (2004) A simple method for reconstructing a high-quality NDVI time-series data set based on the Savitzky–Golay filter. Remote sens Environ. 91(3):332–344

Defries R, Townshend J (1994) NDVI-derived land cover classifications at a global scale. Int J Remote Sens 15(17):3567–3586

Deng X., Su H, Zhan J (2008) Integration of multiple data sources to simulate the dynamics of land systems. Sensors 8(2):620–634

Dong J, Xu X (2009) Land use change especially alternations of farming and grazing in typical agro-pastoral transitional zone in 1988–2000: a case study in Chifeng City of inner Mongolia. J Geo-Inf Sci 4:003

Friedl MA, Mciver DK, Hodges JC, Zhang X, Muchoney D, Strahler AH, et al (2002) Global land cover mapping from MODIS: algorithms and early results. Remote Sens Environ 83(1):287–302

Gao H, Jia G (2012) Spatial and quantitative comparison of satellite-derived land cover products over china. Atmos Oceanic Sci Lett 5(5):426–434

Ge J, Qi J, Lofgren BM, Moore N, Torbick N, Olson JM (2007) Impacts of land use/cover classification accuracy on regional climate simulations. J Geophys Res: Atmos (1984–2012) 112(D5):D05107

Geist HJ, Lambin EF (2002) Proximate causes and underlying driving forces of tropical deforestation: tropical forests are disappearing as the result of many pressures, both local and regional, acting in various combinations in different geographical locations. BioSci 52(2):143–150

Ghose M, Pradhan R, Ghose SS (2010) Decision tree classification of remotely sensed satellite data using spectral separability matrix. Int J Adv Comput Sci Appl 1(5):93–101

Gong P (2009) Accuracy evaluation of the global land cover based on the global flux observation sites. Progr Nat Sci 19:754–759 (In Chinese)

Hasselmann F, Csaplovics E, Falconer I, Bürgi M, Hersperger AM (2010) Technological driving forces of LUCC: conceptualization, quantification, and the example of urban power distribution networks. Land Use Policy 27(2):628–637

Hibbard K, Janetos A, Van Vuuren DP, Pongratz J, Rose SK, Betts R, et al (2010) Research priorities in land use and land-cover change for the Earth system and integrated assessment modelling. Int J Climatol 30(13):2118–2128

Jiang L, Deng X, Seto KC (2013) The impact of urban expansion on agricultural land use intensity in China. Land Use Policy 35:33–39

Kaptué Tchuenté AT, Roujean J-L, De Jong SM (2011) Comparison and relative quality assessment of the GLC2000, GLOBCOVER, MODIS and ECOCLIMAP land cover data sets at the African continental scale. Int J Appl Earth Obs Geoinf 13(2):207–219

Lin B, Liu J (2010) Estimating coal production peak and trends of coal imports in China. Energy Policy 38(1):512–519

Liu J, Diamond J (2005) China's environment in a globalizing world. Nature 435(7046):1179–1186

Liu J, Liu M, Zhuang D, Zhang Z, Deng X (2003) Study on spatial pattern of land-use change in China during 1995–2000. Sci China, Series D: Earth Sci 46(4):373–384

Liu J, Liu M, Tian H, Zhuang D, Zhang Z, Zhang W, et al (2005) Spatial and temporal patterns of China's cropland during 1990–2000: an analysis based on Landsat TM data. Remote Sens Environ 98(4):442–456

Liu J, Gao J, Geng B, Wu L (2007) Study on the dynamic change of land use and landscape pattern in the farming—pastoral region of Northern China. Res Environ Sci 20(5):148–154 (in Chinese)

Liu Y, Wang J, Deng X (2008) Rocky land desertification and its driving forces in the karst areas of rural Guangxi, Southwest China. J Mt Sci 5(4):350–357

Liu W, Lund H, Mathiesen BV, Zhang X (2011) Potential of renewable energy systems in China. Applied Energy. 88(2):518–525

Lutz W, Samir K (2010) Dimensions of global population projections: what do we know about future population trends and structures? Philos Trans Roy Soc B: Biol Sci 365(1554):2779–2791

Munroe DK, Müller D (2007) Issues in spatially explicit statistical land-use/cover change (LUCC) models: examples from western Honduras and the Central Highlands of Vietnam. Land use policy 24(3):521–530

Northam RM (1971) Vacant urban land in the American city. Land Econ 47(4):345–355

Patarasuk R, Binford MW (2012) Longitudinal analysis of the road network development and land-cover change in Lop Buri province, Thailand, 1989–2006. App Geogr 32(2):228–239

Ran Y, Li X, Lu L, Li Z (2012) Large-scale land cover mapping with the integration of multi-source information based on the Dempster-Shafer theory. Int J Geogr Inf Sci 26(1):169–191

Samir K, Barakat B, Goujon A, Skirbekk V, Sanderson W, Lutz W (2010) Projection of populations by level of educational attainment, age, and sex for 120 countries for 2005–2050. Demogr Res 22(15):383–472

Sertel E, Robock A, Ormeci C (2010) Impacts of land cover data quality on regional climate simulations. Int J Climatol 30(13):1942–1953

Simard M, Saatchi SS, Grandi GD (2010) The use of decision tree and multi-scale texture for classification of JERS-1 SAR data over tropical forest. IEEE Trans Geosci Remote Sens 38(5):2310–2321

Veldkamp A, Fresco L (1996) CLUE: a conceptual model to study the conversion of land use and its effects. Ecol Model 85(2):253–270

Verburg P, De Koning G, Kok K, Veldkamp A, Bouma J (1999) A spatial explicit allocation procedure for modelling the pattern of land use change based upon actual land use. Ecol Model 116(1):45–61

White R, Engelen G (2000) High-resolution integrated modelling of the spatial dynamics of urban and regional systems. Comput Environ Urban Syst 24(5):383–400

Wigley T, Raper S (1992) Implications for climate and sea level of revised IPCC emissions scenarios. Nature 357(6376):293–300

Yin RS, Xiang Q, Xu JT, Deng XZ (2010) Modeling the driving forces of the land use and land cover changes along the Upper Yangtze River of China. Environ Manage 45(3):454–465

Zhao H, Uchida E, Deng X, Rozelle S (2011) Do trees grow with the economy? a spatial analysis of the determinants of forest cover change in Sichuan, China. Environ Res Econ 50(1):61–82

Chapter 4
Projected Impacts of Cultivated Land Changes on Surface Climates in China

Qingling Shi, Haiming Yan, Ruijie Qu and Zhaohua Li

China, as a typical agricultural country with large demand for grain in the world, is vitally important to international grain market. According to *Medium and Long Term Planning Outline of National Food Security* (2008–2020), the grain output of China would reach 545 billion kg by 2020. Substantial cultivated land would be reclaimed in China in order to meet the growing food demands, which would greatly influence the future surface climate. The cultivated land reclamation in Northeast China has lasted for many years since the last century due to population continual growth and economic development at the cost of large-scale overconsumption of resources. As a result, the frequent and uneven occupation and reclamation of cultivated land have led to the significant dynamic change of the spatial pattern of cultivated land in Northeast China. This chapter analyzes the possible effects of cultivated land change on the climate in Northeast China and North China Plain based on the simulation result of the Weather Research and Forecast (WRF) model.

The possible effects of the climate change on the grain yield and the potential influence on the food security were analyzed in the first part. In the second part, we also focus on the Northeast China and analyze the possible biogeophysical effects of

Q. Shi (✉)
Institute of Geographic Sciences and Natural Resources Research,
Chinese Academy of Sciences, Beijing 100101, China
e-mail: shiql.ccap@igsnrr.ac.cn

Q. Shi
Center for Chinese Agricultural Policy, Chinese Academy of Sciences,
Beijing 100101, China

H. Yan
State Key Laboratory of Water Environment Simulation, School of Environment,
Beijing Normal University, Beijing 100875, China

R. Qu
College of Geomatics, Xi'an University of Science and Technology, Xi'an 710054, China

Z. Li
Faculty of Resources and Environmental Science, Hubei University, Wuhan 430062, China

X. Deng et al. (eds.), *Land Use Impacts on Climate*, Springer Geography

DOI: 10.1007/978-3-642-54876-5_4,

cultivated land change on the climate in northern China during 2010–2030 on the basis of simulation with WRF model. In terms of the climatic effects of past land use change, the last part of this chapter explores the impacts of land use/cover change on the near-surface temperature in the North China Plain in year 1992 and 2005.

4.1 Impacts of Cultivated Land Reclamation on the Climate and Grain Production in Northeast China in the Future 30 years

Northeast China as an important commodity grain production base in China makes important contribution to the global food security, while the historical large-scale cultivated land reclamation is of great importance to the formation and development of this commodity grain production base. Northeast China currently provides 30–35 million tons of grain every year, accounting for 13 % of the national total grain output. Besides, Northeast China as the core region of grain production of China will undertake the tasks of making the grain output increase by 15.05 billion kg, which will account for 30.1 % of the newly increased grain output. Therefore, the grain production in Northeast China will have great impacts on the Asian and even global food security (Deng et al. 2010a).

Except for the restriction of the cultivated land area, the grain production in Northeast China is also influenced by the climate change. The heat resource during the growth season of crops has shown an increasing trend in Northeast China, and the temperature has increased significantly in the past decades. For example, the relevant research indicates that the temperature in Northeast China has increased by 1.43 °C in the past century (Sun et al. 2006), which is two times higher than the global average level and three times higher than the national average level. The rapid temperature rise will surely have significant impacts on the growth of crops. It has been widely accepted that the climate change is influenced by the human activities (Pielke et al. 2011), and the land use change as one of the major approaches through which the human activities influence the climate change, has received more and more attention (Anderson et al. 2012). The change of the spatial pattern of cultivated land in Northeast China will surely lead to the climate change at local and regional scales. The historical data indicate that along with the cultivated land reclamation, there has been significant climate change in Northeast China, including the obvious change of the spatial pattern of temperature, and precipitation. (Deng et al. 2006).

Some of previous studies predict the climate change in the future just simply according to history climate data and their variation trends (Peterson et al. 2002). It is well known that there is uncertainty in climate change and abnormal weather always occur especially in recent decades, which made the history trend unreliable to represent the real one. Therefore, the shortage of this method was obvious. For that reason, some scientists devoted to predict future climate with

models (Hijmans and Graham 2006). The WRF model is a next-generation mesoscale numerical weather prediction system developed by a group of scientists from different institutes. This model is of strong robustness for predicting the climate changes with various parameters, such as temperature, precipitation, radiation, and heat flux. Besides, in this study, the underlying surface data adopted in WRF model was simulated data given by the Dynamics of Land Systems (DLS) model.

4.1.1 Data and Methodology

4.1.1.1 Introduction of the Study Area

Northeast China (115°05′ ~ 135°02′ E, 38°40′ ~ 53°34′ N) has a total land area of 1.24 million km^2 and covers 209 counties in Heilongjiang Province, Jilin Province, Liaoning Province, and Inner Mongolia Autonomous Region (Fig. 4.1). It is the largest producing area of the corn, high quality japonica rice, and soybean as well as the major production base of the agriculture, forestry, animal husbandry, and industry in China. The total cultivated land area in this area is approximately 227 million hectare, accounting for 18.5 % of the national cultivated land area. The area under crops is approximately 173 million ha and the total grain output is approximately 87 million t in Northeast China, which account for 16.4 and 17.6 % of the national total amount, respectively.

As a monsoon climate of medium latitudes, the amount of precipitation in Northeast China decreases from the east and southeast to the west and northwest on the whole area. The winter is cold and long, while there are frequent winds and little rainfall in the spring in Northeast China. In the summer, the temperature is high and the rainfall is very rich, the amounts of precipitation range from 400 to 700 mm in most part of Northeast China in the summer, accounting for 50–70 % of the annual precipitation. According to the observation data of climate change from 2000 to 2010, we calculated the change trend of temperature and precipitation in Northeast China. The results showed that the temperature increased slightly in the decade, the average growth rate per annum was 0.44 %. While the average annual precipitation was in similar circumstance, its average growth rate per annum was 1.16 %. There are often sunny days and the southwest winds prevail in the autumn, but the amount of precipitation is slightly more than in the spring. Northeast China is the coldest area in China since it is at the high altitudes, the temperature in this region is very low in the winter and the annual temperature difference is very large, showing obvious characteristics of the continental climate. Besides, Northeast China can be divided into three climatic zones from north to south, i.e., the cold temperate zone, the cool temperate zone, and the warm temperate zone since it extends across a wide latitude and longitude. In addition, it can be further divided into several climatic zones from east to west, i.e., Three River Plain Humid Climate Zone, Lesser Khingan Mountains Climate Zone, Great

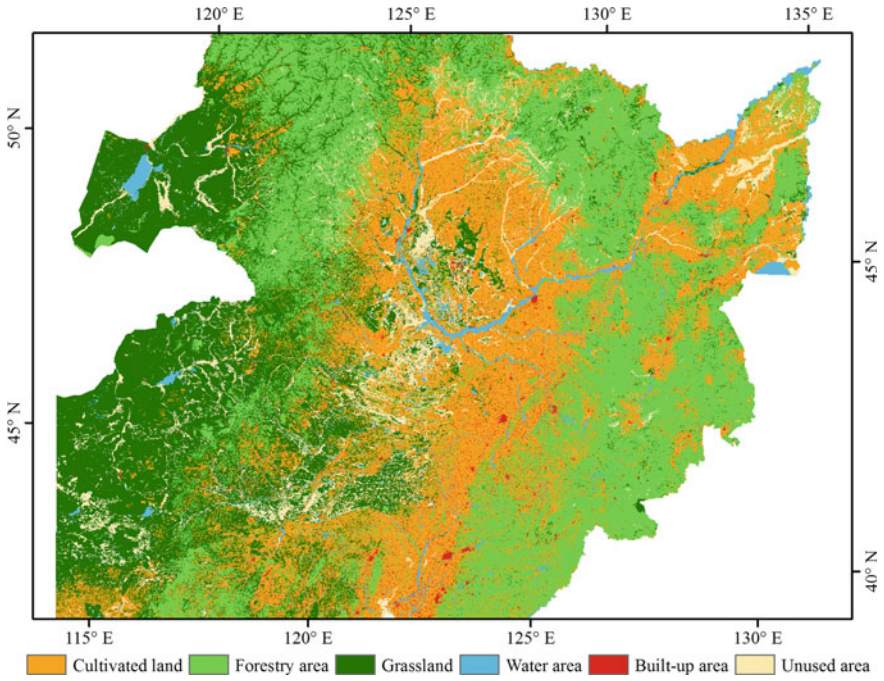

Fig. 4.1 Main land use types of Northeast China in 2010

Khingan Mountains Sub-humid Climate Zone, Songliao Plain Sub-humid Climate Zone, West Liaohe Plain, and Eastern Inner Mongolia Arid Climate Zone.

Northeast China is the fertile grain production area with great potential capability of development and significant contribution to the national food security. Most part of the Northeast Plain and the valleys and tablelands between Changbai Mountains has been reclaimed for cultivated land so far. These regions have been the major farming area for agricultural production in Northeast China, but at the cost of the disappearance of primary forests and grasslands. The scale of the grain production is very large, the major crops including the corn, soybean and rice, because high level of agricultural mechanization in Northeast China have been developed as the earliest reclamation area of agricultural mechanization with its best cultivatable soil conditions since the last century of China. In addition, total 6 billion km^2 of the forest area accounts for 28.1 % of the total national forest stock in Northeast China.

This chapter analyzes the impacts on the climate change of cultivated land reclamation by analyzing the change of temperature and precipitation numerical predicted on the basis of cultivated land change in 30 years in Northeast China, which was simulated by DLS model in previous study (Deng et al. 2010b). The changing trend of the climate in the future is predicted in the context of the change of the spatial pattern of cultivated land, and the impacts of the climate change on

grain production is also analyzed. This will not only provide a typical case study to the research on the global climate change, but also some reference for the development of social industry structure.

Meanwhile, the trend of climate change and regional climate effects of Land Use and Cover Change (LUCC) in Northeast China indicate that there will be more complex and significant climate change in Northeast China. Which means the change trends of temperature and precipitation were not simply increasing or reducing by year, they were up and down and what's more, they showed different tendencies in different seasons. Therefore, it is of great significance to study the impacts of cultivated land reclamation on the climate and grain production in Northeast China and the results can provide significant technical support and policy suggestions for the development of Northeast China.

4.1.1.2 Experiment Design

In order to draw the impact on climate change of cultivated reclamation, two simulated tests were designed in this study; control test and sensitivity test (Table 4.1).The two sets of test used the climate forcing data between January of 2000 and December of 2010, and the difference between them is the underlying surface data. In the control test, the test period is from January of 2000 to December of 2010. The land cover data of 2000 is used as underlying surface data in the test. As to sensitivity, its test period is from January of 2030 to December of 2040. And with land cover data of 2040 as its underlying surface data. The experiment is designed to avoid the influence of forcing data and simultaneously to focus the impact of land use change, specially the cultivated land reclamation on the climate variation. Thereby, the effect on grain production of the reclamation of cultivated land in the Northeast China would be uncovered in this study.

4.1.1.3 Data and Processing

As the simulation time is January of 2000 to December of 2010 and January of 2030 to December of 2040, the underlying surface data used in this study are the land use/cover data in 2010 and 2040 as mentioned in the experiment design section. The former period of data is the real land use/cover data provided by Data Center for Resources and Environmental Sciences, CAS. And the latter data is simulated by DLS model with the land use/cover data of 1 km resolution in 1985, 1995, 2000, and 2005 as its simulated initial year data. The data of four time periods were obtained from Data Center for Resources and Environmental Sciences, CAS. The database is constructed from remote sensing digital images by the US Landsat TM/ETM satellite with a spatial resolution of 30 by 30 m (Deng et al. 2010c). According to the simulated results, the cultivated land reclamation data during 2030–2040 were obtained in Northeast China (Fig. 4.2) (Deng et al. 2010d). According to the simulation results with the DLS model, the cultivated

Table 4.1 Schemes of the simulation test with WRF model

Test	Test period	Underlying surface data	Climate forcing data
Control test	2000.01–2010.12	Land cover data of 2010	Climate forcing data between 2000.01 and 2010.12
Sensitivity test	2030.01–2040.12	Land cover data of 2040	Climate forcing data between 2000.01 and 2010.12

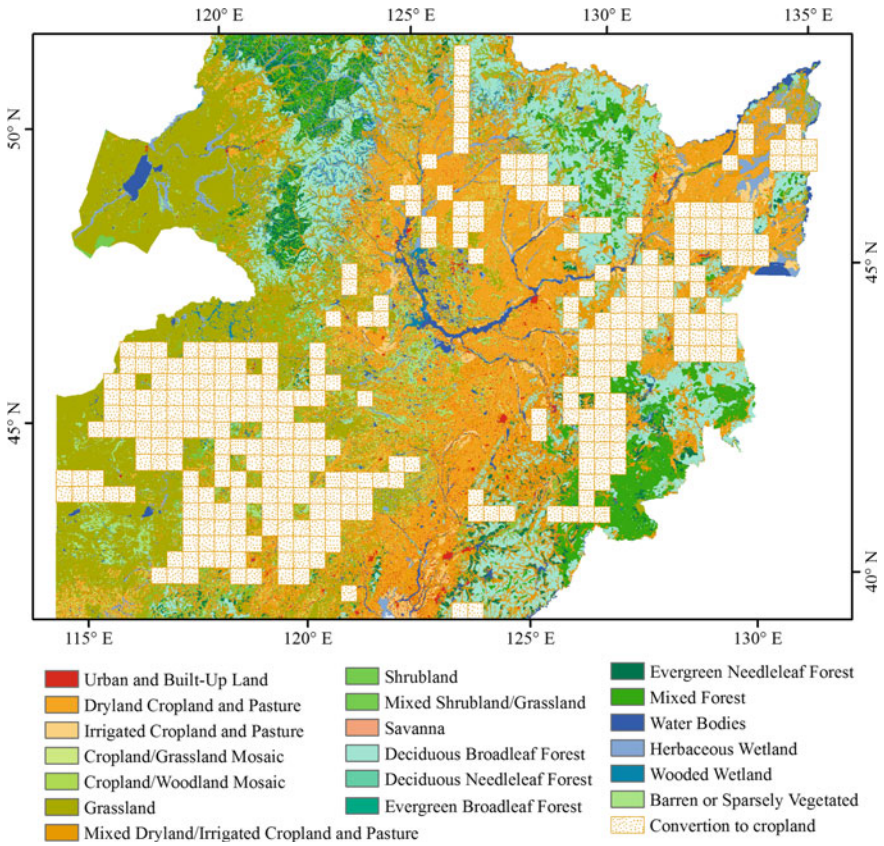

Fig. 4.2 Conversion amount of other land use types into cultivated land in Northeast China during 2030–2040

land area in Northeast China will increase by 288 thousand km^2 during 2030–2040, with an increment rate of 21.62 %. The newly increased cultivated land will mainly be located in Eastern part of Three River Plain, western part of Songnen Plain, Hilly, and mountainous area in Great Khingan Mountains and Lesser Khingan Mountains, and Hulunbuir Region. Besides, the newly increased cultivated land will be mainly converted from the forests, grasslands, and unused land (Deng et al. 2010d).

Table 4.2 Land use/cover types of the USGS classification system

Code	Description	Code	Description
1	Urban and built-up land	14	Evergreen needle leaf forest
2	Dryland cropland and pasture	15	Mixed forest
3	Irrigated cropland and pasture	16	Water bodies
4	Mixed dryland/irrigated cropland and pasture	17	Herbaceous Wetland
5	Cropland/Grassland Mosaic	18	Wooded Wetland
6	Cropland/woodland Mosaic	19	Barren or sparsely vegetated
7	Grassland	20	Herbaceous Tundra
8	Shrubland	21	Wooded Tundra
9	Mixed shrubland/Grassland	22	Mixed Tundra
10	Savanna	23	Bare ground Tundra
11	Deciduous broadleaf forest	24	Snow or Ice
12	Deciduous needle leaf forest	99	Interrupted areas (goodes homolosine projection)
13	Evergreen broadleaf forest	100	Missing data

Due to the land use/cover data classification mechanism in WRF model is the USGS classification system (Table 4.2), and the simulated land use/cover data in 2040 with DLS model were classified by the land cover classification of IGBP. The simulated data were reclassified into USGS classification system with classifier we developed before. In addition, the scale of these data is 1:100000 and the interpretation accuracy exceeds 92 % (Liu et al. 2010).

The climate forcing data used in this study were the geographically segmented (GEOG) data obtained from NCEP FNL (Final) Operational Global Analysis data, which is updated every 6 h. This dataset has been constructed and updated since July of 1999 with the data assimilation of almost all kinds of observation data (e.g., the remote sensing data and ground-based observation data), it has the spatial resolution of $1^\circ \times 1^\circ$ and the vertical height of 27 layers. And the time period of the data were truncated from the January of 2000 to December of 2010. Then the climate forcing data were prepared on the basis of these data. The NCEP/FNL dataset has higher accuracy and spatial resolution and includes more kinds of environmental variables than the datasets of NCEP I, NCEP II and EAR40. This study has used the Noah land surface parameterization scheme, with which the simulation result is more stable and reasonable. The data of the temperature field and precipitation field in this scheme were interpolated with the large scale information.

4.1.2 Results

The change of cultivated land in Northeast China is directly caused by the human activities in the context of the special regional geographical conditions, such as the plenty of the complex mountains in this region. The population growth is the fundamental reason for the expansion of cultivated land in Northeast China, the

economic development is an important human driving factor, and the macro policy is also one of the driving factors of the land use change. With the continual population growth and rapid economic development in Northeast China, there will be more demand for the land resources, which will surely lead to the change of the amount, structure, mode, and intensity of land use. It is forecasted that the population of China will rise to the peak during 2030–2040, reaching 1.5–1.6 billion. The cultivated land area in China will certainly be increased so as to meet the enormous demand of the large population for grain, forage, dairy products, etc. It is inevitable that a lot of land will be reclaimed for agricultural cultivation in Northeast China Since it is the most important commodity grain base with the greatest development potential in China. For these reasons, this study simulated the climate change under the condition of cultivated land reclamation during 2030–2040 based on the WRF model and predicted the future changing trend of the temperature, precipitation in Northeast China. The simulation results indicate that the temperature in Northeast China will show an increasing trend, while the precipitation will show a decreasing trend. The average temperature in Northeast China shows an increasing trend on the whole during the simulation period. The temperature will increase in most parts of Northeast China in January except few areas where it shows a decreasing trend; while in August, it shows an increasing trend in almost all the parts of Northeast China. The temperature change varies greatly among regions; it shows an increasing trend from the southeast to the northwest on the whole, with the largest increment of 2 °C. The temperature increases most obviously in the northern part of Great Khingan Mountains and Lesser Khingan Mountains, while it increases most slightly in Liaohe Plain, Liaodong Peninsula and southern part of Changbai Mountains (Fig. 4.3). The temperature rise in these regions is closely related with the land use conversion in the future, for example, the conversion from forests and grasslands into cultivated land. Great Khingan Mountains and Lesser Khingan Mountains lead to the increase of the regional near-surface temperature not only in the regions with land use conversion, but also in the regions without land use conversion.

The simulation result indicates that there is no significant change of the annual precipitation in Northeast China during 2030–3040, but there is some fluctuation of the seasonal precipitation. The precipitation will increases most greatly in the middle part of Heilongjiang Province and the eastern part of Jilin Province and Liaoning Province. Besides, the precipitation will increase most significantly in the summer, and it will decrease in some regions in the winter. The precipitation will show a decreasing trend on the whole in January; it will show very different changing trends in different regions in August, but still show a decreasing trend on the whole. The precipitation will decrease by 80 mm on average in January, with the largest decrement reaching 120 mm. By comparison, it will change more significantly in August (Fig. 4.4). The precipitation will decrease most greatly in Liaodong Peninsula and the southern part of Changbai Mountains, while it will increase obviously in the northern part of Great Khingan Mountains and Songnen Plain. In addition, it will show great difference at the local scale during different periods since there are some instabilities of the precipitation.

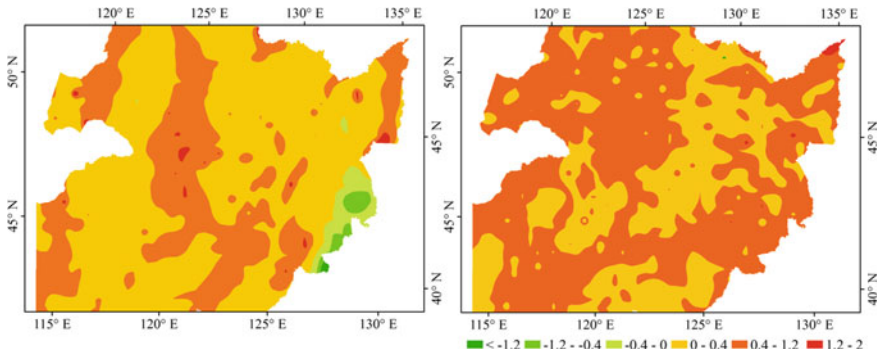

Fig. 4.3 Temperature change in Northeast China in DJF (December, January and February) (*left*) and JJA (June, July and August) (*right*) during 2030–2040

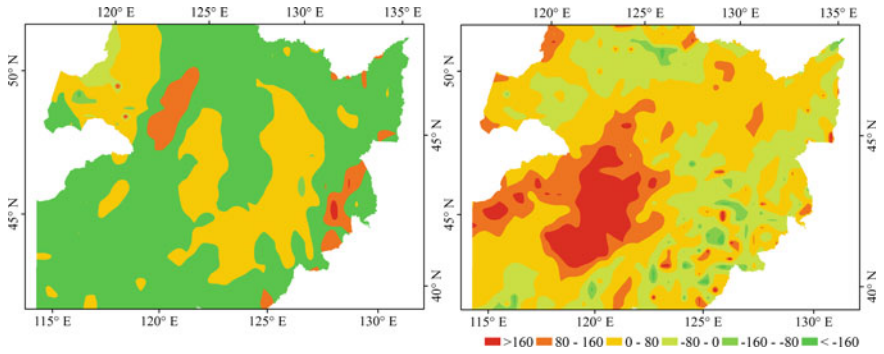

Fig. 4.4 Change of precipitation in Northeast China in DJF (*left*) and JJA (*right*) caused by land use/cover change during 2030–2040

The previous researches have indicated that the climate change will have significant impacts on the crop yields, and there is significant regional difference of these impacts (Deng et al. 2010c; Sun et al. 2006b). When the temperature increases by 1 °C, the per unit area yields of the wheat and soybean may increase by 2–40 %, and the decrement is higher in the northeast part than it is in the southwest part of Northeast China. When the precipitation increases by 10 %, the grain yield will increase by approximately 10 % in the western and southwest part, while it is the contrary in the southeast part (Ma 1996). However, the temperature rise may aggravate the decrease of precipitation, since they generally appear simultaneously. In addition, the previous research indicate that when the temperature increases by 2 °C and the precipitation decreases by 20 %, the grain yield in the western part of Northeast China will decrease by 10–18 % (Ma 2008). Therefore, the future grain yield in Northeast China will show a decreasing trend on the whole, and the grain yield and soybean yield may decrease by at least 10 % in the future.

This study simulated the climatic effects of cultivated land reclamation in Northeast China during 2030–2040. The simulation results indicate that it will inevitably aggravate the drought disaster in Northeast China. In summary, the regions with the most extreme temperature change are mainly located in the northern part of Great Khingan Mountains and Lesser Khingan Mountains; while the regions with the significant precipitation change mainly gathered in the northern part of Great Khingan Mountains and Songnen Plain. Since these regions are located in the major grain producing areas in Northeast China, the climate change due to the cultivated land reclamation will have great impacts on the grain yield in Northeast China.

4.1.3 Concluding Remarks on the Cultivated Land Reclamation

The change of the spatial pattern of land use in Northeast China in the future, mainly including the expansion of cultivated land, will influence the supply function of regional ecosystem services to some degree. It should be noted that although the cultivated land area in Northeast China will show an increasing trend, the population will increase more rapidly, which will lead to the reclamation of some marginal land that is not very suitable for reclamation. Since the rapid population growth will lead to more demand for the food and land resources, some problems such as the deforestation, reclaiming land from lakes, and grassland reclamation, may be more serious and lead to a vicious cycle. Besides, some of the newly increased cultivated land may be not reasonably used, and the extensive operation is still very widespread, which will inevitably lead to the deterioration and waste of the land resources. The decline of soil fertility will undermine the potential of grain yield increase, influence grain production capacity of Northeast China, and subsequently influence the grain production capacity of whole China, and consequently threaten the self-supply of grain and national food security. It is necessary to properly implement some measures in the planning of the future agricultural development in Northeast China on the premise of guaranteeing the strategic grain demand of the whole nation. Besides, it is necessary to improve the scientific and technological level of agricultural cultivation, promote the ecological construction, and enhance the land utilization rate. In addition, it is necessary to implement different agricultural production countermeasures according to the impacts of climate change on different crops in different regions, e.g., adjusting the of the layout of crop variety and planting structure, enhance the measure to prevent disasters so as to ensure the long-term and steady development of grain production.

The temperature will show an increasing trend on the whole, which will have negative impacts on the growth of the major crops, such as rice, corn, soybean, and wheat. The regional climate change will also directly and indirectly influence the behaviors of the peasants. For example, it will directly lead to the change of the planting structure and tillage measures; besides, it will lead to the change of the

grain yield, indirectly change the income of peasants, and consequently alter their production activities. In addition, since different crops have different adaptive capacities to climate change, which will greatly influence the peasants' choice of the kinds of crops and consequently lead to more serious imbalance of the plantation structure. For example, in the middle and western part of Northeast China, where one of major crops is the rice, when the temperature increases and the precipitation decreases, the local peasants may replace the rice with other crops or offset the impacts of climate change on the rice by using more fertilizers or irrigating the crops with more water. So the grain production in Northeast China has some potential to adapt to the temperature rise, and it is of great significance to alleviate the negative impacts of the temperature rise on grain production and guarantee food security in Northeast China to give full play to this potential.

This study has mainly aimed at the simulation and prediction of the change of temperature and precipitation caused by the cultivated land reclamation in the future. In order to forecast the climate change in the future more accurately, it is necessary to quantitatively analyze the changing trends of the temperature and precipitation, and comprehensively take into account the future changes of the monsoon, general atmospheric circulation, change of other land use types, etc. in the climate model and data analysis. Therefore, there is still something to explore in the future researches. First, the regional climate change is caused by various factors, including not only the human activities, but also the natural factors such as the solar activity. Besides, there are also various human activities that influence the regional climate change in Northeast China, but only the cultivated land reclamation has been taken into account in this study, so more influencing factors should be included in the future research. Second, there are some uncertainties in the simulation. Due to those influenced factors, the effects of some of them on the climate change may not be captured in the simulation analysis, which will lead to some uncertainties in the simulation results. So it is necessary to make further sensitivity analysis in the future research so as to make the simulation results more accurate.

4.2 Possible Biogeophysical Effects of Cultivated Land Conversion in Northeast China in 2010–2030

Human activities are widely recognized as one of the major contributors to climate change, through both combustion of fossil fuels and land use activities (Lobell et al. 2006), with the LUCC considered as the major influencing factor. Many studies have revealed the extent to which land cover changes have affected local and regional and even global climate (Marland et al. 2003). For example, previous studies suggested that human-induced land cover change from forest to cultivated lands could lead to a cooling of 0.25 °C on a global basis, and northern mid-latitude agricultural regions are about 1–2 °C cooler in the winter and spring compared to the pre-industrial state due to replacement of forest by cultivated lands. A lot of observations and simulation experiments have suggested that the

LUCC at various scales has been the most important approaches through which the human activities influence the climate (Feddema et al. 2005), and it is of great importance to study the influence of LUCC on the regional climate.

Improved understanding of how human activities influence climate is needed to guide policies aimed at mitigating or adapting to climate change (Lobell et al. 2006). However, most of current climate mitigation policies do not generally incorporate the effects of changes in the land surface on the surface albedo, the fluxes of sensible and latent heat to the atmosphere, and the distribution of energy within the climate system, all of which can affect the local, regional, and global climate, and therefore these policies might lead to land-management decisions that do not produce the intended climatic results (Marland et al. 2003). Besides, a number of models have been used to study the impacts of LUCC on the climate, but most of them do not account for geographically explicit changes in land surface characteristics associated with land cover changes (Sitch et al. 2005). In addition, there are many land use changes not reflected in land cover that can potentially influence climate, including both conversion and other modifications (Feddema et al. 2005), e.g., changes occurring within existing cultivated lands that have the potential to affect local and global climate (Lobell et al. 2006). Moreover, scientific understanding and tools are increasingly becoming available to address the broader implications of land surface interactions within the climate system for national and international policy. It is plausible to implement more in-depth researches on the effects of LUCC on the climate change with the geographically explicit tools.

China is one of the largest developing and populous countries. The large demand of grain for feeding increasing population generates a large demand of cultivated land for increasing agricultural production as well as other types of land use demands for rapid economic development. Northern China, as a grain production base with adequate cultivated land resource, is protecting the food security and economic development of whole China (Fig. 4.5). In Northern China, population density with economy growth is relatively high, and continuous population growth and accelerating economic development would further lead to dramatic LUCCs and consequently exert more significant impacts on the climate change. In fact, the land use has changed a lot in this region after the Chinese economy structural reformation was initiated in the early 1980s. The area of high quality cultivated land has shrunk due to the growing land demand of the urban expansion and infrastructure construction in this region (Jiang et al. 2012). Meanwhile the regional climate in Northern China has changed greatly due to the disturbance of human activities, especially the land use change in the past decades. For example, the temperature has risen more and more obviously in the past decades, which further led to the increased drought time, more dramatic precipitation fluctuation, decreased climate productivity, and more frequent climate disasters (Liu et al. 2008). Previous researches have indicated that there is surely some correlation between the significant climate change and the large-scale LUCC in Northeast China in recent decades (Liu 2007). Therefore, it is of great importance to analyze the interaction between the LUCC and climate change to understand the impacts of LUCC on the grain production in Northeast China since the land resource is

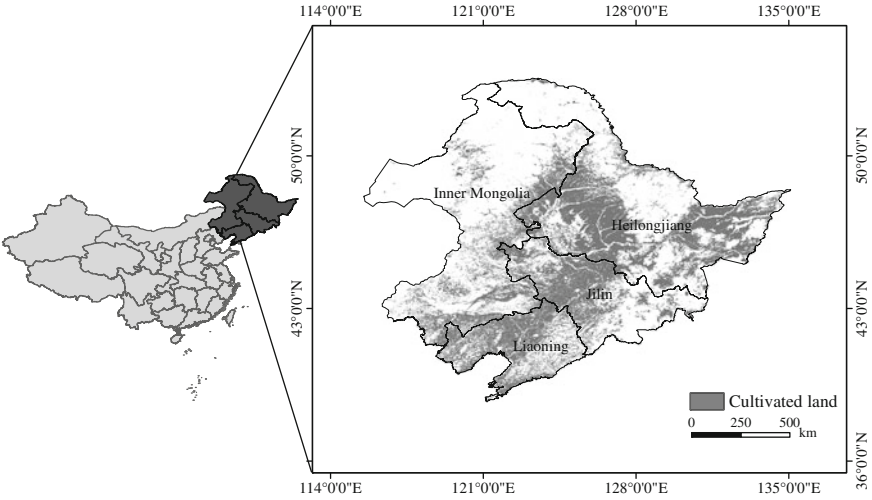

Fig. 4.5 Location of Northeast China. Northeast China mainly covers Heilongjiang Province, Jilin Province, Liaoning Province, and the southeastern part of Inner Mongolia Autonomous Region

indispensable to most essential human activities and provides the basis for agricultural and forest production, recreation and settlement, etc. In this study, the potential biogeophysical effects of cultivated land change were analyzed on the base of the scenario analysis on the land use change and simulation of climate change with WRF model.

4.2.1 Data and Methodology

The simulation is implemented based on the land cover data and forcing data under different scenarios. First, the scenario analysis is carried out on the future LUCC in Northeast China, which provides the time series underlying surface data for the simulation with WRF model. Three scenarios of land use change are designed according to characters of socioeconomic development in the study area, and the structural change of land use is simulated with the module of Agriculture and Land Use in the Global Change Assessment Model (GCAM), with the socioeconomic factors as the driving force. Thereafter, the future spatial pattern of land cover during 2010–2030 is simulated with the DLS model (Deng et al. 2008), and finally the climate effects of the land use change is analyzed based on simulation with WRF model.

4.2.1.1 Scenario Design of Land Use Change

Three scenarios, including the Business as Usual (BAU) scenario, Rapid Economic Growth (REG) scenario, and Coordinated Environmental Sustainability (CES)

scenario, were designed based on the historical changing trends of land cover and the historical and future trends of socio-economic development. This study selected the population, total factors productivity (TFP), gross domestic product, (GDP) and national policy as the variables of socio-economic development, the changing trends of which are different under different scenarios. The BAU scenario mainly reflects historical development trend of the population and economy, which provides the reference to compare with other scenarios. It is assumed that the urbanization and industrialization will continue under the BAU scenario; TFP, which is on behalf of the scientific and technological progress, will develop following the historical development trend, and China's population is expected to peak in 2030, but the population growth rate will gradually reduce. The REG scenario and CES scenario were designed according to the main risks and adjustment directions of the medium and long-term development of China. The REG scenario assumes that the structural reform of industries would be smoothly carried out, the resource allocation and distribution of the industrial structure will be more reasonable, and the economy will develop more and more quickly. Under the CES scenario, the population growth rate is lower than that of BAU scenario, the urbanization rate is relatively lower, and population and GDP would increase with a lower rate. Finally, with the socioeconomic factors as the driving force, the structural change of land use under each scenario is simulated with the module of Agriculture and Land Use in GCAM.

4.2.1.2 Simulation with the DLS Model

This study simulated the spatial pattern of land cover change in the study area with the DLS model, which is a collection of programs that simulates pattern changes in land uses by conducting scenario analysis of the area of land use change (Deng et al. 2008). The DLS model can export a macroscopic map of land use by estimating the effects of driving factors of spatial pattern changes, formulating land use conversion rules and scenarios of land use change, and simulating dynamic spatiotemporal processes of land use changes (Deng et al. 2008). The simulation with the DLS model includes four steps. First, the statistical relationship between the spatial distribution of land use types and the driving factors is analyzed at the regional and grid scales, and the key driving factors were extracted according to the effects of the natural environment and socio-economic factors on the spatial patterns of regional land use. Then the changing trend of the selected key driving factors is predicted based on their historical characteristics and current status at the regional level. Thereafter, a proper scenario is identified and used to foresee the balances between the supply and demand of land resources. Finally, the spatial allocation of land cover is implemented at 1×1 km grid pixel level, and the spatial pattern map of land cover is generated.

4.2.1.3 Simulation with WRF Model

WRF model is a next-generation mesoscale model developed by a group of scientists from different institutes (Hernández-Ceballos et al. 2012).It consists of three parts, including pre-processing module of mode (WPS), main module of model (ARW), and assimilation module of mode and post-processing tools of mode data (WRF-VAR). The ARW is used to analyze the impacts of land use/cover change on the land surface heat flux in this study. This study calculates the flux of momentum, sensible heat, latent heat and radiation, etc. between the land surface and the atmosphere from the perspective of the water balance and energy balance with WRF model. Based on the Noah land surface parameterization scheme, and focused on the sensible heat flux and latent heat flux, the study reveals the impacts of the future land use change on the regional climate change.

The land net radiation is the energy source of near-surface temperature change, and the latent heat flux and sensible heat flux are two key components of the land surface energy balance. Both of them are closely related with the efficient energy of the land surface and are influenced by the land surface characteristics and soil water and heat conditions. Besides, under the condition of certain land surface net radiation the underlying surface influences the temperature through influencing the sensible heat flux, latent heat flux, and soil heat flux.

$$Rn = H + LE + G \tag{1.1}$$

Where Rn is the land surface net radiation, H is the sensible heat flux, LE is the latent heat flux, and G is the soil heat flux.

The land surface net radiation heavily depends on the sensible heat flux and latent heat flux since there is generally very limited heat flux into soil, and the underlying surface can directly influence the latent heat flux and consequently indirectly influence the near-surface temperature. Therefore, this study has mainly focused on the influence of land use change on the latent heat flux and sensible heat flux. Since the temperature is generally very low in the spring and winter in Northeast China, this study has only calculated the sum of the latent heat flux and sensible heat flux in the summer and autumn.

The parameterization scheme of the WRF model in this study includes the Noah land surface parameterization scheme, CAM3 radiation scheme, WSM3-class simple ice microphysics (MP) scheme, Grell-Devenyi ensemble scheme for cumulus convection, and YSU boundary layer scheme. The data of the lateral and boundary conditions came from the NCEP/FNL, being updated every 6 h. This dataset has been constructed and updated since July of 1999 with the data assimilation of almost all kinds of observation data (e.g., the remote sensing data and ground-based observation data), it has the spatial resolution of $1° \times 1°$ and the vertical height of 27 layers. The NCEP/FNL dataset has higher accuracy and spatial resolution and includes more kinds of environmental variables than the datasets of NCEP I, NCEP II, and EAR40. The land surface parameters in WRF model under different conditions of land cover were adjusted according to the result of scenario analysis of the future land use change.

The simulation scheme in this study is as follows. The land cover dataset of year 2010 with the United States Geological Survey's (USGS) classification system is used as the baseline underlying surface data in this study. Then, the structural changes of land use in year 2010 and 2030 under different scenarios were simulated with the module of GCAM and the future spatial pattern of land cover is simulated with the DLS model. Furthermore, the land use data is used as the input underlying surface data of the WRF model to simulate the impacts of land cover change on the climate change.

4.2.1.4 Data and Processing

The input data of WRF model mainly include the underlying surface data and climate forcing data. The 1 km resolution land cover data of the USGS classification system in year 2010 were used as baseline data in this study. The baseline data of land use/cover change were derived from the dataset of the National Key Programme for Developing Basic Science in China (Grant No. 2010CB950900). These data of the 1 km resolution were extracted from Landsat TM/ETM images and classified according to the USGS classification system, the interpretation accuracy of which exceeds 92 % (Liu et al. 2010). The land use/cover data in year 2020 and 2030 were predicted with the data of land conversion among land cover types. Since different communities have different classification systems for the land cover data, this study used the USGS classification, which includes 24 land cover types. First, the 1 km resolution land cover data of USGS classification in year 2010 were extracted from the USGS remote sensing images, and were used as the land cover data in the baseline year. Then the land conversion data, which are used to forecast the land use change (land conversion among different land cover types) during 2010–2030, were simulated with the DLS model based on the different scenarios designed according to the land demand. Finally, the 1 km resolution land cover data were converted into the 10 km resolution data according to the requirement of WRF model.

The forcing data needed in WRF model include the wind field, surface air temperature, long-wave radiation, and short-wave radiation. This study used the climate forcing data from NCEP/FNL (Final) Operational Global Analysis data, which is updated every 6 h. This dataset has been constructed and updated since July of 1999 with the data assimilation of the remote sensing data and ground-based observation data, etc. The NCEP/FNL dataset has higher accuracy and spatial resolution, and it has the spatial resolution of $1 \times 1^{\circ}$ and the vertical height of 27 layers. The static land surface data were the GEOG data provided by WRF model, which were replaced with the land use/cover data under different scenarios in the further simulation. This study has used the Noah land surface parameterization scheme, with which the simulation result is more stable and reasonable. The data of the temperature field and precipitation field in this scheme were interpolated with the large scale information.

4.2.2 Results and Discussion

4.2.2.1 Cultivated Land Change Under Different Scenarios

The simulation results indicate that the land use change in Northeast China during 2010–2030 is mainly characterized by the conversion from cultivated land into forests or urban and built-up land under the three scenarios; the total cultivated land area will show a decreasing trend (Fig. 4.6). The land use change will follow the historical trend under the BAU scenario; the cultivated land will mainly change into urban and built-up land and forests, the newly increased area of which will reach approximately 3,782 and 1,471 km^2 by 2030, respectively. Besides, a few water bodies will convert into cultivated land under the BAU scenario. By comparison, there will be more cultivated land converted into urban and built-up land under the REG scenario and forests under the CES scenario, the newly increased area of which reach 1,889 and 3,798 km^2, respectively. In addition, the cultivated land change will show significant spatial heterogeneity under the three scenarios. The conversion from cultivated land into forests mainly appears in the southern part of Heilingjiang Province, southern and middle part of Jilin Province, and southern and eastern part of Liaoning Province. While the conversion from cultivated land into urban and built-up land will mainly appear in the southern and eastern part of Liaoning Province, middle part of Jilin Province, and eastern part of Helongjiang Province. What is more, compared to the BAU scenario, more cultivated land change will convert into urban and built-up land in the regions around cities under the REG scenario. More cultivated land will change in forests in the regions far from cities under the CES scenario, especially in some important water conservation area such as Three River Plain and Changbai Mountains.

The land use change in Northeast China is greatly influenced by the socioeconomic activities, with the conversion from cultivated land into forests and urban and built-up mainly driven by the governmental policies, socioeconomic development, and urbanization. For example, a series of major ecological construction projects have been implemented, e.g., Three-North Forest Shelterbelt Program and Green for Grain Project, all of which greatly promoted the expansion of the forests in Northeast China. For example, a lot of mixed dryland/irrigated cropland has converted into grassland or mixed forests in the eastern part of Inner Mongolia Autonomous Region, middle, and eastern parts of Heilongjiang Province and Jilin Province; the vegetation degradation in Northeast China has been under control to some degree. Besides, the urban land expansion has led to the occupation of cultivated land around the cities. The simulation results also suggest that more cultivated land around the metropolis and small cities will be occupied since the socioeconomic development leads to more demand for land resources. In summary, under the influence of urbanization and governmental policies, the spatial heterogeneity of cultivated land reclamation and occupation will lead to more significant spatial heterogeneity of cultivated land, which will exert significant impacts on the regional climate.

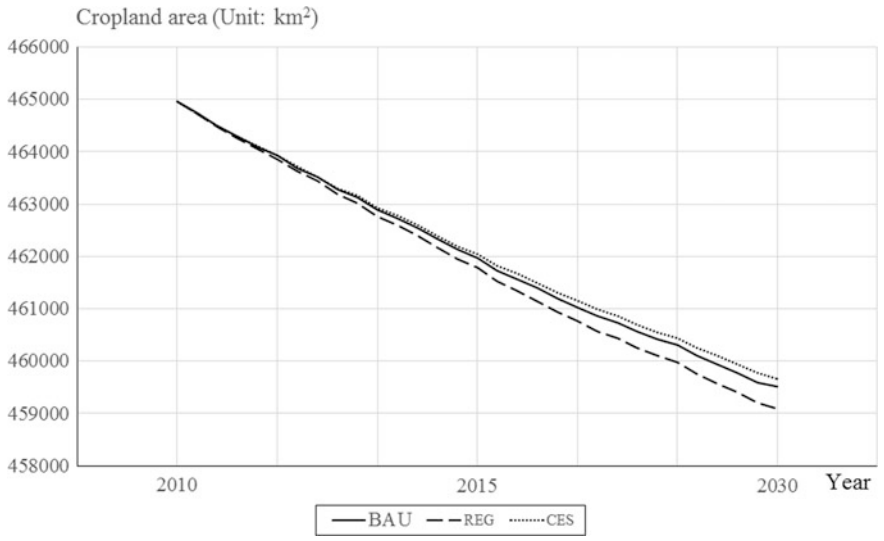

Fig. 4.6 Changing trends of total cultivated land area in Northeast China during 2010–2030 under the three scenarios

4.2.2.2 Influence of Future Cultivated Land Change on the Land Surface Energy Balance

The simulation under the three scenarios all indicate that the average latent heat flux in Northeast China shows a decreasing trend, while the average sensible heat flux shows an increasing trend, but both of them show some regional heterogeneity (Fig. 4.7). Compared to 2010, the latent heat flux in 2030 will decrease by 0.05–0.07 W/m^2 on average and show a decreasing trend on average. The latent heat flux will decrease slightly in most part of the study area. It will decrease significantly in only a few regions, such as the western part of Jilin Province and southern part of Heilongjiang Province, where a lot of cultivated land will change into urban and built-up land, with a decrement of approximately 10 W/m^2 on average. While the latent heat flux will increase obviously in the northeast part of Inner Mongolia Autonomous Region and the eastern boundary regions of Heilongjiang Province and Jilin Province, where the cultivated lands occupy a large fraction of the total land area, and the cultivated land will mainly convert into forests.

The sensible heat flux in 2030 will show an increasing trend on the whole compared to that in 2010, with the average value increasing by 0.06–0.07 (Fig. 4.8). The simulation result indicates that the sensible heat flux will increase slightly in most part of the study area, with the increment of approximately 0.3 W/m^2. The simulation results under the three scenarios suggest that the sensible heat flux will increase most obviously in the northern part of Great Khingan Mountains and Lesser Khingan Mountains, where a lot of cultivated land will change into urban and built-

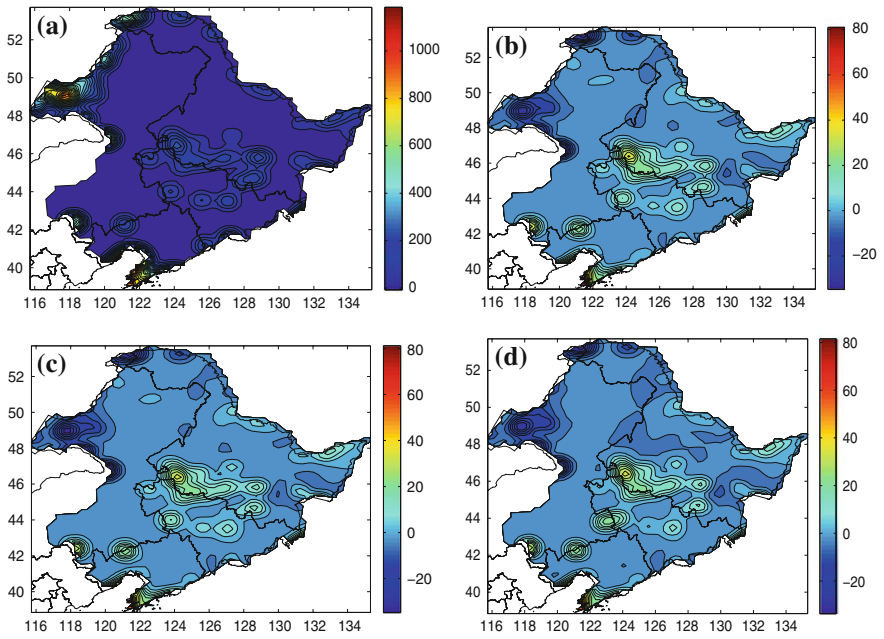

Fig. 4.7 Difference between the latent heat flux in Northeast China in 2010 and 2030 under different scenarios (W/m^2). **a** Spatial pattern of the latent heat flux in 2010, **b** Difference of the latent heat flux between 2010 and 2030 under the BAU scenario, **c** Difference of the latent heat flux between 2010 and 2030 under the REG scenario, **d** Difference of the latent heat flux between 2010 and 2030 under the CES scenario

up land. While it will increase most slightly in Liaohe Plain, Liaodong Peninsula, and southern part of Changbai Mountains, where the cultivated land will mainly change into forests or grassland and the decreased albedo will substantially increase the evaporative flux. In summary, in the regions of returning cultivated land to forests, the forest expansion will increase the evapotranspiration, increase the latent heat flux, decrease the sensible heat flux, and consequently lead to the decrease of the near-surface temperature (Deng et al. 2010d). While in the regions of urbanization, the decrease of evapotranspiration due to conversion from cultivated land into urban and built-up land will lead to significant decrease of latent heat flux and obvious increase of sensible heat flux, which is the main cause of the near-surface temperature rise (Liu 2011).

The difference in the change of the latent heat flux and sensible heat flux under the three scenarios is mainly due to the difference in the land use change, especially the difference in cultivated land change. The simulation results in this study suggest that more cultivated land will convert into urban and built-up land in the regions around cities under the REG scenario, while more cultivated land will convert into forests in the regions far from cities under the CES scenario. All these conversions will lead to obvious vegetation cover change, which will further lead to significant spatial heterogeneity of the latent heat flux and sensible heat flux.

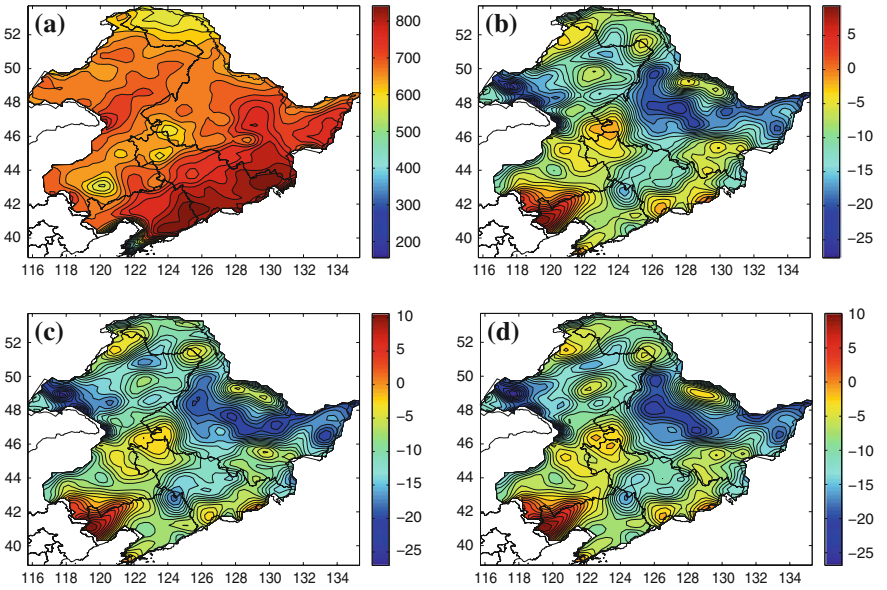

Fig. 4.8 Difference between the sensible heat flux in Northeast China in 2010 and 2030 under different scenarios (W/m^2). **a** Spatial pattern of the sensible heat flux in 2010, **b** Difference of the sensible heat flux between 2010 and 2030 under the BAU scenario, **c** Difference of the sensible heat flux between 2010 and 2030 under the REG scenario, **d** Difference of the sensible heat flux between 2010 and 2030 under the CES scenario

The result indicates that the latent heat flux increases most obviously in the regions where the cultivated land mainly converts into forests, while the sensible heat flux increases most obviously in the regions where the cultivated land mainly converts into urban and built-up land in Northeast China. A lot of research has indicated that the terrestrial vegetation cover change can influence the land surface energy budget through altering the land surface albedo, roughness, etc., and consequently change precipitation and temperature. In Northeast China, the conversion from cultivated land into nonagricultural land has been the main reason for the soil moisture change in regions around cities. The irrigation to cropland can increase the latent heat flux and decrease sensible heat flux, and consequently have cooling effects on the land surface. However, the conversion from irrigated cropland into urban and built-up land has greatly weakened this cooling effect since it decreases the land surface roughness and increases the land surface albedo, which leads to the decrease of evapotranspiration as well as the land surface net radiation, and consequently decreases the latent heat flux and increases the sensible heat flux. Furthermore, returning cultivated land to forests have positive effects on restoring the soil water environment, and afforestation can significantly increase the solar radiation absorbed by the land surface, making the evapotranspiration increase, which will increase the latent heat flux and decrease the sensible heat flux, and consequently decrease the temperature. In fact, the land use has changed greatly

due to the urbanization, but returning cultivated land into forests, etc. in Northeast China in the past decades led to more significant spatial heterogeneity of cultivated land that further lead to spatial heterogeneity of impacts of land use on the climate.

4.2.2.3 Implication for the Land use Management

Human activities have contributed to anthropogenic climate change through a variety of processes, including both of growth or degradation of surface vegetation and the changes in the land surface; however, impacts of the latter one are not currently being incorporated into the development of climate change mitigation policies (Marland et al. 2003). For example, some previous researches have quantified the potential of crop management changes to sequester greenhouse gases, but the biogeophysical effects of most management changes have been less widely considered (Lobell et al. 2006). The cultivated land change in Northeast China is directly caused by the human activities (Deng et al. 2010d), and the land use management can exert great influence on the cultivated land change, especially the conversion between the cultivated land and other land use types, which will further influence the climate change. The population growth is still the fundamental reason for the expansion of cultivated land in Northeast China, and the economic development and the macro policy are important driving factors of the land use change. With the rapid economic development and accelerated urbanization, more cultivated land will be converted into urban and built-up land (Deng et al. 2010a). Meanwhile, with more attention paid to the environmental protection, some cultivated lands will also be returned to forests, especially in Northeast China, where there were once a lot of forests converted into cultivated land due to the population growth and improper land management. Therefore, there will surely be more demand for the land resources as the population continually increases and the economy rapidly develops in Northeast China, which will lead to further land use change and subsequently exert more influence on the regional climate.

Improved understanding of how human activities influence climate is needed to guide policies aimed at mitigating or adapting to climate change since the land use management can exert great influence on the land use change and subsequently influence the regional climate change (Lehmann 2013). Over the past several centuries, human intervention has markedly impacted land surface characteristics and atmospheric composition in Northern China, in particular through large-scale land conversion for cultivation and burning of fossil fuels (Sitch et al. 2005). These land cover change may play a significant role in driving future climate change (Lobell et al. 2006). The land use change in Northern China influences the climate change through not only the expansion of agriculture into natural ecosystems, but also the changes occurring within existing cultivated land. For example, historical clearing of forests for cultivated land is likely to have a cooling effect due to the greater albedo of croplands relative to forests (Lehmann 2013). Besides, changes occurring within existing agricultural lands can also have important consequences for climate, for example, the increases in irrigation and leaf area index and

reductions in tillage all have a physical cooling effect through increasing the planetary albedo (Liu 2011). In addition, some researches showed how reforestation in the temperate and boreal zones can also lead to a net warming, with the biogeophysical (snow-albedo feedback) exceeding biogeochemical effects, thereby accelerating rather than mitigating climate change (Sitch et al. 2005). However, more information on the sensitivity of climate to these management changes is needed to identify the climate-related trade-offs associated with future policy and management decision (Lobell et al. 2006). In summary, more and more attention should be paid to LUCC, since it is one of the major ways the human activities influence the climate change, and more in-depth researches should be carried out on the climate effects of LUCC since there are still some uncertainties in current research results.

More rational land use management measures should be implemented according to the local conditions of the study area in order to reduce the adverse climate effects of land use change while striving to meet the land demand of economic development. For example, it is necessary to control the loss of forests during the land reclamation in order to fulfill their role in regulating the climate and preventing water and soil erosion in Northern China. It is urgent to improve the forest management to minimize the loss of existing forests in order to minimize human-induced climate change at all scales. Meanwhile, more efforts should be made to restore the structures and functions of native ecosystems to minimize the human impacts on the climate system. Besides, it is feasible to alleviate the climate change through returning cultivated land to forests or grassland, and it is necessary to further implement the ecological construction projects such as the Project of Three North Shelterbelt. In addition, it is feasible to promote management changes such as reduced tillage and increased irrigation in consideration of their climate effects, and management practices that demonstrably mitigate regional or global climate change might be encouraged through incentives to farmers (Lehmann 2013). In addition, it is also necessary to adjust the crop composition and convert dry cropland into irrigated cropland in order to regulate the climate and increase the grain yield and consequently contribute to the sustainable development of the regional agriculture.

4.2.3 Concluding Remarks on Biogeophysical Effects of Cultivated Land Conversion

In this chapter, we analyzes the potential climate effects of cultivated land change in Northeast China during 2010–2030 based on the scenario analysis on the land use change and the simulation. The simulation results indicate that the land use change in Northeast China will be mainly characterized by the conversion from cultivated land into forests and urban and built-up land during 2010–2030, with the total cultivated land area showing a decreasing trend, which will inevitably influence the regional climate. Besides, the result of the simulation indicates that

average latent heat flux in the whole Northeast China would show a decreasing trend during 2010–2030 under the three scenarios, while the average sensible heat flux will show an increasing trend. In addition, there is significant spatial heterogeneity in the change of both the latent heat flux and sensible heat flux. The latent heat flux will decrease slightly in most parts of the study area, but it will decrease most obviously in some regions where a lot of cultivated land will change into urban and built-up land, while it will increase most obviously in some parts of the study area where the cultivated land will mainly change into forests.

By comparison, the sensible heat flux will show an increasing trend on the whole during 2010–2030, the simulation results under three scenarios suggest that it will increase most obviously in the northern part of Great Khingan Mountains and Lesser Khingan Mountains, where a lot of cultivated land will change into urban and built-up land, while it will increase most slightly in the regions where the cultivated land will mainly change into forests or grassland. Although there are some uncertainties in the simulation result, it still can provide some useful information for the land managers to regulate the land use more scientifically.

4.3 Estimated Effects of Land Cover Changes on the Near-Surface Temperature in North China

The North China Plain has been selected as the study area in this study. First, it has long been one of the most densely populated regions in China, its current city density is relative high, and industries and agriculture are well-developed in this region. The rapid economy growth and increasing population have led to dramatic land use/cover change in this region, and human disturbance to natural environment is especially significant, which greatly influences sustainable development of whole China. Second, the North China Plain is a typical area of monsoon climate as well as the transient region between the humid and subhumid region and the arid and semiarid region. On the one hand, the plain agriculture can be sustained for a long time due the local climatic conditions. On the other hand, the local climatic conditions also lead to more frequent droughts, make the agricultural production extremely unstable and consequently may lead to greater economic loss and more extensive social influence. Therefore, it is of great importance to study the influence of LUCC on the climate in the North China Plain.

This study first tests the ability of WRF model to simulate the change of the near-surface temperature in the North China Plain, based on which the static land use data in WRF are then replaced. Thereafter, the modified WRF is used to study the influence of the land use/cover change on the near-surface temperature in the North China Plain in year 1992 and 2005. The result can contribute to a better understanding of the influencing factors of the climate in the North China Plain so as to minimize the negative influence and maximize the positive influence on the regional climate, which is helpful to the scientific regional land use planning and management in China in the future.

4.3.1 Method and Data Processing

4.3.1.1 Model and Experiment Design

With the development of the atmospheric models and land surface process models, the numerical simulation has become a widely used approach to study the influence of climate on vegetation. WRF model has been widely used in the global climate and achieved good simulation result, and we use the ARW-WRF (Edition 3.3) in this study.

The location and size of the simulation area have great influence on the simulation result (Seth and Giorgi, 1998) The center line of the simulation area was set to be 36° N, 117° E in this study. The Lambert projection was used, with the two standard parallels being 26 and 46° N, respectively. The spatial resolution was set to be 20 km, and there were 112 grid points in the east-west direction and 97 grid points in the north-south direction in the whole simulation area.

The lateral boundary forcing data, that came from the NCEP/FN dataset, are updated every 6 h. This dataset has the spatial resolution of $1 \times 1°$ and the vertical height of 27 layers, and it has been established and updated since July of 1999 with the data assimilation of almost all kinds of observation data (e.g., remote sensing data and ground-based observation data). In comparison to the datasets of NCEP I, NCEP II, and EAR40, the NCEP/FNL dataset has higher accuracy and spatial resolution, and it includes more kinds of environmental variables.

In the parameterization scheme of physical processes in the model, the cumulus parameterization scheme adopted the Grell–Devenyi ensemble scheme, the boundary layer process scheme was YSU, and the shortwave radiation scheme was the CAM scheme, while the land surface process scheme was Noah land surface model. The boundary buffer was set to be four layers of grid points, and the boundary conditions adopted the relaxation scheme. The time interval of the model integration was set to be 5 min, and that of the radiation process and cumulus convection was 30 and 5 min, respectively. There were 27 layers in the vertical direction and the atmospheric pressure at the top layer was 50 hPa.

The test scheme in this study is as follows (Table 4.3). There are two sets of tests, one is the control test and the other is the sensitivity test. The land cover data of 1985 is used in the control test and that of 2005 is used in the sensitivity test. The two tests are both implemented with the climate forcing data between October of 2005 and December of 2007.

4.3.1.2 Processing of Land Cover Data

It is necessary to reclassify the land use/cover data with the USGS land cover classification, which includes 24 land-cover and land-use types and set the spatial resolution to be 20 km according to the requirement of the WRF model. Therefore, the land use/cover data of the IGBP land cover classification are first reclassified with the USGS land cover classification system, and then the spatial resolution of

Table 4.3 Schemes of the simulation test

Test	Test period	Land cover data used in the WRF model
Control test	2005.10–2007.12	Land cover data of 1985
Sensitivity test	2005.10–2007.12	Land cover data of 2005

the data is converted from 1 to 20 km. The land use/cover data used in this study are extracted from the Chinese subset of the Global Land Cover Characteristics database, which is developed based on the AVHRR data with the support of IGBP-DIS in 1992, and the China subset of the MODIS land cover data product in 2005. The two datasets have the spatial resolution of 1 km and adopt the IGBP classification. On the basis of the data of the IGBP land cover classification, we formulate the transformation method from the IGBP land cover classification to the USGS land cover classification (Table 4.4), and establish the land-use and land-cover dataset of the North China Plain of the USGS classification.

The LUCC data are further upscaled on the basis of the data mentioned earlier so as to embed the high resolution underlying surface data into the large-scale climate model. In this study, the 1 km resolution land-cover and land-use data of USGS classification are upscaled into the 20 km resolution data. Besides, the three kinds of data are integrated in a system of seven land cover types, and their area consistency and spatial consistency are analyzed so as to check the change of the classification accuracy of the land-cover and land-use data before and after the reclassification and upscaling. The result shows the difference of the total area between the land-cover and land-use data after reclassification and upscaling the initial data (Table 4.4).

There is a high overall consistency between the 1 km resolution initial data of the IGBP classification and USGS classification in year 1992 and 2005, except the slight difference in the total area of grassland, water bodies, and unused land. Besides, the 20 km resolution data of USGS classification differed from both of the other two kinds of Land-cover and land-use data. The result of the comparison between the initial data and the upscaled USGS data of year 1992 indicates the area of irrigated cropland and pasture, grassland, and water bodies decreased by 2.69, 7.78, and 41.42 %, respectively; while the area of dryland cropland and pasture, deciduous broadleaf forest, urban and built-up land, and unused land increased by 0.62, 0.46, 1.68, and 153.66 %, respectively. By contrast, that of year 2005 indicates the area irrigated cropland and pasture, deciduous broadleaf forest, water bodies, and urban and built-up land decreased by 6.46, 7.43, 36.35 and 4.87 %, respectively; while the area of dryland cropland and pasture, grassland, and unused land increased by 1.41, 17.29, and 101.11 %, respectively (Table 4.5).

The error matrix is used to assess the spatial consistency between the initial data and the data after reclassification in this study. The result indicates that the consistency of the land use/cover types except the unused land has all exceeded 95 % (Table 4.6). The consistency of the urban and built-up land is the highest, reaching 99.25 %, followed by that of dryland cropland and pasture, which is 98.76 %. The overall consistency has reached 96.84 % and the Kappa coefficient is 0.95, indicating the reclassification result has a high classification accuracy.

Table 4.4 Remapping tables of land-cover and land-use classification

USGS land cover classification	Correspondence	IGBP land cover classification	
01 Urban and built-up land	14 ← 01	01	Evergreen needle leaf
02 Dryland cropland and pasture	13 ← 02	02	Evergreen broadleaf
03 Irrigated cropland and pasture	12 ← 03	03	Deciduous needle leaf
04 Mixed dryland/irrigated cropland and pasture	11 ← 04	04	Deciduous broadleaf
05 Cropland/Grassland Mosaic	15 ← 05	05	Mixed forest
06 Cropland/Woodland Mosaic	08 ← 06	06	Closed shrublands
07 Grassland	09 ← 07	07	Open shrublands
08 Shrubland	08 ← 08	08	Woody savannas
09 Mixed Shrubland/Grassland	10 ← 09	09	Savannas
10 Savanna	07 ← 10	10	Grasslands
11 Deciduous broadleaf forest	17 ← 11	11	Permanent wetlands
12 Deciduous needle leaf forest	02 ← 12	12	Croplands
13 Evergreen broadleaf forest	01 ← 13	13	Urban and built-up
14 Evergreen needle leaf forest	05 ← 14	14	Cropland mosaics
15 Mixed forest	24 ← 15	15	Snow and ice
16 Water bodies	19 ← 16	16	Bare soil and rocks
17 Herbaceous Wetland	16 ← 17	17	Water bodies
18 Wooded Wetland			
19 Barren or sparsely vegetated			
20 Herbaceous Tundra			
21 Wooded Tundra			
22 Mixed Tundra			
23 Bare Ground Tundra			
24 Snow or Ice			

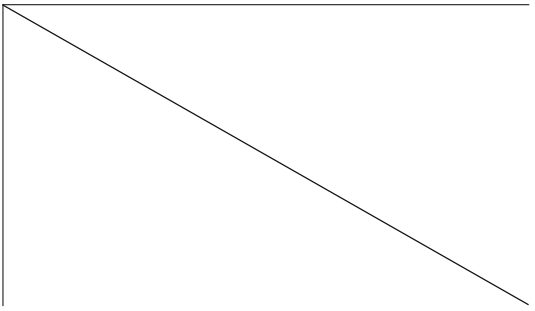

Table 4.5 Comparison table of area percentage (%) of each land-cover and land-use types among various kinds of classification systems

Class	1992			2005		
	IGBP[a]	USGS[b]	USGS[c]	IGBP[a]	USGS[b]	USGS[c]
Irrigated cropland and pasture	4.09	4.09	3.98	3.87	3.87	3.62
Dryland cropland and pasture	66.11	66.11	66.52	64.52	64.52	65.43
Deciduous broadleaf forest	6.48	6.48	6.51	6.55	6.55	6.06
Grassland	7.07	7.37	6.52	6.79	6.78	7.96
Water bodies	3.09	2.00	1.81	3.27	2.43	2.08
Urban and built-up land	12.34	12.34	12.57	14.46	14.46	13.76
Unused land	0.82	1.61	2.08	0.54	1.39	1.09
Total	100	100	100	100	100	100

[a] represents the 1 km resolution data of IGBP classification
[b] represents the 1 km resolution data of USGS classification
[c] represents the 20 km resolution data of USGS classification

Table 4.6 Error matrix of accuracy assessment for reclassifying land-cover and land-use types

	Irrigated cropland and pasture[b]	Dryland cropland and pasture[b]	Deciduous broadleaf forest[b]	Grassland[b]	Water bodies[b]	Urban and built-up land[b]	Unused land[b]
Irrigated cropland and pasture[a]	97.32	0.32	2.04	0.02	0.15	2.88	0.03
Dryland cropland and pasture[a]	0.23	98.74	3.43	2.02	0.05	3.2	0.2
Deciduous broadleaf forest[a]	0.54	0.04	96.45	4.43	0.23	0.3	0.22
Grassland[a]	0.34	0.26	5.23	93	0.4	0.54	0.17
Water bodies[a]	0.37	0.24	0.01	0.05	97.78	0.27	0.23
Urban and built-up land[a]	0	0	0	0	0	99.25	0
Unused land[a]	0.02	0.1	0.07	0.12	0.14	0.69	90.86

[a,b] represent land-cover and land-use types before and after reclassification, Overall accuracy = 96.84 %,Kappa coefficient = 0.9503

4.3.1.3 Processing of meteorological data

The observation data, which are used to make a comparison with the simulated temperature in this study, come from the meteorological stations in the North China Plain. The meteorological data of the same period (January 2006-December 2007) of the simulation are used in this study. The 20 km resolution temperature data are obtained by interpolating the monthly average temperature data from the 57 meteorological stations in the North China Plain with the Kriging interpolation method.

4.3.2 Results

4.3.2.1 Characteristics of LUCC in the North China Plain during 1992–2005

Figure 4.9 shows the LUCC data of the North China Plain, which are obtained by reclassification and upscaling of high resolution data. The map shows that the cropland was mainly located in the plain region and accounted for 70 % of the total area of the North China Plain.

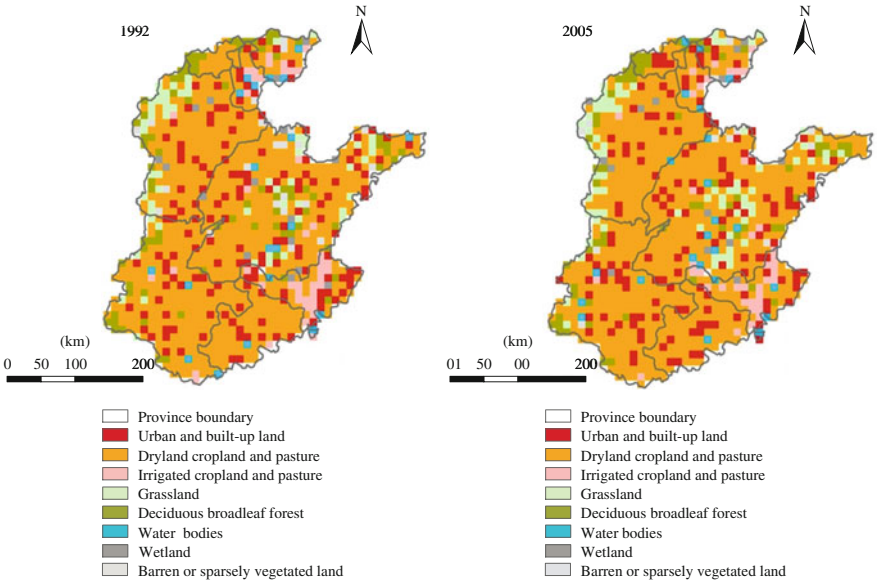

Fig. 4.9 The LUCC map after upscaling in 1992 and 2005

The LUCC data of the North China Plain in 1992 and 2005 are overlaid to further analyze the conversion and inner change of each land cover type. The result indicates that the LUCC is mainly characterized by the increase of the urban and built-up land and decrease of the dryland cropland, the changing rate of which reached 2.12 and 1.59 %, respectively. By contrast, the changing rates of other land cover types are not more than 0.5 %. The result suggests that the newly increased urban and built-up land is mainly located in the Beijing-Tianjin-Tangshan zone and large and around medium-sized cities, such as Shijiazhuang, Zhengzhou, Ji'nan, Qingdao, and Lianyungang; besides, the newly increased urban and built-up land mainly converted from the dryland cropland, accounts for 60.55 % of the conversion of the dryland cropland (Fig. 4.10).

4.3.2.2 Ability of the WRF Model to Simulate the Temperature Change in the North China Plain

The test results obtained with the standard WRF model is first compared with the ground-based observation data to assess the ability of the WRF model to simulate the climate in the North China Plain. The daily average temperature is calculated as the average value of the temperature at 00:00, 06:00, 12:00, and 18:00 so as to keep consistent with the ground-based observation criteria. The results indicate that the WRF model can simulate the spatiotemporal change of temperature very well (Fig. 4.11). According to the monthly change of daily average temperature in the whole study area, the highest temperatures in the observation data and

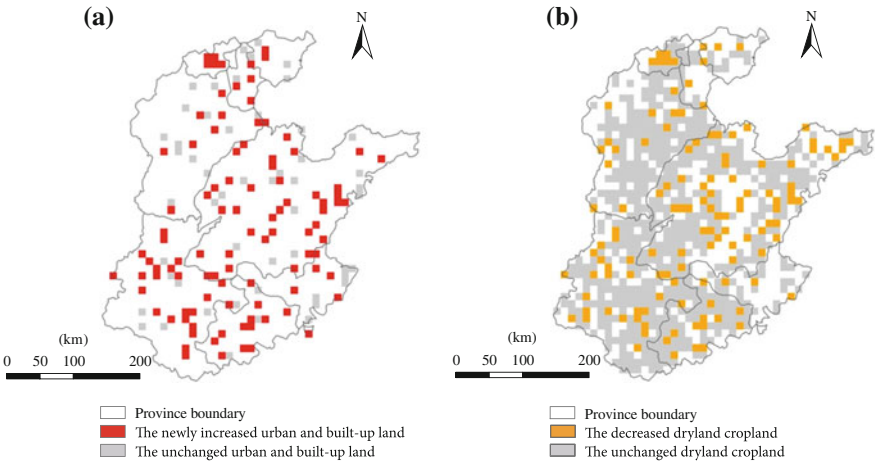

Fig. 4.10 Map of the unchanged and newly increased urban and built-up land (**a**), and map of the unchanged and decreased dryland cropland (**b**)

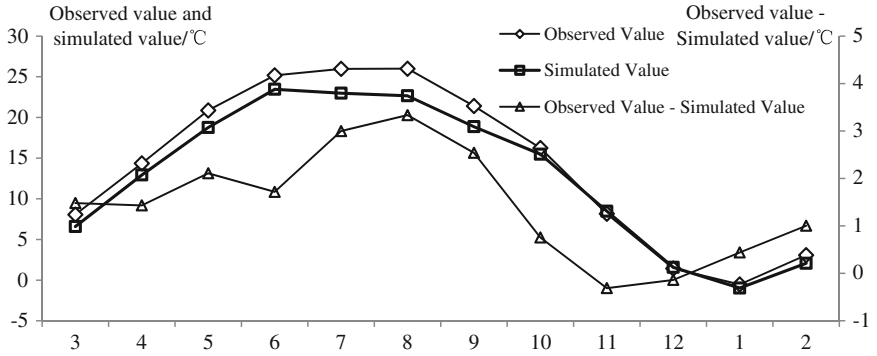

Fig. 4.11 Comparisons of simulated and observed values of the monthly average temperature at 2 m above the ground

simulation data both appear around July, and the lowest temperatures in the observation data and simulation data both appear around January. The decreasing rate of the temperature during September and November is a bit higher than that during March and May, i.e., the temperature decreases a little more quickly in the autumn than it increases in the spring.

According to the spatial pattern of the daily average temperature in February and August, both simulation data and the ground-based observation data indicate the temperature is lower in the north part and higher in the south part, it is colder in the mountainous area and warmer in the plain area in the regions at the same latitude, and it is warmer in the inland region than in the coastal region (Fig. 4.12).

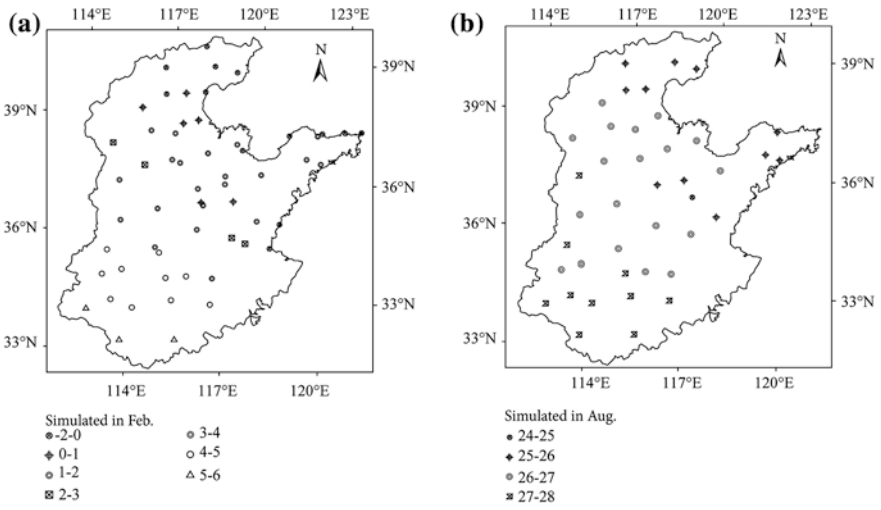

Fig. 4.12 Simulated value of the daily average temperature in the North China Plain in February and August

For example, the temperature difference between the Fuyang observation station in the extreme north and the Zunhua observation station in the extreme north is as high as 5 °C in February and 2–3 °C in August. While that between the Chengshantou observation station in the extreme east and the Shijiazhuang observation station in the extreme west are 1–1.5 and 0.2–0.3 °C, respectively.

There is still some difference between the observed and simulated temperatures, i.e., the simulated temperature is lower than the observed temperature on the whole. For example, the annual daily average temperature of the 57 observation stations is 14.19 °C on average, while the simulated value is 12.74 °C. According to the monthly temperature change, the simulated value is lower than the observed value in most months except November and December, and the maximum difference between them reaches 3.34 °C in August. By contrast, the data of the seasonal temperature change suggests the simulated temperature is lower than the observed temperature in all seasons. The difference is the most significant in the summer, reaching 2.68 °C; while it is relatively small in the spring, autumn, and winter, being 1.67, 0.99, and 0.44 °C, respectively (Table 4.7).

There is also some difference in the spatial patterns of the observed and simulated temperatures (Fig. 4.13). In comparison with the observed temperature, the simulated temperature is higher than in the mountainous area and lower in the plain area. For example, there is a large difference between the observed and simulated daily average temperature in February and August. There are 49 observation stations with the significant difference between the observed and simulated daily average temperatures (reaching the significance level of 95 %) in February, 39 out of which have the simulated value 2.00 °C lower than the observed value on average. While the simulated temperature of the other 10

Table 4.7 Simulated and observed values of the seasonal average temperature at 2 m above the ground surface in the North China Plain (°C)

Season	Winter	Spring	Summer	Autumn
Simulated value	0.89	12.76	23.03	14.27
Observed value	1.33	14.43	25.72	15.27
Ratio between simulated value and observed value	0.44	1.67	2.68	0.99

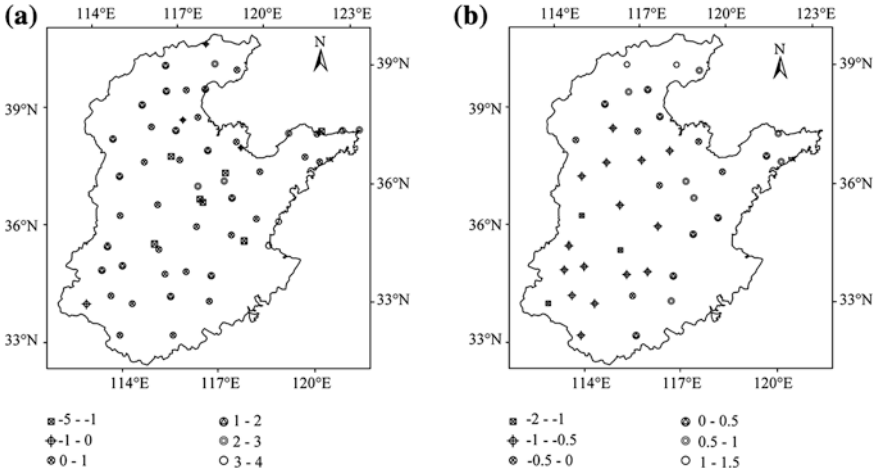

Fig. 4.13 Difference between the observed and simulated daily average temperature in the North China Plain in February and August

observation stations is 1.09 °C higher than the observed temperature on average. The observation stations with the lower simulated temperature are mainly located in the middle part of Hebei Province and Shandong Province, while that with the higher simulated temperature mainly concentrate in the eastern piedmont of Taihang Mountain and inner part of Henan Province. By contrast, the differences between the observed and simulated daily average temperatures in August in 42 observation stations reach the significance level. The simulated value of the 17 out the 42 observation stations is 0.51 °C lower than the observed value on average. While the simulated temperature of the other 25 observation stations is 0.98 °C higher than the observed one on average. The observation stations with the lower simulated temperature are mainly located in Henan Province and Hebei Province.

In summary, the analysis suggests the WRF model can simulate the seasonal change and spatial pattern of temperature in the North China Plain very well. Although there is some difference between the observed and simulated value, with the simulated temperature being lower than the observed temperature on the whole, there is no significant difference in the spatial patterns of the observed and simulated temperatures on the whole. There is only some large difference in very few areas, indicating the WRF model has a great advantage in the simulation of the climate in the plain area.

4.3.2.3 Analysis of Test Results

The LUCC in the North China Plain, which was characterized by the regional urbanization, had led to some changes of the near-surface temperature. The annual average temperature was 14.61 and 14.64 °C in the control test and sensitivity test, respectively. The LUCC in the North China Plain made the regional near-surface temperature increase by 0.03 °C/year. All the months except January and June were characterized by a temperature increase during 1992–2005. Besides, the LUCC in the North China Plain also led to an increase of the near-surface temperature in all the seasons, among which the temperature increment was the highest in the summer and the lowest in the winter, reaching 0.05 and 0.02 °C, respectively. The monthly and seasonal temperature differences in the control test and the sensitivity test were as shown in Fig. 4.14.

The spatial patterns of temperature increase are consistent in the spring and the autumn on the whole, both indicating a significant temperature increase in the North China Plain (Fig. 4.15). The amplitude of the temperature increase is relatively small in the spring (generally around 0.03 °C), while it is very large in the autumn (above 0.04 °C on average). The temperature increases most greatly in the summer, increasing by 0.05 °C/year on average, and exceeding 0.1 °C in the Circum-Bohai-Sea Region and reaching 0.2 °C in the Beijing-Tianjin-Tangshan zone. Besides, there are much wider regions with a significant temperature in the summer than in the other three seasons. Although the temperature increases in the winter on the whole, it still decreases in most regions, especially in the Yanshan Moutain, Circum-Bohai-Sea Region, Shandong Peninsula, etc.

The spatial pattern of the seasonal temperature change corresponded to that of the LUCC on the whole. The temperature generally increased in the regions where the urban and built-up land increases. The temperature increment was very high in these regions, and the degree and the range of influence of temperature increase varied significantly among reasons. Taking the Beijing-Tianjin-Tangshan zone as an example, the temperature increment was very large and the range of the influence of temperature rise was very wide in the summer in this region. The regional temperature increased by 0.06–2.8 °C in the summer, and the temperature change due to expansion of urban and built-up land influenced a wide area around the Beijing-Tianjin-Tangshan zone. The temperature increment was largely the same in the spring and the autumn, reaching 0.03–3 °C. However, the temperature rise mainly influenced Beijing and Tianjing in the spring, and Beijing and some areas in the north part of Hebei Province in the autumn. The temperature rise was only obvious in the regions where urban and built-up land increased, while in other regions the temperature generally decreased by 0.01–0.06 °C, which might be caused by the wind velocity, which was generally high enough in north China in the winter and consequently reduced the tendency of temperature rise resulting from the increase of urban and built-up land (Arnfield 2003; Johnson et al. 1991).

The temperature changes most greatly in the urban and built-up land among all the land use/cover types in the North China Plain (0.1 °C/year), followed by the irrigated cropland and pasture (0.06 °C/year). While the temperature increases most

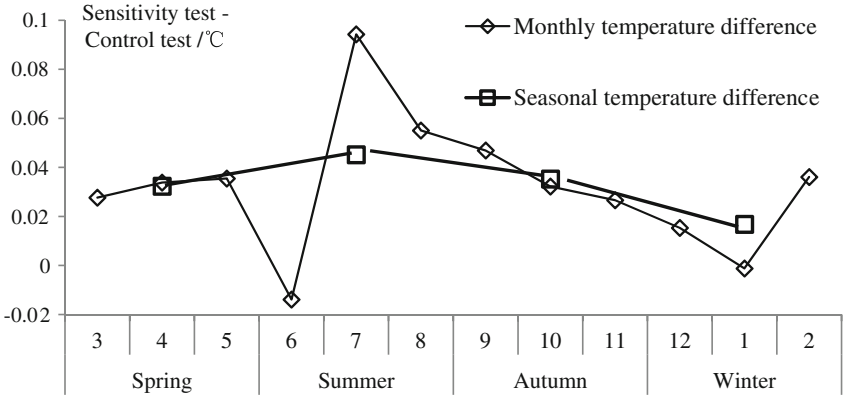

Fig. 4.14 Monthly and seasonal temperature differences in the control test and sensitivity test

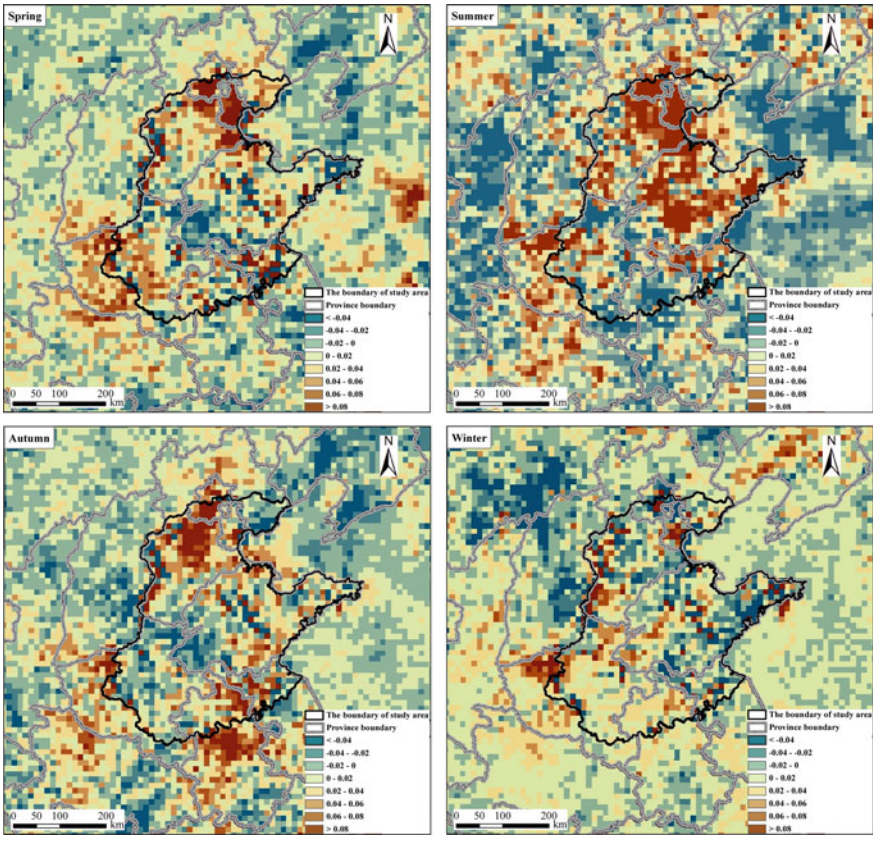

Fig. 4.15 Difference between the near-surface temperature in the four seasons in the sensitivity test and control test (°C)

slightly in the grassland, with an increment of only 0.01 °C/year (Fig 4.16). The result is largely consistent with the result of the research of Lim et al. (2005), in which the climate in the northern hemisphere was simulated with the "CRU-NNR" model at the 5 × 5° resolution (the OMR trend value of the urban and built-up land, crop land, broadleaf forest, and bare land was 0.034/year, 0.02 °C/year, 0.002 °C/year, and 0.02 °C/year, respectively). However, the simulated result is still somewhat higher, which may be because the ERA40 reanalysis indirectly included the ground-based observation data and consequently made the OMR trend values smaller than the results obtained with the numerical simulation.

The vegetation plays an important role in influencing the near-surface temperature. For example, one of the main reasons for the near-surface temperature in different land-cover and land-use types is the amount and the density of the vegetation. On the whole, the better the vegetation cover is, the lesser will be the temperature rise. It may be caused by little evaporation in the barren land, and the land surface heat mainly gets into the atmosphere in the form of sensible heat. By contrast, there is higher soil humidity in the densely vegetated land, which makes the land surface heat mainly get into the atmosphere in the form of latent heat and consequently reduces part of the temperature rise of the land surface. In addition, the heat island effect in the urban region also leads to the rise of the near-surface temperature. By contrast, the temperature increment is less in the water bodies, mainly because the specific heat capacity of water bodies is very large, which makes the temperature increase very slow, and consequently makes the near-surface temperature lower (Su et. al 2005). Furthermore, there is great difference between the irrigation intensities of the dryland cropland and irrigated cropland, which leads to great difference in their physical characteristics, and consequently makes the temperature increments in them differ greatly.

The change of the average near-surface temperature corresponding to each kind of land use/cover change was summarized in this study. The following figure shows the temperature change in the eight major kinds of land use/cover change that involve a large area of land (Fig 4.17). The result showed that the conversion from dryland crop to forest and built-up land made the near-surface temperature increase by 0.13 °C/year, while the conversion from dryland crop to grassland made the near-surface temperature decrease by 0.1 °C/year. By contrast, the other conversion types only made the near-surface temperature increase by 0.01–0.04 °C/year.

The conversion of croplands to built-up lands can lead to the changes in the roughness and albedo of the land surface, which cause the change in the radiation flux of the land surface and consequently make the regional near-surface temperature increase. Besides, changes of the underlying surface due to the urbanization can alter physical processes, such as the energy balance of the land surface and lead to the "five island effects" (i.e., dark islands, heat islands, dry islands, wet islands, and rain islands), decreasing the wind velocity and lead to the variable city climate, and consequently influencing the structure and development of the boundary layer to change the climate in a large area. Moreover, the conversion from grasslands to dryland croplands can decrease the albedo of the land surface,

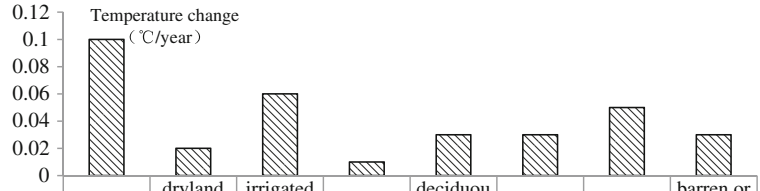

	urban and built-up land	dryland cropland and pasture	irrigated cropland and pasture	grassland	deciduous broadleaf forest	water bodies	wetland	barren or sparsely vegetated land
Temperature change	0.1	0.02	0.06	0.01	0.03	0.03	0.05	0.03

Fig. 4.16 Temperature change in various land use/cover types

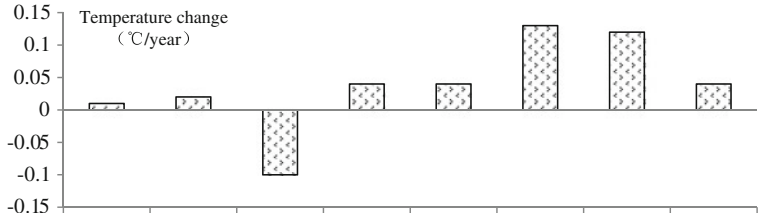

	Conversion from forest to grassland	Conversion from grassland to forest	Conversion from dryland cropland to grassland	Conversion from grassland to dryland cropland	Conversion from forest to dryland cropland	Conversion from dryland cropland to forest	Conversion from dryland cropland to built-up land	Conversion from dryland cropland to water bodies
Temperature change	0.01	0.02	-0.1	0.04	0.04	0.13	0.12	0.04

Fig. 4.17 Change of the near-surface temperature corresponding to each kind of land use/cover change

increase the net radiation of land surface, and consequently make the sensible heat increase and lead to the increase of the daily average temperature.

4.3.3 Concluding Remarks on the Studies of North China

The land use/cover change in the North China Plain during 1992–2005 is mainly characterized by the increase of urban and built-up lands and the decrease of dryland croplands. The urban and built-up lands increased by 2.12 %, and the dryland cropland decreased by 1.59 %, while other land use/cover types changed by no more than 0.5 %. Besides, the newly increased urban and built-up land is mainly located in the Beijing-Tianjin-Tangshan zone and around large and medium-sized cities such as Shijiazhuang, Zhengzhou, Ji'nan, Qingdao, and Lianyungang. In addition, the newly increased urban and built-up lands mainly

converted from the dryland cropland and accounted for 60.55 % of the conversion of the dryland cropland during this period.

There is no significant difference in the spatial patterns of the observed and simulated temperatures on the whole, except some slightly large difference in few areas. The land use/cover change in the North China Plain, which is mainly characterized by the regional urbanization, has caused significant change of the near-surface temperature. It led to a regional near-surface temperature rise of 0.03 °C/year. Besides, the spatial pattern of the temperature change corresponded to that of the land use/cover change on the whole, i.e., the temperature mainly increase significantly in the regions where the urban and built-up land expanded; In addition, the degree and range of the influence of the temperature rise varied greatly among reasons. The temperature changed most significantly in the urban and built-up land (0.1 °C/year), followed by the irrigated cropland and pasture (0.06 °C/year). The temperature generally change by 0.02–0.05 °C/year in the forest, water bodies, and dryland cropland and pasture, and it changed most slightly in the grassland (0.01 °C/year). Among the all the types of land use/cover change that involved a large area of land, the conversion of dry land into forest and built-up land led to the greatest near-surface temperature increment, reaching 0.13 °C/year. While the conversion of dry land and pasture into grassland made the near-surface temperature decrease by 0.1 °C/year. By contrast, the other conversions only made the near-surface temperature change by 0.01–0.04 °C/year.

In comparison to the increase of the greenhouse gases that has a global influence, the land use/cover changes exert more influence at the regional scale. Generally, the better the vegetation cover is, the lesser will be the temperature rise. For example, the urban heat island effect in the urban regions where there is less vegetation will lead to greater increase of the near-surface temperature. Besides, the temperature increment in the water bodies is generally lower, and consequently leads to a lower near-surface temperature since the water has a large specific heat capacity and its temperature generally increases more slowly. What's more, the change of the underlying surface due to the urbanization can alter the physical processes such as the energy balance of the land surface, and consequently lead to the climate change in a large area. For example, the conversion from the cropland to the urban and built-up land can change the roughness and albedo of the land surface, and consequently cause the change in the radiation flux of the land surface and lead to significant increase of the regional near-surface temperature.

Since this study is preliminary, there are still some deficiencies as follows. First, there is still some difference between the upscaled land use/cover data and the initial data, which leads to some uncertainties in the simulated climatic effects of the land use/cover change. Second, the result may change if the calculus of the data of a long period is carried out since the study of the impacts of the land use/cover change on the temperature in the North China Plain is based on the sensitivity test of the numerical integration of the data of only two years in this study. In addition, there are some uncertainties in the result since there are various feedbacks within the climate system.

4.4 Summary

The studies in this chapter mainly focused on the climate effects of the cultivated land change in China. In the first part, we first generally analyzed the cultivated land reclamation and the climate change, e.g., the change of temperature and precipitation in Northeast China during 2000–2010. Then on the basis of these data, the climatic effects of cultivated land reclamation in Northeast China during 2030–2040 were simulated by the WRF model, which has been elaborately introduced in Chap. 2. Finally, the possible effects of the climate change on the grain yield and the potential influence on the food security were analyzed on the basis of the simulation results. The simulation result indicated that the temperature in Northeast China would be increasing on the whole, while the precipitation would be decreasing. Based on the simulation results, this study proposed some measures and policies to cope with the future drought and guarantee the grain yield so as to meet the increasing demand for grain due to the continual population growth.

In the second part, we analyzed the possible biogeophysical effects of cultivated land change on the climate in northern China during 2010–2030 on the basis of simulation with the WRF model. The simulation results indicate that the total cultivated land area in northern China will decrease during 2010–2030, mainly converting into urban and built-up land and forests due to the urbanization and governmental policies. Besides, the cultivated land change will lead to the increase of the sensible heat flux in the regions where a lot of cultivated land will convert into urban and built-up land; while it will make the latent heat flux increase in the regions where the cultivated land will mainly convert into forests, mainly through influencing the evapotranspiration.

In the last part, we explored the impacts of land use/cover change on the near-surface temperature in the North China Plain in year 1992 and 2005. The results indicated that the land use/cover change in the North China Plain, which was characterized by the regional urbanization, had led to significant changes in the near-surface temperature, making the regional near-surface temperature increase by 0.03 °C/year on average.

Overall, there are still some uncertainties in the research on the climatic effects of the land use/cover change; also it is still necessary to carry out more in-depth researches on a series of issues such as the improvement of the climate model and the resampling method of the land use/cover change data, especially the land cover data.

References

Anderson-Teixeira KJ, Snyder PK, Twine TE, Cuadra SV, Costa MH and DeLucia EH (2012) Climate-regulation services of natural and agricultural ecoregions of the Americas. Nature Climate Change 2(3):177–181

Arnfield AJ (2003) Two decades of urban climate research: a review of turbulence, exchanges of energy and water, and the urban heat island. Inter J Climatol 23(1):1–26

Deng X, Huang J, Rozelle S, Uchida (2006) Cultivated land conversion and potential agricultural productivity in China. Land Use Policy 23(4):372–384
Deng X, Su H, Zhan J (2008) Integration of multiple data sources to simulate the dynamics of land systems. Sensors 8(2):620–634
Deng X, Huang J, Rozelle S, Uchida E (2010a) Economic growth and the expansion of urban land in China. Urban Stud 47(4):813–843
Deng X, Jiang Q, Lin Y, Han J (2010b) Simulation of changes of soil organic carbon stock of cropland in China. Geographical Research, 29(1):93–101 (in Chinese)
Deng Z, Wang Q, Zhang Q, Qing Z, Yang G, Yuan P, Liu J et al (2010c) Impact of climate warming and drying on food crops in northern China and the countermeasures. Acta Meteorol Sinica 30(22):6278–6288 (in Chinese)
Deng X, Jiang QO, Zhan J, He S, Lin Y (2010d) Simulation on the dynamics of forest area changes in Northeast China. J Geogr Sci 20(4):495–509
Feddema JJ, Oleson KW, Bonan GB, Mearns LO, Buja LE, Meehl GA et al (2005) The importance of land-cover change in simulating future climates. Science 310(5754):1674–1678
Hernández-Ceballos M, Adame J, Bolívar J, La Morena BD (2012) A mesoscale simulation of coastal circulation in the Guadalquivir valley (southwestern Iberian Peninsula) using the WRF-ARW model. Atmospheric Research
Hijmans RJ, Graham CH (2006) The ability of climate envelope models to predict the effect of climate change on species distributions. Global Change Biol 12(12):2272–2281
Jiang L, Deng X, Seto KC (2012) Multi-level modeling of urban expansion and cultivated land conversion for urban hotspot counties in China. Landscape Urban Plan 108(2–4):131–139
Johnson G, Oke T, Lyons T, Steyn D, Watson I, Voogt JA (1991) Simulation of surface urban heat islands under 'ideal' conditions at night Part 1: theory and tests against field data. Boundary-Layer Meteorology 56(3):275–294
Lehmann N, Briner S, Finger R (2013) The impact of climate and price risks on agricultural land use and crop management decisions. Land Use Policy 35:119–130
Lim YK, Cai M, Kalnay E and Zhou L (2005) Observational evidence of sensitivity of surface climate changes to land types and urbanization. Geophys Res Lett 32(22):L22712, doi: 10.1029/2005GL024267
Liu J, Deng X (2011) Impacts and mitigation of climate change on Chinese cities. Curr OpinEnviron Sustain 3(3):188–192
Liu J, Gao J, Geng B and Wu L (2007) Study on the dynamic change of land use and landscape pattern in the farming- pastoral region of Northeast China. Res Environ Sci 20(5):148–145 (in Chinese)
Liu M, Tian H, Chen G, Ren W, Zhang C, Liu J (2008) Effects of land-use and land-cover change on evapotranspiration and water yield in China During 1900–20001. JAWRA J Am Water Resour Assoc 44(5):1193–1207
Liu J, Zhang Z, Xu X, Kuang W, Zhou W, Zhang S et al (2010) Spatial patterns and driving forces of land use change in China during the early 21st century. J Geogr Sci 20(4):483–494
Lobell D, Bala G, Duffy P (2006) Biogeophysical impacts of cropland management changes on climate. Geophys Res Lett 33(6):L06708
Ma Q (1996) A simulating study on the influences of climate change on grain yield and the countermeasures in Northeast China. Acta Meteorol Sinica 54(4):484–492. (in Chinese)
Ma S, Wang Q, Luo X (2008) Effect of climate change on maize (Zea mays) growth and yield based on stage sowing. Acta Meteorol Sinica 28(5):2131–2139 (in Chinese)
Marland G, Pielke RA Sr, Apps M, Avissar R, Betts RA, Davis KJ et al (2003) The climatic impacts of land surface change and carbon management, and the implications for climate-change mitigation policy. Climate Policy 3(2):149–157
Peterson AT, Ortega-Huerta MA, Bartley J, Sánchez-Cordero V, Soberón J, Buddemeier RH et al (2002) Future projections for Mexican faunas under global climate change scenarios. Nature 416(6881):626–629

Pielke RA, Pitman A, Niyogi D, Mahmood R, Mcalpine C, Hossain F et al (2011) Land use/land cover changes and climate: modeling analysis and observational evidence. Wiley Interdiscip Rev Climate Change 2(6):828–850

Seth A, Giorgi F (1998) The effects of domain choice on summer precipitation simulation and sensitivity in a regional climate model. J Climate 11(10):2698–2712

Sitch S, Brovkin V, Von Bloh W, Van Vuuren D, Eickhout B, Ganopolski A (2005) Impacts of future land cover changes on atmospheric CO2 and climate. Global Biogeochem Cycles 19(2): GB2013 doi: 10.1029/2004GB002311

Sun F, Yang X, Lu S and Yang S (2006b) The contrast analysis on the average and extremum temperature trend in Northeast China. J Meteorol Sci 26(2):157–163 (in Chinese)

Sun H, Yuan J, Lu S (2006a) The change and test of climate in Northeast China over the last 100 years. Climatic Environ Res 11(1):101–108

Chapter 5
Simulation of the Plausible Climate Effects of Ecological Restoration Programs in China

Qun'ou Jiang, Enjun Ma, Yanfei Li and Anping Liu

This chapter focuses on the climate effect of ecological restoration programs in China. The fourth assessment report of Intergovernmental Panel on Climate Change (IPCC AR4) indicated that the human activities are a significant influencing factor of climate change. Deforestation, grassland degradation, and desertification, which are mainly induced by human activities, have been greatly intensified due to the irrational exploitation of the natural resources, rapid population growth, and the expansion of road network in the past decades. Some ecological restoration programs have been recently carried out, e.g., Green for Grain Project, which can affect the climate through not only the carbon sink but also the thermal properties of the land surface. The land cover affects the surface roughness and consequently influences the transfer of local momentum and heat (Bonan and Pollard 1992).

Since the mid-1970s, scholars studied the impact of deforestation, grassland degradation, desertification, irrigation, and other land cover changes by using the global and regional climate model patterns. According to those researches, it can be concluded that the land use/cover change alters the land roughness, soil hydrological and thermal features, which lead to the further changes of the temperature, precipitation, downward shortwave radiation, sensible heat, and latent heat (Loridan et al. 2011). Therefore, it is meaningful to study the effects of land cover change not only on the climate, but also on the energy balance, and it will provide the significant reference for land use planning and climate adaptation to explore how the land cover impacts the climate and energy balance.

Q. Jiang (✉)
School of Soil and Water Conservation, Beijing Forestry University, Beijing 100038, China
e-mail: jiangqo@bjfu.edu.cn

E. Ma · A. Liu
School of Mathematics and Physics, China University of Geosciences (Wuhan), Wuhan 430074, China

Y. Li
Faculty of Resources and Environmental Science, Hubei University, Wuhan 430062, China

X. Deng et al. (eds.), *Land Use Impacts on Climate*, Springer Geography

DOI: 10.1007/978-3-642-54876-5_5,

This chapter includes three case studies. The first one attempts to predict the potential effects of artificial vegetation change on the regional climate in Jiangxi Province. Based on the Weather Research and Forecasting (WRF) model, a comparative analysis is carried out on the future temperature and precipitation under four hypothetical vegetation cover scenarios. The second case study simulates the land cover in the semiarid grassland area of China under the future scenarios with the DLS model and analyzes the effects of land cover conversion on the energy balance through the numerical simulation, which may provide some valuable information for the land use planning and climate change alleviation. As for the biosphere feedback on regional climate in Northwest China, the potential effects of grassland degradation on regional climate have also been explored in the overgrazing area of Northwest China from 2010 to 2040 in the third case studies.

5.1 A Scenario-Based Analysis of Afforestation and Its Impact on the Regional Surface Climate in Jiangxi Province, China

Jiangxi Province is covered by large forestry area, and a series of afforestation project has been carried out in Jiangxi Province. The Green for Grain project is implemented in 2000, while "one big and four small" project has been in full operation since 2008. As we know, these projects influence land use conversion and climate change (Deng et al. 2011a, b). The assessment of potential effects of artificial vegetation change on the regional climate in Jiangxi Province is meaningful for climate change mitigation and rational land management.

The forestry area in Jiangxi Province had exceeded 63.1 % by 2010, which is much higher than the national average level (Deng et al. 2011a, b). The area of needle-leaved forestry area reaches 5.65 million hm^2, accounting for 68.1 % of the arbor area and 52.7 % of the total forestry area in Jiangxi Province, and it will continue to increase due to afforestation. Meanwhile, the broadleaf forest recovery will be one of the competitors of the needleleaf forest expansion due to the favorable water and heat resources. There are currently five kinds of forests in Jiangxi Province, i.e., the deciduous broadleaf forest, deciduous needleleaf forest, evergreen broadleaf forest, evergreen needleleaf forest, and mixed forest. The needleleaf forests have expanded due to the afforestation in this region, however, the broadleaf forests are recovering owing to the suitable climatic conditions. Based on the simulation with WRF model, we carry out a comparative analysis on the future temperature and precipitation under four hypothetical vegetation cover scenarios.

5.1.1 Data and Methodology

5.1.1.1 Simulation Scheme

On the whole, the forest change in Jiangxi Province is characterized by the competition between the needleleaf forests and the broadleaf forests. To cover the potential effects of the forest vegetation change on regional climate, four hypothetical vegetation cover scenarios are designed in this study, including the scenarios of deciduous broadleaf (DB), deciduous needleleaf (DN), evergreen broadleaf (EB), and evergreen needleleaf (EN), and it means all of the forests are DB, DN, EB, and EN under the four different scenarios, respectively. The forest pattern in year 2000 is regarded as the baseline scenario (BL). The effects of afforestation on the regional climate can be measured with the differences of the simulation results under the four hypothetical scenarios and the BL scenario.

$$E_i = R_i - r_i$$

where i refers to the precipitation and temperature; E_i is the effects of the vegetation change on the climate under the four hypothetical scenarios; R_i is the simulation results under the four hypothetical scenarios with extreme vegetation cover; and r_i is the simulation results under the BL scenario.

5.1.1.2 Atmospheric Forcing Data

The Global Forecast System (GFS) is a global spectral data assimilation and forecast model system produced by National Centers for Environmental Prediction (NCEP), and dozens of atmospheric are available through this dataset which is on 0.5-degree by 0.5-degree grids prepared operationally every six hours (00:00, 06:00, 12:00, and 18:00 UTC). The NCEP GFS final (FNL) gridded analysis datasets from January 2000 until the current day can be obtained from its official website, while this study used the data of NCEP GFSFNL version of 2010 as the atmospheric forcing dataset of WRF model.

5.1.1.3 Underlying Surface Data

The underlying surface data under the scenarios of DB, DN, EB, and EN as well as BL, which are required in the scenario-based simulation, were derived from the dataset of National Basic Research Program of China. The dataset was originally established with the 1 km × 1 km grid data based on the satellite remote sensing images and ground information of year 2000, and it used the land use and land cover classification system of the United States Geological Survey (USGS). In this study, the 1 km grid data were first resampled into the 5 km grid data. The

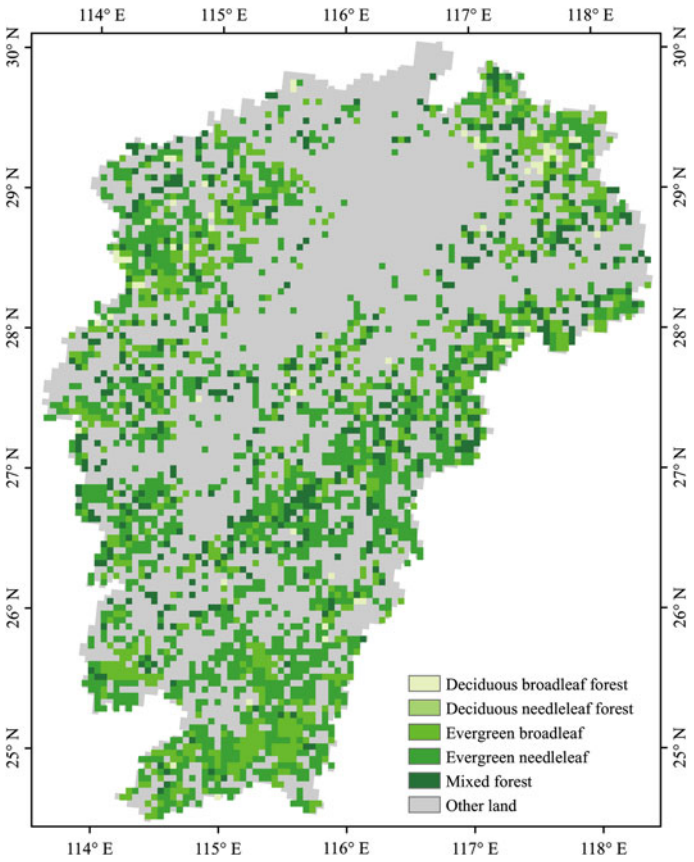

Fig. 5.1 Forest area of Jiangxi Province in 2000

statistical results of the underlying surface data suggest that more than 40 % are covered by the forests (2,717 pixels) in Jiangxi Province (Fig. 5.1), and about 30 % of them were covered by the broadleaf forests, while the needleleaf forests accounted for more than 52 % of the total forestry area.

The underlying surface data under the DB, DN, EB, and EN scenarios are generated by replacing all the forests with one specific type of forests, respectively. For instance, the underlying surface data under the DB scenario was generated by replacing all the forestry area by the deciduous broadleaf forests, and consequently all the forestry area in Jiangxi Province is covered by the deciduous broadleaf forests under the scenario of BD. And similarly, the underlying surface data of DN, EB, and EN were generated by altering the property of pixels.

5.1.2 Impacts of Afforestation on the Regional Surface Climate

The simulation results in 2010 are finally obtained under the scenarios of DB, DN, EB, and EN as well as BL.

5.1.2.1 Effects on the Annual Average Temperature

The simulation results showed that there were significant effects of the vegetation change on the annual average temperature in Jiangxi Province. Among the results under the four hypothetical extreme scenarios, there were overall cooling effects under the scenarios of DB and DN, while warming effects under the scenarios of EB and EN (Fig. 5.2). The statistics indicates that the deciduous broadleaf expansion under the scenario of DB will make the annual average temperature decrease by 0.08 °C. This cooling effect will mainly happen in the southern part of Jiangxi Province. For some area there, the annual average temperature will even decline by more than 0.2 °C. By comparison, the expansion of deciduous needleleaf forests under the scenario of DN only shows slight cooling effects, it is notable that the cooling effects also mainly happen in the southern part of Jiangxi Province, but are not as significant as that under the scenario of DB. The results under the scenarios of DN indicate there are some warming effects in the areas near the northern and western boundary of Jiangxi Province, while the overall effects of the expansion of deciduous needleleaf forests make the annual average temperature decrease by 0.02 °C under the scenario of DN.

The spatial pattern of the warming effects under the scenario of EB is consistent with the pattern of forests in Jiangxi Province, and the evergreen broadleaf expansion will make the annual average temperature increase by 0.03 °C (Fig. 5.2). The annual average temperature under the scenario of EN will increase by 0.01 °C more than that under the scenario of BL. In summary, the deciduous forest plays a positive role in decreasing the annual average temperature while evergreen forest contributes to the increase of annual average temperature, and the effect of needleleaf forest expansion on annual average temperature is much more significant than that of broadleaf forest. This may be due to the differences between the thermal properties of the deciduous and evergreen forests.

5.1.2.2 Effects on the Annual Average Precipitation

The expansion of deciduous forests leads to significant change of the spatial pattern of the annual average precipitation in Jiangxi Province regardless of the scenarios. The simulation results showed that the expansion of deciduous broadleaf forests will make the annual average precipitation in the southeast part of Jiangxi Province decrease by more than 400 mm (Fig. 5.3). Besides, the annual

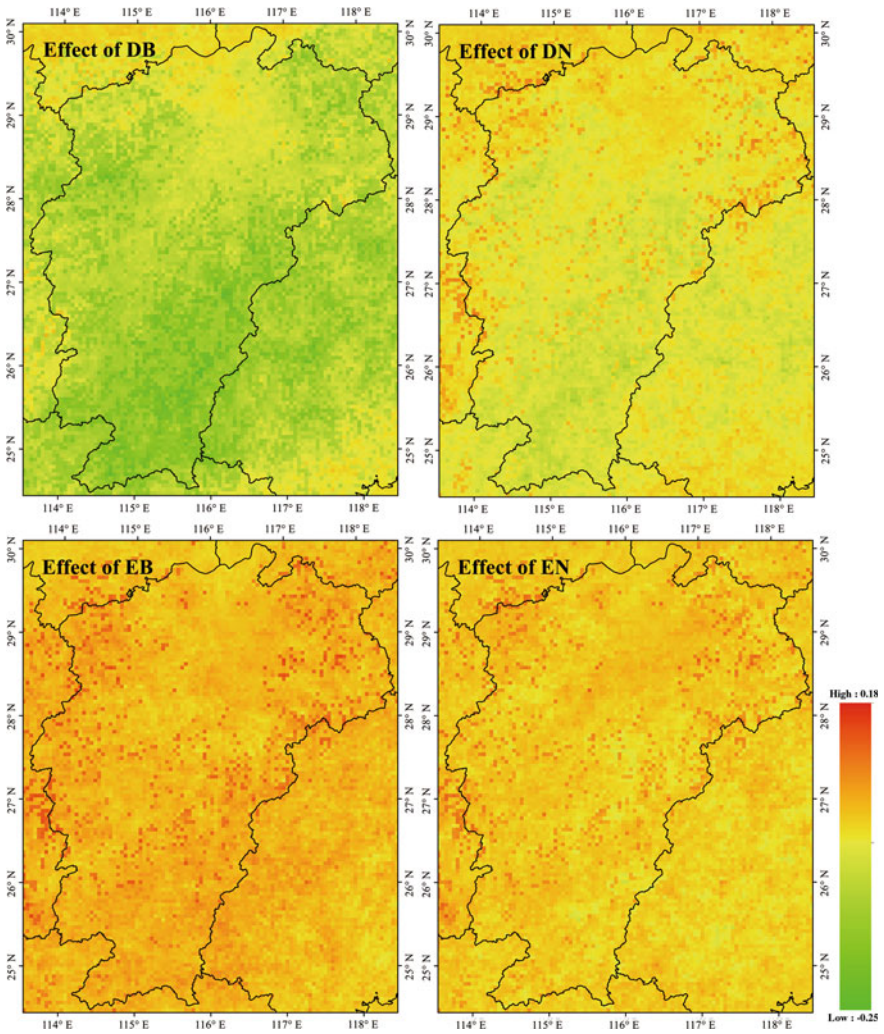

Fig. 5.2 Simulated effects of afforestation on the annual average temperature (measured in degrees Celsius) in Jiangxi Province

average precipitation in the northwest part of Jiangxi Province will also increase by more than 250 mm. However, the expansion of the deciduous broadleaf forests will make the overall annual average precipitation in the simulation area decrease by 47 mm under the scenario of DB. By comparison, the drought effects of the deciduous needleleaf forest expansion under the scenario of DN area is little slighter than that of under the scenario of DB, it will make the annual average precipitation decrease by 33 mm in the study area on the whole. What's more, the spatial pattern of the climatic effects under the scenario of DN is similar with that under the scenario of DB.

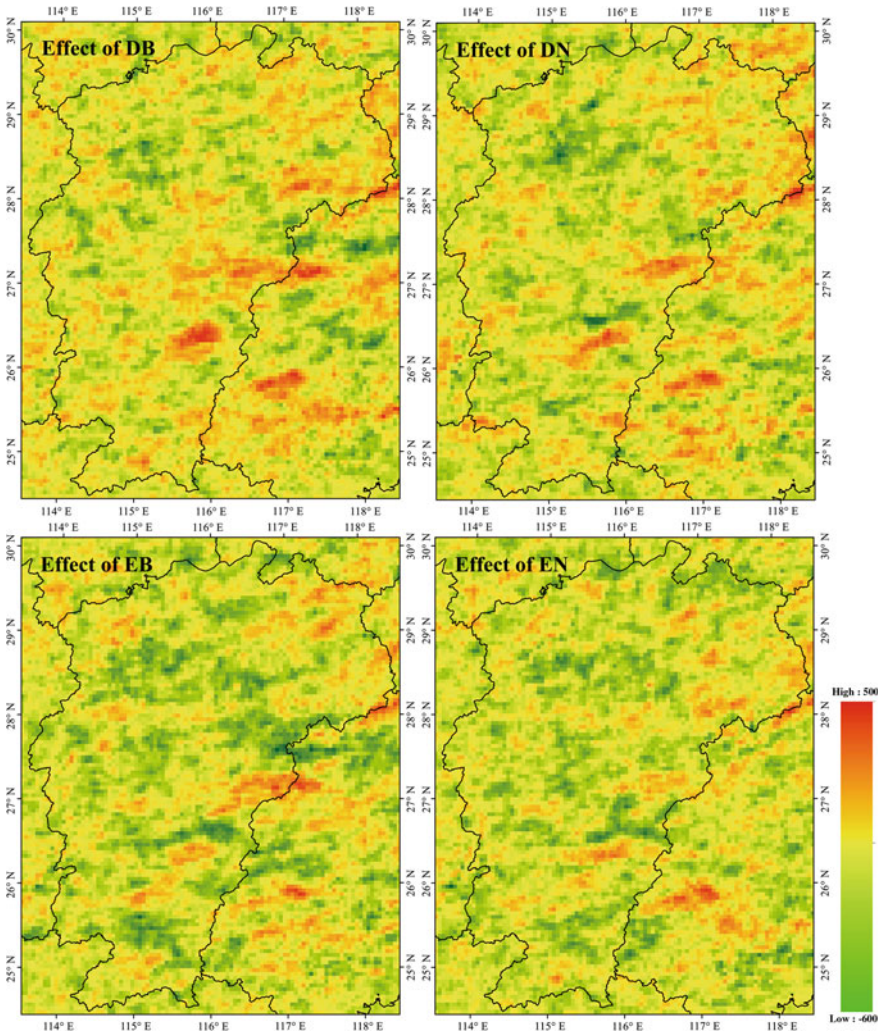

Fig. 5.3 Simulated effects of afforestation on the annual average precipitation (measured in millimeters) in Jiangxi Province

In comparison, the simulation results under the scenarios of EB and EN indicated that the overall effects of the evergreen forest expansion on the annual average precipitation are not as significant as that under the scenarios of DB and DN. In most part of Jiangxi Province, the evergreen forest expansion will make the annual average precipitation increase by 50–200 mm under the scenarios of EB and EN (Fig. 5.3). The drought effects under the scenarios of EB and EN will mainly happen in the area near the eastern boundary of Jiangxi Province. The annual average precipitation will decrease by 2.6 and 3.9 mm under the scenarios

Table 5.1 Simulated effects of afforestation on the monthly average temperature in Jiangxi Province (measured in degrees Celsius)

Month	DB		DN		EB		EN	
	Mean	Std.	Mean	Std.	Mean	Std.	Mean	Std.
Jan	−0.12	0.09	−0.06	0.06	0.05	0.06	0.03	0.05
Feb	−0.09	0.07	−0.05	0.06	0.03	0.05	0.02	0.05
Mar	−0.07	0.07	0.00	0.05	0.05	0.05	0.02	0.05
Apr	−0.07	0.06	−0.03	0.05	0.02	0.04	0.01	0.04
May	−0.08	0.07	−0.02	0.05	0.01	0.05	−0.01	0.05
Jun	−0.08	0.08	−0.03	0.06	0.01	0.06	0.00	0.06
Jul	−0.05	0.08	−0.02	0.07	0.00	0.07	−0.01	0.07
Aug	−0.06	0.08	−0.01	0.07	0.00	0.06	−0.01	0.07
Sep	−0.08	0.08	−0.03	0.06	0.00	0.06	−0.01	0.06
Oct	−0.07	0.06	−0.01	0.04	0.03	0.04	0.01	0.04
Nov	−0.08	0.07	0.00	0.06	0.05	0.06	0.02	0.05
Dec	−0.07	0.07	0.00	0.05	0.05	0.06	0.03	0.05

of EB and EN, respectively. On the whole, the deciduous forest expansion may aggravate the drought, while the expansion of evergreen forests may increase the annual average precipitation in most of the regions in Jiangxi Province. So the expansion of evergreen forests is more favorable than the expansion of deciduous forests since the seasonal drought is one of the main problems that restrain the agricultural production in Jiangxi Province.

5.1.2.3 Effects on the Monthly Climate

The effects of afforestation on the monthly average temperature vary from month to month under all the four scenarios (Table 5.1). Under the scenario of DB, the deciduous broadleaf forest expansion will result in a relatively stable decrease of the monthly average temperature in most of the months, by about 0.07–0.08 °C, and it will decrease most in January and least in July, by about 0.12 and 0.05 °C, respectively. By comparison, there is a slighter decrease of the monthly average temperature due to the deciduous needleleaf forest expansion under the scenario of DN than that of under the scenario of DB, moreover, it will decrease by no more than 0.03 °C from April to October. The afforestation even has no effects on monthly average temperature in March, November, and December under the scenario of DN.

In contrast to the effects under the scenarios of DB and DN, the evergreen broadleaf forest expansion will lead to some increase of the monthly average temperature (Table 5.1). The simulation results show that the monthly average temperature will increase by 0.03–0.05 °C from October to March under this scenario, and it will decrease by 0.01–0.02 °C in April, May, and June. Besides, there are no significant effects of the evergreen broadleaf forest expansion on the monthly average temperature in July, August, and September. There are more

Table 5.2 Simulated effects of afforestation on albedo in Jiangxi Province (magnified by 10^{-3})

Month	DB		DN		EB		EN	
	Mean	Std.	Mean	Std.	Mean	Std.	Mean	Std.
Jan	11.31	30.52	3.59	27.43	−7.61	28.73	−7.61	28.73
Feb	11.56	30.37	3.75	27.17	−7.57	28.36	−7.56	28.39
Mar	11.51	31.18	3.70	28.05	−7.71	29.26	−7.71	29.25
Apr	11.75	27.83	3.93	24.15	−6.57	25.03	−6.57	25.03
May	12.05	22.80	4.24	17.93	−4.78	18.16	−4.78	18.16
Jun	12.35	20.04	4.54	13.99	−3.58	13.54	−3.58	13.54
Jul	12.34	19.75	4.52	13.59	−3.47	13.12	−3.47	13.12
Aug	12.33	19.92	4.52	13.84	−3.54	13.39	−3.54	13.39
Sep	12.31	20.44	4.49	14.60	−3.77	14.27	−3.77	14.27
Oct	11.80	24.03	3.99	19.62	−5.31	20.22	−5.31	20.22
Nov	11.58	27.10	3.77	23.40	−6.40	24.40	−6.40	24.40
Dec	11.26	28.63	3.57	25.42	−7.10	26.62	−7.08	26.63

complex effects of expansion of the evergreen needleleaf forests under the scenario of EN, which makes the monthly average temperature decrease from May to September and increase from October to April (Table 5.1). On the whole, the variation of the monthly average temperature change under the scenarios of DN, EB, and EN is similar to that of under the scenario of DB.

Afforestation can affect the monthly average temperature via multiple ways such as albedo, potential evapotranspiration, and leaf area index. Considering the plentiful water and heat resources in Jiangxi province, albedo is most likely to be the principal cause resulting in the monthly average temperature changes. The changes of albedo under all the four scenarios are provided to help to identify the reasons of monthly average temperature changes (Table 5.2). A larger increase in albedo shows a severer decrease trend in monthly average temperature. It implies that the cooling effect is due to the low surface net radiation caused by high albedo under the scenarios of DB and DN. And on the contrary, the declines of albedo under the scenarios of EB and EN may be the major causes of monthly average temperature increase in Jiangxi Province. The variation of monthly average temperature change also has a convergence trend with that of albedo change. The correlation coefficient of monthly average temperature change and albedo change reaches -0.77, which also implies that the temperature changes are mainly derived from the changes of albedo driven by afforestation.

The effects of afforestation on the monthly average precipitation are more significant than that on the monthly average temperature. The precipitation in Jiangxi Province will decrease greatly in the summer under the scenarios of DB and DN (Table 5.3). Under the scenario of DB, the monthly average precipitation will decrease by 10.63, 11.50, and 8.63 mm in June, July, and August, respectively. Although the decrement of the monthly average precipitation is smaller than that of under the scenario of DN, it still reaches 10.42 mm in July. The drought effects of the deciduous forest expansion will last throughout the year

Table 5.3 Simulated effects of afforestation on the monthly average precipitation in Jiangxi Province (measured in millimeters)

Month	DB		DN		EB		EN	
	Mean	Std.	Mean	Std.	Mean	Std.	Mean	Std.
Jan	−0.16	5.01	−0.18	4.96	−0.06	5.09	−0.01	4.92
Feb	−1.03	10.98	−0.89	11.85	0.03	10.60	0.25	10.65
Mar	−0.57	10.43	−0.86	11.87	0.07	10.79	0.20	9.93
Apr	−2.39	21.93	−1.77	20.83	0.20	22.28	1.44	22.67
May	−5.10	43.83	−4.01	41.78	0.34	48.23	−0.99	46.52
Jun	−10.63	61.72	−6.37	55.74	−1.20	57.79	−0.34	55.14
Jul	−11.50	59.29	−10.42	61.17	−0.89	61.26	−2.95	60.15
Aug	−8.63	42.27	−4.86	42.42	−1.29	40.29	−1.89	42.31
Sep	−6.79	39.63	−3.48	39.87	0.11	40.48	0.06	38.69
Oct	−0.29	9.19	−0.29	8.96	0.09	8.74	0.23	9.01
Nov	−0.25	1.40	−0.21	1.35	0.03	1.30	0.07	1.32
Dec	−0.03	1.77	−0.08	1.72	−0.03	1.77	0.02	1.69

under the scenarios of DB and DN. By contrast, there are slight effects of the evergreen forest expansion on the monthly average precipitation under the scenarios of EB and EN (Table 5.3).The monthly average precipitation will decrease most in August under the scenario of EB, with a decrement of 1.29 mm, while it will decrease by no more than 3 mm under the scenario of EN. Overall, there are no significant variations for the monthly average temperature change among the scenarios of DB, DN, EB, and EN.

Above all, the effects of annual average temperature show a decreasing order: EB > EN > DN > DB. By comparison, the expansion of deciduous needleleaf forests under the scenario of DB shows evident cooling effects. In addition, the cooling effects mainly happen in the southern part of Jiangxi Province and the effects of annual average precipitation of the evergreen forests are larger than the deciduous forests.

5.1.3 Concluding Remarks on Afforestation in Jiangxi Province

This study analyzes the impacts of afforestation on the regional climate at different temporal scales under four designed scenarios in Jiangxi Province. The main conclusions are follows:

(i) The deciduous forest expansion plays a positive role in decreasing the annual average temperature, while the evergreen forest expansion makes the annual average temperature increase. On the whole, the effects of the needleleaf forest expansion on the annual average temperature are not as significant as that of the broadleaf forest. The expansion of deciduous forests

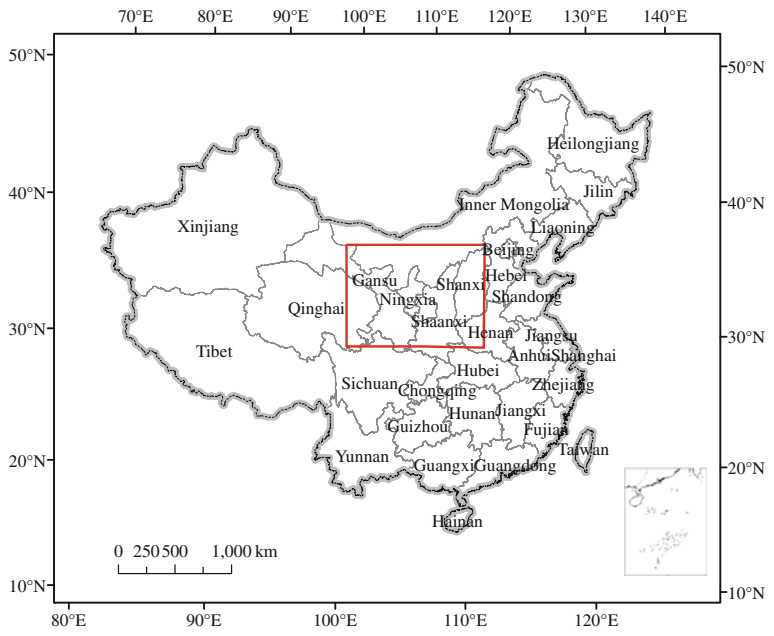

Fig. 5.4 Location of study area

may aggravate the seasonal drought in Jiangxi Province, while the expansion of evergreen forests is more favorable since it may increase the annual average precipitation in most part of Jiangxi Province.

(ii) There are significant effects of afforestation, especially the deciduous forest expansion, on the monthly average precipitation. There is only slight change in the monthly average temperature caused by afforestation. What's more, the deciduous forest expansion may result in severe drought at the local scale in the summer in Jiangxi Province.

5.2 Projection of the Biogeophysical Effects of Green for Grain Project in the Semiarid Grassland Area

Loess Plateau is mainly located in the arid and semiarid area of China with a fragile ecological environment (Fig. 5.4). Poor land use practices have resulted in the serious soil erosion, land degradation, desertification, and deterioration of the ecological environment (Clarke 2000). To speed up the construction of ecological environment in Western China, the government had implemented the project of Green for Grain, which has achieved desirable results. It not only prevents the soil erosion and ecological environment degradation effectively, but also promotes the development of grass industry, animal husbandry, and agriculture industries after the policy is implemented comprehensively (Kang 1985). However, when we are

concerned about the benefits of the Green for Grain project, it should be noted whether such large-scale land cover changes will impact the regional climate. Will it relieve the drought to some extent or make it more serious? Does it have effects on energy balance of near surface? Returning cropland to forestry area or grassland will continue in the next few decades to protect the ecological environment; therefore, the contribution of land cover changes to the energy flux of near surface becomes one of the significant issues (Kang 1985).

To quantify the effects of land cover changes on energy balance in the Loess Plateau, it is essential for regional ecological environment construction. This study simulates the spatial heterogeneity of land cover changes based on the Dynamics of Land System (DLS) model, estimates the surface energy variation at a regional scale based on the principle of energy balance and similarity theory of boundary layers with the WRF model, and finally explores the response mechanism of the temporal and spatial variation of surface energy on land cover changes. The results will provide the scientific reference for the land use planning and climate change mitigation.

5.2.1 Data Source and Handling

5.2.1.1 Land Cover Data

Different communities have different land cover classification systems, and this study applies the classification system of USGS with 24 types of land cover. First, 1 km land cover data in 2010 are extracted from the remote sensing images, and the year 2010 is taken as the baseline year. Then two kinds of scenario, e.g., coordinated environmental sustainability (CES) scenario, rapid economic growth (REG) scenario, etc., are designed. The land cover data during 2010–2050 are simulated by DLS model based on the land demand estimated under the two scenarios. Finally, the 1 km resolution land cover data from 2010 to 2050 were resampled into 10 km resolution data according to the requirement of the WRF model.

5.2.1.2 Forcing Data

The forcing data required in the WRF model, including wind field, surface air temperature, longwave radiation, shortwave radiation, and so on, are derived from the dataset of the fifth phase of the Climate Model Intercomparison Project (CMIP5). CMIP5 consists of 29 global climate models, and the dataset of Geophysical Fluid Dynamics Laboratory CM3 (GFDL-CM3) model are adopted in this study. It incorporates an atmospheric chemistry model within the fully interactive framework of the atmosphere, ocean, land, and sea ice components, and has four Representative Concentration Pathways (RCPs) scenarios such as RCP2.6, RCP4.5, RCP6.0, and RCP8.5. This study analyzed the energy balance under the RCP6.0 scenario, the CO_2 concentration under this scenario rank in the

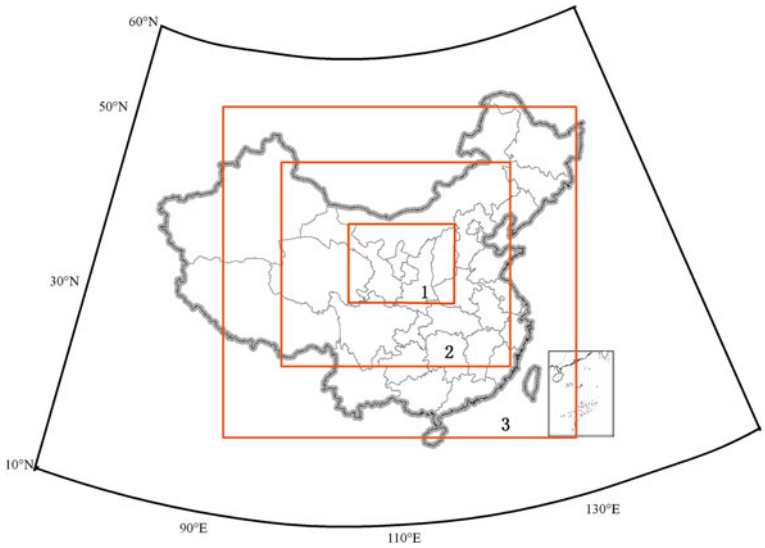

Fig. 5.5 Schematic diagram of scheme design for three-layer nested WRF model

intermediate level, and it is more tally with the actual situation in China. Since the dataset has been established and updated since July 1999, all the data needed in this study can be obtained, e.g., the surface observation data and the remote sensing data.

5.2.2 Methodology

5.2.2.1 Experiment Design

The WRF model is developed into two versions, one is for business, another one is for research, and this study adopts the latter one, namely ARW (Advanced Research WRF), to carry out the relevant simulation. To simulate the energy distribution of near land surface more accurately, this study applies three-layer nested structure including D01, D02, and D03, and the area ratio of three layers is 3:2:1. The spatial resolution of output of D03 is set to 1 km (Fig. 5.5). The air temperature, sea ice, and soil moisture data required by the model are updated every day.

The parameterization scheme of physical processes in the WRF model is as follows. The longwave radiation scheme and shortwave radiation scheme adopted RRTM and Dudhia, respectively, the boundary layer process scheme utilized YSU, and the land surface process scheme used NOAH Land surface model (Table 5.4). The simulation was implemented with the climate forcing data from January of 2010 to December of 2050.

Table 5.4 Design of WRF model and relative description

WRF	Designation	Description
Simulation period	2010_01_01–2050_12_31	
Time resolution	Day	
D01/02/03 land cover data	USGS	
Microphysics parameterization scheme	WSM3	It includes water vapor, cloud water, rain, cloud ice, snow, and cloud water
Longwave radiation scheme	RRTM	It uses pre-set tables to accurately represent longwave processes due to water vapor, ozone, CO_2, and trace gases (if present) as well as accounting for cloud optical depth
Shortwave radiation scheme	Dudhia	It is a simple downward integration of solar flux, accounting for clear-air scattering, water vapor absorption (Lacis and Hansen 1974), and cloud albedo and absorption. It uses look-up tables for clouds from Stephens (1978)
Land surface process scheme	Noah land surface model	Unified NCEP/NCAR/AFWA scheme with soil temperature and moisture in four layers, fractional snow cover and frozen soil physics
Boundary layer process scheme	YSU	Non-local-K scheme with explicit entrainment layer and parabolic K profile in unstable mixed layer
Cumulus parameterization scheme	Kain–Fritsch	It utilizes a simple cloud model with moist updrafts and downdrafts, including the effects of detrainment, entrainment, and relatively crude microphysics

5.2.3 Scenario Design

Based on the characteristics of socialeconomic development in the past 30 years, we design two kinds of socialeconomic development scenarios, that is, REG scenario and CES scenario. Among the two scenarios, the social and economic development process such as population, factor endowments, and technological advances are all taken into account in Loess Plateau. Under the REG scenario, it assumes that the reforms will be put forward quickly and smoothly, the role of market in the allocation of resources will be enhanced obviously, structural adjustment will be vigorously promoted, and the economic growth pattern will make progress. CES scenario mainly considers that it is developed with slower urbanization, slow recovering of the world economy, serious trade protection, slow export growth, higher international energy prices, restricted energy imports, slow progress in system reform, and slow technological innovation and efficiency improvement.

5.2.4 Land Cover Changes from 2010 to 2050 in the Semiarid Grassland Area of China

This study simulates the land cover of the semiarid grassland area of China from 2010 to 2050 under two kinds of scenarios by DLS model, and the robust of the DLS model has been proven through investigation, so the simulation results is trustworthy. The simulation results illustrate that the spatial distribution of land cover in the study area has no disruptive changes from 2010 to 2050, but the changing ratio will gradually slow down. The analysis on land cover change between different periods indicates that the conversion types are mainly dominated by the conversion between cropland and grassland, but the tendency and scale of the major land cover changes are various under different scenarios.

Under the CES scenario, the grassland cover shows an increasing trend. Although the forestry area will rise in some parts of the study area to some extent, the total forestry area will show a slight downward trend from 2010 to 2050. Maybe the harsh natural conditions restrict the forestry area expansion, and it is notable that the largest part of the newly increased forest cover is shrubland. Additionally, the CES scenario takes the Green for Grain project into account, which promotes the growth of grassland area and the decrease in the cropland area. In the period of 2010–2030, the grassland will grow by 4.8 %, and it will increase 4.4 % during the period of 2030–2050. Most of the increased grasslands are converted from cropland, and are mainly distributed in the Shanxi Province, southern Shaanxi Province, southeast of Gansu Province, and some areas of Ningxia. As for the cropland, it will reduce by 22.6×10^3 km^2 from 2010 to 2030, and by about 19.8×10^3 km^2 in the period of 2030–2050. Barren or sparsely vegetated land is another kind of land cover which is mainly converted to

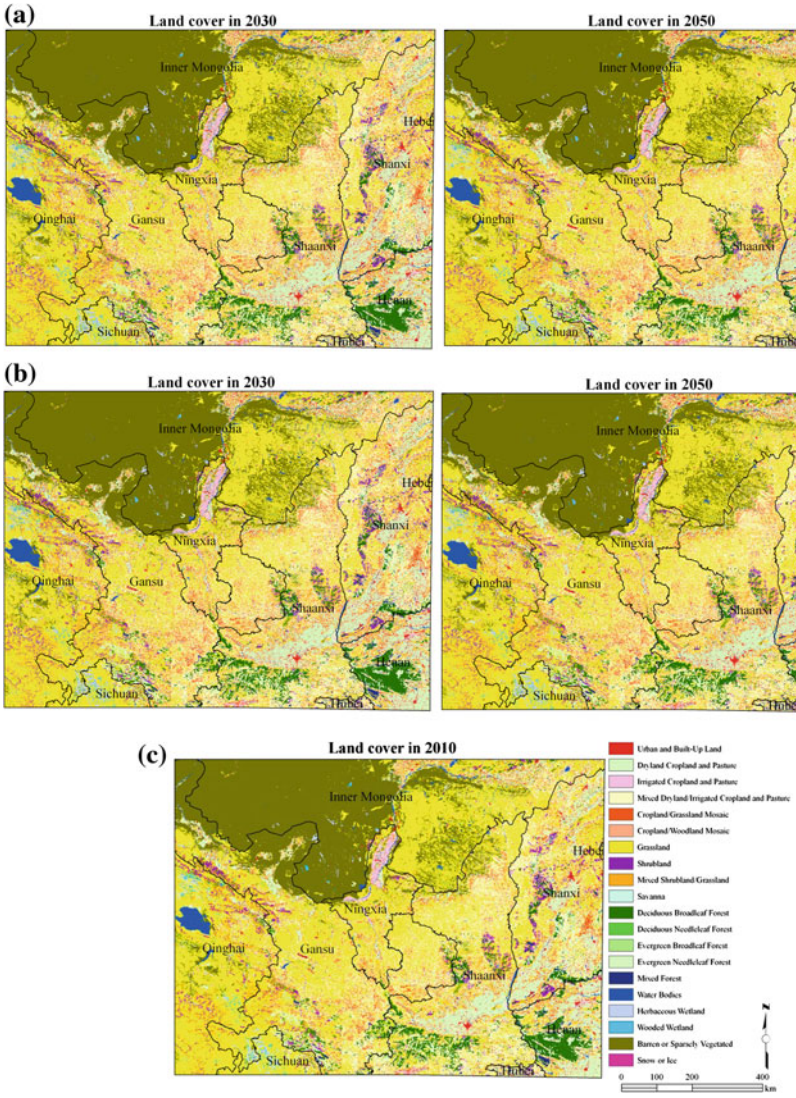

Fig. 5.6 Land cover change under different scenarios from 2010 to 2050 **a** REG scenario, **b** CES scenario, **c** Baseline year

grassland or shrubland in the north and middle of the semiarid grassland area of China due to ecological recovery construction (Fig. 5.6). Another significant conversion is cropland to urban area, and the expanded urban area is mainly located in the surroundings of the cities. Western China is in the rapid process of urbanization and industrialization; therefore, urban area expansion cannot be prevented in the immediate future.

Table 5.5 Statistics of heat flux and radiation (measured in W/m^2) of different land covers

land cover types	Latent heat flux	Downward shortwave radiation
Cropland and pasture	24.9	279.6
Grassland	25.3	284.0
Forestry area	36.0	289.9
Urban area	15.0	295.0

The socioeconomic development and rapid urbanization mean that more lands are converted to urban area. During the period of 2010–2050, there will be an increase of 5.3×10^3 km^2 for urban area in the semiarid grassland area of China under the REG scenario, most of which is converted from cropland. Correspondingly, there is less cropland converted to grassland or forestry area. Compared to the CES scenario, the grassland will increase only by 23.3×10^3 km^2 during the period of 2010–2030, while with an increase of 4.2 % in the period of 2030–2050. The expansion of grassland is mostly concentrated in the eastern part of Loess Plateau (Fig. 5.6). On contrary, most of the cropland is located in the southern part of the study area including the central and southern Shanxi Province, southern Shanxi Province, and southeastern Gansu Province. It is notable that there are more water resources in the eastern and southern part of study area, which is beneficial for forest growing. Under the REG scenario, some areas of grasslands are degraded to bare land or are turned into cropland in the western part of the semiarid grassland area of China.

5.2.5 Effects of Land Cover Conversion on Energy Balance in the Semiarid Grassland Area of China

This study simulates the latent heat flux and downward shortwave radiation by the WRF model, and then summarizes the latent heat flux and downward shortwave radiation on different types of land cover. The results indicate that the energy fluxes vary with the land covers, so the land cover conversion will produce different effects on regional environment and climate, however, the extent of their impacts and sensitive region has obvious temporal and spatial disparity. In addition, the statistical results show that forestry area has highest latent heat flux with 36.0 W/m^2, while urban area has relative low latent heat flux which is 15.0 W/m^2 (Table 5.5). As for the downward shortwave radiation, the urban area is highest with 295.0 W/m^2, while it is lowest for cropland and pasture.

5.2.5.1 Latent Heat Flux

The simulation results show that the barren or sparsely vegetated land in the western parts of Inner Mongolia Autonomous Region and northern Shaanxi Province has lower latent heat flux, while it is higher in the southern areas which

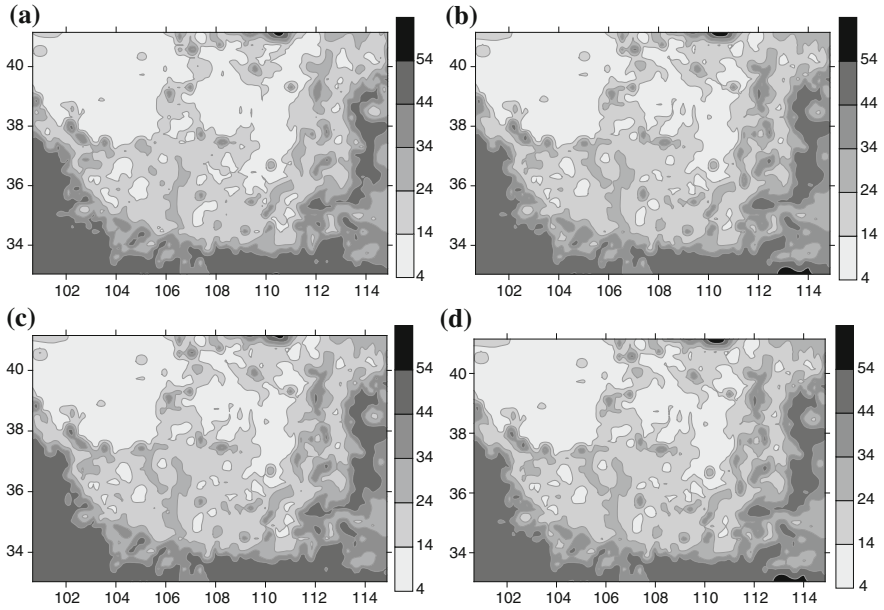

Fig. 5.7 Latent heat flux changes under different scenarios in 2030 and 2050 in the semi-arid grassland area of China (W/m^2) **a** REG scenario in 2030, **b** CES scenario in 2030, **c** REG scenario in 2050, **d** CES scenario in 2050

are mostly covered by grassland, shrubland, cropland, and pasture. Actually, the forestry area also has higher latent heat flux; however, it has no obvious effects on energy flux since the forestry area in the study area is extremely small.

The annual average latent heat flux in the semiarid grassland area of China will not change obviously from 2010 to 2050, with only 3.2 W/m^2 increment. However, there will be various climate effects in different areas from 2010 to 2050 (Fig. 5.7). Due to the impacts of the Green for Grain project, the latent heat flux will increase in the middle part of Shanxi Province, southern part of Ningxia Province, southern and southeast part of Gansu Province, with the increment ranging from 1.2 to 20.4 W/m^2. The grassland degradation could lead to the decrease of latent heat flux in the middle part of Inner Mongolia Autonomous Region, north of Ningxia Province, northwest of Shaanxi Province because of the conversion from grassland to barren or sparsely vegetated land, with a decrease of 3.2 W/m^2 (Fig. 5.7).

To predict the energy balance in the future, this study simulates the energy flux under two scenarios. The results illustrate that the latent heat flux under the CES scenario is higher than that of under the REG scenario due to the fact that more ecological constructions are conducted under the CES scenario, which will produce more latent heat flux. It can be seen from the Fig. 5.7 that the two scenarios have similar spatial distribution of latent heat flux, but there are regional

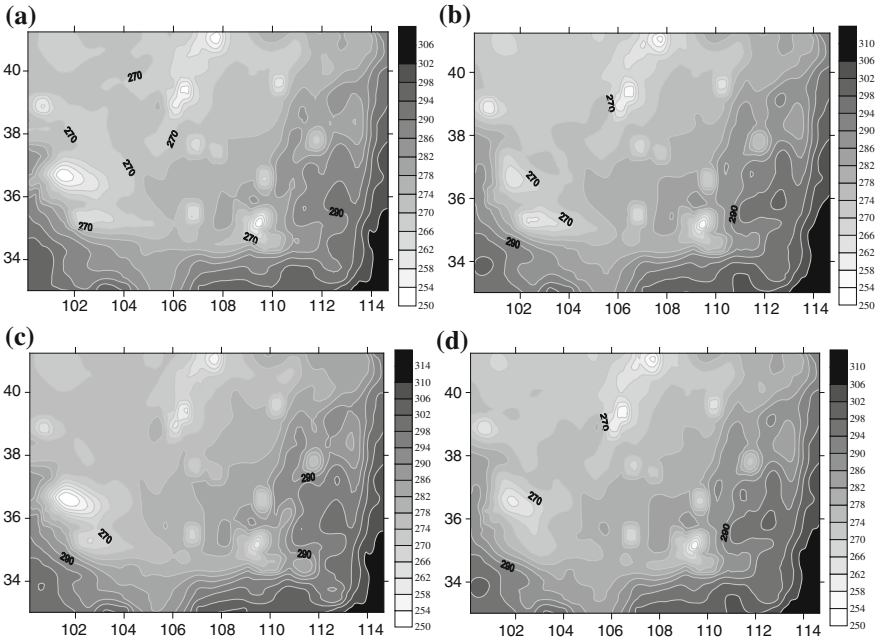

Fig. 5.8 Downward short wave radiation changes under different scenarios in 2030 and 2050 in the semi-arid grassland area of China (W/m^2) **a** REG scenario in 2030, **b** CES scenario in 2030, **c** REG scenario in 2050, **d** CES scenario in 2050

differences as well. The CES scenario has smaller areas within the range of 4–14 W/m^2 especially in the central regions, but larger areas within the range of 44–64 W/m^2.

5.2.5.2 Downward Shortwave Radiation

Downward shortwave radiation is one of the significant factors influencing the energy balance of climate system. This study simulates the downward shortwave radiation in different periods under the REG scenario and CES scenario from 2010 to 2050. The results indicate that the downward shortwave radiation is weak in the Inner Mongolia Autonomous Region, the northern part of Shaanxi Province, and Ningxia Hui Autonomous Region, while it is stronger in the southeastern area of Loess Plateau. This is because the northern part of Loess Plateau is covered mainly by the overlapped zone of the grassland and barren or sparsely vegetated land, while the land cover in the southeastern part is dryland cropland pasture. It can be seen from here that the Green for Grain project will reduce the downward shortwave radiation. However, different scenarios have different kinds of land cover changes, so the downward shortwave radiation under two different scenarios has significant spatial and temporal disparity.

According to the statistical analysis on the downward shortwave radiation at the grid scale, it can be found that the annual average downward shortwave radiation will have no obvious changes from 2010 to 2050 without regarding the scenarios, which will grow consistently from 280.4 to 282.1 W/m^2 under the CES scenario, and that under the REG scenario will increase from 276.2 to 280.5 W/m^2 (Fig. 5.8). Although the Green for Grain project can reduce the downward shortwave radiation, the urban area expansion will lead to more downward shortwave radiation, and that is why there is a higher increment of downward shortwave radiation under the REG scenario. On comparing the downward shortwave radiation under two different scenarios, it can be seen that it is higher under the REG scenario than that of under the CES scenario in the period of 2010–2050. The spatial distribution of downward shortwave radiation in 2030 and 2050 under the REG scenario represents that the area, whose downward shortwave radiation is less than 265 W/m^2, is expanding especially in the northern and middle region and the western part of the semiarid grassland area of China due to the ecological recovery (Fig. 5.8). For example, the barren or sparsely vegetated lands are improved to be grassland gradually.

5.2.6 Concluding Remarks on Biogeophysical Effects of Green for Grain Project

This study applies the DLS model to simulating the land cover distribution from 2010 to 2050 under the CES scenario and REG scenario, and then analyzes the effects of land cover change on the regional energy balance in the semiarid grassland area of China through implementing the numerical simulation with the WRF model. Latent heat and radiation are the main factors influencing the energy balance, so this study selects two indexes including latent heat and downward shortwave radiation to explore the energy balance in the study area. The conclusions are as follows:

(i) There will be no significant change in the spatial pattern of the land cover in the study area during 2010–2050. The changing ratio of all the land cover types will show a decreasing trend with time. Under the CES scenario, the grassland shows an increasing trend, while the forest cover is shrinking because the harsh natural conditions restrict the forestry area expansion, and shrubland accounts for the largest percentage of the newly increased forest cover. Barren or sparsely vegetated land will be mainly converted to grassland or shrubland. During the period of 2010–2050, there will be an increase in urban area under the REG scenario, and the main land cover converted to urban area is cropland. Compared to the CES scenario, the rate of increase of grassland will be lower, and the expansion of grassland is mainly concentrated in the western part of Loess Plateau.

(ii) The simulation results indicate that there will be no obvious changes in energy flux of near surface under the CES scenario, and the latent heat flux and downward shortwave radiation will all have small-scale increase.

Therefore, the land cover conversion maybe has no great impact on climate in the coming 40 years. However, the spatial disparity of energy flux is extremely significant. The Green for Grain project makes the latent heat increase to some extent, while the grassland degradation could lead to the decrease of latent heat due to the conversion from grassland to barren or sparsely vegetated land. As for the downward shortwave radiation, it can be seen that it is higher under the REG scenario than that of under the CES scenario in the study period. Urbanization and the decrease in forestry area will offset the energy flux reduction brought by grassland expansion to some extent.

Although we have carried out an estimation for the effects of land cover change on energy balance by the WRF model, there are certain limitations in our analysis. First, there is uncertainty on the prediction of socialeconomic developments, moreover, the accuracy of the prediction for the socialeconomic development determines the prediction for the land cover change, which further impacts the simulation of regional climate. Therefore, there is uncertainty on all of the simulations. Second, there are various factors that influence the regional energy flux, but in this study, only the land cover change is taken into account to analyze its impacts on the regional energy flux.

5.3 Numerical Simulation of the Effects of Grassland Degradation on the Surface Climate in Overgrazing Area of Northwest China

As one of the most widespread land use type, grassland covers about 40 % of the total area of China. It can not only provide amount of food and materials such as milk, meat, forage, etc., but also can regulate the regional climate, e.g., the mitigation of greenhouse gas (GHG) emissions through soil organic carbon (C) and nitrogen (N) sequestration (Fan et al. 2008; Barthold et al. 2013). In the past decades, the grassland degradation and desertification in Northwest China have greatly intensified due to the livestock overgrazing, rapid population growth, irrational exploitation of the natural resources, and the expansion of road network in recent years (Xu et al. 2012; Deng et al. 2011a, b). Furthermore, the grassland degradation has led to the decline of grassland productivity and increased the frequency of extreme climate events such as droughts and fierce freeze-up, which have seriously influenced the sustainable development of animal husbandry (Deng et al. 2011a, b). Therefore, it is of great importance to study the influence of grassland degradation on the climate in the overgrazing area of Northwest China (Bounoua et al. 2002).

Some studies have found that the grassland degradation in overgrazing areas of Northwest China has brought about obvious effects on the regional climate (Nobre et al. 1991; Foley et al. 1996; Gibbard et al. 2005). However, those researches mainly focused on the effects of grassland degradation in the historical period,

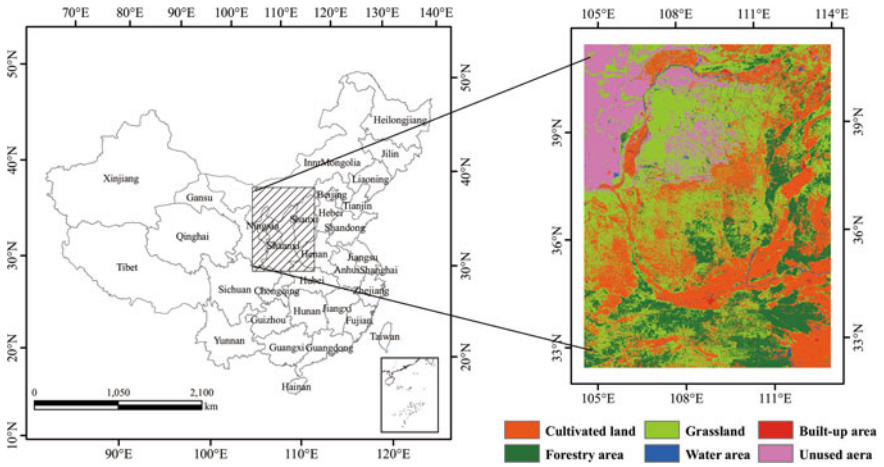

Fig. 5.9 Location of the study area and the distribution of land use type in the overgrazing areas of Northwest China

while this study aims to explore the potential impacts of grassland degradation on climate change in overgrazing area of Northwest China from 2010 to 2040.

5.3.1 Data and Methodology

5.3.1.1 Case Study Area

The overgrazing area of Northwest China is located between 104° 04′ and 114° 02′ E, 32°40′ and 41° 20′ N, with a total land area of 811,856 km^2, and covers five provinces including Ningxia Province, the southeast part of Gansu Province, Shaanxi Province, the western part of Shanxi Province, and the middle and southwest part of Inner Mongolia Autonomous Region (Fig. 5.9). This area stretches across the eastern monsoon region and northwest arid region, with an annual average temperature of 5–10° and the annual precipitation of 200–800 mm, and is close to the Qinghai–Tibet alpine region, approximately located in the transition zone of the three major natural zones of China. There is very limited water resource, the spatiotemporal distribution of which is very imbalanced, and there are frequently meteorological disasters. It is one of the largest grazing areas, and is also the major production base of the animal husbandry industry in China.

The grassland and cultivated land are the dominant land use types in this region, accounting for 36.19 and 29 % of the total area, respectively. The irrational utilization of grassland resources is very common due to overgrazing and over-reclamation under the background of one-sided pursuit of economic benefit since the 1980s, which has led to the continual degradation of the grassland. The

Table 5.6 Parameterization scheme of physical processes in the WRF model

Classification of schemes	Scheme option
Physics parameterization scheme	WSM 3-class simple ice
Cumulus parameterization scheme	Grell-Devenyi ensemble
Boundary layer process scheme	YSU
Radiation scheme	CAM 3 radiation
Land surface process scheme	Noah land surface model

proportion of grassland accounting for the total area of Northwest China has decreased from about 36 % in 1995 to 31 % in 2008, and most of grassland degraded into barren land and croplands. The intensive grassland degradation has resulted in more and more acute contradiction between the human and nature, economic development, and eco-environmental conservation.

5.3.1.2 Data Resource

The data required in this study are similar to the ones in the second case study, and have the same derivation. The differences are that the data in this case study are from 2010 to 2040, so we will not illustrate them again over here.

5.3.1.3 Test Design

The parameterization scheme of physical processes in the WRF model in this study is as follows (Table 5.6). It mainly includes the WSM 3-Class simple ice physical scheme, ensemble cumulus convection schemes of Grell-Devenyi ensemble, YSU, CAM3 radiation schemes, and consolidated NOAH land surface parameterization scheme (Snyder et al. 2004).

In this study, two numerical simulation tests, including the control test and sensitivity test, are designed and performed with the same horizontal resolution and parameterization scheme in order to analyze the effects of grassland degradation on the regional climate more accurately. The control test is designed as a reference case, which uses the land cover data of 2010 and assumes that the land cover will not change during 2010–2040. On contrary, the sensitivity test supposes that the land cover change with time, therefore, it will apply the simulated land cover from 2010 to 2040, in which part of grassland converted into bare land, croplands, or urban area. The center of the simulated area is located at 37°53′ N, 109°1′ E with two standard parallels of 39° N and 35° N, including 27 grid points in the east–west direction, and 48 grid points in the north–south direction. The simulation period is 30 years from January 1st, 2010 to December 31st, 2040.

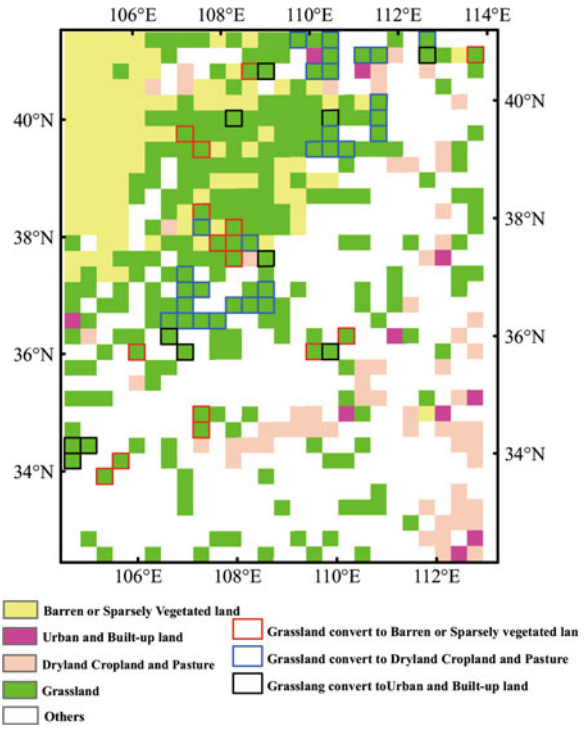

Fig. 5.10 Conversion from grassland to other land use types between 2010 and 2040 of the overgrazing areas in Northwest China

5.3.2 Results

5.3.2.1 Forecast of Future Grassland Degradation in Overgrazing Areas of Northwest China During 2010–2040

The grassland in Northwest China mainly concentrates in the southern and middle part of Inner Mongolia and Ningxia Province, the northeast of Gansu Province and southern part of Shaanxi Province, accounting for about 35 % of the total area of overgrazing areas in Northwest China. This study stimulates the grassland change in overgrazing areas of Northwest China from 2010 to 2040, and the results indicated that the grassland degradation is still severe in the future 30 years because of the increasing population and unreasonable use of the grassland, and the conclusion is coherent with that of previous study (Wu et al. 2013). The main conversion will be between grassland and croplands, bare land and urban land.

This study also statistically analyzes the number of grid cells converting from grassland into other land types between 2010 and 2040. The result indicates that there will be 55 grids converting from grassland into other land types from 2010 to 2040 in the study area (Fig. 5.10). About 48 % of the converted grassland will convert into croplands, which mainly distributed in the southeast part of Inner Mongolia Autonomous Region, northwest part of Shaanxi Province, and northeast

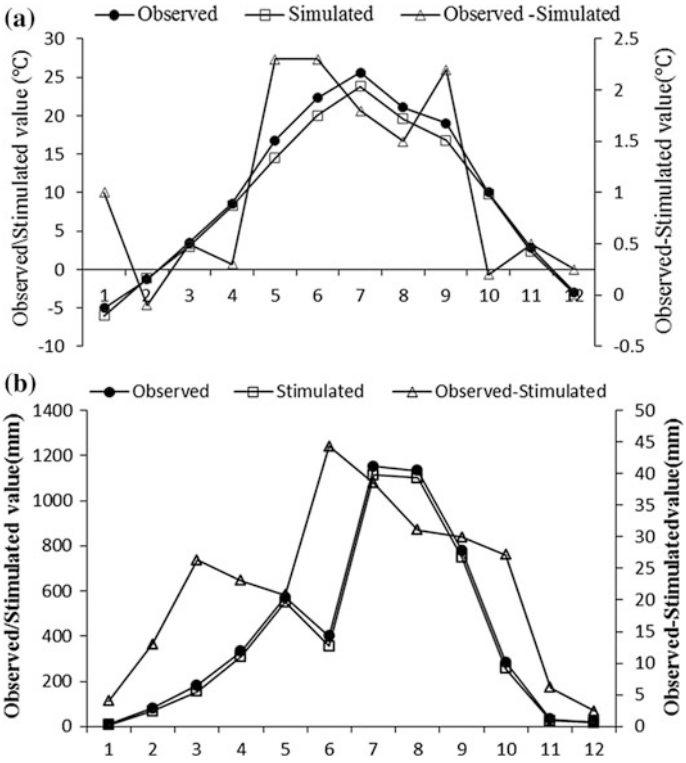

Fig. 5.11 Difference between the observed and simulated monthly temperature (**a**) and precipitation (**b**) in 2010 in the overgrazing areas of Northwest China

part of Gansu Province. The obvious conversion from grassland into barren land will mainly occur in southern and central part of Inner Mongolia and Shanxi Province, southern part of Ningxia Province, and southeast part of Gansu Province, accounting for 42 % of the total number of converted grids. There will be nine grids converting from grassland into urban land, accounting for about 10 % of the total number of converted grids. In summary, the grassland in overgrazing areas of Northwest China will be mainly converted into barren land and croplands.

5.3.2.2 Result of the Control Test

This study first simulates the temperature and precipitation in 2010 with WRF model, then validates the correction of simulation, and the results indicate that WRF model can simulate the temporal change of temperature very well (Figs. 5.11a and 5.12a). According to the monthly temperature change in the entire study area, the simulated temperature is roughly consistent with the observed value in the spring and winter, and the difference between them ranges from 0 to 0.5 °C

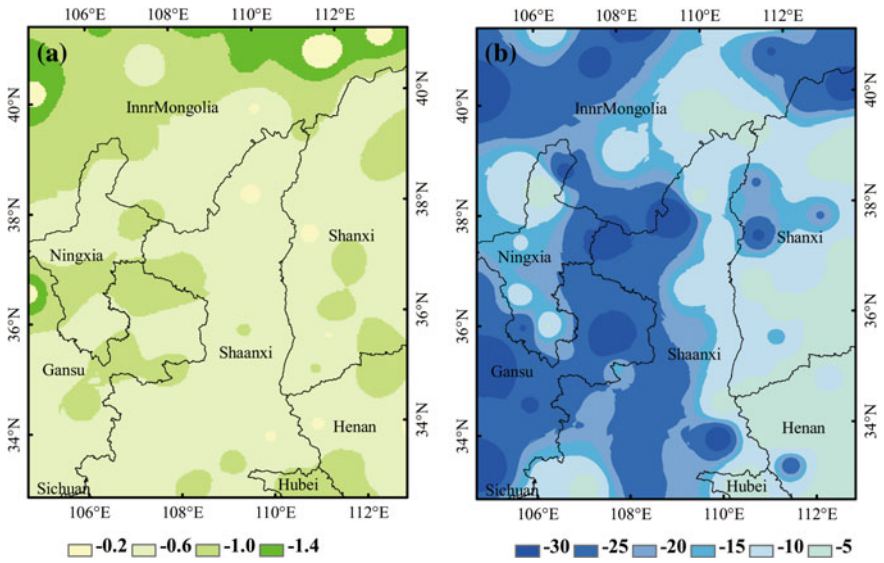

Fig. 5.12 Difference between the simulated and observed annual average temperature (**a**, °C) and annual precipitation (**b**, mm) in the overgrazing areas of Northwest China in 2010

(Fig. 5.11a). However, the temperature is obviously lower than the observed value in both the summer and autumn, with the difference ranging from 0.5 to 2.5 °C. As shown from Fig. 5.12a, the stimulated annual average temperature is lower than the observed value, and the difference between them ranges from 0.2 to 1.4 °C, indicating that there is only slight difference between the stimulated and observed annual average temperature.

The simulated precipitation in the spring and autumn of 2010 is lower than the observed value, and the difference between them ranges from 5 to 40 mm in most of the months except June (Fig. 5.11b). Figure 5.12b reveals that the annual precipitation of 2010 in overgrazing areas of Northwest China, especially the southeast part of Gansu Province and northwest of Shaanxi Province, is lower than the observed value, and the difference between them generally ranges from 5 to 30 mm. Overall, the difference between the simulated and observed monthly and annual change of precipitation is not extremely obvious. Therefore, the WRF model can also simulate the monthly and annual change of precipitation very well.

5.3.2.3 Effects of Grassland Degradation on the Land Surface Temperature

The impacts of grassland degradation on the temperature in overgrazing areas of Northwest China can be analyzed through calculating the difference in the annual average near-surface temperature (air temperatures at 2 m above the ground)

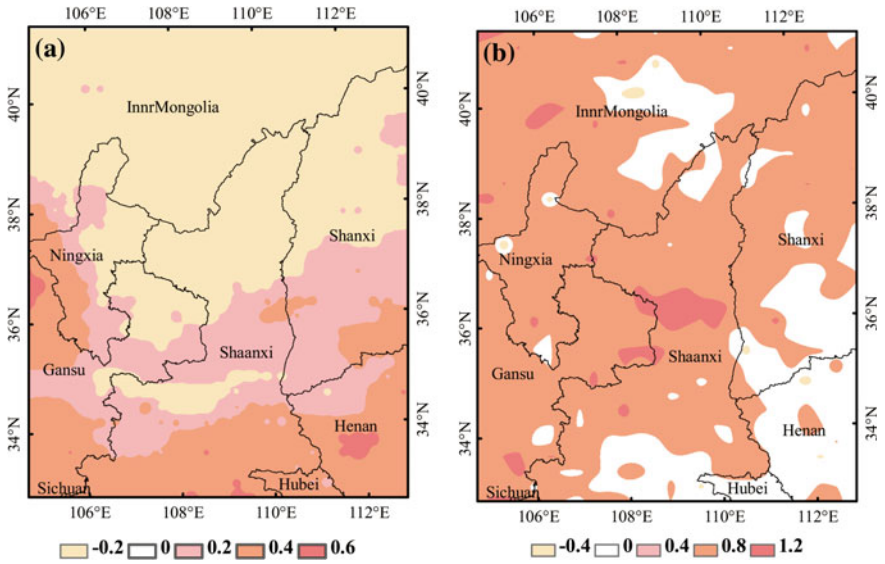

Fig. 5.13 Difference in the annual average temperature (°C) in winter (**a**) and summer (**b**) from 2010 to 2040 in the overgrazing areas in Northwest China between the sensitivity test and the control test

between the results of the control test and sensitivity test. The simulation result indicates that there will be different climate effects of the grassland degradation in different areas and seasons from 2010 to 2040 in the overgrazing areas of Northwest China (Fig. 5.13). Besides, the results of the two tests showed that the grassland degradation would increase the land surface albedo, which could lead to the decrease of near-surface temperature in the winter in the middle part of Inner Mongolia Autonomous Region, southwest of Ningxia Province, northwest of Shanxi Province due to the conversion from grassland to barren land and urban land with the decrement reaching 0.2 °C (Fig. 5.13a). Although the near-surface temperature of the winter increased in the middle part of Shaanxi Province and northern part of Shanxi Province due to the decrease of land surface albedo caused by conversion from grassland to croplands. The grassland degradation can mainly result in the decrease of the near-surface temperature in winter in the study area.

The impacts of grassland degradation are more complicated and widespread in the summer than those in winter. The grassland degradation can decrease the surface albedo, which will result in the increase of the near-surface temperature in the overgrazing areas of Northwest China, with an increment of about 0.4–1.2 °C (Fig. 5.13b). The temperature most obviously rise in the southwest of Inner Mongolia and middle part of Shaanxi with the increment of about 1.2 °C. Although surface temperature of summer decrease in the southern part of Inner Mongolia, the southern part of Shaanxi Province, southeast of Gansu Province with the drop scale of about 0.4 °C (Fig. 5.13b), which would be caused by the conversion from grassland to croplands since there is obvious difference between

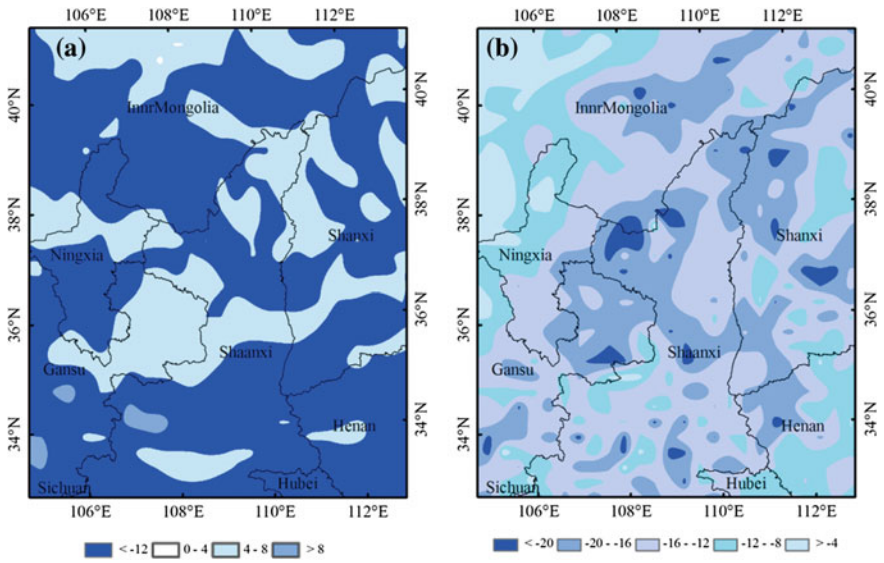

Fig. 5.14 Difference in the annual precipitation (mm) in the winter (**a**) and summer (**b**) from 2010 to 2040 in overgrazing areas of Northwest China between the sensitivity test and control test

the surface albedo of croplands and grassland and the higher evapotranspiration of the croplands. The grassland degradation would mainly lead to the increase of surface temperature in summer in the overgrazing areas of Northwest China.

5.3.2.4 The Effect of Grassland Degradation on Precipitation

The simulation result indicates that the grassland degradation can cause the decrease of precipitation in the winter in most parts of the overgrazing areas in Northwest China, with a decrement from 0 to 12 mm (Fig. 5.14a). Particularly, the annual precipitation in the northwest part of Shanxi Province, southern part of Inner Mongolia Autonomous Region will decline most obviously due to the serious grassland desertification, with a decrement of about 12 mm. Besides, in the summer, the conversion from grassland to barren land can result in the obvious decrease of precipitation in northern and central part of Shanxi Province, northern part of Inner Mongolia and Ningxia Province, with the decrement ranging from about 4 to 20 mm (Fig. 5.14b).

The numerical simulation of temperature and precipitation in the next 30 years shows that the grassland degradation in the overgrazing areas of Northwest China will make the climate change to show a dry-warm trend according to the results of the control test and sensitivity test. The results are consistent with theoretical analysis results that the underlying surface change will lead to regional climate change (Boucher et al. 2012), i.e., the vegetation degradation will cause the increase of surface albedo, and thereby leads to the decrease of precipitation and increase of temperature.

5.3.3 Concluding Remarks on the Surface Climatic Effects of Grassland Degradation

Based on the analysis of grassland change in the future, this study analyzed the impacts of grassland degradation on the regional climate in the overgrazing areas of Northwest China through implementing the numerical simulation with the WRF model. The conclusions of this study are as follows.

(i) WRF model can simulate the spatial pattern and change of temperature and precipitation very well, although the simulated value is a bit lower than the observed value. Besides, the grassland of Northwest China would mainly degrade into croplands, bare land, and urban land over the next 30 years. The most obvious grassland change will occur in the central part of Inner Mongolia Autonomous Region, northwest part of Shaanxi Province.

(ii) The grassland degradation will make the climate change show a dry-warm trend in the overgrazing areas of Northwest China in the future 30 years. The impacts of grassland degradation on the climate will vary in different seasons. In summer, the grassland degradation will lead to the increase of surface temperature and decrease of precipitation. While in winter, it will lead to the decrease of both the precipitation and temperature.

(iii) There are generally various impacts of land cover change on the climate change. However, this study has only analyzed the effects of grassland degradation on the temperature and precipitation. Actually there are other kinds of land use conversion which will also have effects on climate change, therefore, more land use conversions should be taken into account in the future research. In addition, there are various factors that influence the regional climate, but only the land cover change is used to analyze the impacts of grassland degradation on the regional climate in this study, which leads to some uncertainties of the results. Therefore, more efforts should be made in the future researches on the sensitivity test to reduce the uncertainties of the results.

5.4 Summary

This chapter focused on the climate effect of ecological restoration programs in China, and carried out three case studies in China. In the first case, we assessed the potential effects of artificial vegetation change on the regional climate in Jiangxi Province, China. Based on the simulation with the WRF model, a comparative analysis was carried out on the future temperature and precipitation under four hypothetical vegetation cover scenarios. The simulation results indicated that the vegetation change would have significant effects on the regional climate. The simulated effects of annual average temperature showed a decreasing order: evergreen broadleaf > evergreen needleleaf > deciduous needleleaf > deciduous

broadleaf, and the effects of annual average precipitation of the evergreen forests would be bigger than the deciduous forests. The deciduous forests play a positive role in decreasing the annual average temperature, while the evergreen forests promote the annual average temperature rise. Besides, the expansion of deciduous forests may result in severe drought in the summer in Jiangxi Province.

In the second case, we simulated the land cover under the future scenarios, and analyze the effects of land cover conversion on energy balance in the semiarid grassland area of China through the numerical simulation with the WRF model. The results indicate that the grassland will show a steadily upgrowing trend under the CES scenario. Compared to the CES scenario, the rate of increase in grassland cover is lower, while the rate of increase in urban land cover will be higher under the REG scenario. Although the conversion from cropland to grassland will reduce the energy flux, the expansion of urban area and decreasing of forestry area will bring about more energy flux. As a whole, the energy flux of near surface will obviously not change under the CES scenario, and the climate therefore will not be possible to be influenced greatly by land cover change. The energy flux under the REG scenario is higher than that under the CES scenario.

The last case study investigated the effects of biosphere feedback in grassland of Northwest China. Based on the forecast of the conversion pattern from grassland to other land use types in next 30 years, the potential effects of grassland degradation on regional climate in the overgrazing area of Northwest China from 2010 to 2040 have been explored with the WRF model. The analysis results show that grassland will mainly convert into bare land and croplands, which account for 42 and 48 % of the total converted grassland area, respectively. The grassland degradation during next 30 years will result in the increase of temperature in summer, with an increment of 0.4–1.2 °C, and the decrease of temperature in winter with a decrement of 0.2 °C. In addition, grassland degradation will cause the decrease of precipitation in both summer and winter, with a decrement of 4–20 mm. On the whole, those research conclusions can offer valuable information for the land use planning and climate change adaptation.

References

Barthold F, Wiesmeier M, Breuer L, Frede HG, Wu J, Blank F (2013) Land use and climate control the spatial distribution of soil types in the grasslands of Inner Mongolia. J Arid Environ 88:194–205

Bonan GB, Pollard D (1992) Effects of boreal forest vegetation on global climate. Nature 359:716–718

Boucher JF, Tremblay P, Gaboury S, Villeneuve C (2012) Can boreal afforestation help offset incompressible GHG emissions from Canadian industries? Process Saf Environ Prot 90(6):459–466

Bounoua L, Defries R, Collatz GJ, Sellers P, Khan H (2002) Effects of land cover conversion on surface climate. Clim Change 52(1–2):29–64

Clarke JM (2000) Effect of drought stress on residual transpiration and its relationship with water use of wheat. Can J Plant Sci 71(3):695–702

Deng X, Huang J, Uchida E, Rozelle S, Gibson J (2011a) Pressure cookers or pressure valves: do roads lead to deforestation in China? J Environ Econ Manage 61(1):79–94

Deng X, Huang J, Huang Q, Rozelle S, Gibson J (2011b) Do roads lead to grassland degradation or restoration? a case study in Inner Mongolia, China. Environ Dev Econ 16(6):751–773

Fan J, Zhong H, Harris W, Yu G, Wang S, Hu Z, Yue Y (2008) Carbon storage in the grasslands of China based on field measurements of above-and below-ground biomass. Clim Change 86(3–4):375–396

Findell KL, Shevliakova E, Milly P, Stouffer RJ (2007) Modeled impact of anthropogenic land cover change on climate. J Clim 20(14):3621–3634

Foley JA, Prentice IC, Ramankutty N, Levis S, Pollard D, Sitch S, Haxeltine A (1996) An integrated biosphere model of land surface processes, terrestrial carbon balance, and vegetation dynamics. Global Biogeochemical Cycles 10(4):603–628

Gibbard S, Caldeira K, Bala G, Phillips TJ, Wickett M (2005) Climate effects of global land cover change. Geophys Res Lett 32(23):L23705

Kang SZ (1985) Calculating method of potential atmospheric evaporation in the arid and semiarid areas. Agric Res Arid Areas 1(2):41–50

Lacis AA and Hansen JE (1974) A parameterization for the absorption of solar radiation in the Earth's atmosphere. J Atmos Sci 31:118–133

Loridan T, Grimmond C, Offerle BD, Young DT, Smith TE, Järvi L, Lindberg F (2011) Local-scale urban meteorological parameterization scheme (LUMPS): longwave radiation parameterization and seasonality-related developments. J Appl Meteorol Climatol 50(1):185–202

Nobre CA, Sellers PJ, Shukla J (1991) Amazonian deforestation and regional climate change. J Clim 4(10):957–988

Snyder P, Delire C, Foley J (2004) Evaluating the influence of different vegetation biomes on the global climate. Clim Dyn 23(3–4):279–302

Stephens GL (1978) Radiation profiles in extended water clouds. Part II: Parameterization schemes. J Atmos Sci 35:2123–2132

Wu F, Deng X, Yin F, Yuan Y (2013) Projected changes of grassland productivity along the representative concentration pathways during 2010–2050 in China. Adv Meteorol 2013: Article ID 812723, 9 pages, doi: 10.1155/2013/812723

Xu G, Kang M, Jiang Y (2012) Adaptation to the policy-oriented livelihood change in Xilingol Grassland, Northern China. Procedia Environ Sci 13:1668–1683

Chapter 6
Regional Climate Impacts of Future Urbanization in China

Xinli Ke, Jinyan Zhan, Enjun Ma and Juan Huang

Urbanization is one of the most important anthropogenic influences on surface climate. The process of urbanization has a profound impact on local, regional, and global climate change by natural to artificial land use/cover changes and anthropogenic heat emissions. Therefore, with the rapid urbanization, the impact of urbanization especially urban land expansion on global climate change has been one of the hot topics in research fields (Lei et al. 2008). In some specific areas, urban land use change even surpasses greenhouse gases in regulating climate, becoming an important factor which exerts impact on regional and global climate change (Jin et al. 2005). Previous studies have analyzed the effects of urban land surface change at the microscale; however, it is also necessary to study how both the past and future urbanization might affect the weather and surface climate.

Urban agglomeration has gradually become the main form of urbanization in China. This chapter presents three case studies on surface climatic impacts of further urbanization in China. The first case study aims to identify the impact of urban land use change on regional temperature and precipitation in summer in the Beijing-Tianjin-Tangshan Metropolitan (Great Beijing) area during 2030–2040. The second study carries out scenario analysis of land use change, and simulated the future regional temperature with Weather Research and Forecasting (WRF) model in Southern Jiangsu province, another typical region of urbanization in China. Finally, the last case study analyzes the impact of urbanization on surface climate under different urbanization patterns, i.e., baseline scenario, centralized urbanization scenarios, and decentralized urbanization scenarios in Wuhan Metropolitan region.

X. Ke (✉)
College of Land Management, Huazhong Agricultural University, Wuhan 430079, China
e-mail: kexl@igsnrr.ac.cn

J. Zhan · J. Huang
State Key Laboratory of Water Environment Simulation, School of Environment, Beijing Normal University, Beijing 100875, China

E. Ma
School of Mathematics and Physics, China University of Geosciences (Wuhan), Wuhan 430074, China

X. Deng et al. (eds.), *Land Use Impacts on Climate*, Springer Geography
DOI: 10.1007/978-3-642-54876-5_6,

6.1 Simulated Climate Impacts of Future Urbanization for the Great Beijing Area

In recent years, with the development of remote sensing technology, the studies of the impacts of urbanization on regional climate has made a great progress by using remote sensing technology to extract information on land use changes, land surface temperature, and precipitation (Mitra et al. 2012). These methods provided a good support to describe the impacts of urbanization on surface climate rather than the impact mechanism of urbanization on surface climate. Therefore, it is necessary to introduce numerical simulation in investigating the key process that urbanization affects regional climate change from the perspective of the mechanism. Sensitivity experiments of two-dimensional scale model showed that sensible heat fluxes caused by urban surface changes played a key role in climate change, and roughness changes affected the spatial heterogeneity of climate change. Sensitivity test of RAMS/TEM coupled model indicated that UHL plays a key role in inducing downwind convective systems (Rozoff et al. 2003).

Metropolitan cities in China have shown the "spread" and "aggressive" expansion accompanied by regional urban development and megalopolis formation since the reform and opening up, resulting in increasing effects on climate change (Tang et al. 2013). Great Beijing area is the economic center of northern China, and it plays a strategically important role in the political and economic development of the whole China (Kuang et al. 2011). Therefore, the primary objectives of this study are (i) to analyze the relationship between urbanization and climate in the Great Beijing area during 1995–2005 and (ii) to identify the impact of urbanization on temperature and precipitation in summer based on scenario-based simulaiton results during 2030–2040.

6.1.1 Data and Methodology

6.1.1.1 Study Area

The Great Beijing area is located in North China Plain between 38°25′–41°5′ N, 115°25′–119°25′ E. It covers Beijing Municipality and Tianjin Municipality and the cities of Tangshan, Langfang, and Qinhuangdao (TLQ) of Hebei Province, with a total area of 55,000 km^2 and a resident population of 29,368,600. Most of the area is plain and the hilly area is only 1.98 km^2. The area belongs to the continental monsoon climate. The average annual temperature is from 10 to 12 °C, with the mean temperature of −1.9 °C in January and 26.4 °C in July. The average annual precipitation is from 75 to 500 mm with an uneven time distribution, which mainly occurs during summer with 72 % of the total annual rainfall.

Great Beijing area is defined as the political, cultural, and economic center of China. The Eleventh National Five-Year Plan concluded development of this region.

The Great Beijing area developed quickly with high land use intensity, especially the large-scale science and technology parks, economic zones, industrial parks, and other new development zones. Thus the conflict between rapid city growth and water and soil resources has become increasingly pronounced.

6.1.1.2 Simulation Scheme

This study simulates the climate change in the Great Beijing area during 2030–2040 based on the control and sensitivity tests with WRF model. Two simulation tests are conducted for summer (June–August) during 2030–2040 (Table 6.1) under the same condition except the underlying surface in order to indicate the impact of urbanization on temperature and precipitation. First, the underlying surface data of 1992–1993 in WRF model is replaced since it cannot exactly reflect the land surface condition after 2000. The land cover data in 2010 are used as the underlying surface data for the control test, and the land cover data in 2030 predicted on the basis of the trend of social-economic simulation is used for the sensitivity test. The simulation results of the control test and sensitivity test are then compared, and the effects of urbanization on summer temperature and precipitation are finally examined. The effects of future urban expansion on surface climate can be explained with E_i.

$$E_i = R_i - r_i$$

where i refers to the precipitation and temperature; E_i is the effect of the future urbanization on the climate; R_i is the result of the simulation with the predicted underlying surface, and r_i is the result of the simulation with the baseline underlying surface.

The parameterization schemes in this study are listed in Table 6.2. The Grell-Devenyi ensemble scheme was adopted in the cumulus parameterization scheme, with YSU being the boundary layer process scheme, and the CAM scheme being both long-wave radiation and shortwave radiation scheme, while the land surface process scheme was the Noah land surface model. The boundary buffer was set to be four layers of grid points, and the relaxation scheme was adopted in the boundary conditions. The time interval of the model integration was set to be 5 min, and that of the radiation process and cumulus convection was 30 and 5 min, respectively. There were 27 layers in the vertical direction and the atmospheric pressure at the top layer was 50 hPa.

The lateral boundary forcing data was from the National Centers for Environmental Predictions (NCEP) operational Global Final (FNL) Analyses (NCEP/FNL) and was updated every 6 h. The dataset was established on the basis of the assimilation of almost all kinds of observational data (e.g., remote sensing data and ground-based observation data) with a spatial resolution of $1° \times 1°$ gird and a vertical height of 27 layers, and it has been updated to now since July, 1999. Compared with dataset of NCEP I, NCEP II, and EAR40, the NCEP/FNL not only

Table 6.1 Schemes of the simulation test

Test	Test time	Land cover data used in WRF
Control test	2030.01.01–2040.12.31	Land cover data of 2010
Sensitivity test	2030.01.01–2040.12.31	Land cover data of 2030

Table 6.2 Configuration of the physical parameterization schemes in WRF

Physical processes	Scheme option
Microphysics scheme	Lin et al.
Cumulus scheme	Grell-Decenyi ensemble
Land surface process	Noah land surface model
Short wave radiation	CAM scheme
Long-wave radiation	CAM scheme

has the higher accuracy and spatial resolution, but also involves more kinds of environmental variables. The data of future force filed were from the fifth phase of the Coupled Model Intercomparison Project (CMIP5) which produces a state-of-the-art multimodel dataset. The model output analyzed by researches forms the basis for the Fifth Assessment Report of the Intergovernmental Panel on Climate Change (Taylor et al. 2012), and two time scales of projections of future climate change are provided. The first one is the near term (out to about 2035), and the other one is the long term (out to 2100 and beyond). Model output of the RCP 6.0 such as air temperature, specific humidity, sea level pressure, eastward wind, northward wind, geopotential height from 2010 to 2040 were used as the atmospheric forcing dataset of WRF model.

Urban land use data, which were extracted from Landsat TM images in 1995 and Landsat ETM, images from the China–Brazil Earth Resources satellite (CBERS) in 2005 (Liu et al. 2003, 2010), was acquired from the data center of the Chinese Academy of Sciences. The land use change during 1995–2005 has been described Table 6.3. The predicted land use and land cover data in 2030 were derived from the database of Representative Concentration Pathway (RCP6.0). The new urban area pixels during 2010–2030 derived from RCP 6.0 was overlaid to the map of baseline underlying surface, then the underlying surface data in 2030 was transformed to grid data of 30*30 km of USGS data by resampling.

6.1.2 Results and Discussion

6.1.2.1 Spatiotemporal Pattern of Urban Expansion Since 1995

Urban expansion is one of the key characteristics of land use change in the Great Beijing area from 1995 to 2005, the spatiotemporal pattern of which was analyzed according to remote sensing data (Table 6.3). During 1995 and 2005, the total area of cultivated land and forests decreased by 0.98 and 2.15 %, respectively, while the urban land area increased by 3.34 %, with an average annual rate of 0.33 %.

Table 6.3 The area precentage and the changes of main land use (%) in Beijing-Tianjin-Tangshan Metropoliatn area, 1995–2005

Year/period	Cultivated land	Forestry area	Grassland	Water	Built-up area	Unused land
1995	48.48	24.59	6.32	5.54	14.14	0.92
2005	47.50	22.45	6.74	5.08	17.48	0.76
Change[a]	−0.10	−0.21	0.04	−0.05	0.33	−0.02

Note [a] represents the change rate calculated with the following equation: $\left(A_i^{2005} - A_i^{1995}\right)/(10)$, where A_i^{2005} means the area proportion of land use type i in 2005, A_i^{1995} means the area proportion of land use type i in 1995

Urban expansion is the main driving factor of the shrinkage of cultivated land and forests. The socioeconomic development and geographical factors, such as the population growth, policy, and economic development, all affect the urban expansion and subsequent landscape changes.

6.1.2.2 Spatiotemporal Dynamics of Temperature and Precipitation in the Great Beijing Area during 1995–2005

There was slight temperature change in the Beijing-Tianjin-Tanghsan Metropolitan area from 1995 to 2005 (Fig. 6.1). Overall, temperature showed an increasing trend in most part of the study area, especially around the metropolitan Beijing and in the costal metropolitan area of Tianjin and Tangshan, with an average increasing rate of 0.023 °C/year. However, temperature has decreased to some degree in northeast and northwest part of the study area. The regions that converted from other land use types into cities has shown relatively higher temperature rise, indicating that urbanization has some influence on temperature in the Great Beijing area. At the same time, precipitation showed an increasing trend in metropolitan Tangshan and northeast part of Beijing Metropolitan, while it showed a downward trend in the west and south part of Beijing. According to the results mentioned above, it can be concluded that the process of urbanization has affected regional temperature and precipitation to a certain extent in the Great Beijing area.

6.1.2.3 Urban Area Change from 2010 to 2030

There will be obvious conversion from other land use types to urban area in Great Beijing area during 2010–2030 (Fig. 6.2). Urban area in this region would continue to increase during 2010–2030, and the newly increased urban land will mainly concentrate in the regions around downtown of Beijing and Tianjin City. Land use conversion mainly results from the joint effects of both the internal factors and external factors such as terrain, traffic, economic factors, cultural tradition, and behaviors of the government officials.

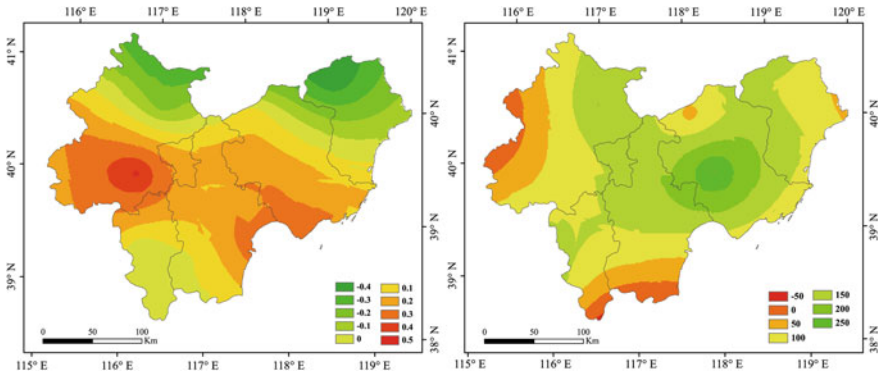

Fig. 6.1 Simulated changes of temperature (*left*) and precipitation (*right*) in Beijing-Tianjin-Tangshan Metropolitan area during 1995–2005

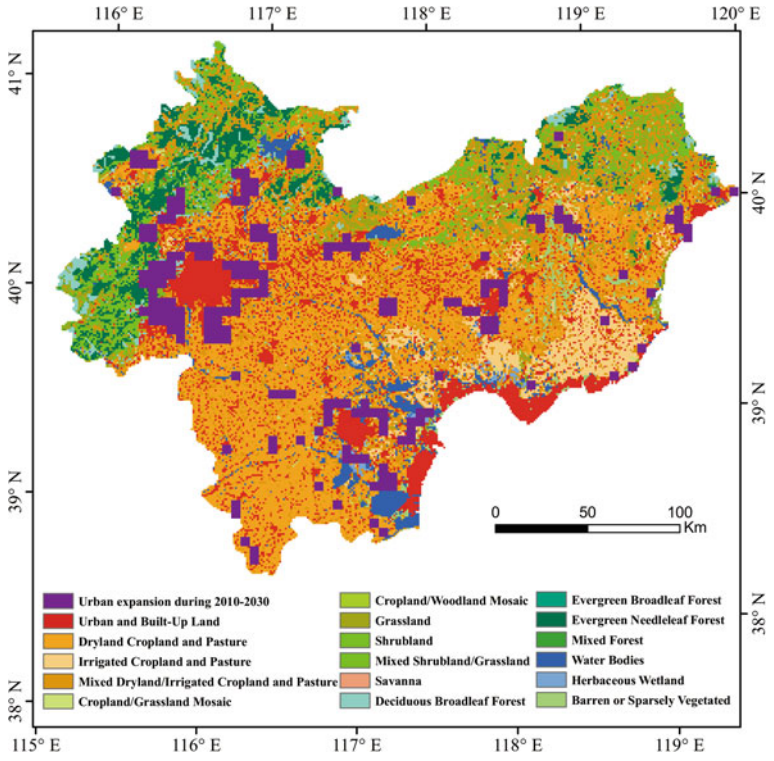

Fig. 6.2 Conversion from other land use types to urban area in Beijing-Tianjin-Tangshan Metropolitan area during 2010–2030

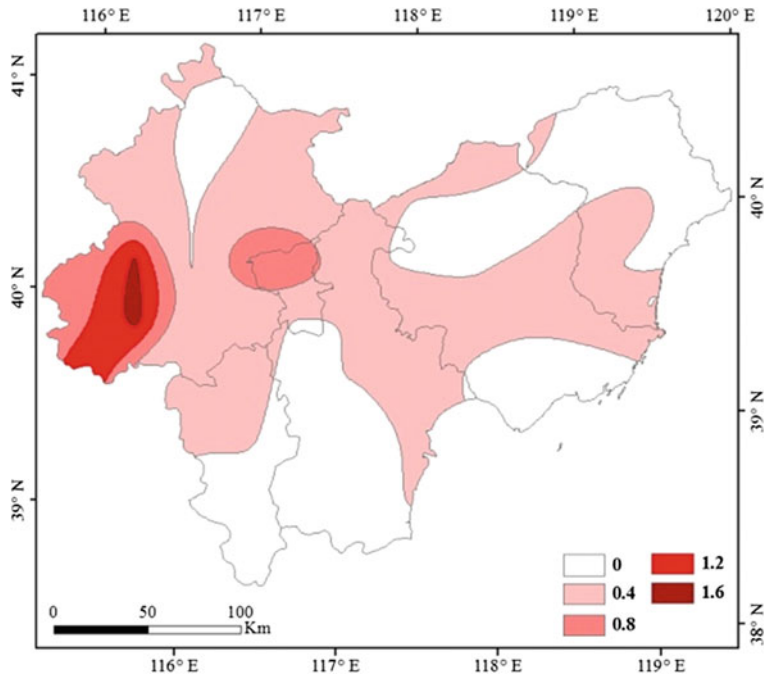

Fig. 6.3 Difference in the projected monthly average temperature in summer between the control test and sensitivity test in the Beijing-Tianjin-Tangshan Metropolitan area during 2030–2040

6.1.2.4 Results of the Numerical Simulation

Figure 6.3 depicted the simulated impact of future urban expansion on average annual temperature in the study area during 2030–2040. There will be significant warming effects in the summer, mainly occurring in the downtown and eastern part of Beijing Metropolitan. Transformation from vegetated land to urban land results in significant differences of near-surface temperature. As a result, the temperature would increase obviously in the regions with urban expansion, mainly owning to UHL effect, which is consistent with the results of previous researches (Wang et al. 2002).

Surface temperature is determined with surface energy balance equation.

$$-\rho L_v(\overline{w'q'})_{\text{sfc}} + R_n - S - \rho c_p C_h u(T_{\text{sfc}} - T) = 0$$

where the first item refers to latent heat flux; the second item refers to net radiation flux; the third item refers to soil heat flux; and the forth item refers to sensible heat flux.

Part of net radiation flux is absorbed by the earth's surface, which further influences latent heat flux and sensible heat flux, with the rest transformed into soil and soil heat flux. The heat transfer in soil complies with the thermal diffusion equation.

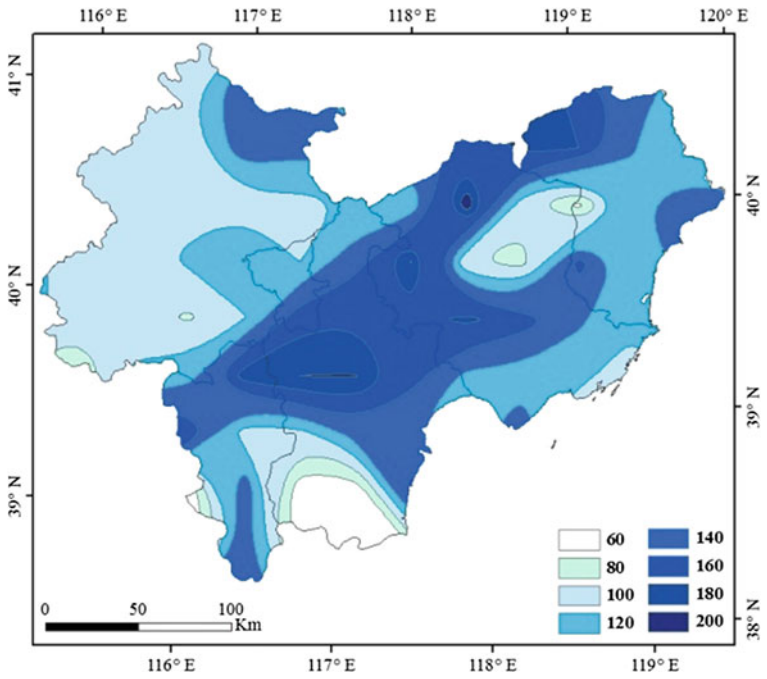

Fig. 6.4 Projected summer precipitation difference of monthly average temperature between control test and sensitivity testin Beijing-Tianjin-Tangshan Metropolitan area, 2030–2040

$$C(\Theta)\frac{\partial \Theta}{\partial t} = \frac{\partial}{\partial z}\left(K_t(\Theta)\frac{\partial T}{\partial t}\right)$$

where T is soil layer temperature; Θ refers to soil water content; C means specific heat of soil layer; K_t is thermal conduction system.

There will be much more population in new cities, which will need and consume a lot of heat/power due to their activities (transportation, air conditioning, industries), thus exerting significant impacts on the balance of surface energy. It has been reported that surface temperature is determined by radiation flux, sensible heat flux, latent heat flux, specific heat of soil layer, and thermal conduction system, while surface temperature also affects sensible heat flux and latent heat flux (Miglietta et al. 2009). In urbanized area surface temperature, which magnifies sensible heat flux and soil heat flux, will rise due to the increase of net surface shortwave radiation and decrease of latent heat flux. All these changes along with the increase of human-induced heat emission will lead to temperature increase.

Urban expansion has significant impacts on precipitation in summer during 2030–2040 in the study area (Fig. 6.4). In general, there is an obvious heterogeneity of local precipitation change, and there will be some precipitation increase in urban areas, which may be due to the extended urban boundary and increased secondary

outflow activity. Shepherd also showed that expansion of future urban land might result in a more expensive area of rainfall (Shepherd et al. 2010). Urbanization would increase the emission of atmospheric pollutants, cause the heat island effect, and lead to land use change. The volatile air layer can lead to thermal convection easily due to UHL effect, which can increase thermal convection and convective precipitation. Moreover, buildings of different heights can not only cause mechanical turbulence, but also hinder the moving slow precipitation system, thus leading to increase of precipitation. At the same time, there are intensive human activities in urban regions, which lead to the emission of a large amount of greenhouse gases, aerosol, and other particulate matters. On one hand, these materials increase the condensation nucleus for precipitation; on the other hand, these materials intensify the UHL effect in urban regions. Under the condition of sufficient moisture, there will more precipitation due to increased condensation nucleus above the municipal areas and relatively high underlying surface temperature, which may account for the increase of precipitation in this region in summer.

6.1.3 *Concluding Remarks on Future Urbanization and its Climate Effects in the Great Beijing Area*

Urban climate change results from the interaction between human activities and local climate change in essence. The change of underlying surface properties and human-induced heat emission will lead to the difference between urban and rural temperature, which will further change local climate forcing field and consequently lead to the redistribution of climate factors, such as the wind, cloud, and precipitation. This study investigated the contribution of urban land use change to the change of temperature and precipitation in Great Beijing area during 2030–2040 with the WRF model based on the latest actual urban land cover data from 1995 to 2005.

The impact of urbanization on regional climate change is a very complex and challenging problem and it is necessary to carry out more in-depth research since there are still some uncertainties in the current research. For example, more efforts should be made to comprehensively investigate the contribution of urbanization to the change in annual temperature and precipitation, extreme climate, latent heat flux at land surface, wave flux at ground surface. Meanwhile, it is necessary to carry out further research on how to quantitatively measure the inner link between urban development and climate factors and how this inner link will change when climate factors change. Urban area in this region would increase continuously, and urban expansion leads to continual increase of local temperature and will make precipitation in summer show an increasing trend during 2030–2040.

The results of this study indicated that the anthropogenic land cover change has significant impacts on regional climate in the Great Beijing area, which can provide scientific reference for optimizing land use management and planning to mitigate and adapt to regional climate change in the future. For example, government can

increase the proportion of urban green land in urban land use planning and take urban forests as an important component of the ecological infrastructure to promote the ability of cities to mitigate and adapt to climate change.

6.2 Estimated Biogeophysical Effects of Urbanization in Southern Jiangsu Province

Southern Jiangsu province is located in the Yangtze River Basin in China (Fig. 6.5), with superior geographical environment, pleasant climate and convenient irrigation, vast plains, and fertile soil. There are five cities in Southern Jiangsu province, including Nanjing, Zhenjiang, Changzhou, Wuxi, and Suzhou. Southern Jiangsu province has been China's most prosperous place because of due to the well-developed agriculture. Southern Jiangsu province also has a geographical advantage that it neighbors Shanghai and is Shanghai's largest hinterland. Because of its natural connection with Shanghai in geography, Southern Jiangsu province becomes Shanghai's most direct economic radiation zone, taking and digesting its industrial transfer, absorbing and creating a lot of employment opportunities. Southern Jiangsu province seized the opportunity and thus became a typical model of China's economic development since China's reform and opening up.

With Shanghai's role in driving the economic development, the Southern Jiangsu province grows rapidly in economic development and urbanization. In 2008, the regional GDP of Southern Jiangsu province was 1.85 trillion Yuan, accounting for 6.4 % of the whole country. Southern Jiangsu province is also relatively dense with cities and towns, and urbanization level is high. In 2008, the urbanization rate in Southern Jiangsu province reached 67.7 %, and per capita GDP reached 61,823 Yuan reaching the level of moderately developed countries.

In this study, we first simulate the region's future land use change scenarios based on DLS (Dynamics of Land System) model, and then processed the DLS simulation results in order to satisfy the requirements of underlying surface of WRF model. On this basis, WRF model is used to simulate the impacts of future land use change on regional climate change to scientifically understand the core parameters and the key process of the impacts of future land use change on regional climate change, and thereafter to provide scientific basis for rational regional land use planning to mitigate climate change.

6.2.1 Data and Methodology

6.2.1.1 Data Sources

Data used in this study includes land use data, socioeconomic data, and natural environmental indicators of Southern Jiangsu province.

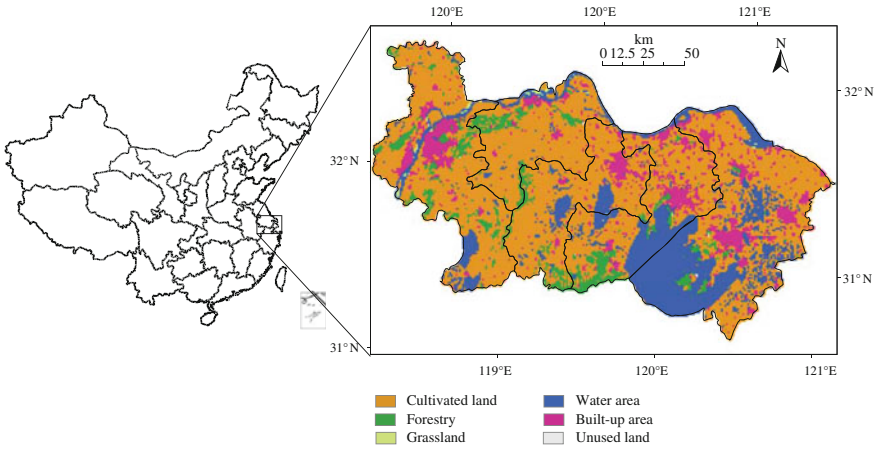

Fig. 6.5 Location of Southern Jiangsu

Land use data is mainly used for scenario-based simulations of land use change. In this study, land use data of Southern Jiangsu province in 2000 and 2008 are obtained through remote sensing images interpretation. These land use data are composed of six land types, including farmland, forestry land, grassland, built-up land, water bodies, and bare land. Among them, land use data in 2000 came from the Land Use Database of Data Center Resources and Environment, Chinese Academy of Science (Liu et al. 2002). The database consists of interpretation results from Landsat TM/ETM+ images with a spatial resolution of 30 × 30 m. Land use data in 2008 is interpreted from Landsat ETM+ images by the authors.

Social and economic statistical data includes the population of Southern Jiangsu province, per capita retail sales of social consumer goods, the total investment in fixed assets, per capita fiscal revenue, the gross output of the second industry, and grain yield per unit area from 2000 to 2008. The above data comes from Jiangsu Statistical Yearbook.

Natural environmental indicators include DEM, the distance from the city at all levels, the distance from the railways, the distance from the roads, and the distance from the rivers. DEM data comes from Shuttle Radar Topography Mission (SRTM) of NASA. This part hierarchically calculated the distance from the city at all levels to each 100 × 100 m grid. Using the Landsat TM/ETM+ geometric correction in 2000 that covered Southern Jiangsu province to outline the major river systems and the network of transport of the study area and to work out the distance from each 100 × 100 m grid to railways, roads and rivers.

6.2.1.2 DLS Model

DLS is a land use dynamic simulation model based on land use change mechanism, DLS model consists of four modules, including scenario analysis module,

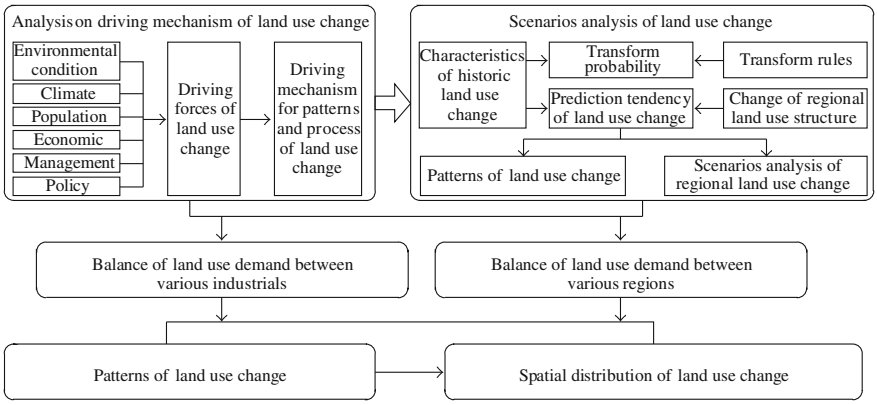

Fig. 6.6 Framework of DLS model

spatial analysis module, the conversion rules module, and spatial analysis modules (Fig. 6.6). Scenario analysis module is used to express the changed needs of a variety of land use types under different scenarios. Spatial analysis module is used to calculate the probability values of various land use types in each grid unit through spatial regression analysis for driving factors. Transfer rules module is used to express possibility and ease of a certain type of land transfer to another type of land on each grid cell. Space allocation module implements spatial distribution pattern of various land use types under different scenarios on the grid.

There are mainly four steps to carry out dynamic simulation of land use based on DLS. First, conversion rules module analyzes statistical relationship between land use types distribution and driving factors from the two scales of region and grid, measures effects of the natural environment and socioeconomic factors on temporal patterns of regional land use, and extracts the key factors which affect land use types distribution. Second, based on the history of land use characteristics and the status of regional land use changes, spatial analysis module predicts the trends that key factors influence land use patterns, and then select a reasonable scenario. Third, according to supply–demand situation of different industries on land under this scenario during the time cross-section of forecast period, scenario analysis module allocates area demand of different land types to various industries. Finally, by balance analysis of grid-scale land type area's demand and supply, spatial allocation module achieves spatial distribution of different kinds of land use types on the grid scale and generate spatial pattern of land use.

According to the estimated result of experiential model, the contribution on land use change of various independent variables can be calculated. Based on this, prediction of land use in 2010 and 2050 in Southern Jiangsu can be worked out. Under the linear hypothesis, land use change process can be presented as the following formula.

$$\triangle Yi = f(\ldots, x_i^t, \ldots) - f(\ldots, x_i^{t-1}, \ldots) = f(\triangle xi) \tag{6.1}$$

where, $\triangle Yi$ is the change area of land useYi, x_i^t and x_i^{t-1} are the value of independent variables in time t and $t-1$ respectively, and $\triangle x$ is the changed value of independent variables.

6.2.2 Results

6.2.2.1 Scenario Analysis of Future Land use in Southern Jiangsu Province

Future land use conditions in Southern Jiangsu province are simulated under two scenarios in this part (Fig. 6.7). After 30 years' development under the reform and opening up policy in China, the Southern Jiangsu province has achieved rapid socioeconomic progress. Meanwhile, resources and environment in Southern Jiangsu province are also under tremendous pressure and have become increasingly prominent in the process of rapid economic development. Particularly, farmland resources in this area are facing significant stress of reduction with rapid urban expansion. Therefore, the development of Southern Jiangsu province is facing new opportunities and challenges. In this context, this part sets future land use scenarios as REG scenario and CES scenario for the study area. The core of REG scenario is that land use demands have the priority in land use change. Land use change in Southern Jiangsu province has served the purpose of economic development in the past 30 years; therefore, it can be considered that land use scenario in Southern Jiangsu province was REG scenario in the past 30 years. The core of CES scenario is to achieve coordination between economic development and environmental protection. Therefore, the purpose of land use in CES scenario is to realize the transformation of economic development so as to protect natural resources and environment by sacrificing the speed of economic development rationally.

This study simulates land use change in Southern Jiangsu province during 2010 to 2050 under REG scenario and CES scenario with DLS model (Fig. 6.6). The result under REG scenario suggests that built-up land expansion in 2010 mainly concentrates on the core urban areas of Nanjing, Zhenjiang, Suzhou, Wuxi, and Changzhou, which is consistent with the trend of current land use change in Southern Jiangsu province. While the simulation result under CES scenario indicates that built-up land will expand dispersedly in the whole study area, including the main urban areas of Nanjing, Zhenjiang, Suzhou, Wuxi, and Changzhou will be restrained to some degree.

The simulation result in year 2050 indicates that there is still a great demand of economic development for the land resource under REG scenario due to a high speed of development in Southern Jiangsu province. Built-up land will expand most obviously around the main urban areas of Nanjing, Zhenjiang, Suzhou, Wuxi, and Changzhou, where the area of cultivated land and forests will further decrease.

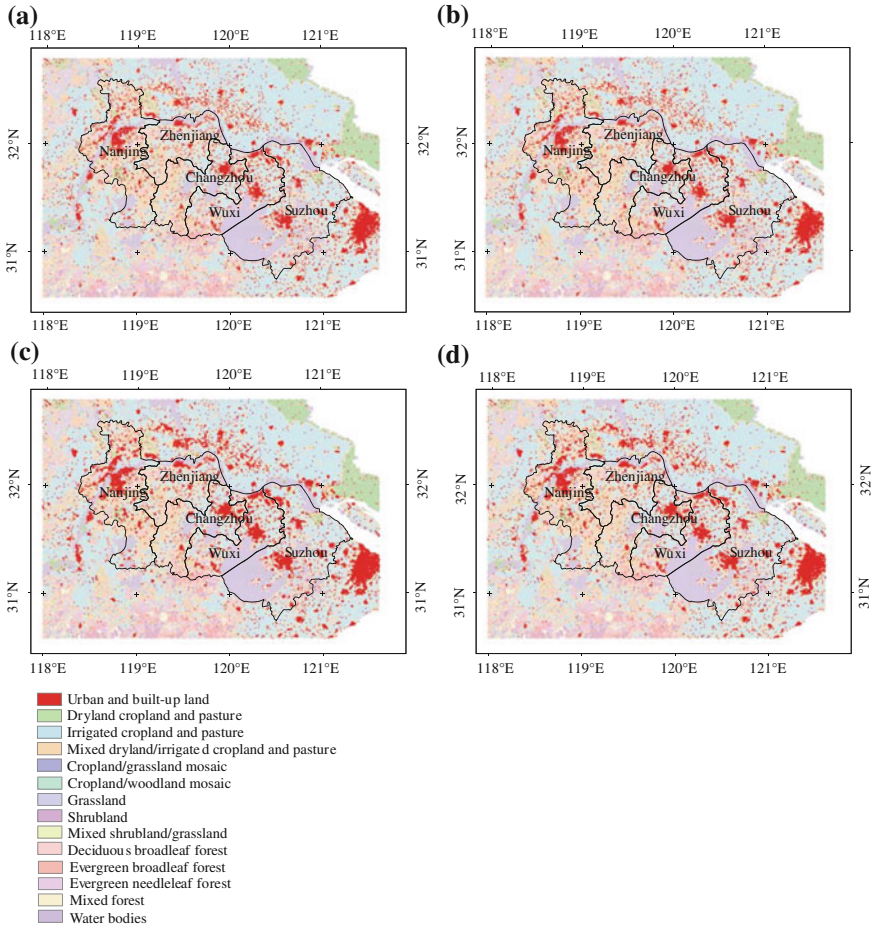

Fig. 6.7 Results of land use change simulation. **a** and **b** Show the simulation results of land use in Southern Jiangsu in year 2010 under REG scenario and CES scenario, respectively; **c** and **d** show the simulation results of land use in Southern Jiangsu in year 2050 under REG scenario and CES scenario, respectively

There will also be some expansion of built-up land in small–medium cities, which puts great pressure on the surrounding cultivated land and forest. Under CES scenarios, the speed of economic development will be restrained to some degree, and land use intensity will be further improved and the consumption of land resources due to economic development will also be restrained. Although there will be some expansion of built-up land around the main urban areas of Nanjing, Zhenjiang, Suzhou, Wuxi, and Changzhou, the expansion degree is much limited compared to that under REG scenario. The area of cultivated land and forest will decrease slightly due to built-up land expansion, but the decreased area has been under

control compared to that under REG scenarios, in particular, the shrinkage of forest is well controlled in these regions. By comparison, built-up land in small–medium cities still expands dispersedly, but the expansion speed is obviously restrained.

6.2.3 Impacts of Future Land use Change on Regional Temperature in Southern Jiangsu Province

Based on the simulation results of future land use change in Southern Jiangsu province, the WRF model was used to simulate the impacts of land use change on regional climate change under different scenarios. The underlying surface data were first generated through up-scaling and reclassifying the simulation results of land use change according to the requirement of WRF model. The static underlying surface data in the WRF model were then replaced with the dynamic ones in 2010 and 2050 under REG scenario and CES scenario, thereafter future regional climate change was simulated and finally the climate effects of different underlying surfaces were analyzed (Fig. 6.8).

The simulation results indicate that the changing trends of monthly average temperatures under different scenarios are consistent on the whole. The highest monthly average temperatures all appear in June, July, and August, and the lowest ones all appear in November, January, and February. This result shows that the changes of underlying surface do not affect monthly temperature change trend; it only affects the values of average temperature. There is significant difference on monthly average temperatures during different periods under different scenarios. The simulation results indicate that regional monthly average temperature in 2010 under CES scenario is the lowest on the whole, while that in 2050 under REG scenario is the highest. Besides, monthly average temperature in 2010 under REG scenario is slightly higher than in 2050 under CES scenario. In addition, there are also some differences in monthly average temperatures between different underlying surfaces during different periods. Overall, the greatest difference in monthly average temperatures appears in summer, while there is no significant difference in winter, with that in January being the slightest.

The simulation results indicate that there are significant impacts of the underlying surface on the spatial pattern of monthly average temperature under different scenarios, especially in 2050 under REG scenario and in 2010 under CES scenario (Fig. 6.9). Figure 6.9a and b suggest that there is no significant difference between the spatial pattern of monthly average temperature on the underlying surfaces under REG scenario and CES scenario in 2010, and monthly average temperature under REG scenario is only slightly higher than that under REG scenario. However, Fig. 6.9c and d indicate that the regions with high temperature in 2050 under REG scenario are much wider than that under CES scenario, especially around the center of big cities such as Nanjing, Zhenjiang, Suzhou, and Wuxi. According to the comparison of results between monthly average temperature in 2050 under

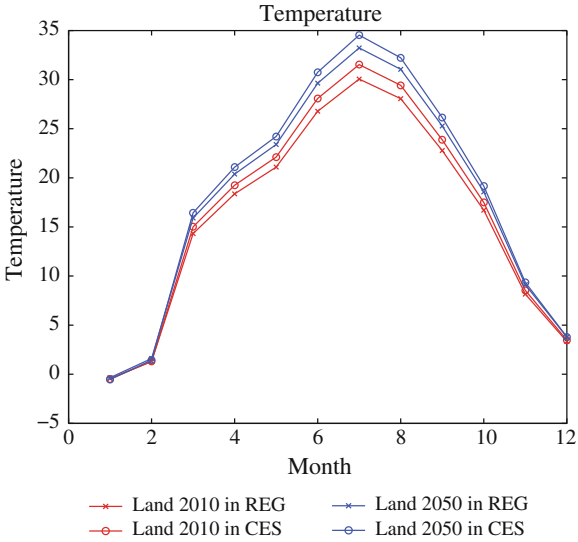

Fig. 6.8 Simulated monthly average temperature in Southern Jiangsu under different scenarios (°C). Land 2010 in REG scenario and Land 2010 in CES scenario represent the monthly average temperature simulated with the Land Use and Cover Change (LUCC) data in 2010 under the REG scenario and CES scenario as the underlying data, respectively. Land 2050 in REG scenario and Land 2050 in CES scenario refer to that in 2050

REG scenario and the other scenarios, the range of high-temperature regions is much wider in 2050 under REG scenario than the other scenarios.

The biggest difference in monthly average temperature under different scenarios is in July, therefore, the impacts of different underlying surfaces on temperature can be more clearly revealed through comparing the spatial pattern of monthly average temperature in July (Fig. 6.10). The impacts of different underlying surfaces on the spatial pattern of temperature in Southern Jiangsu province in July are consistent with that on monthly average temperature, but it is more significant in July. Taking the results in 2050 under REG scenario and CES scenario (Fig. 6.10c and d) as examples, the high-temperature region in Nanjing has expanded into a separate continuous region in 2050 under CES scenario, while the scope of the high-temperature region in Zhenjiang is still very limited. Besides, the high-temperature regions in Suzhou, Wuxi, and Changzhou have also expanded into a large continuous district, but its scope and temperature range are both smaller than that in 2050 under REG scenario.

6.2.4 Key Impact Mechanisms of Future Land use Change on Regional Temperature in Southern Jiangsu Province

According to surface energy budget equation, there is close relationship between surface net radiation, land surface albedo, downward shortwave radiation, downward long-wave radiation, and land surface emissivity.

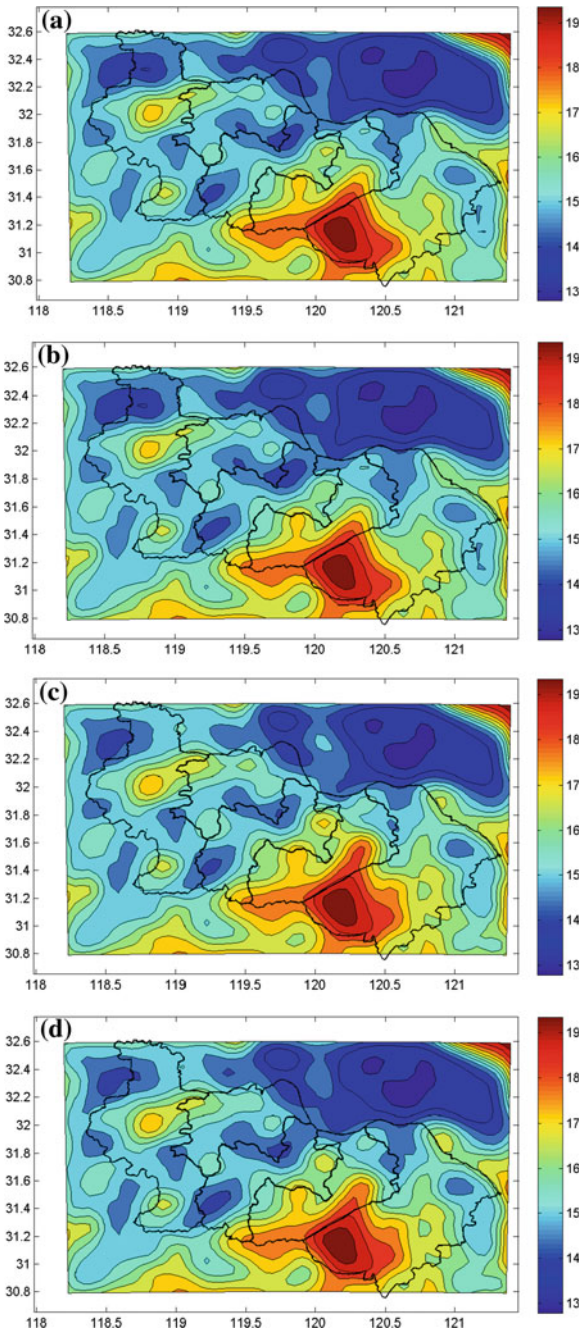

Fig. 6.9 Spatial pattern of the monthly average temperature in Southern Jiangsu under different scenarios (°C). **a** and **b** Show the simulation result of average temperature of land use in Southern Jiangsu in year 2010 under REG scenario and CES scenario, respectively; **c** and **d** show the simulation result of average temperature of land use in Southern Jiangsu in year 2050 under REG scenario and CES scenario, respectively

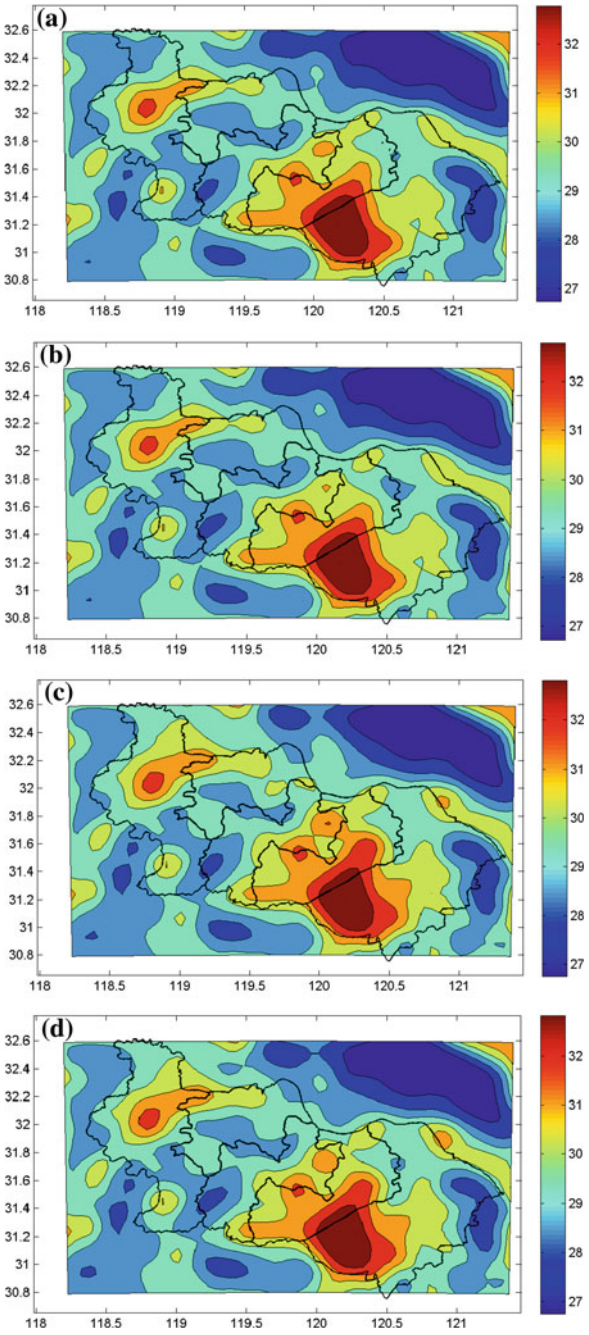

Fig. 6.10 Spatial pattern of the monthly average temperature in Southern Jiangsu in July under different scenarios (°C). **a** and **b** Show the simulation result of monthly average temperature in Southern Jiangsu in July of land use in year 2010 under REG scenario and CES scenario, respectively; **c** and **d** show the simulation result of monthly average temperature in Southern Jiangsu in July of land use in year 2050 under REG scenario and CES scenario, respectively

$$Rn = R_n^S + R_n^l = (1 - \alpha)F_d^s + \varepsilon F_d^l - \sigma\varepsilon T^4 \quad (6.2)$$

where Rn is surface net radiation, R_n^S is shortwave radiation, R_n^l is long-wave radiation, α is land surface albedo, F_d^S is downward shortwave radiation, .ε is land surface emissivity, F_d^l is downward long-wave radiation, T is land surface temperature. Land net radiation is the energy source of land surface temperature change. This study has focused on how the underlying surface change influences land surface albedo, downward shortwave radiation, downward long-wave radiation, and land surface emissivity in order to clarify the key influencing mechanism of future land use change on regional temperature in Southern Jiangsu province (Fig. 6.11).

Land use change in Southern Jiangsu province mainly influences land net radiation through exerting impacts on land surface albedo and emissivity, and land use change influences the spatial heterogeneity of land surface emissivity most greatly under both scenarios (Fig. 6.11). Figure 6.11a suggests that land surface albedo will be the lowest in 2050 under REG scenario, while it will show no significant difference under the other scenarios. Moreover, Fig. 6.11b suggests that land surface emissivity will be obviously lower in 2050 under REG scenario than the other scenarios, under which it will show no significant difference. In addition, Fig. 6.11c and d indicate that there will not be significant difference in downward long-wave radiation and downward shortwave radiation under all scenarios. In summary, under the condition that there is no significant difference between downward long-wave radiation and downward shortwave radiation, there will be lower land surface albedo and emissivity in 2050 under REG scenario, which consequently greatly increases land surface net radiation and thus lays foundation for the warming effects.

This study analyzed the impacts of the spatial heterogeneity of land surface emissivity on the spatial pattern of temperature in the hottest month (July) since the difference in land surface emissivity is the main reason for the warming effects in 2050 under REG scenario (Fig. 6.12).

Under all four scenarios, there are always continuous districts with lower land surface emissivity in Nanjing, Zhenjiang, Suzhou, Wuxi, and Changzhou, where urban land is the main part of the underlying surface (Fig. 6.12). However, the result clearly shows that land surface emissivity in these continuous districts is obviously lower in 2050 under REG scenario than the other scenarios, which may be mainly because that the underlying surface will change more greatly in 2050 under REG scenario.

What's more, land surface energy budget equation suggests that under the condition of certain land surface net radiation, the underlying surface mainly influences temperature through influencing sensible heat flux, latent heat flux, and soil heat flux.

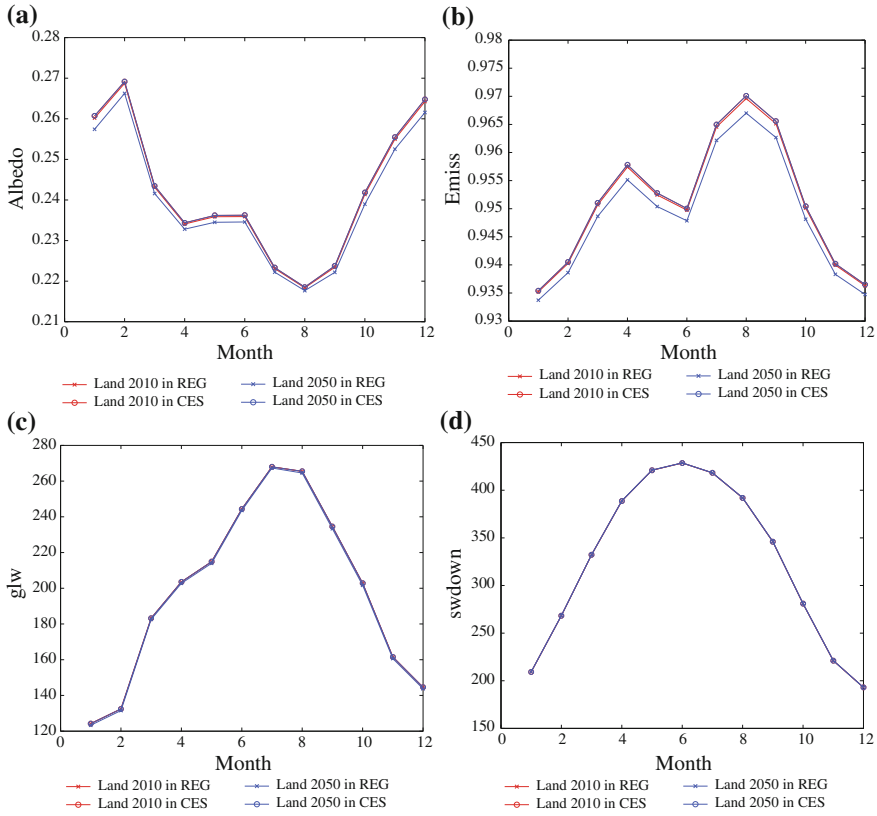

Fig. 6.11 Influence of the future land use change on the key biogeophysical parameters in Southern-Jiangsu. **a** and **b** Show the influence of the future land use change on albedo and surface emissivity; **c** and **d** show the influence of the future land use change on downward long-wave radiation and downward shortwave radiation (W/m^2)

$$Rn = H + LE + G \tag{6.3}$$

where Rn is land surface net radiation, H is sensible heat flux, LE is latent heat flux, and $G$is soil heat flux.

Since there is generally very limited heat flux into the soil layer, land surface net radiation is mainly influenced by sensible heat flux and latent heat flux, while the underlying surface can directly influence latent heat flux and consequently influence near-surface temperature (Fig. 6.13).

In order to further analyze the impacts of the variation in latent heat flux on the spatial pattern of temperature, we investigate the spatial pattern of latent heat flux under different scenarios (Fig. 6. 14). It can be seen that there is no significant difference in the spatial pattern of latent heat flux in Southern Jiangsu province under different scenarios. However, the variation range of latent heat flux in 2050 is smaller under REG scenario than under the other scenarios.

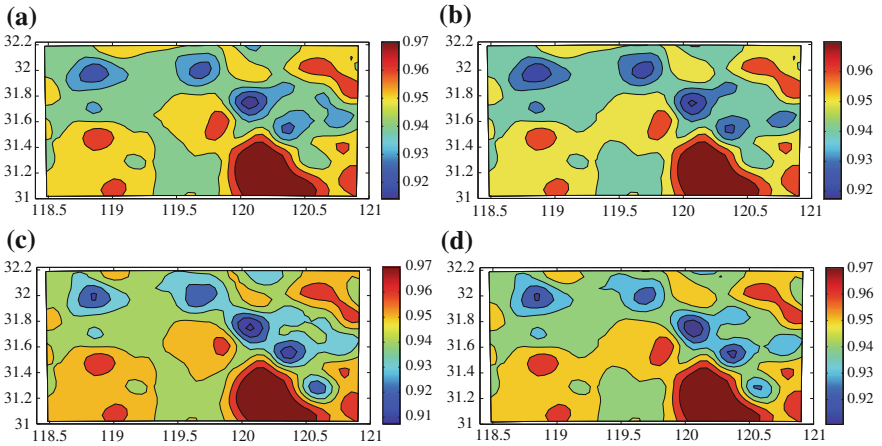

Fig. 6.12 Spatial pattern of the land surface emissivity in Southern Jiangsu under different scenarios. **a** and **b** Show the simulation result of land surface emissivity of land use in Southern Jiangsu in year 2010 under REG scenario and CES scenario, respectively; **c** and **d** show the simulation result of land surface emissivity of land use in Southern Jiangsu in year 2050 under REG scenario and CES scenario, respectively

Fig. 6.13 Comparison of the latent heat flux in Southern Jiangsu under different scenarios (W/m^2)

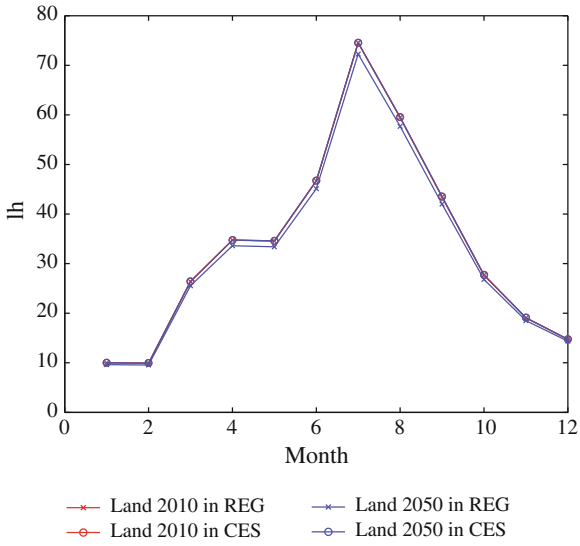

6.2.5 *Concluding Remarks on Urbanization and its Climate Effects in Southern Jiangsu Province*

(i) Land use change in Southern Jiangsu province shows different changing trends under different scenarios, but it is mainly characterized by the expansion of urban land and shrinkage of cultivated land and forest. Under

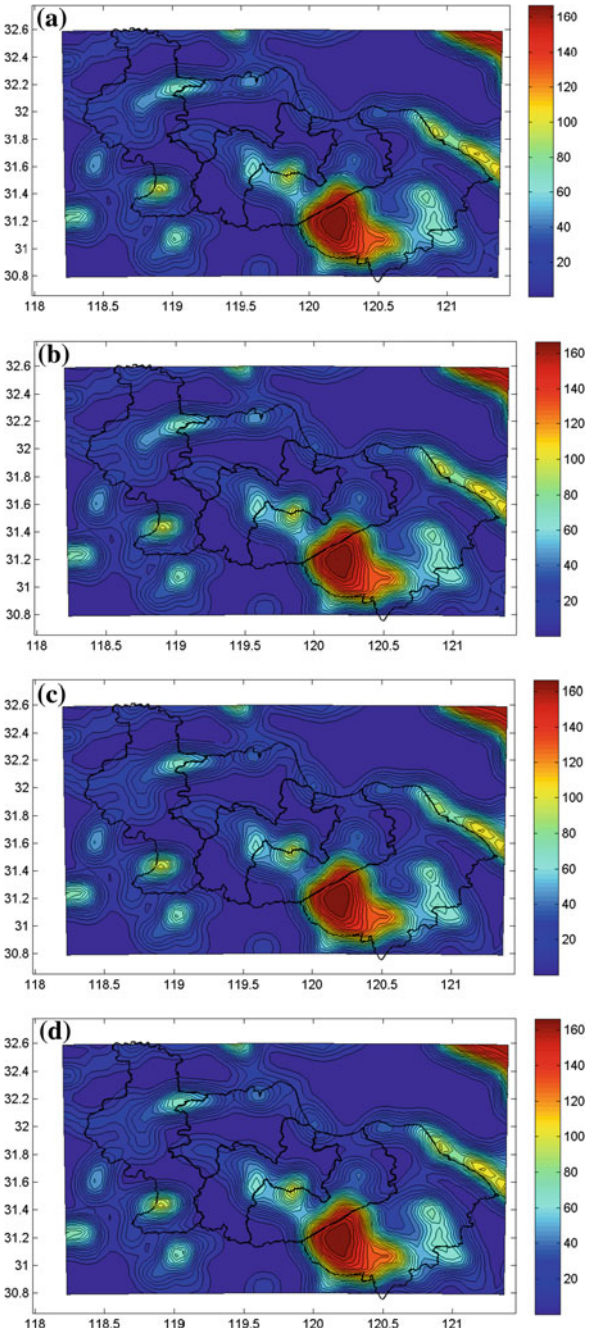

Fig. 6.14 Spatial pattern of the latent heat flux in Southern Jiangsu under different scenarios (mm). **a** and **b** Show the simulation result of latent heat flux of land use in Southern Jiangsu in year 2010 under REG scenario and CES scenario, respectively; **c** and **d** show the simulation result of latent heat flux of land use in Southern Jiangsu in year 2050 under REG scenario and CES scenario, respectively

REG scenario, urban land expansion in Southern Jiangsu province will keep at a fast rate; urban land will mainly expand around the central cities, mainly occupying cultivated land and forests. By contrast, built-up land will expand dispersedly in the whole study area under CES scenario, and built-up land expansion around the main cities will be restricted to some degree.

(ii) Monthly average temperature in Southern Jiangsu province shows a consistent changing trend under different scenarios, but temperature range shows significant difference. The highest value of monthly average temperature appears in July under all scenarios, while the lowest one appears in January. Besides, regional monthly average temperature is the highest in 2050 under REG scenario and the lowest in 2010 under CES scenario. In addition, the difference in monthly average temperatures is the greatest in summer and the smallest in winter.

(iii) There is significant influence of the underlying surface on the spatial pattern of temperature. The spatial pattern differs most greatly in 2050 under REG scenario and in 2010 under conservation scenario, especially in July. The range of high-temperature regions is much wider in 2050 under REG scenario than in 2010 under CES scenario. The high-temperature regions are much wider in 2050 under REG scenario than it is under CES scenario, especially in big cities such as Nanjing, Zhenjiang, Suzhou, and Wuxi.

(iv) Land use change in Southern Jiangsu province mainly influences regional temperature through altering land surface net radiation and latent heat flux. Land surface net radiation, which depends on land surface albedo and emissivity, downward long-wave radiation and downward shortwave radiation, plays a dominant role in influencing temperature. Meanwhile, there is no significant influence of land use change on the spatial pattern of latent heat flux. In addition, land surface albedo and emissivity play the most important roles in influencing land surface net radiation, and there is no significant influence of the underlying surface on downward long-wave radiation and downward shortwave radiation.

This study revealed the influence of future land use change (especially urban land expansion) on regional temperature in Southern Jiangsu province, and analyzed the impacts of land use change on the key biogeophysical parameters from the perspective of land surface radiation budget and energy balance. The result of this study is of great significance to the selection of reasonable land use mode to mitigate regional climate change. The precipitation as another important aspect of regional climate change has not been involved in this study. Therefore, it is still necessary to carry out more in-depth research on the influence of land use change on regional climate change.

6.3 Projected Climate Impacts of Urbanization in Wuhan Metropolitan

Rational choice of urbanization patterns is the hot issue for government and academia. On one hand, many economists have conducted comparative study of urbanization pattern from the perspective of economic efficiency, and given the basis of urbanization model selection. On the other hand, natural scientists have proved that urban land expansion is one of the most important reasons for global climate change. Urban land expansion has a non-negligible impact on regional climate by changing the underlying surface. As an important place for human settlements, urban development should be evaluated form both environmental effects and its impact on human welfare when pursuing economic efficiency. Therefore, not only economic efficiency differences but also the environmental effects of urban development and its impact on human living conditions should be considered to choose a rational urban land expansion pattern. Especially in the context of global climate change, studying impacts of underlying surface on regional climate change has an important guiding significance for selection of rational urbanization patterns. China is currently in the period of rapid urbanization. In the coming period, China will maintain a high speed of urbanization. Therefore, rational choice of urbanization model has a special significance for China.

Wuhan Metropolitan is an important urban agglomeration after the rise of Central China following the Yangtze River Delta, Pearl River Delta, and the Bohai Sea Rim in China. It is also the first batch of pilot area of the "resources-saving and environment-friendly" society construction in China. Therefore, it is urgent to figure out the impact of different urban land expansion patterns on climate change in Wuhan Metropolitan, which will find out a reasonable urban land expansion pattern to mitigate regional climate change in Wuhan Metropolitan.

In this case study, we set up three kinds of urbanization scenarios: baseline scenario, centralized urban land expansion scenario, and decentralized urban land expansion scenario. The Partitioned and Asynchronous Cellular Automaton Model is then employed to simulate urban land expansion patterns under different scenarios in Wuhan Metropolitan in 2020. The results are taken as a land use/cover underlying surface data to be input into WRF model, and impacts of urban land expansion on regional climate change under three different scenarios of urban land expansion pattern are simulated. Through comparative analysis urban land expansion under three different scenarios, we generate the spatiotemporal variation of its impacts on surface climate, which will provide a reasonable response of urbanization patterns to climate change in Wuhan Metropolitan.

6.3.1 Study Area and Data Sources

6.3.1.1 Study Area

Wuhan Metropolitan is located in the middle of Hubei province, China. It is the urban agglomeration which takes Wuhan as the center, and is composed of eight cities of Huangshi, Ezhou, Huanggang, Xiaogan, Xianning, Xiantao, Tianmen, and Qianjiang within 100 km, with a total area of about 5.78×10^4 km^2, accounting for 31.1 % of land area in Hubei Province (Fig. 6.15). By the end of 2008, the resident population of Wuhan Metropolitan was 2994.6 million, the annual GDP reached 697.211 billion Yuan, accounting for 61.5 % of the province's total GDP, it is also an important economic development centers in Hubei Province, and an important strategic fulcrum of "rise of central China." Wuhan Metropolitan faces many development opportunities as the comprehensive reform pilot area of "resource-saving and environment-friendly" society. However, to this end, the rapid development of Wuhan Metropolitan could not only focus on socioeconomic development but also concentrate about ecological and environmental effects in the fast urbanization process. Therefore, it is beneficial to analyze effects of different urbanization pattern on regional climate and select reasonable urbanization patterns for Wuhan Metropolitan region accordingly.

6.3.1.2 Data Sources

Land use data, interpreted from remote sensing images in 2000 and 2008, is mainly used for scenario simulations of future land use change, for Wuhan Metropolitan region. It includes five land types, i.e., farmland, forestland, grassland, built-up land and water bodies, and built-up land contains urban land, rural residential and other construction land. Among them, land use data in 2000 came from the Land Use Database of Data Center Resources and Environment, Chinese Academy of Science. The resource of this database is Landsat TM/ETM$^+$ image interpretation with a spatial resolution of the 30 × 30 m. Land use dataset are then resampled to 100 × 100 m raster dataset. Land use data in 2008 came from the CBERS (China–Brazil Earth Resource Satellite) image interpretation with a spatial resolution of 20 × 20 m. The interpretation results are also resampled to 100 × 100 m grid. Specific process includes geometric correction, radiometric correction, boundary cropping, supervised classification, and visual interpretation, and accuracy assessment.

Natural environmental indicators in this study are the same to the previous case study for Southern Jiangsu province, namely DEM, distance from the city at all levels, distance from the railway, road and river. Social and economic statistical data in this study include population data of Wuhan Metropolitan cities, per capita retail sales of social consumer goods, the total investment in fixed assets, per capita income, and second industry gross grain yield per unit area from 2000 to 2008. These data comes from Hubei Statistical Yearbook.

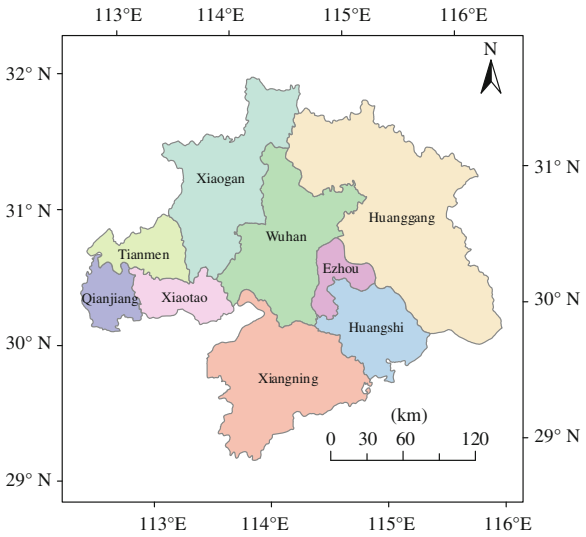

Fig. 6.15 Study area

Climate data includes annual precipitation and annual average temperature data. Based on China weather site observation data, spline interpolation arithmetic method is employed to interpolate meteorological site's observation data to get grid form of annual precipitation and annual average temperature surface in research region.

6.3.2 Methodology

6.3.2.1 Research Framework

The basic idea of scenario analysis on the impacts of urban land expansion on climate change is performed by Fig. 6.16. Based on setting urban land expansion scenarios in Wuhan Metropolitan, the Partitioned and Asynchronous Cellular Automata Model is employed to carry out the scenarios simulation of urban land use expansion in Wuhan Metropolitan, so as to get spatiotemporal pattern of urban land expansion. By converting urban land expansion simulation results to underlying surface data to be input into WRF model, regional climate change under different scenarios in Wuhan Metropolitan can be carried out. By comparing analysis on climate change effects of urban land expansion under different scenarios, it is helpful to get reasonable urban land expansion pattern for mitigation climate change in Wuhan Metropolitan.

Urban land Expansion Scenario

Urban land expansion pattern scenarios of Wuhan Metropolitan are set up first. In this part, three urbanization pattern scenarios are setup. They are baseline scenario,

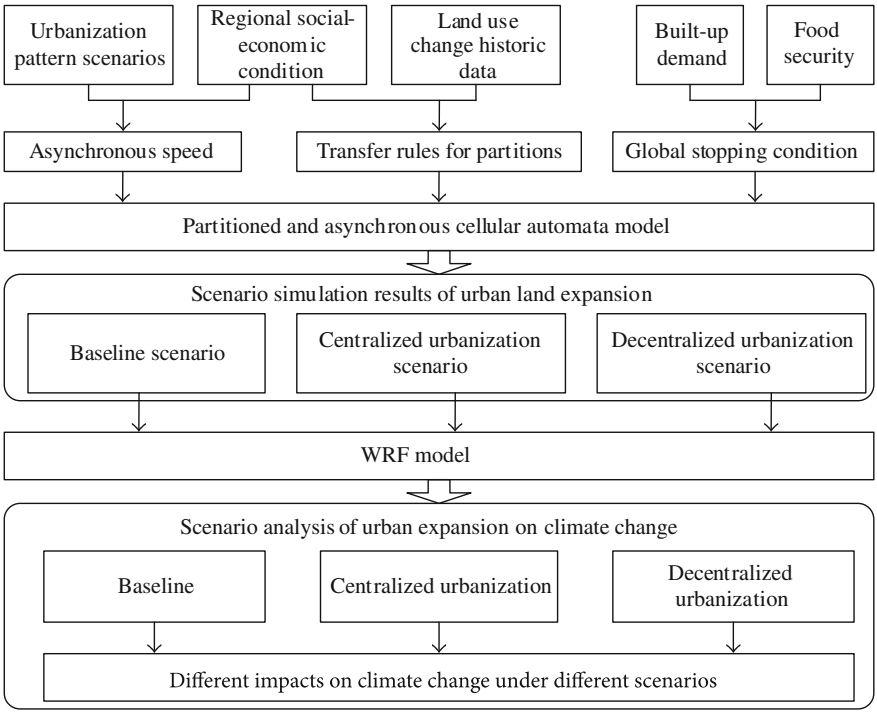

Fig. 6.16 Research framework of scenario analysis of urban land expansion on climate change impacts

centralized urban land expansion scenario, and decentralized urban expansion scenario. On this basis, the Partitioned and Asynchronous Cellular Automata model is employed to simulate urban land expansion under different scenarios. In Partitioned and Asynchronous Cellular Automata model, urban land expansion scenarios and regional socioeconomic development conditions are used to calibrate asynchronous evolving speed, regional land use change laws and regional differences of socioeconomic conditions are used to calibrate transformation rules in each partition, and built-up demand decided by economic development and farmland demand decided by food security are used to calibrate global stopping condition. After these, urban land expansion patterns under different scenarios in Wuhan Metropolitan can be carried out.

Scenario Analysis of Urban Land Expansion on Surface Climate

The underlying surface data of Wuhan Metropolitan for climate model are processed first. By scale transformation and type transformation, scenario simulation results of urban land expansion can be converted to underlying surface data for

WRF model. Keeping lateral boundary conditions and all other parameters of WRF model unchanged, processed land use/cover underlying surface data are input into WRF model to simulate regional climate change in Wuhan Metropolitan. After these processes, regional climate change under different urbanization patterns in Wuhan Metropolitan can be figured out. Through scenario analysis of regional climate change under different urbanization patterns, optimal urbanization patterns which can mitigate climate change in Wuhan Metropolitan can be worked out.

6.3.2.2 Partitioned and Asynchronous Cellular Automata Model

Cellular automata model has the ability to simulate spatial and temporal evolution of complex systems. The "bottom-up" research idea fully reflects the concept that local individual behaviors of complex systems will produce global and orderly pattern. Therefore, cellular automata model has natural advantages in urban land expansion simulation (Li et al. 2007). However, most cellular automata models have some limitations in simulating urban land expansion. On one hand, it ignores spatial heterogeneities existing in urban land expansion and its influencing factors to use the unified cellular transformations rules for all cells in urban land expansion simulation. On the other hand, it ignores the spatial heterogeneities of urban land expansion speed to employ same evolving speed for all cells. Both of them become the barrier of simulation accuracy improving for cellular automata model (Ke and Bian 2010). In this model, spatial data mining methods are employed to dig out partitions for cellular automata model and separately cellular transformation rules for each partition are dig out by Decision Tree Algorithm.

Transformation rules for each partition are made up of three sections: transformation probability for each partition, unit constraints, and neighborhood development density (Li et al. 2007). It can be showed by the following formula.

$$P_{d,ij}^{t} = [1 + (-ln\gamma)^{\alpha}] \times P_g \times \mathrm{con}(s_{ij}^{t}) \times \Omega_{ij}^{t}$$

where $p_{d,ij}^{t}$ is transformation probability for each partition, γ is random number ranging from 0 to 1, α is the parameter which controlling random variable effect level. It is an integer which ranges from 1 to 10, P_g is transformation probability which decided by urban expansion influencing factors, $\mathrm{con}(s_{ij}^{t})$ is constraint condition of unit, Ω_{ij}^{t} is neighborhood function which means effect of neighborhood to cellular automata transformation probability.

In these above parameters, γ and α is introduced to add random factors in cellular automata model to imitate effect and intervention of all kinds of uncertain factors in land use processes. P_g is obtained from geographical phenomenon change data and is related to impact factors by the method of spatial data mining. It remains unchanged in the process of the whole simulation. $\Omega_{ij}^{t}$is a very important factor. It changes over time and can be performed by the following formula.

$$\Omega_{ij}^{t} = \frac{\sum_{3\times3}(s_{ij} = target)}{3 \times 3 - 1}$$

$\mathrm{con}\left(s_{ij}^{t}\right)$ is unit constraint condition represent cellular which cannot transform to urban land, such as water and high mountain. For example, when a cell represents basic farmland preservation area, $\mathrm{con}\left(s_{ij}^{t}\right) - 0$, because it is constraint to development in this area.

P_g is regional land use change regulations mined from data of regional land use and related influencing factors. In our research, C5.0 Decision Tree Algorithm is applied to calculate regional land use change rules. Decision Tree Algorithm is a typical data mining classification algorithm. Its main role is to reveal the structured information of the data. The created tree structure is visual, easy to understand, and deal with nonlinear data. The hidden knowledge rules in data can also be extracted. Therefore, Decision Tree Algorithm can be used to dig out cellular transformation rule (Ke et al. 2009). In C5.0 Tree Decision Algorithm, clusters are determined by the fellow formula.

$$I(r_1, r_2, \ldots, r_m) = -\sum_{i=1}^{m} p_i \cdot \log_2(p_i)$$

where r_i is the subset of dataset S which belongs to cluster C_i, P_i is the probability of every sample belongs to C_i, and I is the information gain.

Asynchronous evolving speed is determined by two parts, level of social-economic development and urbanization scenario. Compared with the conditions of social and economic development level, urbanization patterns play much more important role in urban land expansion speed. Therefore, in order to clarify the influential difference of urban land expansion on regional climate change in different urbanization pattern of Wuhan Metropolitan, asynchronous evolving speed for Partitioned and Asynchronous Cellular Automata Model is decided by urbanization patterns. Under baseline scenario, the evolving speed for each cellular in Wuhan Metropolitan follows in the history of law, mainly determined by the regional differences of socioeconomic development. Under centralized urbanization scenario, the greater the cities are, the higher the urban land expansion prefers and the faster urban land expands. Under decentralized urbanization scenario, the smaller the size of cities is, the higher priority and the slower speed of urban land expansion is. Asynchronous evolving speed in Partitioned and Asynchronous Cellular Automata Model can be figured out by the following formula.

$$v_{ij\_pri} = \frac{priority_{ij}}{priority_{\max} - priority_{\min}} \times (v_{\max} - v_{\min}) + v_{\min}$$

Where v_{ij} is transformation speed of cell (i, j), $\mathrm{priority}_{ij}$ is urban land development priority of cell (i, j), $\mathrm{priority}_{\max}$ is the maximum of all-region's urban land

development priority, $\text{priority}_{\min}$ is the minimum of all-region's urban land development priority, $v_{\max}$ and $v_{\min}$ are all-region's maximum and minimum of cellular transformation speed.

Since cellular automaton model does not have the concept of transform speed but only evolution interval, so we need to convert evolutionary speed to evolution interval here.

$$Interval_{ij\_pri} = \left[\frac{1}{v_{ij\_pri}}\right]$$

The above formula is the corresponding evolution interval of evolving speed. Accordingly, we can estimate asynchronous evolution interval of urban land expansion for Wuhan Metropolitan.

6.3.3 Results

6.3.3.1 Urbanization Pattern Scenarios for Wuhan Metropolitan

Urbanization patterns are divided into two categories: centralized and decentralized urbanization. Centralized urbanization has three main features: First, urban scale structure is centralized. It is mainly performed that large cities, metropolitan, and medium-sized cities lead in development. Second, cluster is the main feature of city metropolitan. It is mainly showed that formation and development of various levels and influential metropolitan intensive areas. Third, urban land use become more intensified spatially. In our research, centralized urbanization mainly refers to the first characteristic, namely, cities, metropolitan, and medium-sized cities lead in development. Corresponding decentralized urbanization, the main characteristics is that small towns lead in development.

According to urbanization patterns, three scenarios of urban land expansion are designed. They are baseline scenario, centralized urban land expansion scenario, and decentralized urban land expansion scenario in this research. Under baseline scenario, urban land expansion in Wuhan Metropolitan follows its historical law. Under centralized urban land expansion scenario, large cities lead in development, while small towns' urban land use expansion speed is controlled. Under decentralized urban land expansion scenario, priority in the development is achieved by small towns, metropolitan urban land expansion are controlled. Accordingly, by setting the asynchronous evolution interval of Partitioned and Asynchronous Cellular Automata Model, urban land expansion patterns in Wuhan Metropolitan under different scenarios can be simulated. Taking centralized urbanization scenario for example, large cities will receive the prior development. At the same time, cities have higher evolving speed, and the corresponding evolution should be given a smaller interval. Accordingly, we could set three asynchronous evolution intervals of urban land expansion under different scenarios in Wuhan Metropolitan

(Table 6.4). Under each scenario, the demand of urban land for whole Wuhan Metropolitan is 819,784 hm^2, while the demand of farmland in the whole is 25,741,94 hm^2.

6.3.3.2 Scenario Simulation of Urban Land Expansion for Wuhan Metropolitan

According to asynchronous evolution intervals that set by urban land expansion scenario for Wuhan Metropolitan and combing transform rules for each partition and global stopping conditions which were determined by socioeconomic conditions and natural resource endowments in Wuhan Metropolitan, the Partitioned and Asynchronous Cellular Automata Model can be employed to carry out urban land expansion patterns under each scenario in Wuhan Metropolitan (Fig. 6.17). As could be seen, spatial patterns of urban land use results in very similar results under baseline scenario and centralized scenario for Wuhan Metropolitan. The difference lies in that the speed of urban land expansion in big cities and small cities are different but both developed under baseline scenario. However, under centralized urbanization scenario, the speed of urban land use expansion for big cities and small cities has a very significant variation. Urban land use expansion in Wuhan and its surrounding areas is very rapid, but urban land use of other areas in Wuhan Metropolitan expanded very slowly. Compared with former two scenarios, urban land use expansion law of Wuhan Metropolitan is distinctly different in decentralized urbanization scenario: Wuhan and its surrounding areas urban land expansion are very small although urban land expansion is obvious in corresponding small urban areas.

The underlying surface of WRF model is classified based on classification criteria of USGS data, while Land Use/Cover in urban land expansion simulation was divided into five categories: farmland, forestland, grassland, water bodies, and built-up land. Therefore, the simulation results cannot be directly used as underlying surface input data. Based on original underlying surface data of WRF model, urban land expansion simulation results are converted to raster datasets which have same scale with underlying surface data of WRF model by spatial analysis tools in ArcGIS. Grid data in original underlying surface data are then displaced by urban land use type in corresponding grid in processed urban land expansion simulation results. The obtained new underlying surface data contains urban land expansion in Wuhan Metropolitan under various scenarios (Fig. 6.18).

6.3.3.3 Scenario Analysis of Urban land Expansion on Climate Change Impacts

We kept boundary conditions and other initial field of WRF model constant, and substituted Wuhan Metropolitan's underlying surface data under different scenarios for WRF model. Regional climate change under different scenarios in

Table 6.4 Asynchronous evolution interval of urban land expansion in Wuhan metropolitan under different scenarios

District	Urban land expansion scenarios			District	Urban land expansion scenarios		
	Baseline	Centralized	Decentralized		Baseline	Centralized	Decentralized
Wuhan	1	1	20	Qichun	4	20	1
Caidian	7	5	15	Huangmei	5	20	1
Jiangxia	7	5	15	Xiaogan	3	10	10
Huangpi	4	5	15	Yingcheng	5	20	1
Xizhou	4	5	15	Anlu	5	20	1
Ezhou	4	10	10	Hanchuan	4	20	1
Huangshi	2	10	10	Dawu	5	20	1
Daye	5	20	1	Yunmeng	4	20	1
Yangxin	4	20	1	Xianning	8	10	10
Huanggang	4	10	10	Chibi	5	20	1
Macheng	6	20	1	Jiayu	5	20	1
Wuxue	4	20	1	Tongcheng	3	20	1
Tuanfeng	6	20	1	Chongyang	3	20	1
Hong'an	6	20	1	Tongshan	3	20	1
Luotian	4	20	1	Xiantiao	5	20	1
Yingshan	2	20	1	Tianmen	5	20	1
Xishui	4	20	1	Qianjiang	7	20	1

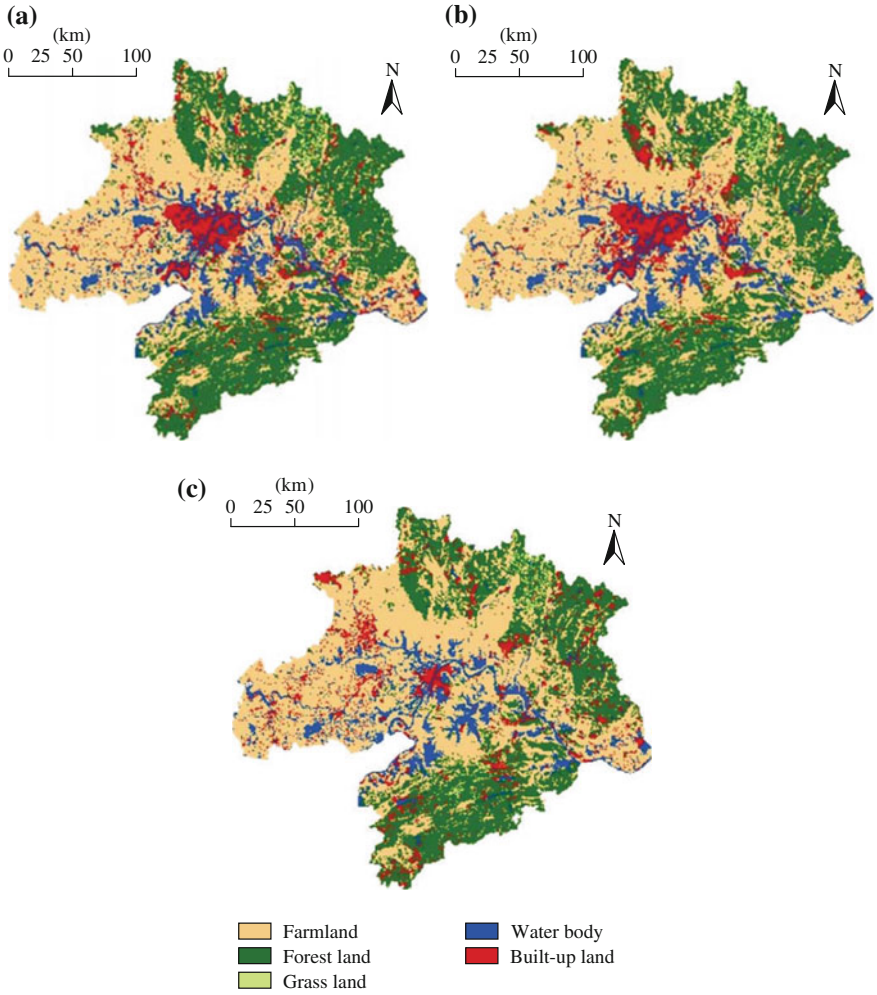

Fig. 6.17 Spatial pattern of land use under different urbanization scenarios in Wuhan Metropolitan. **a** baseline scenario. **b** Centralized urbanization scenario. **c** Decentralized urbanization scenario

Wuhan Metropolitan can thus be figured out, especially the spatial pattern of temperature and precipitation.

Under different scenarios of urbanization patterns, the impact of underlying surface changes on temperature had obvious differences (Fig. 6.19). Overall, the warming effect under three scenarios is significantly different. Among these three scenarios, the most obvious warming effect is centralized urban land expansion scenario, followed by baseline scenario, while the smallest warming effect is decentralized urban land expansion scenario. Temporally, the strongest warming

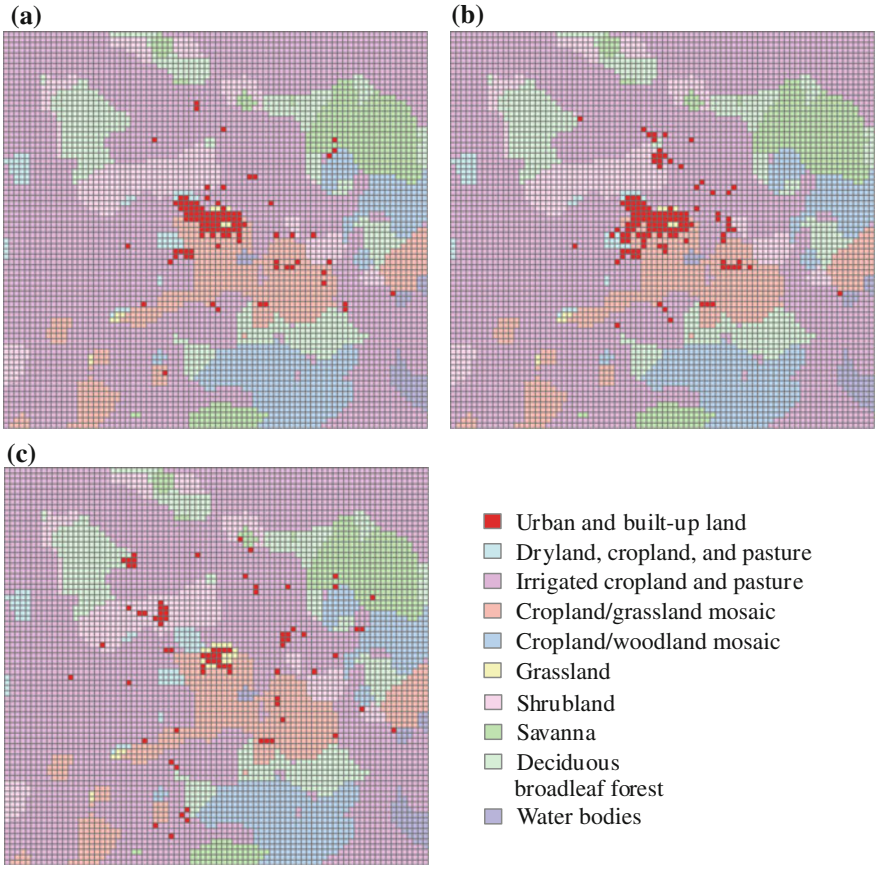

Fig. 6.18 Underlying surface data of Wuhan Metropolitan under different scenarios. **a** Baseline scenario. **b** Centralized urbanization scenario. **c** Decentralized urbanization scenario

effect difference of three scenarios appears at the hottest month of the year (June, July, and August). In colder months (January, February, November, and December), the difference of warming effect under three scenarios is small.

Under different scenarios of urbanization, there are significant differences of spatial patterns of impacts of land surface on temperature change (Fig. 6.20). From the differences of three scenarios, variation between centralized and decentralized urban land expansion scenario is the biggest, while there are small differences between centralized urban land expansion scenario and baseline scenario. Compared to decentralized urban land expansion scenario, the spatial range of warming effect is much stronger under centralized urban land expansion scenario, and the magnitude of temperature difference was greater too. Compared to baseline scenario, the spatial range of warming effect was a little stronger and more concentrated in centralized urban land expansion scenario, and the magnitude of

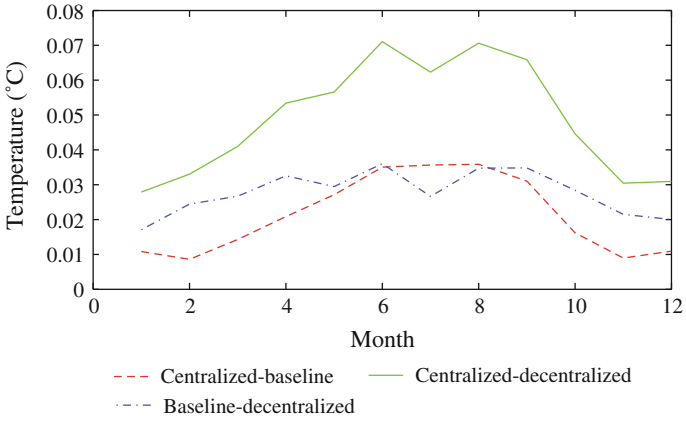

Fig. 6.19 Temperature difference under different scenarios

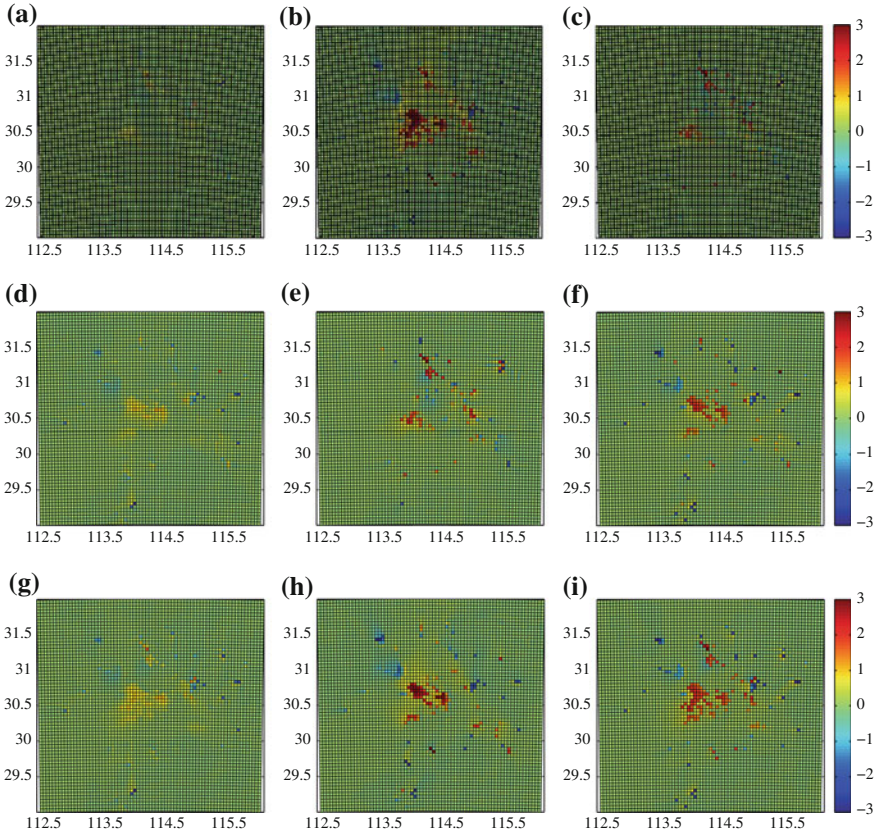

Fig. 6.20 Spatial pattern of warming effect under different scenarios (°C)

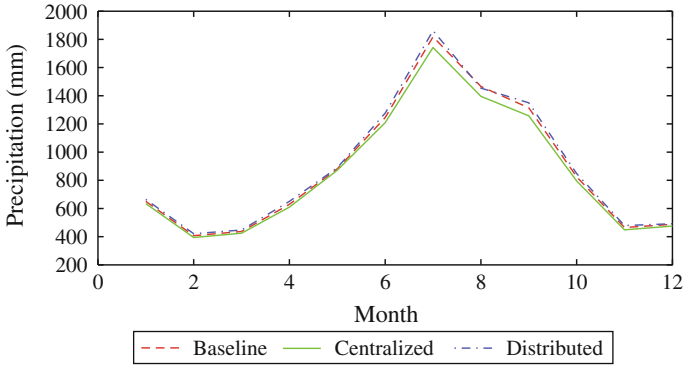

Fig. 6.21 Precipitation under different scenarios

temperature difference is also smaller. Temporally, colder month (in January as an example) warming differences are small, but the hotter months (in July for example) warming differences are much significant. From the perspective of annual average level, the biggest warming difference still lies between centralized urban land expansion scenario and decentralized urban land expansion scenario, the minimum warming difference lies between centralized urban land expansion scenario and baseline scenario. Among three scenarios, the warming effect caused by underlying surface changes is widest and strongest under centralized urban land expansion scenario. Under decentralized urban land expansion scenario, the warming scope and magnitude caused by the underlying surface changes is the smallest.

Under different scenarios of urban land expansion, the difference of impact of underlying surface changes on precipitation is not particularly significant (Fig. 6.21). Overall, the precipitation of decentralized urban land expansion scenarios is maximum, slightly higher than the other two scenarios. The precipitation of centralized urbanization scenarios is minimal, slightly lower than the other two scenarios. From the aspects of time series, precipitation under different scenarios presents an appearance of consistent monthly, the peak of precipitation appeared in July. Precipitation differences among three scenarios are largest near precipitation peak.

As the spatial distribution is concerned, precipitation under centralized urban land expansion scenario and baseline scenario is relatively concentrated, while spatial precipitation under decentralized urban land expansion scenario is relatively dispersed (Fig. 6.22). There is a wider scope, greater intensity of rainfall centers under centralized urban land expansion scenario and baseline scenario. Under decentralized urban land expansion scenario, precipitation center presented decentralized characteristic, namely, there were two smaller and weaker precipitation centers which are more evenly distributed in space.

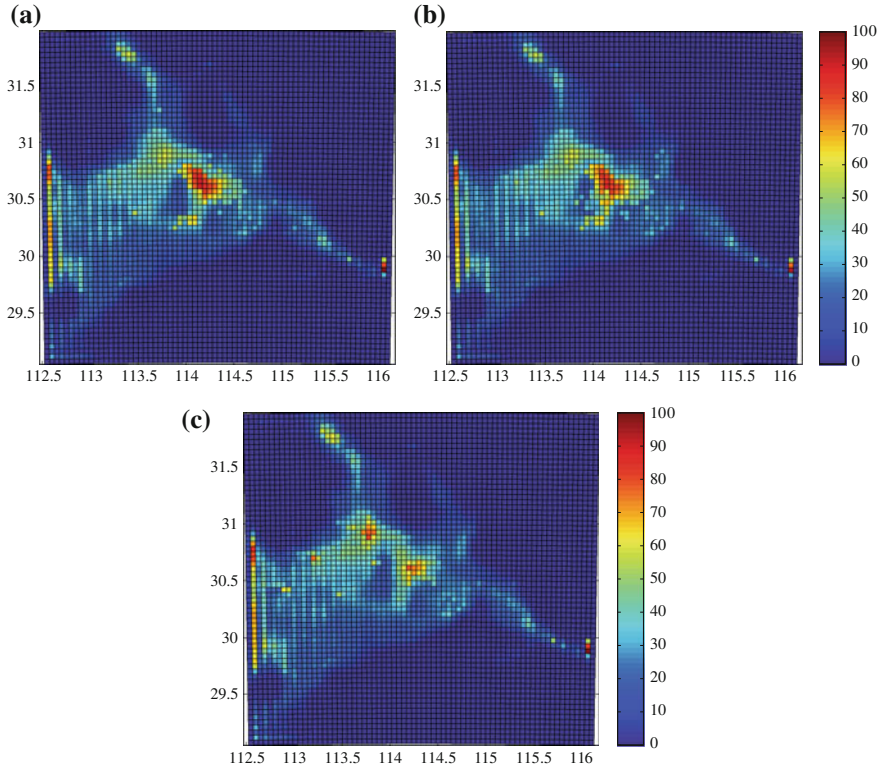

Fig. 6.22 Spatial distribution of precipitation under different scenarios (mm). **a** Baseline scenario. **b** Centralized scenario. **c** Decentralized scenario

6.3.4 Concluding Remarks on Urbanization and its Climate Effects in Wuhan Metropolitan

We carried out urban land expansion scenario simulation under different urbanization patterns based on Partitioned and Asynchronous Cellular Automata Model for Wuhan Metropolitan region. The impact of the underlying surface changes on regional temperature and precipitation under different urbanization scenarios are simulated and analyzed by WRF model. Results showed that:

(i) Under different urban land expansion scenarios, warming effect of urban land expansion has significant variations. Warming effect under centralized urbanization pattern is the most significant, far higher than it under decentralized urbanization scenario. Warming effect under decentralized urban land expansion scenario is much weaker than the other two scenarios. Besides, the spatial distribution of warming effect also has significant differences. The warming effect of centralized urban land expansion

is widest and strongest among three urban land expansion scenarios. The warming effect of decentralized urban land expansion scenario is on the opposite.

(ii) The different effects of different urban land expansion scenarios on regional average precipitation are not very significant. Overall, regional precipitation is largest under decentralized urban land expansion scenario, slightly higher than the other two scenarios. On the opposite, regional precipitation under centralized urban land expansion scenario is smallest. Precipitations under difference scenarios are comparatively consistent temporally. Meanwhile, spatial distribution of precipitation has significant differences. The spatial distribution of precipitation is more concentrated under centralized urban land expansion scenario, and presents a wider scope, greater intensity of rainfall center. The distribution of precipitation is more dispersed and the rainfall centers are still dispersed under decentralized urban land expansion.

(iii) Decentralized urban land expansion pattern is the suitable urbanization pattern for mitigating climate change. Under decentralized urban land expansion scenario, underlying surface change has little effect on climate change, and showing a uniform distribution pattern in space. Under centralized urban land expansion scenario, there is a greater impact on climate change, and the distribution is more concentrated in the space.

By analyzing effects of urban land expansion on regional temperature and precipitation under different urban land expansion patterns, we concluded that decentralized urban land expansion pattern is rational for "resources-saving and environment-friendly" society construction. In further studies, we need to discuss in-depth the spatial and temporal laws of regional underlying surface change on other parameters that could affect ecological environment and its effect on human welfare under different urban land expansion scenarios.

6.4 Summary

This chapter includes three case studies on the impact of future urbanization on surface climate in China.

First, we analyzed the impact of urban land use change on regional temperature and precipitation in summer in the Great Beijing area during 2030–2040 based on the simulation results of WRF and archived data land use change and climate change during 1995–2005. Results showed that urbanization in this area has affected regional climate and has the potential to the increase of temperature and precipitation in summer during 2030–2040. These results can support sustainable urban planning to mitigate and adapt to climate change in the future.

Second, we performed a scenario-based simulation of influence of land use change on regional temperature in Southern Jiangsu province, a typical region of

urbanization in China. This study projected future land use change, and then simulated the future regional temperature with WRF model. The influencing mechanism of land use change on regional temperature was analyzed from the perspective of land surface radiation budget and energy balance. The results indicated that: (i) the monthly average temperature was obviously higher under Rapid Economic Growth (REG) scenario than under Cooperate Environmental Sustainability (CES) scenario in 2050, especially in the hottest month (July). (ii) The extent of high-temperature regions is much wider under REG scenario than it is under CES scenario in 2050. (iii) The land surface net radiation and latent heat flux are two key factors through which land use change affects regional temperature in Southern Jiangsu province, and latent heat flux plays a dominant role. (iv) Land use change mainly influences land surface net radiation through altering land surface albedo and emissivity.

Last, we further simulated climatic impacts of urban land expansion under different urbanization patterns in Wuhan Metropolitan. We designed three urbanization patterns scenarios, i.e., baseline scenario, centralized urbanization scenarios, and decentralized urbanization scenarios. We applied Partitioned and Asynchronous Cellular Automata Model to simulate spatial patterns of urban land expansion under these scenarios. The results showed that decentralized urbanization is a reasonable urbanization pattern to mitigate climate change in rapid urbanization period in this study area. It can provide a scientific basis for the rational choice of urban land expansion pattern in Wuhan Metropolitan in the context of climate change, and also shed lights on choosing rational urban development models for the other regions.

References

Jin M, Dickinson RE, Zhang D (2005) The footprint of urban areas on global climate as characterized by MODIS. J Climate 18(10):1551–1565

Ke X (2009) A partitioned and asynchronous CA model and its sensitivity to scales. Ph.D. dissertation, Wuhan University

Ke X, Bian F (2010) A Partitioned and Asynchronous CA based on spatial data mining. J Image Graph 15(6):921–930

Kuang W, Liu J, Shao Q (2011) Simulating dynamic urban expansion at reginal scale in Beijing-Tianjin-Tangshan Metropolitan Area. J Geogr Sci 66(2):178–188

Lei M, Niyogi D, Kishtawal C, Pielke R Sr, Beltrán-Przekurat A, Nobis T et al (2008) Effect of explicit urban land surface representation on the simulation of the 26 July 2005 heavy rain event over Mumbai, India. Atmos Chem Phys 8(20):5975–5995

Li X, Yeh AGO, Liu X (2007) Geographical simulation systems: cellular automata and multi-agent systems. Science Press, Beijing

Liu J, Liu M, Zhuang D (2002) Spatial pattern analysis of China's recent land-use change. Chinese Sci 32(12):1031–1040

Liu J, Liu M, Zhuang D (2003) Study on spatial pattern of land-use change in China during 1995–2000. Sci China Ser D Earth Sci 46(4):373–384

Liu J, Zhang Z, Xu X (2010) Spatial patterns and driving forces of land use change in China in the early 21st century. J Geogr Sci 20(4):483–494

Miglietta F, Gioli B, Brunet Y, Hutjes R, Matese A, Sarrat C et al (2009) Sensible and latent heat flux from radiometric surface temperatures at the regional scale: methodology and evaluation. Biogeosciences 6(10):1975–1986

Mitra C, Shepherd JM, Jordan T (2012) On the relationship between the premonsoonal rainfall climatology and urban land cover dynamics in Kolkata city, India. Int J Climatol 32(9):1443–1454

Rozoff CM, Cotton WR, Adegoke JO (2003) Simulation of St. Louis, Missouri, land use impacts on thunderstorms. J Appl Meteorol 42(6):716–738

Shepherd JM, Carter M, Manyin M, Messen D, Burian S (2010) The impact of urbanization on current and future coastal precipitation: a case study for Houston. Environ Plann B Plann Des 37(2):284–304

Tang T, Ran S, Tan M (2013) Urbanization and its impact on the evapotranspiration in Beijing-Tianjin-Tangshan Area. J Geo-inf Sci 15(2):233–240 (in Chinese)

Taylor KE, Stouffer RJ, Meehl GA (2012) An overview of CMIP5 and the experiment design. Bull Am Meteorol Soc 93(4):485–498

Wang J, He C, Dong Y, Gao L, Xu W (2002) Analysis of land use/cover driving forces in the urban fringe of Beijing City. Adv Sci 17:201–208

Chapter 7
International Comparisons of the Modeled Climate Effects of Land Use Changes

Yingzhi Lin, Fan Zhang, Yi Qu, Zhihui Li and Tao Zhang

Previous chapters focus on the climate effects responding to different types of land use changes in China. This chapter furthers the researches on the land use impacts on climate from a global perspective. Five distinguished cases for estimating the impacts of land surface changes on climate through the world are introduced separately. The first one still focuses on the possible impacts of underlying cultivated land reclamation on the future climate change, but we move the study area to India where land reclamation became the dominated land conversion comparing with other economies. Specifically, the future cultivated land reclamation is projected for the climate model's performance to estimate the potential effects on local energy flux and temperature in summer and winter.

Further, global deforestation plays a vital role in regulating climate through biogeophysical and biogeochemical effects (Bonan 2008). Currently, deforestation is one of the typical land cover changes, and its impacts on climate are not the same at different scales. Tropical deforestation will induce lower evaporate rates and make the local climate drier and warmer (Costa and Foley 2000). However, the boreal forests will change the climate in different ways in comparison with other forests. In order to understand the biogeophysical effects of different forests change on the climate, the European Russia boreal forest region is firstly chosen as the study area to study the regional temperature variation induced by future boreal deforestation. Besides, the tropical forest in Brazilian Amazon is also considered to model the potential climatological variability caused by future forest vulnerability over the twenty-first century.

As mentioned in Chap. 5, the grassland plays an important role in the ecosystem services supply, but it can rarely find out the influences of grassland change

Y. Lin (✉) · F. Zhang
School of Mathematics and Physics, China University of Geosciences (Wuhan), Wuhan 430074, China
e-mail: linyz.simlab@gmail.com

Y. Qu · Z. Li · T. Zhang
Institute of Geographic Science and Natural Resource Research, Chinese Academy of Sciences, Beijing 100101 China

X. Deng et al. (eds.), *Land Use Impacts on Climate*, Springer Geography
DOI: 10.1007/978-3-642-54876-5_7,

on regional climate. In the next study, we aim to simulate the climatological changes caused by future grassland change in Mongolia under Representative Concentration Pathways (RCPs) for the years 2010–2020 and 2040–2050.

In terms of the urbanization impacts on climate in developed megalopolis, there are still no sufficient evidences for understanding the relationships between future urban expansion and regional climate at the scale of megalopolis, whose urban area are still expanding, such as New York, Beijing, Seoul, Chicago, and Moscow. Therefore, we present some evidences for supporting the effects of future urban expansion on regional climate based on the model simulation of precipitation and temperature in the Northeast megalopolis of the United States of America (USA).

7.1 Potential Climate Impacts of Land Reclamation in India

India is a typical region of the reclamation of cultivated land in the global land use and land cover change (Delucchi). Cultivated land expansion is usually caused by the intermediate needs of the growing population. According to the fifteenth population survey in 2011, the total population of India has exceeded 1.21 billion, accounting for 17.5 % of the world population and ranking second all over the world. It is assumed that the population of India is expected to exceed that of China in 2030 (Kunzig 2011). The continuous population growth has posed a great challenge to the food security, so Indians have progressively reclaimed the cultivated land while promoting modern agriculture so as to meet the domestic food demand. Subsequently, these large scale anthropogenic reclamation leads to the land use and land cover changes, which inevitably influences the exchange and distribution of the energy, moisture, and momentum between the biosphere and atmosphere, and affects the radiation balance and water cycle (Feddema et al. 2005; Pielke et al. 2002). Hence, this study attempts to quantitatively project the potential biogeophysical effects caused by the future large-scale reclamation of cultivated land with the WRF model performance.

7.1.1 Model and Data

7.1.1.1 Simulation Schemes

The simulation domain is illustrated in Fig. 7.1. The spatial resolution of land cover maps is 30 km × 30 km, and there were 79 grid cells in the east-west direction and 111 grid cells in the north-south direction in the whole simulation area (Only a small eastern part of India is not included in the study area). The temporal duration of the WRF simulation is set to 2010–2050 in this study. The parameterization schemes mainly include the Noah land surface parameterization scheme (Ek et al. 2003),

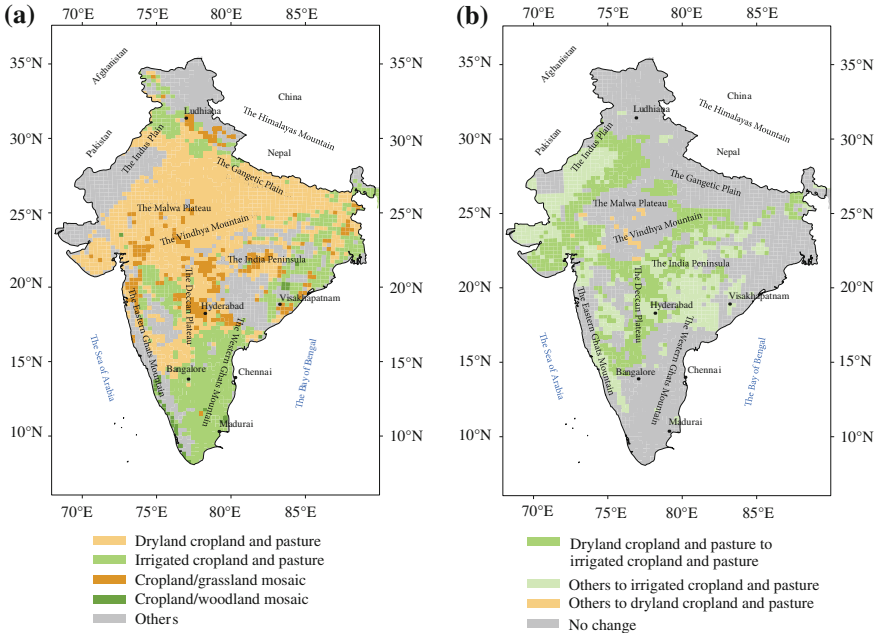

Fig. 7.1 Spatial pattern of cultivated land in the base year of 2010 (**a**) and its possible changes in future (**b**) in India

CAM3 radiation scheme (Gettelman et al. 2008), WSM3-class simple ice microphysics (MP) scheme (Challa et al. 2009), Grell-Devenyi ensemble scheme for cumulus convection, and YSU boundary layer scheme (Hong et al. 2006).

The fifth phase of the Coupled Model Intercomparison Project (CMIP5) produced a state-of-the-art multi-model dataset advancing our knowledge of climate variability and climate change. This model output, which is analyzed by researchers worldwide, underlies the Fifth Assessment Report by the Intergovernmental Panel on Climate Change (Taylor et al. 2012). It provides projections of future climate change on two timescales, near term (out to about 2035) and long-term (out to 2100 and beyond). Model output of the latter of Representative Concentration Pathway (RCP) 6.0, such as air temperature, specific humidity, sea level pressure, eastward wind, northward wind, and geopotential height from 2010 to 2050 was used as the atmospheric forcing dataset of WRF model.

The parameters of the Noah land surface parameterization is adjusted for the application in India case. In addition, the vegetation parameters related with the land cover as well as the land cover change are revised since this study mainly focuses on the effects of the land cover changes rather than those of the radiation process.

Table 7.1 Description of the experimental design

Test	Test period	Forcing data	Land cover data in WRF model
Control test	2010–2050	2010–2050	Land cover data of 2010
Prediction test tetest	2010-2050	2010–2050	Land cover data of 2050

Table 7.2 The simulated and observed values of the annual average near-surface temperature (°C) in India for the year of 2010

City	Coordinates	Location	Observed	Simulated	Difference
Ludhiana	(31.05 N,77.34E)	North	14.2	13.0	−1.2
Madural	(10.19 N,79.23E)	South	35.0	33.5	−1.5
Chenni	(14.05 N,80.29E)	Plain	16.6	17.4	0.8
Bangalore	(13.92 N,77.12E)	Mountainous area	33.2	32.9	−0.3
Visakhapatnam	(18.90 N,83.28E)	Coastal area	30.9	30.3	−0.6
Hyderabad	(18.23 N,78.27E)	Inland	32.8	32.7	−0.1

Note The historical data is collected from http://sdwebx.worldbank.org/climateportal/index.cfm

7.1.1.2 Data

There are two sets of tests included in the experimental design, one is the control test and the other is the prediction test (Table 7.1). The land cover data in 2010 and the predicted land cover data in 2050, both in the classification of US Geological Survey (USGS), were used as the underlying land surface data in the control test and prediction test, respectively. The land cover data in 2010 were obtained from the National Basic Research Program of China, and the land cover data in 2050 is projected based on the work of the Asia-Pacific Integrated Model (AIM) modeling team at the National Institute for Environmental Studies (NIES), Japan. The reason why we choose RCP6.0 scenario is that it is a stabilization scenario where total radiative forcing is stable after 2100 without overshoot by employment of a range of technologies and strategies for reducing greenhouse gas emissions (Fujino et al. 2006). Only the underlying cultivated land is highly concerned to focus on the research purpose in which the reclamation's effects would be modeled.

7.1.2 Results

7.1.2.1 Cultivated Land Changes in India

2Cultivated land is widely distributed in India, and the total area of the cultivated land and pasture reaches around 2.07 million km^2, accounting for 73.03 % of the study area. There are mainly four kinds of cultivated land in India according to the USGS classification, i.e., the dryland cropland and pasture, irrigated cropland and pasture, cropland/grassland mosaic, and cropland/woodland mosaic. The dryland

cropland and pasture owns the largest area among the four kinds of cultivated land, reaching nearly 1.18 million km^2 (56.76 % of the total cultivated land area), mainly located in Gangetic Plain, Malwa Plateau, and the northern part of Deccan Plateau. The irrigated cropland and pasture ranks second with the coverage of 0.67 million km^2 (32.10 % of the total cultivated land area), and it is mainly distributed in the northern part of Indus plain, eastern part of India Peninsula, and the coastal plain in the southern part of India. There are only a few cropland/grassland mosaics (9.82 %) in the northern part of Indus plain and the middle part of India Peninsula, and the cropland/woodland mosaic is kept with the least area (1.32 %), which is sparsely distributed in the coastal area in the southwest part of India (Fig. 7.1a).

According to the projected land cover data in 2010–2050, the total conversion area of the cultivated land will be about 1.16 million km^2, and changed cells cover most part of India except Gangetic Plain and the coastal area in the southeast part of India, including the conversion from other land use types into the cultivated land as well as the conversion from the dryland cropland into the irrigated cropland (Fig. 7.1b). The dominated land use change is the conversion from the dryland cropland into the irrigated cropland, accounting for 50.23 % of the total conversion area. The corresponding converted grid cells are mainly located in the flat regions, e.g., Indus Pain and the middle part of India Peninsula. Additionally, the cells of conversion from other land use types into the irrigated cropland (48.15 % of the total conversion area) mainly distributes in the plain and coastal area in the northeast part of Eastern Ghats Mountain, the northern part of Western Ghats Mountain, and some undeveloped regions with certain water sources in the southwest part of India. In the second conversion type, 93 % of the expanded cultivated land is from grassland and shrub, with only 7 % from forest. The least proportion of changed land is converted from other land use types into the dryland cropland, and only sparsely distributed in Malwa Plateau. Totally, there has been a large proportion of dryland cropland in India, and most of them will be changed into the irrigated land with higher productivity due to the improvement of the irrigation conditions, progress of irrigation techniques, and increase of the food demand.

7.1.2.2 Model Validation

The result indicates that the maximum temperature of both the historical data and the simulation result appears around March, while the minimum occurs in November. The decrease rate during the period from September to November is a little bit higher than that during January and March (Fig. 7.2).

The simulation result showed that the modeled temperature is lower than the observations on the whole. Specifically, the observed data indicate the annual daily average temperature is 29.06 °C, while the simulation result is 27.70 °C. As for the monthly temperature change, the simulated temperature is lower than the observed one in all months except February, and the difference in September is the most significant, reaching 2.69 °C. With regard to the seasonal change, the simulated temperature is less than the observations of all seasons except the winter.

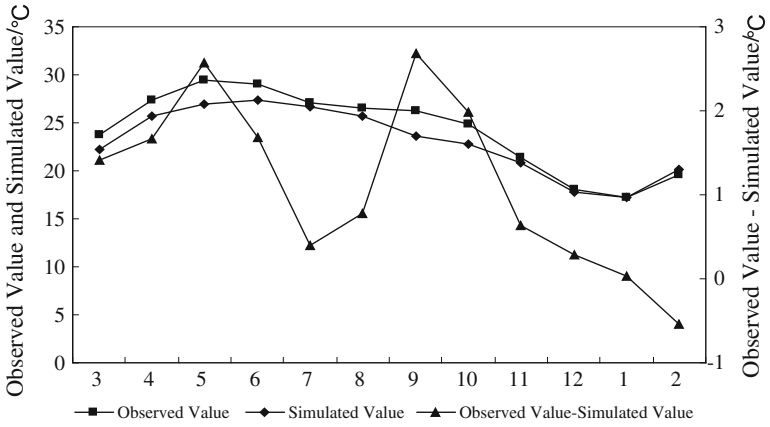

Fig. 7.2 Simulated and observed values of the monthly average near-surface temperatures in India for the year of 2010The spatial pattern of the annual daily average temperature indicates that the simulated and observed temperatures are both higher in the south part and lower in the north part, higher in the mountainous area and lower in the plain at the same latitude, and that of inland is warmer than the coastal area. For example, the temperature in Madural City (south) is 20.5 °C higher than that of Ludhiana (north); while it is 15.5 °C higher in Bangalore City (mountain area) than that of the Chenni City (plain). Meantime, the temperature in Hyderabad City in the inland is 2.4 °C higher than that in Visakhapatnam City in the coastal area (Table 7.2)

The difference between the simulated and observed data in the spring and autumn is 1.89C and 1.77 °C, respectively, and it is relatively small in the summer and winter, only reaching 0.95 °C.

In summary, WRF model has a high ability to simulate the temperature in India at different temporal and spatial scales with accepted tolerance. The simulated results is a little bit lower than the observations, and the spatial pattern indicates that there is no significant difference between the simulated and observed values in most regions.

7.1.2.3 Possible Impacts of the Cultivated Land Reclamation on the Energy Flux

The reclamation of cultivated land in study area may lead to significant change of the energy flux, which might augment the temperature variation through the land–atmosphere interaction and the atmospheric circulation. Table 7.3 shows the simulated monthly and annual differences of latent heat flux and sensible heat flux between 2010 and 2050. These differences are caused by the reclamation of cultivated land (Deng et al. 2013; Liu and Deng 2011). The result shows that the cultivated land reclamation will induce the increase of the latent heat flux increases (0.84 W/m^2) and decrease of the sensible heat flux (1.03 W/m^2).

The simulation result indicates that there is obvious seasonal fluctuation of heat fluxes (Table 7.3). For example, on average, the latent heat flux in the monsoon

Table 7.3 Projected differences of monthly and annual heat fluxes (W/m^2) between 2010 and 2050 in India

	Latent heat flux	Sensible heat flux
Jan	0.14	−0.42
Feb	0.54	−0.78
Mar	0.68	−0.95
Apr	1.80	−2.00
May	1.06	−1.17
Jun	1.40	−1.54
Jul	1.99	−2.18
Aug	0.47	−0.64
Sep	1.50	−1.61
Oct	0.23	−0.45
Nov	0.18	−0.33
Dec	0.11	−0.29
Average	0.84	−1.03

season (roughly August to October) increases by 0.73 W/m^2, while the sensible heat flux decreases by 0.90 W/m^2. By comparison, on average, the latent heat flux before the monsoon season (roughly April to July) increases by 1.56 W/m^2, while the sensible heat flux decreases by 1.72 W/m^2. This indicates that the changes on heat fluxes before the monsoon season are larger than that in the monsoon season.

7.1.2.4 Possible Impacts of the Cultivated land Reclamation on Air Temperature

(i) Overall conditions of the near-surface temperature

Since the near-surface temperature is extreme in the summer and winter, we have mainly focused on the forecast of the monthly average temperature in the summer and winter for the study area of India. The spatial heterogeneity of the monthly average temperature in the summer and winter from 2010 to 2050 is shown in Fig. 7.3. The result indicates that the future reclamation of cultivated land in India will have some impacts on the monthly average temperature in the summer and winter. In comparison to the base year 2010, the land reclamation will drive the monthly average temperature decrease and increase by 0.22 °C and 0.11 °C in the summer and winter, respectively, for 2050 in India. It has a cooling effect on the temperature in India on the whole and it is consistent with the conclusion of Feddema et al. (Feddema et al. 2005) that agriculture expansion can contribute to the decrease of the daytime temperature at the low or middle latitudes. This may be caused by the conversion from some other land use types into the irrigated cropland during the reclamation of cultivated land in India, and the increased irrigation plays an important role in decreasing the temperature. Besides, the conversion from grasslands and forest land into the dryland cropland can

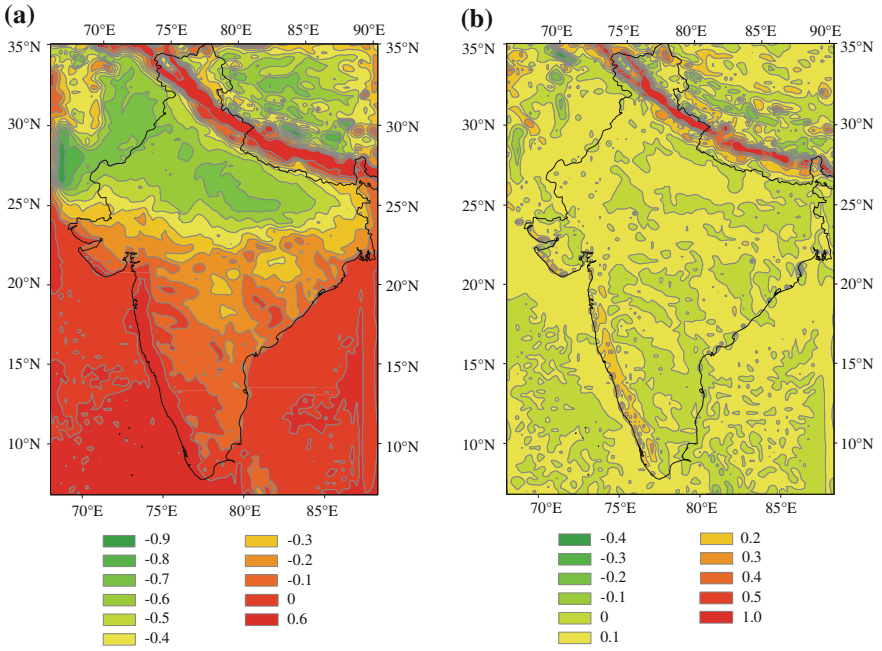

Fig. 7.3 Change of the monthly average temperature in the summer (**a**) and the winter (**b**) due to the cultivated land reclamation in India

increase the surface sensible heat flux while decreasing the latent heat flux and evapotranspiration. Consequently, the monthly average temperature increases.

Our simulation results indicate the temperature variability also varies at spatial scales. In summer, the monthly average temperature in most regions of India decreases to some degree, among which it decreases most significantly in Gangetic Plain in the north part, with the decrement of 0.70 °C. As this region has good irrigation conditions, the newly reclaimed cultivated land can be irrigated and consequently makes the temperature decrease. In contrast, the temperature has not changed that much in some parts of the Eastern Ghats Mountain and the Western Ghats Mountain where the altitude is relatively high. The temperature increases by 0.57 °C in the regions along Himalayas Mountain and the west part of the Western Ghats Mountain. In winter, the monthly average temperature increases to some degree in most parts of India (approximately 64.52 % of the study area) due to the reclamation of cultivated land. These regions are mainly located in the plateaus and part of the plain, where there is very limited agricultural irrigation in the winter and the reclamation of cultivated land has limited cooling effects. Conversely, the monthly average temperature keeps stable in the rest of the study area (approximately 35.15 %) where mainly in the plain the agriculture industry is originally well developed. In addition, the monthly average temperature shows a decreasing trend in only 0.32 % of the whole region, which is sparsely distributed

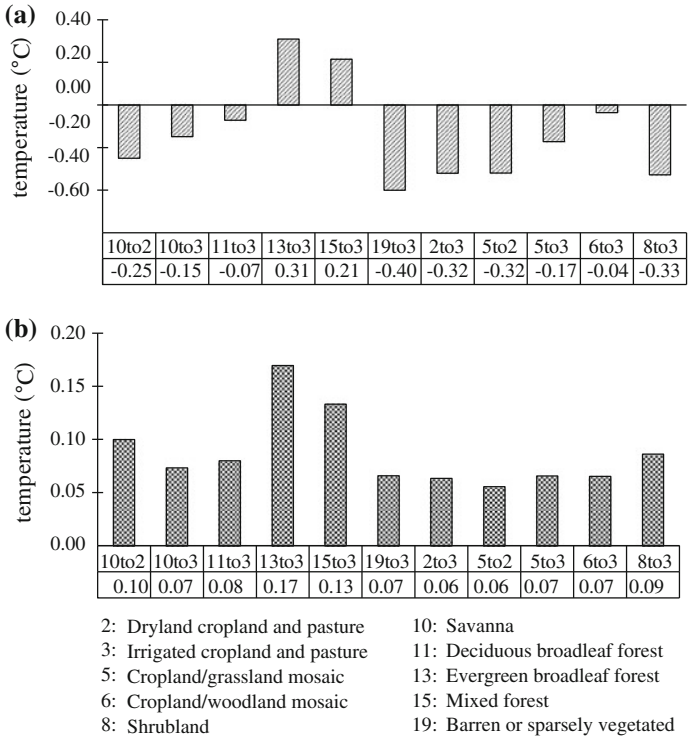

Fig. 7.4 Change of the monthly average temperature of different types of LUCC in the future reclamation of cultivated land in summer (**a**) and winter (**b**). Note: *i* to *j* (*i*, *j* are codes of land use/cover types) refers to the conversion from the land use/cover of *i* to that of *j*

in some areas near the Himalayas Mountain. Generally from the Fig. 7.3, we can also conclude that the impacts of land reclamation will not only be exerted on the local climate but also transmitted to neighboring areas.

(ii) Relationship between Land Use and Cover Change (LUCC) and the changes of near-surface temperature

The results show that the changes from evergreen broadleaf forest to irrigated cropland and pasture (designated as the conversion of 13–3 for convenience, the same below) or the changes from mixed forest to irrigated cropland and pasture (15–3) will cause an increase on the monthly average temperature separately by 0.31 and 0.21 °C in summer (Fig. 7.4a). These two types of land conversion will induce the decrease on latent heat flux and increase on sensible heat flux, leading to an overall increase on land surface temperature. The warming effect caused by the deforestation will not be offset by the cooling effect of cropland irrigation in this case. In addition to these two types of cultivated land reclamation, other land

use changes have cooling effect on the surface temperature, among which the conversion from barren or sparsely vegetated land to irrigated cropland and pasture (19–3) will lead to a maximum decrease of the monthly average temperature (i.e., −0.40 °C), this is because the vegetation coverage is relatively low in the less vegetated land. While they are converted into irrigated cropland and pasture, latent heat flux would be increased and sensible heat flux decreased resulting in the reduction of the monthly average temperature. Besides, the cooling effect of conversion from cropland/woodland mosaic to irrigated cropland and pasture (6–3) is the least (i.e., −0.04 °C). In winter (Fig. 7.4b), different types of reclamation will cause an universal rise on the monthly average temperature. The conversion from evergreen broadleaf forest to irrigated cropland (13–3) will lead to a maximum increase on the monthly average temperature, with 0.17 °C.

In conclusion, the effects of cultivated land reclamation on temperature vary between seasons. Meanwhile, the impacts of different cultivated land reclamation types on temperature are also different; this is because different types of cultivated land reclamation will lead to different changes in vegetation types and farmland management modes, which will result in changes of latent heat flux and sensible heat flux, and thus lead to different effects.

7.1.3 Concluding Remarks on Land Reclamation in India

After testing and verifying the WRF model in simulating the temperature of India, we updated the land cover data, and simulated the possible impacts of cultivated land reclamation on the temperature in India. India is with vast cultivated land reclaimed for agricultural production; there is, however, still a trend of reclamation of cultivated land in the future since the population growth. The area of LUCC due to the reclamation of cultivated land is projected to reach 1.16 million km^2, among which includes around 584.33 thousand km^2 of converted area from the dryland cropland to the irrigated cropland as well as nearly 560.12 thousand km^2 of converted area from other land use types into irrigated cropland, accounting for 50.23 and 48.15 % of the total conversion area, respectively. The proportion of cultivated land and pasture in the study area will increase from 73.03 to 85.28 %.

The land reclamation will increase the latent heat flux and decrease the sensible heat flux, which may be the reason for the downward trend of the monthly average temperature in India on the whole. Specifically, it mainly decreases the temperature in summer, while increases the temperature in the winter. Besides, the reclamation of cultivated land influences not only the local climate, but also the regional climate in the neighboring districts.

This study is still preliminary and there are still some uncertainties to be further mitigated in simulating the climatic effects of the LUCC. For example, there are many factors influencing the regional climate and they generally act synthetically,

such as other land use and land cover changes and atmospheric circulations. Besides, the reclamation of cultivated land in India also influences many other climatic indicators, such as precipitation and runoff, only some of which have been taken into account in this study. There may be some uncertainties and interactions between these indicators and it is necessary to complement the sensitivity analysis in the forthcoming researches.

7.2 Possible Impacts of Boreal Deforestation on the Near-Surface Temperature in the European Russia

There have been many researches focusing on the impacts of the high-latitude boreal deforestation on climate change. As boreal forest is the largest continuous terrestrial ecosystem in the world, boreal forest has the potential to influence the climate by altering the radiation budget. Bonan (2008) found that loss of boreal forests provided a positive feedback for glaciation, whereas boreal forest expansion during the mid-Holocene amplified warming. Bathiany et al. (2010) identified that in the future 100 years, the deforestation at the northern latitudes (45–90°N) will lead a decrease of 0.25 °C in global annual mean temperature, while the afforestation had equally large warming effects combining both biochemical and biophysical effects. And through latitude-specific large-scale deforestation experiment, Bala et al. revealed that the difference of the global average temperature between the standard case without deforestation and the experiment with boreal deforestation at high latitude in year 2100 is −0.8 °C (Bala et al. 2007). Based on observations, Lee et al. found that for the site pairs at 45°N, the mean annual temperature difference induced by deforestation is 0.85 ± 0.44 °C (± mean standard deviation) (Lee et al. 2011). Overall, most researches identified that at higher latitudes, boreal deforestation will results in cooling effects due to that the boreal forests with lower albedo being replaced by other types of vegetation with higher albedo, such as crops and grasslands. (Pielke et al. 2002). Boreal deforestation will lead to a large increase in albedo especially in winter (Lawrence and Chase 2010), Also boreal deforestation can alter surface heat balance by altering evaporative heat transfer caused by evapotranspiration from vegetation, and by changes in surface roughness(Ellis and Pontius 2007).

European Russia with high coverage of boreal forest has gone through intensive human activities. The largest part of the boreal forests is located in Russia, and about half of the boreal forests are still primary, with very limited impacts from forestry and other human activities. While the most intensely managed part of the boreal forest is in Scandinavia and western Russia (European Russia), where only patches of old-growth forests remain in reserves. Some researchers have showed that European Russia has experienced fluctuant forest cover change. Baumann

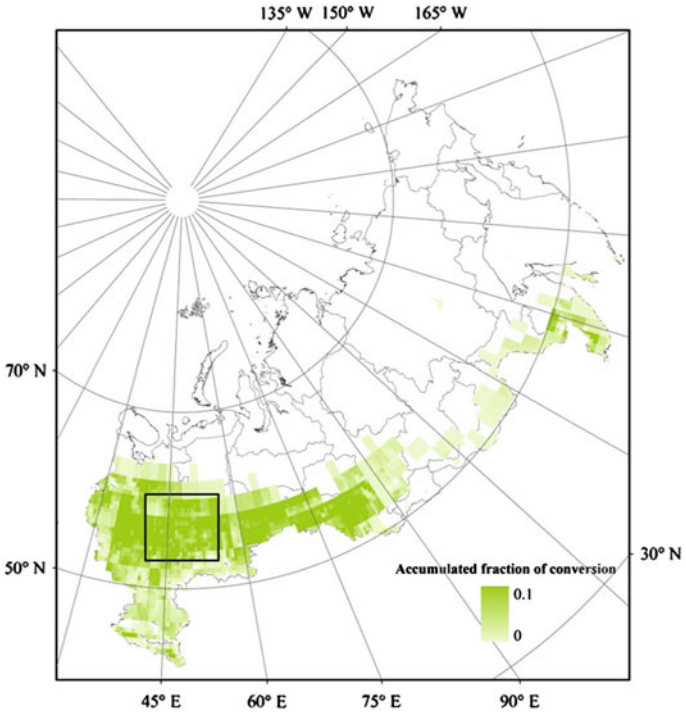

Fig. 7.5 Accumulated fraction of conversion from forests to croplands between 2000 and 2100 in the study area. The *black* box is the boundary of the study area

et al. found that the temperate forests in European Russia underwent substantial change during 1990–2010, with a decrease rate of 1 % in total area between 1990 and 1995 and an increase rate of 1.4 % between 2005 and 2010, which may be caused by the logging and afforestation on abandoned croplands (Baumann et al. 2012). Hansen et al. reported that Russia has the third largest area of gross forest cover loss. Russia's forest loss is geographically widespread due to deforestation in the European and far-eastern parts of the country and forest fires throughout Siberia (Hansen et al. 2010). Potapov et al. (2011) indicated that the forest cover is central part of European Russia was between 16 and 50 % (average forest cover of 36 %). The low forest cover within these regions is a result of a long history of conversion from forests to croplands.

Thus, the European Russia where has experienced fluctuant land cover change and serious forest loss due to the intensive human activities is selected as a typical area to detect the impacts of deforestation on the near-surface temperature (Fig. 7.5).

7.2.1 Data and Methodology

7.2.1.1 Data Processing

The data used in this study include land cover data, climate forcing data, and meteorological observation data. In this study, the 1 km × 1 km resolution land cover data of the USGS classification system in year 2000 derived from USGS Land Cover Institute, including 24 land cover types, were used as the baseline data. The land cover data of year 2010 and 2100 were predicted with the data of land conversion data, which were derived from the Asia-Pacific Integrated Model with the global economy model (AIM/CGE) based on RCPs 6.0 scenario. In the AIM/CGE model, land resource was treated as a production factor for agriculture, livestock, forestry, and biomass energy production. Urban land area expanded due to the population and economic growth, while the cropland area expanded for meeting the increasing food demand. The land cover data and underlying land surface change data during 1500–2100 can be obtained through data fusion at 0.5° × 0.5° resolution (Hurtt et al. 2011).

As there is difference in the spatial resolution and classification system between the land cover data of the USGS classification system and the RCP-based land conversion data, it is necessary to project the future land use and land cover data and upscale it to a higher resolution (1–10 km) as the requirement of WRF model. As it is well acknowledged that regional climate models (RCMs) with spatial resolution at or coarser than 30 km are unable to produce accurate climate forecasts (Jin and Miller 2007). Higher resolution allowed the model to feature the regional geophysical conditions and predict the regional climate with more accuracy. For example, WRF simulations can be done at a resolution of 4 km, which allows many small scale features, such as mountains and coastlines, for our purposes (Mawalagedara and Oglesby 2012). In this study, we set the resolution of the land cover data to be 5 km × 5 km in WRF model. Taking the processing of land cover data of year 2100 as an example, first, the accumulated fraction of different kinds of land conversion in each 0.5° × 0.5° grid from 2000 to 2100 was calculated (Fig. 7.5). Then the dominant conversion type (with maxima conversion amount) of each grid cell could be identified, and thereafter whether the land cover type of grids changed or not was identified through setting threshold value of the conversion rate. The threshold values were mainly set to reveal the conversion trend, as to each type of conversion, the threshold value was set to be the 50^{th} percentile of the conversion rate. The land cover data in year 2010 and 2100 were further obtained from the land cover data of the USGS classification in year 2000 and the land conversion data during 2000–2010 and 2000–2100. Finally the underlying land surface data were transformed to grid data of 5 km × 5 km through resampling.

Model output of RCP 6.0, such as air temperature, specific humidity, sea level pressure, eastward wind, northward wind, and geopotential height from 2000 to 2100 were used as the atmospheric forcing dataset in the WRF model. In addition,

Table 7.4 Parameterization scheme of physical processes in the model

Classification of schemes	Scheme option
Microphysics parameterization scheme	Bulk microphysics schemes introduced by Lin et al.(1983)
Cumulus parameterization scheme	Grell-Devenyi ensemble
Boundary layer process scheme	YSU
Long-wave radiation scheme	CAM Long-wave radiation
Shortwave radiation scheme	CAM Shortwave radiation
Land surface process scheme	Noah land surface model

the meteorological observation data, which were used to validate the WRF model in this study, were collected from European Climate Assessment & Dataset.[1]

7.2.1.2 Scenario-Based Experiment Design

The Advanced Research WRF (ARW-WRF) is used in this study. The Lambert projection is used, with the two standard parallels both being 57° N, central meridian 48° E. The study area is located in European Russia, and it contains 192 grid cells in the east-west direction and 174 grid cells in the north-south direction.

The parameterization scheme of physical processes in the model (Table 7.4) is as follows. The Microphysics parameterization Scheme adopted the scheme introduced by Lin et al. (1983). The cumulus parameterization scheme adopted the Grell-Devenyi ensemble scheme. The boundary layer process scheme was followed the scheme of Yonsei University (YSU). The long-wave radiation scheme and shortwave radiation scheme were both the Community Atmosphere Model (CAM) scheme, and the land surface process scheme was Noah land surface model. The boundary buffer was set to be four layers of grid points, and the boundary conditions adopted the relaxation scheme. The time interval of the model integration was set to be 5 min, and that of the radiation process and cumulus convection was 30 and 5 min, respectively. There were 27 layers in the vertical direction, and the atmospheric pressure at the top layer was 50 hPa.

The experiment design in this study is as follows (Table 7.5). The simulation was implemented with the land cover data in three separated years as the land surface. The land cover data of the year 2000 (Fig. 7.6) with the USGS classification system was used in the baseline scenario, while the land cover data of year 2010 and 2100 were used in the sensitivity tests. The monthly and seasonal simulation results were compared. Firstly, the simulation results of monthly temperature in year 2010 was used to validate the WRF model, then spatial difference of the near-surface temperature in the winter between 2000 and 2010 were analyzed, and at last the monthly near-surface temperature between 2010 and 2100 was compared.

[1] For more information, please refer to http://eca.knmi.nl/dailydata/predefinedseries.php.

Table 7.5 Design of the simulation scheme

Simulation	Period of forcing data	Land cover data used in WRF model
Control simulation: Year 2000 as the baseline year	2000	Land cover data of year 2000
Sensitivity simulation I: Year 2010	2010	Land cover data of year 2010
Sensitivity simulation II: Year 2100	2100	Land cover data of year 2100

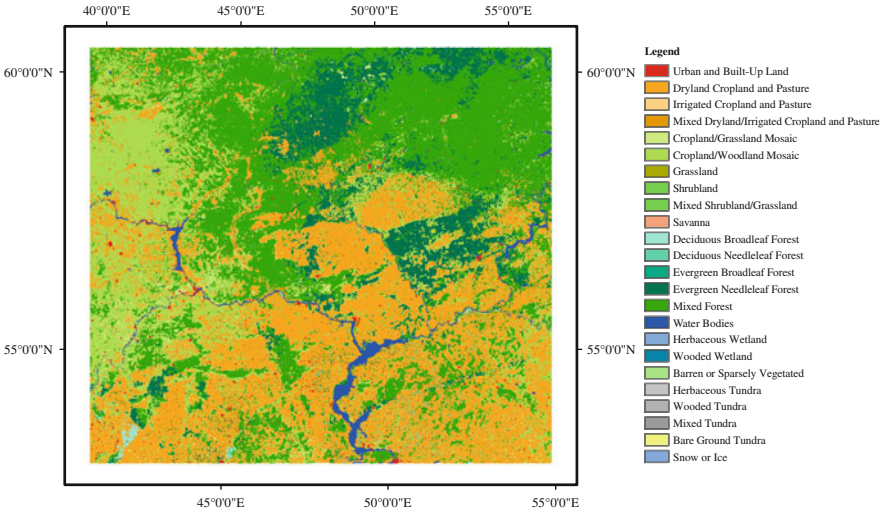

Fig. 7.6 Land cover of the study area in year 2000

7.2.1.3 Land Cover Change in the Study Area of European Russia

The main land cover types in the study area are the croplands (four types of cropland in USGS classification, with "Dryland Cropland and Pasture" (DCP) and "Cropland Woodland Mosaics" (CWM) dominating) and forests (four types of forest in USGS classification, with "Evergreen Needleleaf Forest" (ENF) and "Mixed Forest" (MF) dominating), accounting for about 53 and 44 % of the total land area, respectively. The land conversion types in the region are mainly dominated by the conversions between croplands and forests.

From 2000 to 2010, the land cover conversion is dominated by the conversion from croplands to forests (mainly from CWM type to MF in the northern part of the study area) and conversion from forests to croplands (mainly from MF to DCP in the southern part of the study area) in different parts of the study area. Statistics analysis shows that the grids dominated by the conversion from croplands to forests account for 26.18 % of all the grids in the study area, and grids dominated by the conversion from forests to croplands accounts for 27.80 % of all the grids.

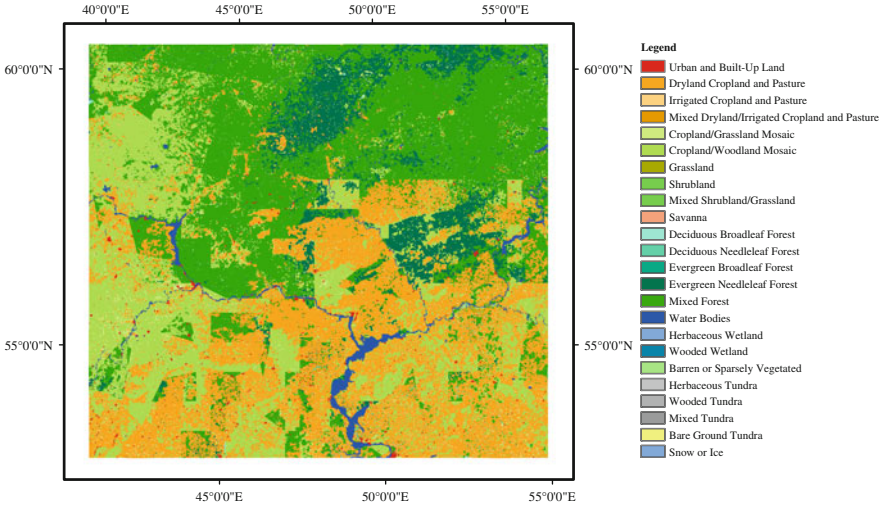

Fig. 7.7 Land cover of the study area in year 2010

Totally, the forests coverage in the study area will decrease from 44.40 to 44.07 %, while that of the croplands will increase from 53.04 to 53.37 %. The conversion between the forests and croplands will be in balance during 2000–2010. However, the spatial heterogeneity of the land conversion will redistribute the land cover types. For example, the croplands in the northern part of study area have a tendency to be converted to forests, while the scattered forests in the southern part tend to be converted to croplands (Fig. 7.7).

By 2100, the conversion from forests to croplands will dominate in the study area. The grids presenting the conversion from forests to croplands will account for 37.4 % of all the grids. Then the croplands coverage will go up to 72.27 % of the total land area, while the forests coverage will decrease to 25.31 % (Fig. 7.8). It indicates that there is a strong tendency of conversion from forests to croplands in this region in the future 100 years.

The coverage percentage of different land cover type in year 2000, 2010, and 2100 which were calculated based on the amount of grids of each land cover type are shown in Table 7.6.

7.2.1.4 Validation of the Simulation Result

As shown in Fig. 7.9, the change trends of both simulated and observed monthly average temperature in the study area were relatively similar, and the difference between the observed and simulated values generally fluctuates around zero. To examine whether the difference was significant or not, a paired *T*-test was conducted to test the difference between simulated values and observed values. The

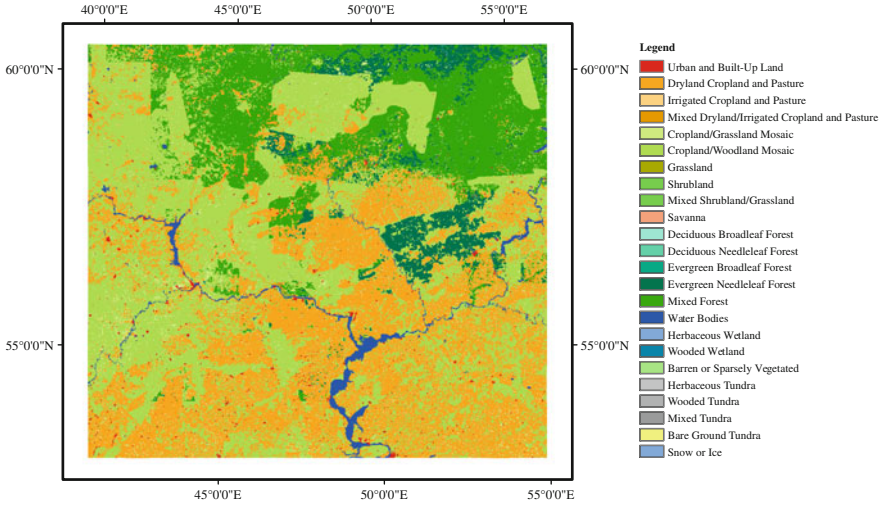

Fig. 7.8 Land cover of the study area in year 2100

null hypothesis was that there was no significant difference between those two samples, and the *P* value of the paired *T*-test was 0.91 at the significance level of 0.05, which indicated that there was no significant difference between the simulated values and observations. Thus, the WRF model has the ability to simulate the temperature change.

7.2.2 Results

7.2.2.1 Analysis of Temperature Change

As a result of the land conversion during 2000–2010, the simulated monthly average temperature during the winter (December, January, and February) increased in most part of the study area compared with that in year 2000 (Fig. 7.10). The spatial pattern of the temperature change during winter is highly related to the land cover and land cover change. The average temperature in the winter generally increased in the regions where mainly covered by croplands or where the boreal forest expands. In the southern part of the study area, which was mainly covered by dryland cropland, the forests were converted into croplands; consequently the temperature increment was relatively higher. The average temperature increment generally declines as the distance to forested regions decreases. In general, the land cover change in the study area is almost in balance from 2000 to 2010, there was very slight change of the average temperature in the winter (no more than 0.023 °C/year), and the spatial distribution of temperature change corresponds to land use and land cover change.

Table 7.6 Coverage percentage of various land cover type (%)

USGS land cover classification	Coverage percentage		
	2000	2010	2100
1 Urban	0.65	0.59	0.62
2 Dryland cropland and pasture	31.07	28.59	32.21
3 Irrigated cropland and pasture	0.00	0.00	0.00
5 Cropland/Grassland mosaic	1.07	0.78	1.01
6 Crop/woodland mosaic	20.90	24.00	39.05
Sum of Cropland	**53.04**	**53.37**	**72.27**
7 Grassland	0.18	0.12	0.03
8 Shrub land	0.01	0.01	0.01
10 Savanna	0.12	0.07	0.00
11 Deciduous broadleaf forest	0.24	0.06	0.01
12 Deciduous broadleaf forest	0.27	0.13	0.02
14 Evergreen needleleaf forest	9.87	8.54	6.76
15 Mixed forest	33.85	35.33	18.51
16 Water bodies	1.74	1.74	1.74
Sum of forests	**44.22**	**44.07**	**25.30**
18 Wooded Wetland	0.00	0.00	0.00
19 Barren or sparsely vegetated	0.02	0.02	0.01
21 Wooded tundra	0.00	0.00	0.00
22 Mixed tundra	0.01	0.01	0.01
Total	100	100	100

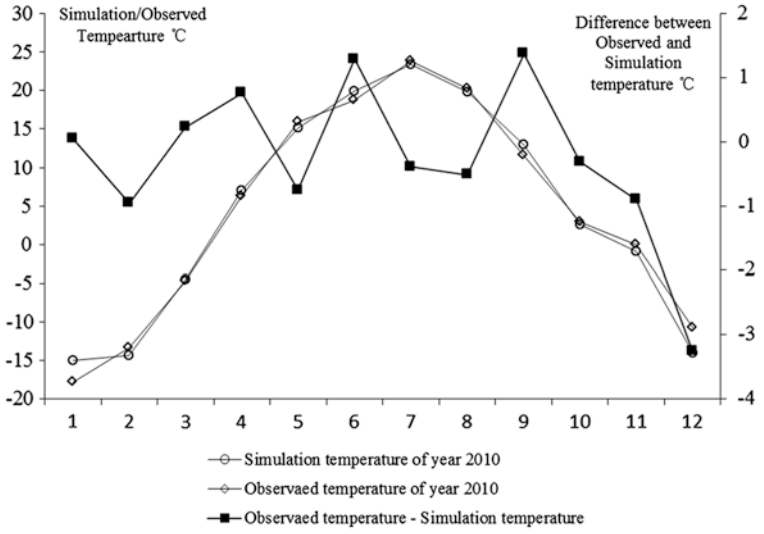

Fig. 7.9 Comparison of simulated and observed values of the monthly average near-surface temperature at 2 meters above the ground of the study area

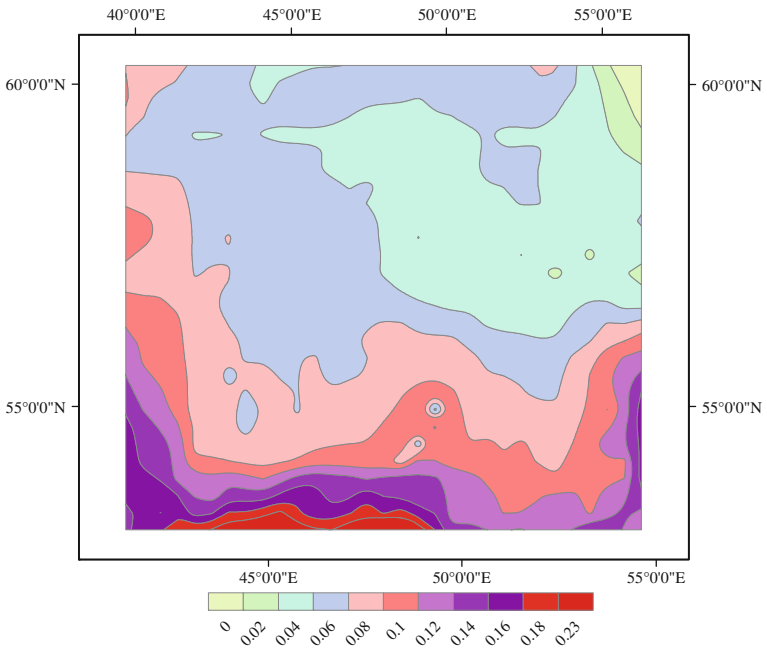

Fig. 7.10 Difference of simulated monthly average temperature in the winter between year 2000 and 2010 (°C) in the study area

The land cover change in the study area in year 2100 is mainly characterized by the conversion from forests to croplands, and it will lead to change of the near-surface temperature. The annual temperature will decline, while the monthly average temperature will increase from February to June and decrease from July to January (Fig. 7.11). In the boreal forest region, the temperature change mainly results from the change of albedo due to snow masking (Bathiany et al. 2010). As snow covers the surface and boreal forests are converted to croplands, the albedo of the land surface will increase and the net surface solar radiation will reduce, thus leading to the cooling effect, which offsets the warming effect due to the decrease of evaporation-transpiration. Therefore, near-surface temperature during the winter will change most intensively, decreasing by 1.81 °C on average. In the northern hemisphere, solar radiation begins to strengthen in June, and becomes the strongest around July and August. The conifer forests (needle-leaf forests) have lower evapotranspiration rate (defined as ratio of latent heat flux to available energy) than the deciduous broadleaf forests in the summer, which can lead to the higher rates of sensible heat flux(Bonan 2008). From 2010 to 2100, most Evergreen Needleleaf forests will be converted to croplands, and thus the cooling effect due to the albedo increase is also stronger than the warming effect due to the decrease of evapo-transpiration in the previous needle-leaf forest area during July and August, and consequently makes the average temperature decrease by 0.30 °C. While in the

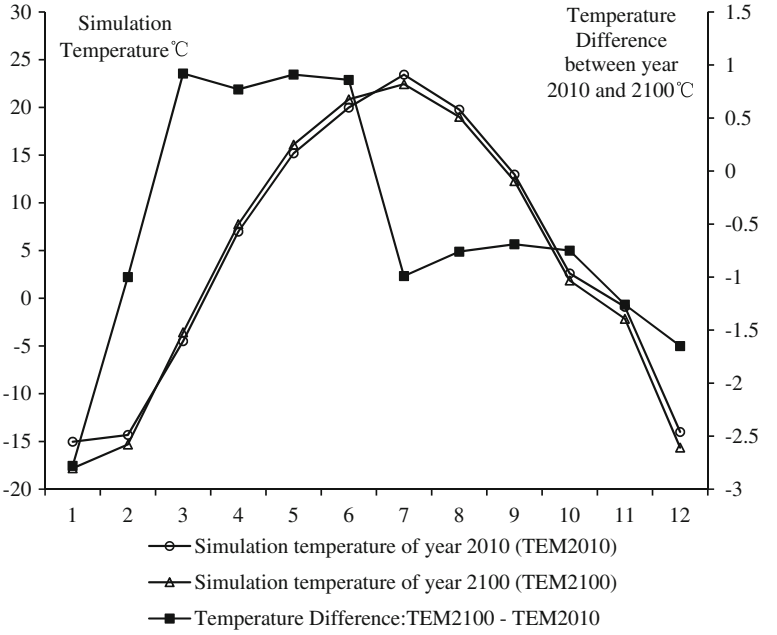

Fig. 7.11 Comparison of simulated monthly average temperature at 2 m above the ground in year 2010 and year 2100 in the study area

spring, snow will melt and the solar radiation is not very high, the warming effect due to the evapotranspiration reduction of evergreen needle-forests cannot be offset by the cooling effect due to the increase of surface albedo, and consequently the monthly average temperature will increase by 0.86°C in the spring. In general, the result indicated that the high albedo resulting from deforestation of boreal forests has negative impacts on the temperature, i.e., boreal deforestation will make the temperature decrease, especially during the snow season.

7.2.3 Concluding Remarks on Case Study of Boreal Deforestation in European Russia

The land cover change in the study area, which was mainly characterized by the conversion between boreal forests and croplands, will lead to significant change of the near-surface temperature, especially in the next century. It will make the regional near-surface temperature decrease by 0.58 °C in future 100 years (0.0058 °C/year on average) with the temperature change varies greatly in different seasons. The temperature changes most drastically in the winter, with an average decrease of 1.81 °C. And the temperature will decrease by 0.30 °C in the summer, while in the spring it will increase by 0.87 °C. The temperature change is

mainly due to the increase of surface albedo caused by boreal deforestation, which offset the warming effect due to evapotranspiration reduction.

The results of this study basically reveals the impacts of boreal deforestation on regional climate changes, but there are still some uncertainties about the influence of the future land cover change since only biogeophysical effects were taken into consideration, without considering the biochemical effects through some other key influencing factors, such as carbon emission. Since the impacts of land cover change are very complex, it is still necessary to carry out more in-depth researches on a series of issues, such as combination of biochemical and biophysical models, which take both the biogeophysical and biogeochemical processes into account. In addition, there are still some aspects that should be improved to better detect the impacts of deforestation on climate changes. First, it is still necessary to further explore the data assimilation methods to harmonize the data from different sources. Second, there are many factors that may influence the climate change, and it is necessary to do some sensitivity experiments to detect the main factors and minimize the uncertainties.

7.3 Potential Impacts of Future land Surface Changes on Regional Climate over the Brazilian Amazon

Forests, covering more than 30 % of terrestrial land (Deng et al. 2010), mainly comprise tropical, temperate, and boreal types from which provide invaluable ecological, socioeconomic, and mental public goods and services for humanity. Among these forest types, tropical forest occupies nearly 20 % of total forest land area, appropriates more than 30 % of net primary production (NPP) in the terrestrial ecosystem. This outstanding biomass can sequester a great deal of CO_2, maintaining above 25 % on land surface (Bonan 1997), which doubles or triples that of temperate and boreal forests (Malhi et al. 2008). Well-functioned tropical forests could effectively accelerate the evapotranspiration rate, cool the atmospheric temperature, and increase the rainfall. Some earlier experimental simulations in which the tropical forest was entirely replaced with less vegetated lands (Bonan 1997; Negri et al. 2004) suggested that these changes would induce slightly unstable in surface temperature, in comparison to the decrease of precipitation, evapotranspiration, and soil moisture. The tropical deforestation will also reduce the cloud cover caused by the increase of surface albedo and decrease of surface roughness. Though tropical forest could mitigate surface warming through considerable evaporative cooling effect, the temperature would increase if the surface albedo rose to a large extent induced by deforestation, which would offset the water and energy exchange feedback effects, compared with the reduction of convection and precipitation (Phillips et al. 2009). Therefore, no debate of this issue would be complete without taking the tropical forest as a significant component into account in climate change researches.

Table 7.7 The forest area and biomass stock in Brazil from 1990 to 2005

Categories		1990	2000	2005
Forest area (10^6 hectares)				
	Primary	460.51	433.22	415.89
	Modified natural	54.44	54.71	56.42
	Productive plantation	5.07	5.28	5.38
	Total	520.03	493.21	477.70
Biomass stock (10^3 million metric tonnes oven-dry weight)				
	Above ground biomass	86.09	82.68	79.22
	Below ground biomass	24.43	22.86	22.02
	Dead wood	6.88	6.56	6.36
	Total	117.40	112.10	107.60

Note This table shows a dramatic reduction in both forest quantity and quality. The data is obtained from the website of Food and Agriculture Organization of the United Nations, global forest resources assessment, 2005. For more information, please refer to http://www.fao.org/forestry/country/32185/en/bra/, http://www.fao.org/forestry/country/32183/en/bra/

The Amazonia tropical forest with an area of 6 million km^2, nearly 80 % of its original area, covers half of the global remaining tropical forests, and approximately 60 % is located in the Brazilian Amazon region. The annual average forest clearing rate in Brazil has accelerated during the period from 1994 to 2005 and showed a decreasing trend in recent years, increased from 1.3×10^4 km^2 in 1990–1994 to above 2.0×10^4 km^2 in the next two years, then slightly declined to 1.9×10^4 km^2 until 2005 and less than 0.7×10^4 km^2 in 2011 (Duchelle et al. 2013). Meantime, the quality of forest has also experienced a significant loss, which can be illustrated by the figures in Table 7.7. Given the massive ecological services in water maintaining and climate regulation, the annual average precipitation in Amazon reaches 2,500 mm, and it can discharge over a trillion m^3 of water into the ocean. Without these tropical forest featured by low albedo, great radiative forcing, and high evapotranspiration rate, the local residents should not have had such habitable zones with a cool and wet boundary (Werth and Avissar 2002). Although the tropical forests are an indispensable component of regional ecological system and humanity, anthropogenic activities have caused the shift of climatic states by disturbing and clearing the tropical forests (Ramos da Silva et al. 2008). This land surface change would destabilize regional climatic and hydrometerological variability (Baidya Roy and Avissar 2002), and then induce the climate anomalies, such as change in precipitation and temperature (Schneider et al. 2004).

Numerous researches have been conducted to assess the potential climatological changes of tropical deforestation in (Brazilian) Amazon using the global or regional climate models (Ke et al. 2012), and shared a common view that the vast tropical forest plays a pivotal role in changing climatic conditions. But these studies are lacking thorough and profound investigation due to the demerits of numerical models and data availability. As to the Global Climate Models (GCMs),

its rough resolution is inappropriate to reveal the land surface–atmosphere interactions for regional simulation cases. Importantly, it is worth pointing out that the entire Amazon forests have been entirely converted into less vegetated lands in terms of pasture, savanna, and cropland in the GCMs performances. Though this unrealistic assumption could help to understand the importance of tropical deforestation to regional and global climate changes as a whole, it is unable to help reveal the regional anthropogenic climate changes mechanism. In contrast, although the regional climate models (RCMs) with higher resolution are better at revealing the mesoscale effects of land surface changes on regional climate variability, the potential climate uncertainties induced by future land surface modification and vegetation alteration are still far from known.

Thus, the scientific objective of this case study is to estimate the potential impacts of future tropical deforestation on regional climate changes in Brazilian Amazon during 2090–2100 with WRF model performance. For this purpose, a relative rational underlying land surface with high resolution should be projected firstly. Given the observations and investigations showed that remarkable progress in curbing tropical forests recession has been made in recent years, the prevailing unreasonable land surface scenarios in which the entire forests are replaced with lower coverage vegetation would not be used in this part. We analyze the characteristics of forest land conversion between 2005 and 2100, and then the land surface map in particular years could be identified. Thereafter, the control and simulation experiments are designed for WRF modeling.

7.3.1 Data and Methodology

7.3.1.1 Data

The data used in this part include land surface data and lateral climate forcing data. The respectable land cover product, generated by the GCAM model under the state-of-the-art scenario (RCPs), is used to analyze the land cover conversions, such as the changing trend and the fraction, which is critical to project the future land surface properties (Hurtt et al. 2011). These data harmonized the historical land uses and the future land surface scenarios for studying the anthropogenic impacts and the annually fractional landscape patterns and land surface transitions for the period 1500–2100 at $0.5^{\circ} \times 0.5^{\circ}$ resolutions. For the purpose of this study, the forest land conversions during the period from 2005 to 2100 will be identified.

There are three steps to predict and generate the future land surface maps. Firstly, the fraction of transitioned cells that converted from the primary forest and the secondary forest into other land cover types, including cropland, pasture,

and built-up land, was calculated during 2005–2100. Then the transformation thresholds were set to identify the targeted grid cells with vast changed area. In this study, by considering the potential joint efforts to curb the deforestation in the future that may result in reaching the saturation point of forest clearing rate, we then set quite lower thresholds than current deforestation rate (0.7 %). The fraction thresholds of grid cells that converted from forest land to dryland cropland and pasture (pasture) and cropland/woodland mosaic (woodland) were 0.15 and 0.02, respectively, and the grid cells would be considered converting from forest to pasture if both thresholds were reached. Therefore, the conversion thresholds might have had influences on the future land surface projection. Finally, label and replace the initial land surface map in 2005, which is processed with USGS land cover classification at the resolution of 30 km × 30 km and will be used in the control experiment. By doing this, a relative reasonable future land surface in 2100 is generated as compared with that of most researches in which replacing the entire tropical forest with cropland or savanna vegetation types (Schneider et al. 2004). Thereafter, a rectangle region was selected as the study area covering the changed grid cells as many as possible (Fig. 7.12). High resolution with this grid size can also help to reveal the land-atmosphere interactions as well as the cumulus parameterization and weather. The climate forcing data is same as the data used in previous section (Sect. 7.2 boreal deforestation). The buffer zone of the lateral boundary is set to four layers of grid points. WRF model integrates at a 5-minute step, as well as the cumulus convection processes operation, but run the radiation process at a 0.5 hour step. Additionally, the observations of certain climate indicators in the year 2010 are collected for validation.

7.3.1.2 WRF Model and Experiments

The ARW-WRF is used in this study. To assess the model performance, the land cover data and meteorology data in 2010 is used to validate the WRF model. This model is set up with a grid of 63 × 49 cells, and each one representing a 30 km × 30 km area, centered at 5°S, 56°W.

For assessing the impacts of tropical deforestation on climate change, other variables are controlled but to modify the land surface and relative properties in the model schemes. To achieve this goal, two experiments are designed, including the control experiment and simulation experiment. In the control experiment, which is regarded as the reference case, the current land surface map in 2005 is used as the basic land cover data, maintaining constant in the whole simulation process. By contrast, the simulation experiment is designed with the implementation of project land surface map in 2100 in which certain numbers of grid cells are converted from the forests into dryland cropland and pasture (pasture) and cropland/woodland mosaic (woodland) (Fig. 7.12). This replacement will result in changing of corresponding biogeophysical parameters, such as root depth, canopy height, and other variables in WRF model. The climatic metrics in terms of

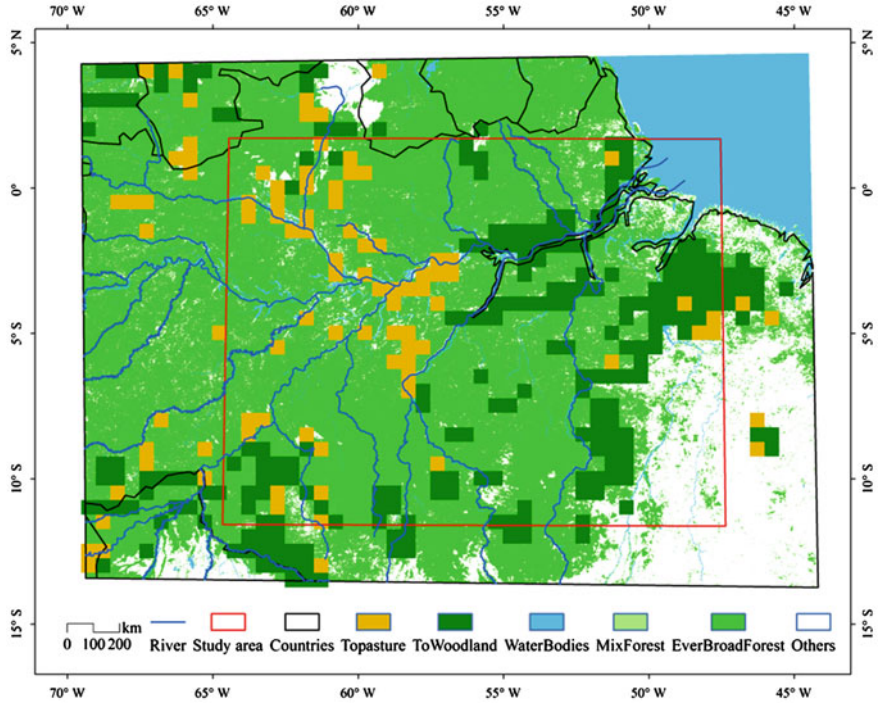

Fig. 7.12 The land surface properties in Brazilian Amazon. Only forests and water bodies are showed in the land cover layer (1 km × 1 km, USGS land cover classification). Grid cells in which forests are converted into the pasture (*yellow*) and woodland (*darkgreen*) are provided in the land surface change layer (0.5° × 0.5°). The study area (*red rectangle*) covers most changed forest land cells

sensible heat flux, latent heat flux, precipitation, and temperature in two experiments are simulated and processed into annual domain-averaged variables during the simulation period of 2090–2100.

7.3.2 Results and Discussion

7.3.2.1 Future land Surface Properties

In the Brazilian Amazon, the entire forest accounts for 78.07 % of the total area in the year 2005, totally contributed by the evergreen broadleaf forest. According to the statistical analysis, the projected deforested land occupies 18.23 % of the study area during the period from 2005 to 2100. The ratio of cells, in which forest is converted into pasture and woodland, to the total grid cells in the study area is 5.12 and 13.11 %, respectively. Specifically, the primary forest degrades by 13.36 % of

the study area, among which 32.04 % is converted into the pasture and 67.96 % is transitioned into the woodland. The secondary forest decreases by 4.33 % in the study area, among which 19.40 % is transitioned from forest into pasture and 80.60 % into the woodland. Furthermore, the proportions of each cell in which primary forest is converted to pasture and woodland range from 0 to 56.51 % and from 0 to 20.70 % separately from 2005 to 2100, in comparison to those of the secondary forest range from 0 to 37.70 % and from 0 to 15.31 %, respectively.

Figure 7.12 provides the geographical distribution of changed forest land. The degraded and transitioned grid cells primarily distribute in the periphery of the entire Amazon, or along the rivers. Particularly, most grid cells in which forests are converted into pasture are mainly located in the northwest part of the study area, where contains a great deal of water resource supplied by the dense water network. By contrast, the cells in which forest is converted into cropland are principally distributed in the most disturbed and populated area, especially the transition zones between forests and other land cover types.

7.3.2.2 Heat Fluxes

The yearly averaged sum of sensible and latent heat flux serves as an indicator for estimating the energy exchange between land surface and atmosphere during 2090–2100. Generally, based on the model analysis, deforestation will cause a reduction in surface heat flux with approximate 5 W/m^2 per month (Fig. 7.13). In the control simulation, the surface heat flux in the east is greater than that in the west, but the eastern area will see a decline in the deforestation simulation. This progressive decrease in the total heat flux illustrates the importance of increase in surface albedo and radiation caused by deforestation. Specifically, the annual average sensible heat flux will increase to some extent, especially in the west region covering most deforested areas during the period of 2090–2100, while the latent heat flux shows a significant downward trend in the same period. Such spatial gradient of heat flux will increase the convection by generating a thermally driven circulation, leading to rising of the sensible heat flux over the west part and falling over the east part, which will redistribute the temperatures.

7.3.2.3 Precipitation and Temperature

On the whole, the annual domain-averaged precipitation will decrease, while the temperature will increase during the simulation period. Deforestation in Brazilian Amazon will induce a monthly reduction in precipitation (1.05 mm) and a monthly increase in surface temperature (0.12 °C). The Fig. 7.13 also shows that the deforestation will cause a significant precipitation reduction in rainy season, but a slight decrease in dry season. Correspondingly, the surface temperature nearly increases to a large extent in rainy season and moderately goes up to a higher level in dry season.

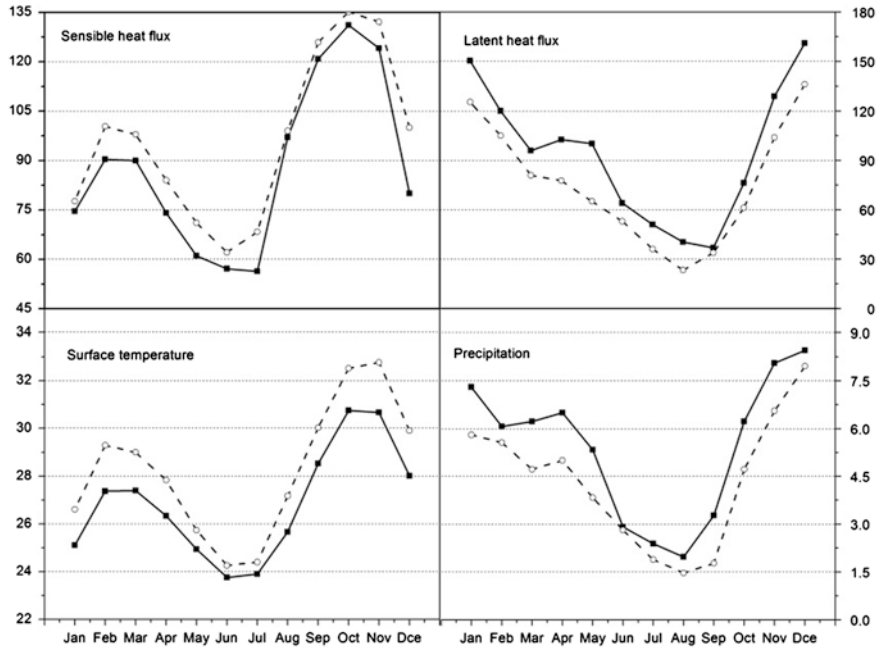

Fig. 7.13 Annual cycles' domain-averaged in the years 2090–2100 between 49 and 63°W and 12°S–2°N. All flux is in W/m^2, surface temperature in°C, precipitation in mm. *Solid line* is the control simulation, and the *dashed line* is deforestation simulation

The spatial distribution of differences in surface temperature between the control test and sensitivity test is significantly influenced by the forest land changes. Obviously, the surface temperature increases over the western region, associated with the reduction of precipitation and soil moisture that will reduce the latent heat flux discharge from the land surface into atmosphere. Massive deforested areas experience a significant increase of temperature and decrease of precipitation. In addition, deforestation will intensify the precipitation shift by increasing its amount in the southeast region and even further, and decreasing the precipitation in the northwest region (Fig. 7.14). The precipitation variability can be explained by that deforestation may influence the propagation of squall lines, which will reduce the water supply in these regions. Meanwhile, the convection and speed effects will also impose a negative feedback in these regions.

To study the spatial heterogeneity of these climatic metrics in longitude and latitude direction, the average surface temperature and precipitation in different zones were calculated (Fig. 7.14, down panels). Apparently, the surface temperature fluctuates dramatically in the western region and almost remains stable in the eastern part, which means that the surface temperature has a longitudinal distribution characteristic. Meanwhile, the zonally average temperature of north region increases most greatly by 0.0350 °C in year 2100 induced by deforestation, while

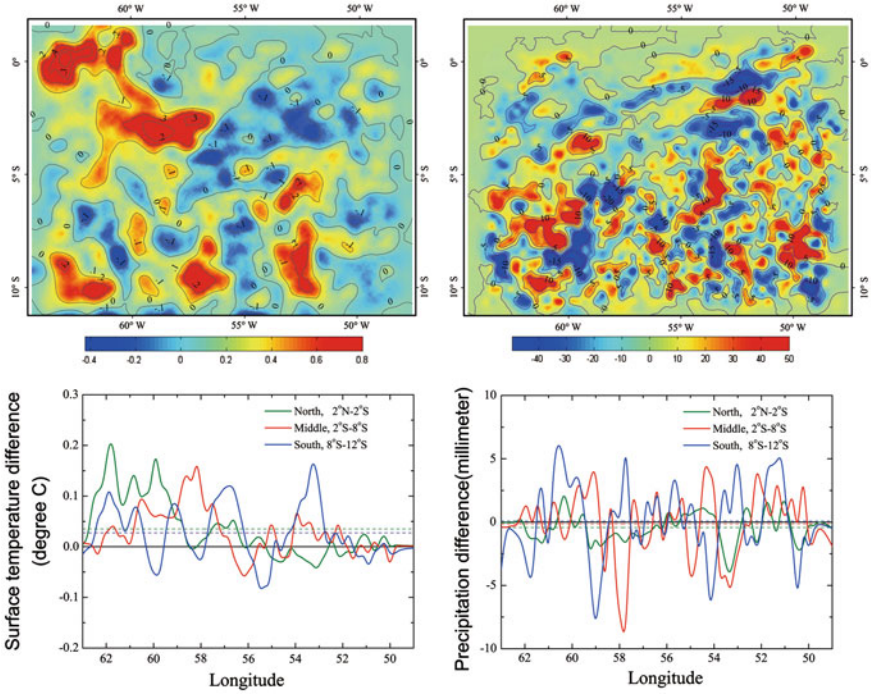

Fig. 7.14 The *top panels* show the yearly-averaged deviations of surface temperature (*top-left*) and precipitation (*top-right*) in the year 2100 (deforestation minus control). The surface temperature is contoured at a 0.2 °C interval, and the precipitation is contoured at a 5 mm interval. The *down panels* are zonally averaged surface temperature and precipitation differences (deforestation minus control). *Green line* indicates the north region between 2°N and 2°S of the Brazilian Amazon, *red line* is the central region between 2 and 8 °S, and blue line is the south region between 8 and 12 °S, the *dash lines* are averages of zonally surface temperature and precipitation

that of central region has a less increment of 0.0272 °C, as compared to that of south region with a similar growth by 0.0274 °C. For the precipitation, those of the central region and the southern region fluctuate more strongly than that of the northern region. The zonally annual average precipitation in northern region and central region will decrease by 0.433 and 0.147 mm, respectively, while it will slightly increase by 0.09 mm in the south region.

Variability of climate is also calculated on each land cover type according to the model results in 2100 with the resolution of 30 km × 30 km (Fig. 7.15). The statistical analysis indicates that the average precipitation and latent heat flux in the evergreen broadleaf forest area will experience a decrease of 0.15 mm and 0.40 W/m^2, respectively, while the temperature will increase by 0.02 °C. Since forests are converted into pasture and woodland, the corresponding climatic conditions in pasture will have a significant reduction of precipitation and latent heat flux, and increase of surface temperature. Unexpectedly, though the latent heat flux of cropland will drop at a significant level, the precipitation will grow to

some extent, as well as the temperature. This can be explained by that the flux and wind speed gradient will accelerate the convection and telecommunication in the study area, which will offset the negative effects of hydrometerological anomalies. Thus, the land cover structure, which means the area and continuity of each land cover type, will also rouse uncertainties to regional climate changes.

7.3.3 *Concluding Remarks on the Anthropogenic Tropical Forests Changes*

In this case study, WRF model is used to simulate the effects of future tropical deforestation on regional climate between 2090 and 2100 in Brazilian Amazon. High resolution land surface maps (30 km × 30 km) with USGS land use and land cover classification, projected from the respectable land surface product, are utilized in this model. Land surface changes are quite different from previous studies. Forests are mainly converted into pasture and woodland, distributed along the edge of the study area and river branches. The simulated climatic results caused by these potential future land surface changes show that expanding deforestation will principally trigger the reduction of precipitation and increase of surface temperature in the deforested area. The sum of sensible heat flux and latent heat flux tends to show a decline at the same period.

However, only the impacts of deforestation on climate are evaluated in this study. In fact, various intangible factors will impose a synthetic effect on regional and global biogeophysical and biogeochemical processes, which will influence the hydrological cycle and energy budget, and further result in the climate changes. Thus, the sensitivity analysis on other factors should be required in further studies.

7.4 Impacts of Future Grassland Changes on Surface Climate in Mongolia

Mongolia is located in the middle of Asia with bordering Russia to the north and the Inner Mongolia of China to the south, east, and west. It is the second-largest inland country all over the world with total area of 1.56 million km^2, ranking the 18th in the world. Much of the country's area (∼70 %) is covered by steppes (Fig. 7.16). Mongolia is located in the Mongolian Plateau. Most areas are mountainous region with eastern part comprising hills and plains, and the southern part is Gobi desert. Mongolia is far away from the coast and has obvious inland climate characteristics. There is a large difference of the daily and seasonal temperatures. The winter in Mongolia is cold and long and the summer is warm and short. According to the data from Mongolia Meteorological Administration from 1960 to 2006, the temperature is relatively low with annual average temperature of

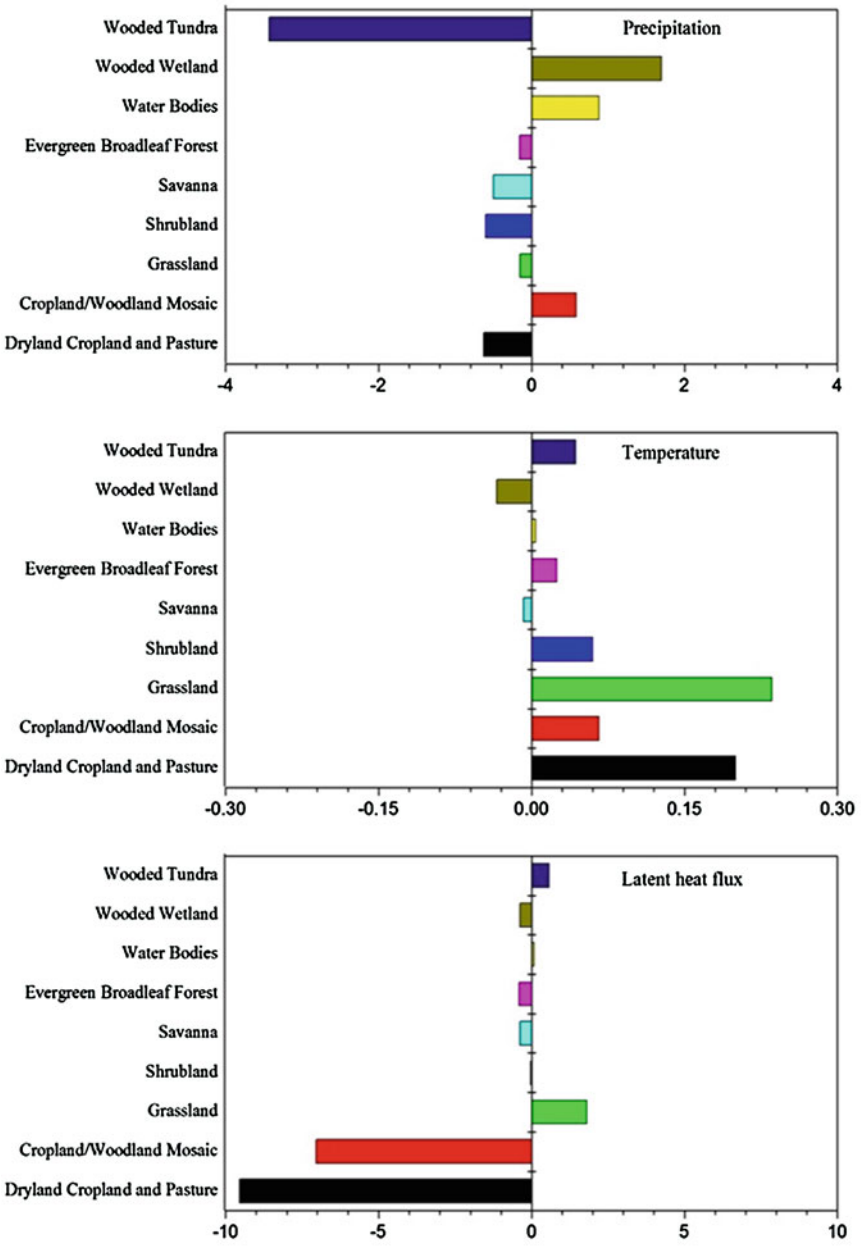

Fig. 7.15 The zonally averaged difference of precipitation (mm), temperature (°C) and latent heat flux (W/m^2) of different land covers in Brazilian Amazon in 2100

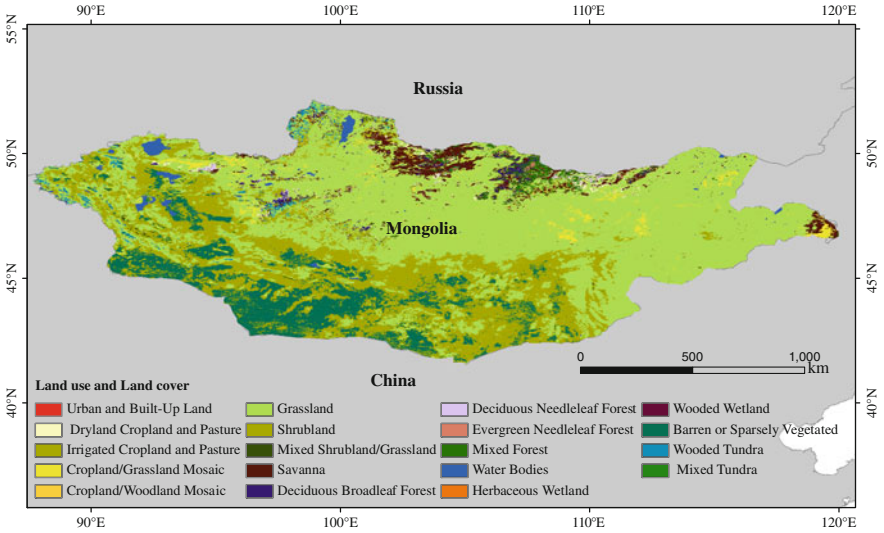

Fig. 7.16 Land use and Land cover of Mongolia in 1993

−5 °C or even much lower while it is 4 °C in the southern part of plain (Хауленбек 2009). The hottest month is July, the average temperature in the areas of Altai County, Bat-olzi County, and Batkhorob County reaches 10–15 °C. The temperature in Gobi desert and the eastern plains of Mongolia is more than 20 °C (Humphrey 1978). And average annual precipitation in Mongolia is 200–300 mm from 1980 to 2006 (Zhang et al. 2007; Хауленбек 2009). In recent 20 years, the global average temperature has risen by 0.74 °C, while average temperature of Mongolia rose from 1.5 to 2.5 °C, which is two or three times of the world average level (Yatagai and Yasunari 1994). Storm and drought are the two main nature disasters for the agriculture and animal husbandry production.

The pillar industry in Mongolia's national economy is always stock farming. Given approximately 30 % of the population is nomadic or semi-nomadic, grassland is quite important in Mongolia. Revealing the effects of grassland change on climate is of global importance in such a typical region. Its grassland is mainly divided into Forest Grassland, Typical Grassland, Mountain Grassland, Desert Grassland, and Desert. Since the 1960s, due to overgrazing, herds imbalance, the excessive use of pastures, and the effects of global warming, the decrement of species in Forest Grassland, Typical Grassland, Mountain Grassland, Desert Grassland, and Desert are 50, 44.73, 30.3, 23.8, and 26.7 %, respectively. The forage grass of high quality was gradually recessed or replaced by inferior plants (bushes, shrubs, etc.) (Barger et al. 2004). Many species of plants decreased greatly and forage quality declined year by year. From 1961 to 2006, the rates of pasture production in Forest Grassland, Typical Grassland, Mountain Grassland, Desert Grassland, and Desert declined by 40.54, 52.17, 39.28, 33.33, and 39.28 %, respectively (Хауленбек 2009). The above studies have shown that the

Mongolia's grassland degraded seriously, which may lead to the increase of carbon dioxide and other greenhouse gasses. Subsequently, it has driven the temperature rise in Mongolia and redistributed the precipitation, destabilized the natural ecosystems, and even threatened the human food supply and living environment.

7.4.1 Data and Methodology

7.4.1.1 Underlying Surface Data and Atmospheric Forcing Data

There are two types of input data in WRF model, the underlying land surface data and atmospheric forcing data. An advanced very high resolution radiometer (AVHRR) grid data with resolution of 1 km × 1 km of the United States Geological Survey's (USGS) classification system spanning a 12-month period (April 1992–March 1993, henceforth, 1993) is used as the baseline underlying surface data in this study. The predicted land conversion data with 0.5° × 0.5° resolution from 2010 to 2050 are developed by the Asia-Pacific Integrated Model (AIM) modeling team at the National Institute for Environmental Studies (NIES), Japan. This data is used to project the land surface data in the future utilized in the WRF model. To investigate the effects of future grassland degradation on climate, we only focused the grassland conversion of this data, though change information of all kinds of land use and land cover types are available. Supposing other types of land use changes are not considered in this research, the newly grassland conversion pixels derived from AIM (RCP 6.0) were overlaid to the land surface map in the baseline. Thereafter, both of these two major underlying land surface data were transformed to grid data with the resolution of 50 km × 50 km by resampling. Model outputs under RCP 6.0, such as air temperature, specific humidity, sea level pressure, eastward wind, northward wind, and geo-potential height from 2010 to 2050, were used as the atmospheric forcing dataset in the WRF model.

7.4.1.2 Experimental Design

WRF model based on the Eulerian mass solver was used to investigate the temperature and precipitation changes driven by future grassland degradation in this study. Two sets of tests (control test and simulation test) were designed, the land surface in the baseline and the predicted underlying land surface data were used in these two tests from 2010 to 2050, respectively. The effects of future grassland degradation on climate can be measured by the difference of these two series of simulated results.

$$R_i = C_i - S_i \tag{1}$$

where R is the effects of future grassland degradation on climate, refers to average annual and monthly temperatures and average annual and monthly precipitations, and C and S are the simulated results of WRF model with future projected land surface and the land surface in the baseline, respectively.

The effects of grassland degradation on temperature and precipitation for each period of 2010–2020 and 2040–2050 were simulated. Concretely, the temperature and precipitation of each period of 2010–2020 and 2040–2050 with basic land surface were modeled first, then those of 2010–2020 and 2040–2050 under the projected land surface data was simulated. Finally, the effects of future grassland degradation on climate were measured by the difference between these two series of simulated results. By doing this, it can also reduce the biases induced by other factors.

7.4.2 Results

7.4.2.1 Effects on the Annual Average Temperature

The simulated results show that there will be a upward trend of annual average temperature with an increment of 0.1–0.3 °C during 2010–2020 (Fig. 7.17). In addition, the temperature decreases gradually from west to east, and climbs up first, then declines progressively from north to south. The annual average temperature changes significantly by 0.3 °C in the northwest of Mongolia where grassland covers most. Only a small area near the sea in the northeast, the temperature falls by approximately 0.1 °C. Generally, the annual average temperature changes obviously in the most significant degraded areas, such as Alli county, Ada Chad's county, and Altay city. This indicates that the grassland degradation has a great influence on the local temperature change in Mongolia.

We also use the same method to simulate the effects of grassland degradation on the average annual temperature from 2040 to 2050. The simulated result shows that the annual average temperature will increase by 0.1–0.4 °C during 2040–2050 (Fig. 7.18). Compared with the simulated results of 2010–2020, the regions experienced increase of annual average temperature expanded significantly, and these regions are mainly distributed in northwestern and central regions of Mongolia. In this period, the annual average temperature increases by about 0.1 °C. Besides, the temperature decreases by almost 0.1 °C in some areas of southwestern and eastern regions of Mongolia.

7.4.2.2 Effects on the Annual Average Precipitation

The degradation of grassland leads to the significant change of the spatial pattern of the annual average precipitation in Mongolia. The simulated result during 2010–2020 indicates the annual average precipitation will decrease by more than

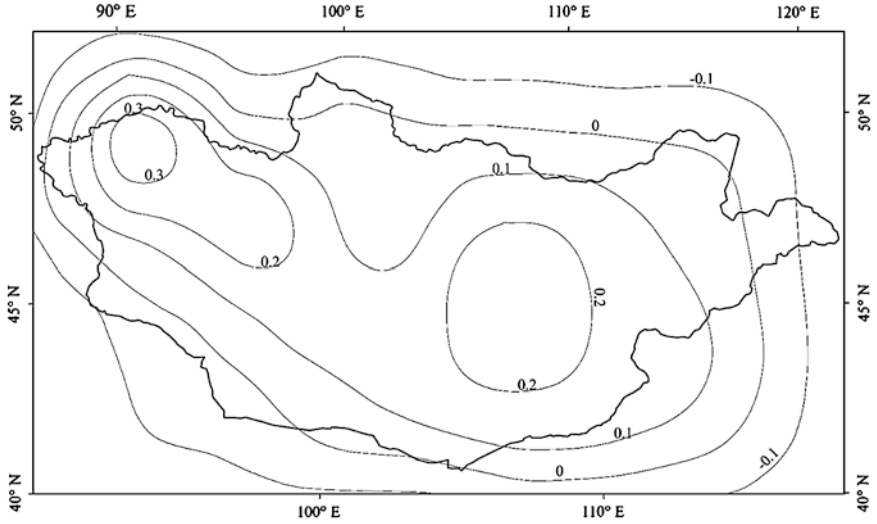

Fig. 7.17 Effects of future grassland degradation on average annual temperature between year 2010 and 2020 (measured in degree Celsius) in Mongolia

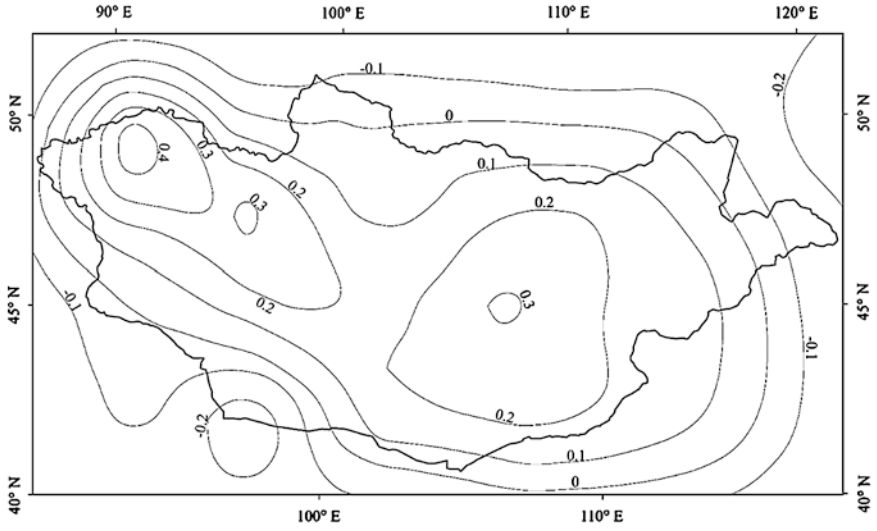

Fig. 7.18 Effects of future grassland degradation on average annual temperature between year 2040 and 2050 (measured in degree Celsius) in Mongolia

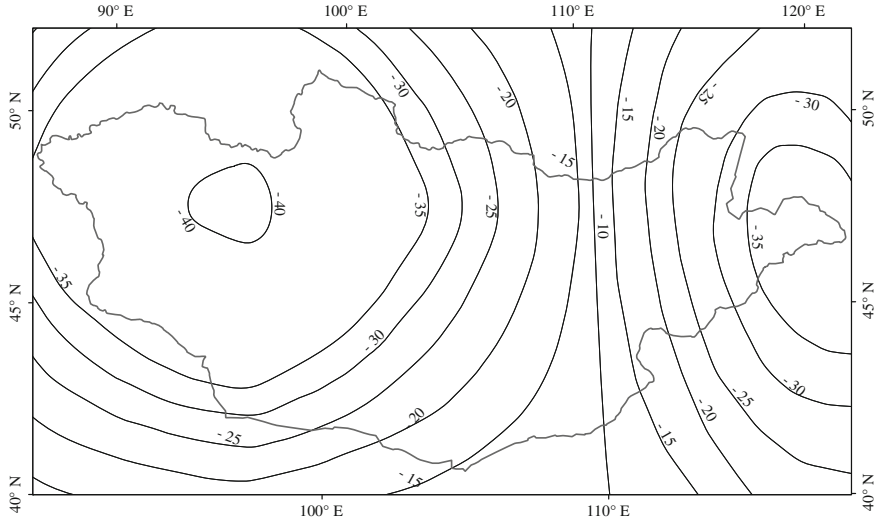

Fig. 7.19 Effects of future grassland degradation on average annual precipitation between year 2010 and 2020 (measured in millimeters) in Mongolia

40 mm in the northwestern and eastern parts of Mongolia (Fig. 7.19) and decrease by over 20 mm in the central part of Mongolia. Totally, the degradation of grassland will make the annual domain-averaged precipitation decrease by 25 mm.

In the future, the annual average precipitation will decrease by 15–50 mm during 2040–2050 caused by grassland degradation in most parts of Mongolia. Simulation results show that there is a downward tendency of annual average precipitation from the outside to the central areas, and the minimum average annual precipitation is 15 mm (Fig. 7.20). The annual average precipitation decreases obviously in the northwestern and eastern parts of Mongolia, while this change in the central part is relatively small. This result also illustrates that the precipitation variance is strongly related to the grassland degradation.

7.4.2.3 Effects on the Monthly Average Temperature and Precipitation

The impacts of grassland degradation on the monthly average temperature vary from month to month during 2010–2020 and 2040–2050 (Fig. 7.21). The simulated result indicates that the monthly average temperature in the above two periods are much similar and have obvious seasonal characteristics. Specifically, grassland degradation has a significant impact on the monthly temperature in Mongolia, the change scale of monthly average temperature are 0.025–0.075 °C. Compared with the results of control test, the monthly average temperature increases continuously, and the growth rate increases first and then decreases. The maximum change of monthly average temperature appears in July with 0.075 °C, while the minimum

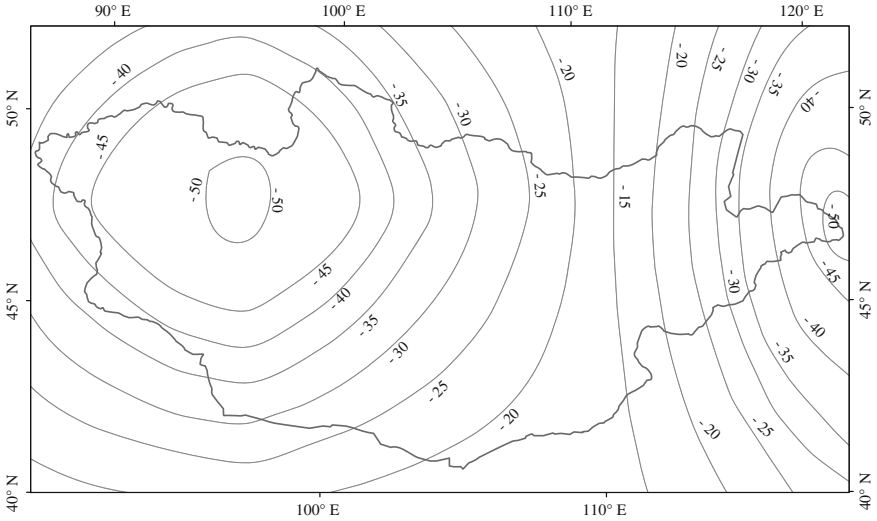

Fig. 7.20 Effects of future grassland degradation on average annual precipitation between year 2040 and 2050 (measured in millimeters) in Mongolia

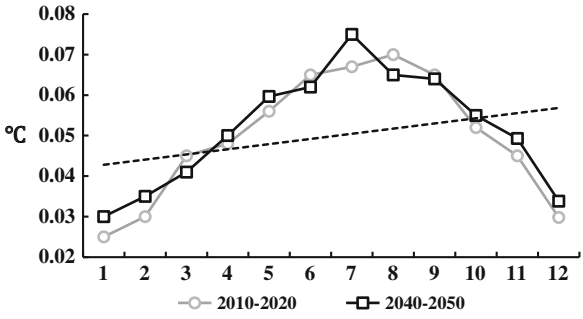

Fig. 7.21 Effects of future grassland degradation on average monthly temperature during two decades (measured in degree Celsius) in Mongolia

change occurs in December and January, the change scale being 0.025-0.03°C. The simulated result about monthly average temperature is further confirmed that the grassland degradation would lead to higher temperature.

The grassland occupies largely in Mongolia and decrease significantly from 1.3 million hectares to 0.9 million hectares from 1990s onward. Overall, the simulated results of the monthly average precipitation during 2010–2020 and 2040–2050 are quite similar. The precipitation in summer is significantly higher than in winter, and the range of monthly average precipitation variation is from –3 to 5 mm (Fig. 7.22). It can be seen clearly that precipitation changes obviously in June-August, the monthly average precipitation in the three months is 3–5 mm higher than that in the baseline year, while in the other months the monthly average precipitation is lower than that in the baseline.

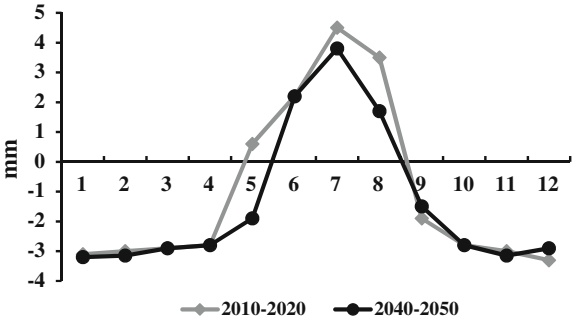

Fig. 7.22 Effects of future grassland degradation on average monthly precipitation during two decades (measured in millimeters) in Mongolia

7.4.3 Concluding Remarks on Grassland Degradation in Mongolia

This study analyzed the impacts of the grassland degradation on annual and monthly average temperature and precipitation climate change with the WRF model at the national levels in Mongolia.

Despite the spatial resolution of the data and simulation duration, the data are still reliable in assessing the impacts of the grassland degradation on the climate change. The results indicate that grassland degradation has an obvious effect on the regional temperature and precipitation in the next 40 years in Mongolia. Annual average temperature and precipitation change significantly from April to September, the maximum change appears in July. The difference between the simulation test and control test is regarded as the impacts of grassland degradation in Mongolia. The results show that the annual average temperature changes obviously in the northwest, southeast, and middle-east of Mongolia, approximately −0.1–0.4 °C, and about 70 % areas of Mongolia have experienced an increment in the annual average temperature with 0.1–0.3 °C. Besides, annual average precipitation change in Mongolia has also obviously regional and seasonal characteristics. Overall, there has been a falling trend of average annual precipitation change in most regions of Mongolia. The most significant changes occur in July and August, with 30–50 mm. Furthermore, the difference between the simulated test and control test showed that in July and August the monthly average temperature increase most obviously by 0.06–0.075 °C from 2010 to 2050. In winter the temperature rise is relatively slow, about 0.02–0.03 °C. The most significant change of monthly average precipitation appears in April and September, the change value is 2–5 mm.

In this study, we only consider the impact of grassland degradation on temperatures and precipitation, without reporting the energy balance, circulation, monsoon, and other climate factors. More importantly, there are still some other issues that need to be resolved in the further studies. Firstly, the climate effect could be caused by some other factors except for grassland degeneration, such as

solar activity and other human activities. Secondly, some uncertainties may hide behind the data processing, parameterization, and WRF model itself. Therefore, there is still further work to do in order to get more accurate assessment.

7.5 Impacts of Future Urban Expansion on Regional Climate in the Northeast Megalopolis, USA

Urban expansion is regarded as one of the most noticeable effects of human activities that cover a very small fraction of Earth's land surface, but notably affects climate. It usually removes and replaces crops and natural vegetation with non-evaporating and non-transpiring surfaces, such as metal, asphalt, and concrete (Basara et al. 2010).These artificial surfaces are characterized by specific thermal properties (albedo, thermal conductivity, and emissivity), which are different from those of nonurban areas (Weng et al. 2004).The alteration of regional thermal properties along with urban expansion will inevitably result in the redistribution of incoming solar radiation and affect the surface energy budgets (Zhang et al. 2009). Consequently, the wind velocity, mixing layer depth, and thermal structures in the boundary layer, as well as the local and regional atmospheric circulations are changed (Lei et al. 2008).

The primary objective of this study is to determine the influences of future urban expansion on regional climate at different temporal scales in developed megalopolis. The major contribution of this case study is that it will provide evidences for influences of future urban expansion on regional climate at the scale of megalopolis and helps to understand the integrated effects of combination and interaction of multiple cities and their surroundings.

7.5.1 Data and Methodology

7.5.1.1 Study Area

The Northeast megalopolis is the most populous and largely developed megalopolis of USA. It is constituted by a number of cities including Baltimore, Boston, Harrisburg, Newark, New York City, Philadelphia, Portland, Providence, Richmond, Springfield, Hartford, and Washington (Gottmann 1964). The megalopolis's population is expected to reach sixty million by 2025. This megalopolis is chosen as case study area because it is one of the most typical megalopolis globally, which can be regarded as the example of future megalopolis development.

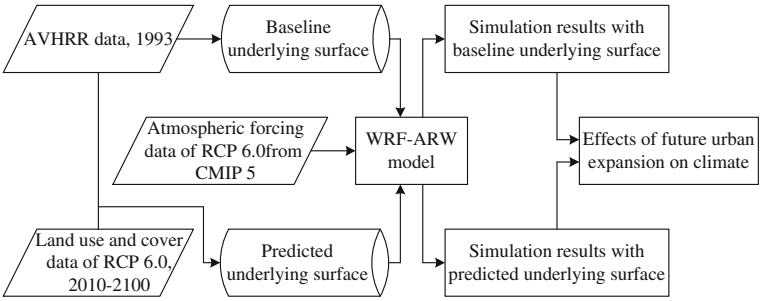

Fig. 7.23 Simulation scheme and data processing framework

7.5.1.2 Data and Process

An AVHRR grid data of 1 km × 1 km of the United States Geological Survey's (USGS) classification system spanning a 12 month period (April 1992–March1993, henceforth, 1993) is used as the baseline underlying surface data in this study (Fig. 7.21). And the predicted land use and land cover data of 0.5° × 0.5° from 2010 to 2100 are derived from the Asia-Pacific Integrated Model (AIM) modeling team at the National Institute for Environmental Studies (NIES), Japan. The reason that we choose RCP 6.0 is because it is a stabilization scenario where total radiative forcing is stabilized after 2100 without overshoot by employment of a range of technologies and strategies for reducing greenhouse gas emissions (Y. Hijioka 2008). Supposing other type of land use and cover remaining stable, the new urban area pixels derived from the AIM output of RCP 6.0 were overlaid to the map of baseline underlying surface. Consequently, two major underlying surface data, including the baseline underlying surface data directly derived from AVHRR data of 1993 and the predicted underlying surface data by overlaying the urban expansion information to the map of baseline underlying surface, were finally obtained (Fig. 7.23). Both of these two underlying surface data were transformed into grid data with a 50 km × 50 km resolution by resampling (Fig. 7.24). According to the AIM data, urban area in the Northeast megalopolis had expanded rapidly during the period 1993–2010 and would continue to expand during the period 2010–2100. Model output, such as air temperature, specific humidity, sea level pressure, eastward wind, northward wind, and geopotential height from 2010 to 2100 were used as the atmospheric forcing dataset of WRF-ARW model (Fig. 7.23).

7.5.1.3 Simulation Scheme

The WRF-ARW model based on the Eulerian mass solver is used in this study to investigate the temperature and precipitation change driven by future urban expansion in the study area. Simulation from 2010 to 2100 with a constant

underlying surface (the pattern of urban area as well as other land use and land cover types in the study area is fixed to that of 1993, namely, baseline underlying surface) was implemented first, whose results are regarded as references. The effects of future urban expansion on climate can be measured by the difference of the simulation results with predicted underlying surface and baseline underlying surface (Fig. 7.23).

$$E_i = R_i - r_i$$

where, i refers to average annual and monthly temperature, and average annual and monthly precipitation; E is the effects of future urban expansion on climate; and R and r are the simulation results of WRF-ARW model with predicted underlying surface and baseline underlying surface, respectively.

The average effects of urban expansion on temperature and precipitation for each period of 2010–2020, 2040–2050, and 2090–2100 were calculated. In the simulation of three periods, the baseline underlying surface data and predicted underlying surface data were used. Concretely, the temperature and precipitation of each period of 2010–2020, 2040–2050, and 2090–2100 with baseline underlying surface were obtained first. And then the simulation of temperature and precipitation of three periods of 2010–2020, 2040–2050, and 2090–2100, were continuously modeled by using the predicted underlying surface of 2010, 2040, and 2090, respectively. By doing this, the impacts of urban expansion can be estimated by the difference of each period, and it can also reduce the simulation bias induced by discontinuous simulation. The original simulation results were hourly and aggregated into average annual data and average monthly data.

7.5.2 Results and Discussion

7.5.2.1 Average Annual Temperature Effects

Figure 7.25 depicts the simulated effects of future urban expansion on average annual temperature in the Northeast megalopolis, USA. From the variation in average annual temperature change, it is shown that temperature will be locally and regionally affected by future urban expansion (Fig. 7.25). The largest change in average annual temperature will occur in the new urban area (expanded urban area during 1993–2100), which can be certainly referred to urban heat island (UHI) effects. The strongest UHI will lead to an increase of 5.73 °C in average annual temperature in some new urban area. And for most newly expanded urban areas, the average annual temperature will increase by 2–5 °C 1993 to the period of 2090–2100. The effects of future urban expansion on average annual temperature will be strengthened along with urban area increase. For instance, conversion

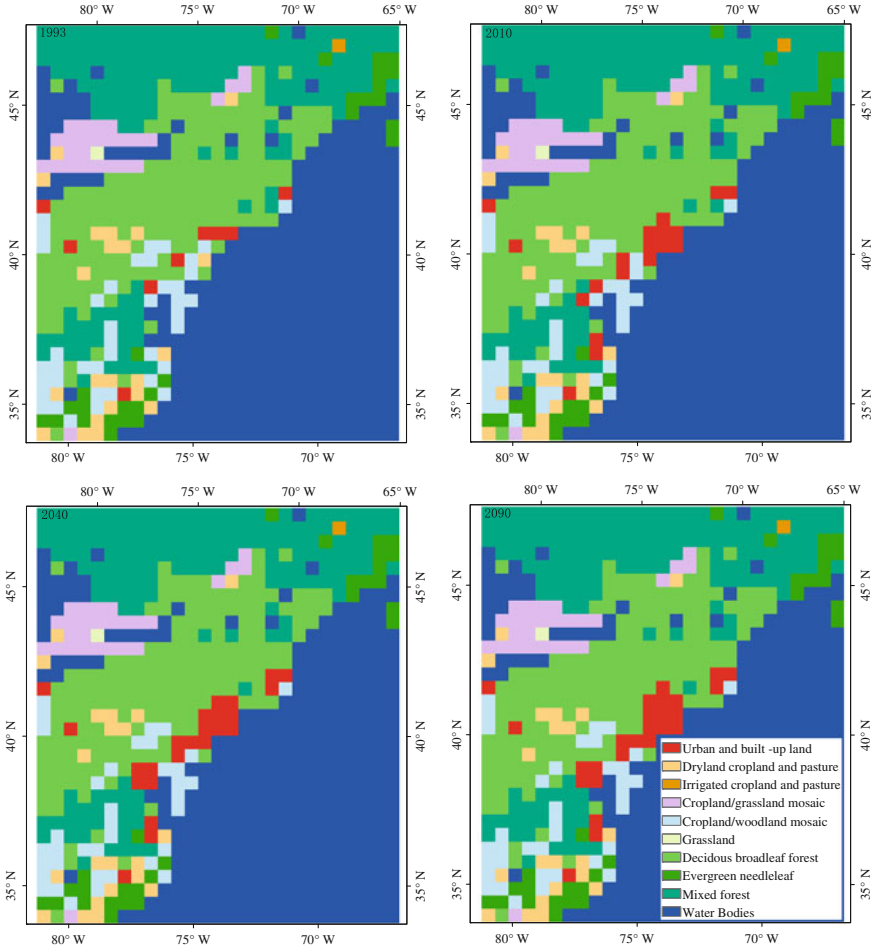

Fig. 7.24 Baseline underlying surface data (1993) and predicted underlying surface data (2010, 2040 and 2090) used in this study

from deciduous broadleaf forest to urban area will drive the average annual temperature of the pixel (39°59́N, 75°50́W) growing by 3.15, 3.53, and 3.76 °C in the period of 2010–2010, 2040–2050 and 2090–2100, respectively.

There will be some nonurban pixels experiencing average annual temperature decrease due to future urban expansion, while the annual average temperature of most nonurban areas will be steady. The significant annual average temperature decrease will mainly happen in the south of the Northeast megalopolis with mixed forest (Fig. 7.25). Statistics shows that this annual average temperature decrease will range from 0.40 to 1.20 °C. Consequently, the cooling effect in this area will

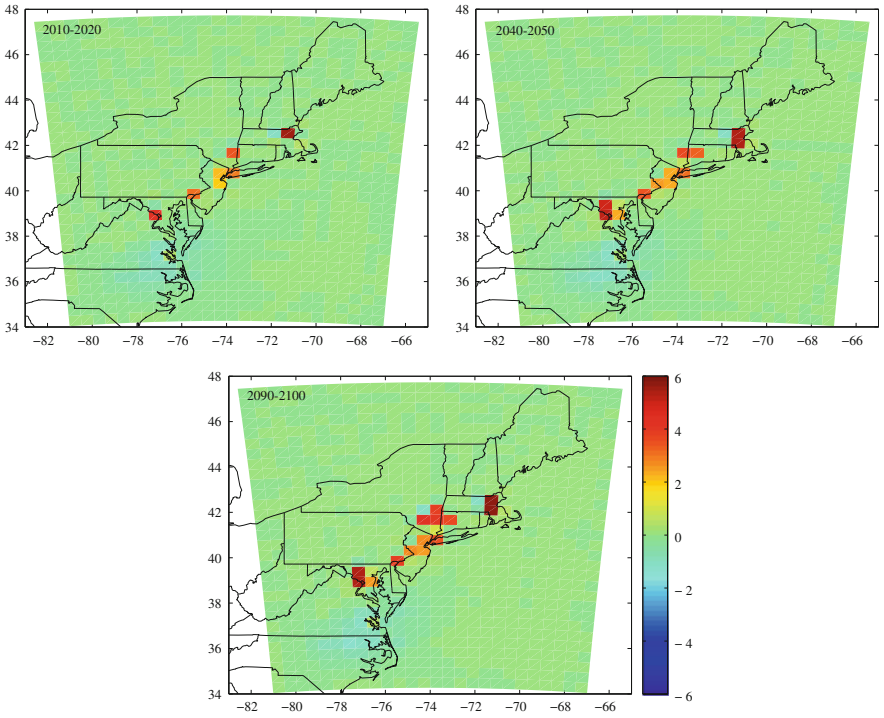

Fig. 7.25 Effects of future urban expansion on average annual temperature in the Northeast megalopolis, USA (°C)

be more and more notable along with the urban expansion. This may be caused by the strengthened UHI effect due to urban expansion, which will enhance the rising flow of urban area and reduce the inflow of cold wet air stream from the sea.

7.5.2.2 Average Annual Precipitation Effects

The urban expansion will mainly decrease the average annual precipitation. The spatial pattern of average annual precipitation change will be approximately opposite with that of average annual temperature change (Fig. 7.26). For some new urban area and nearby pixels, the average annual precipitation will decrease by 10–50 mm, while it will reduce by more than 100 mm for some pixels in the south region of the Northeast megalopolis. This reduction may be caused by changes in surface hydrology that extend beyond the UHI effect. There are lots of researches that argue urban expansion resulting in an increase of urban precipitation (Kleerekoper et al. 2012; Lin et al. 2008). However, our simulation showed that the impact of future urban expansion in Northeast megalopolis with mega cities on precipitation has different rules. This simulation result is consistent with

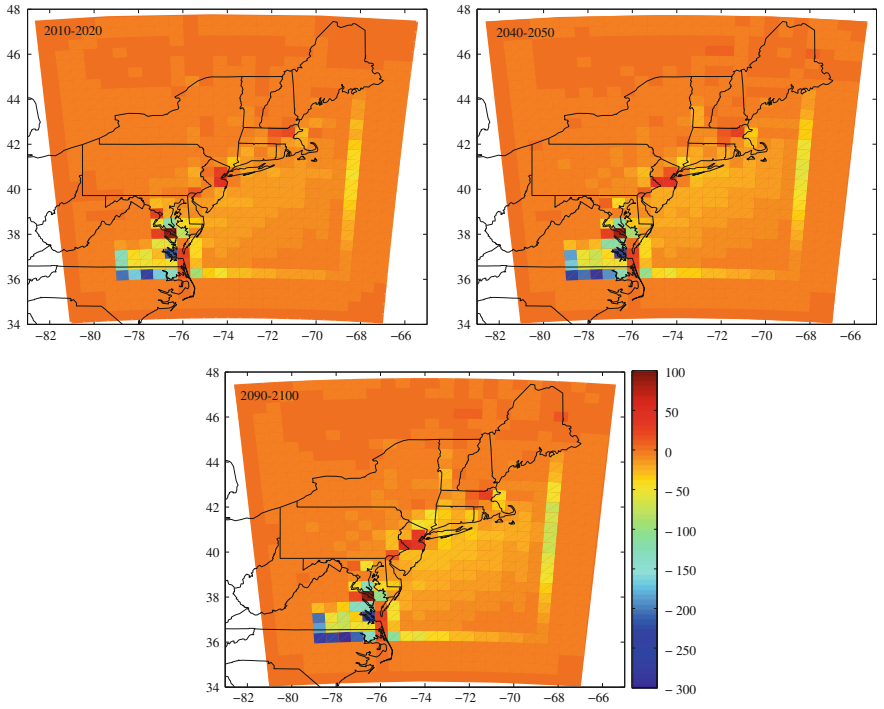

Fig. 7.26 Effects of future urban expansion on average annual precipitation in the Northeast megalopolis, USA (mm)

the findings of Guo et al. and Zhang et al., though their study area of Beijing is much smaller than ours on scale (Guo et al. 2006; Zhang et al. 2009). The urban expansion will produce less evaporation, higher surface temperatures, and larger sensible heat fluxes. This leads to less water vapor and hence less convective available potential energy. Combination of these factors induced by urban expansion contributes to regional precipitation reduction in general. Concretely, due to urban expansion in the Northeast megalopolis, the average annual precipitation of the simulation area will decrease by 5.75 mm, 7.10 mm, and 8.35 mm in the period of 2010–2010, 2040–2050, and 2090–2100, respectively.

7.5.2.3 Average Monthly Temperature Effects

Figure 7.27 depicts the monthly variation of average temperature change driven by future urban expansion. The urban expansion in the Northeast megalopolis will result in an average monthly temperature increase in original urban area (urban area in 1993) in April, May, June, July, and August and decrease in other months in the period of 2010–2020 (Fig. 7.27, Panel A). The cooling effect in winter may be caused by the local circulation change driven by surface energy budgets change.

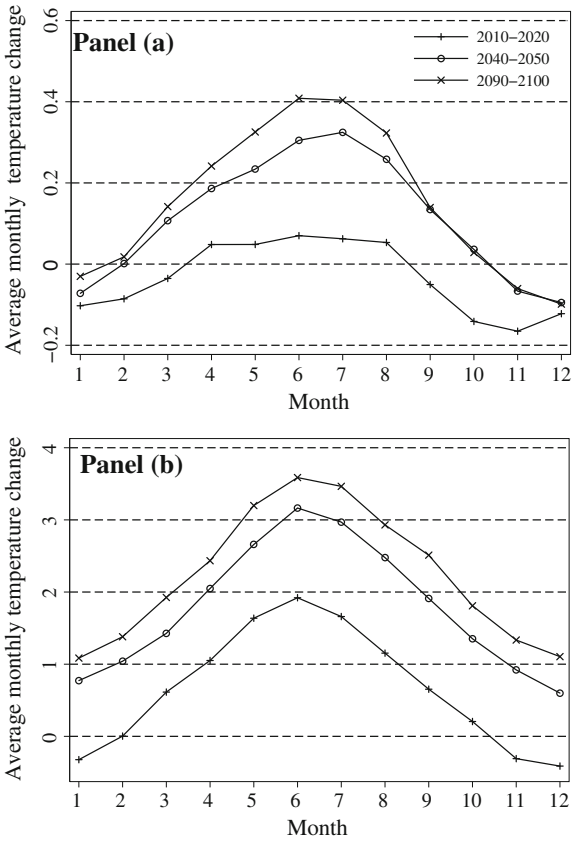

Fig. 7.27 Effects of future urban expansion on average monthly temperature in urban area in the Northeast megalopolis, USA (°C)

Along with urban expansion in the periods of 2040–2050 and 2090–2100, the cooling effect will be underscored, which can be referred to the enhancement of UHI effect. The urban expansion during these two periods will result in an average monthly temperature increase from February to October and decrease in other three months. The average monthly temperature increase in June and July in original urban area will exceed 0.4 °C in the period of 2090–2100 due to urban expansion. On the whole, the future urban expansion will lead to an average monthly temperature increase in original urban area.

The warming effect of future urban expansion in new urban area will be more significant than that in original urban area, especially in summer (Fig. 7.27, Panel B). In June, the average monthly temperature increase by 1.92, 3.16 and 3.59 °C in new urban area in the period of 2010–2010, 2040–2050 and 2090–2100, respectively. There will be also cooling effect in new urban area in November, December, and January during the period of 2010–2020. The differences of average monthly temperature among the three simulation periods indicate that the UHI effect in new urban area will be enhanced along with urban expansion.

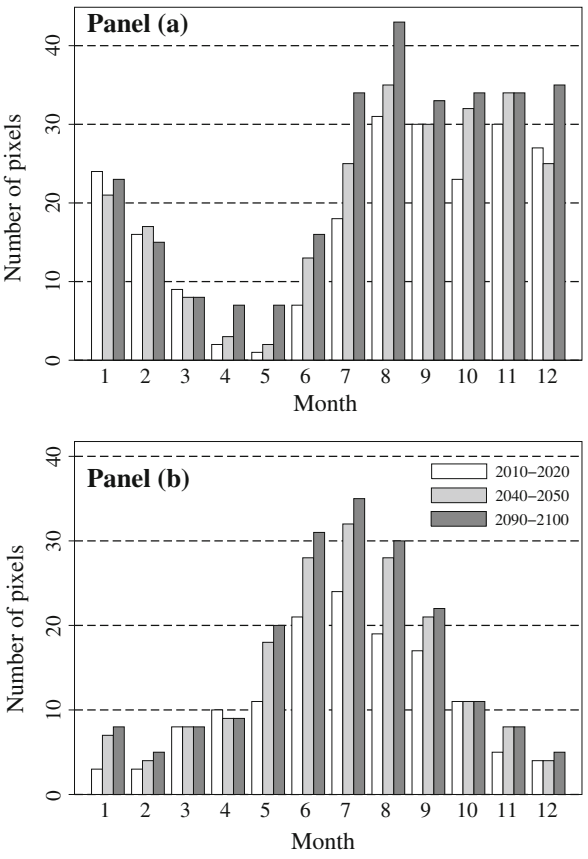

Fig. 7.28 Effects of future urban expansion on average monthly temperature and precipitation in nonurban area in the Northeast megalopolis, USA. *Panel A* number of pixels with average monthly temperature change exceeding ±0.5 °C; *Panel B* number of pixels with average monthly precipitation change exceeding ±1 mm

Moreover, the future urban expansion will also impact the average monthly temperature in nonurban area. We counted the number of pixels with average monthly temperature changes exceeding ±0.5 °C (Fig. 7.28, Panel A). This number indicates these areas severely influenced by future urban expansion on average monthly temperature. The influence will be large during the period from July to January at least 20 pixels, which means an area of more than 5.00×10^4 km^2 will be affected by future urban expansion. Especially in the period of 2090–2100, the urban expansion will lead to the change on average monthly temperature with more than ±0.5 °C in a vast area of 1.10×10^5 km^2. Further, the increase of pixels in which average monthly temperature changes exceeding ±0.5 °C at the temporal scale indicates that more area will be influenced by future urban expansion. In sum, the larger the urban area expands, the more notable will be the effects on average monthly temperature.

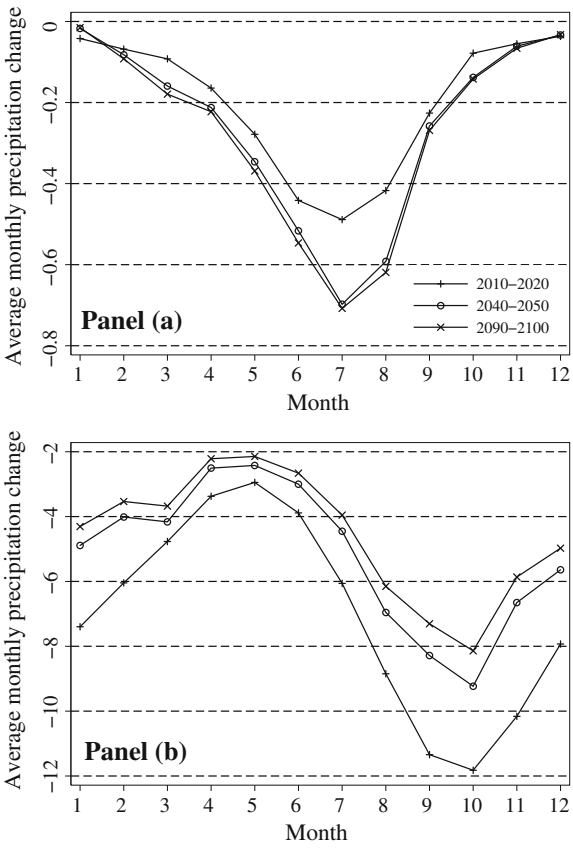

Fig. 7.29 Effects of future urban expansion on average monthly precipitation in urban area in the Northeast megalopolis, USA (mm)

7.5.2.4 Average Monthly Precipitation Effects

There will be slightly negative effects of future urban expansion on average monthly precipitation in original urban area. Similarly with average monthly temperature, the change of average monthly precipitation in original urban area caused by future urban expansion will be more significant in summer than that in winter (Fig. 7.29, Panel A). The average monthly precipitation will decrease in original urban area and reach its maximum of 0.49 mm, 0.69 mm, and 0.71 mm in July in the period of 2010–2020, 2040–2050, and 2090–2100, respectively, and it will fall to its minimum of 0.04 mm in December in the period of 2010–2020, and 0.02 and 0.01 mm in January in the period of 2040–2050 and 2090–2100, respectively. The effects of future urban expansion on average monthly precipitation will continuously increase from January to July, and then start to decline until December. This change of average monthly precipitation in original urban area may be driven by the local circulation change caused by surface energy

budgets change and can be easily found to become increasingly serious along with future urban expansion.

The drought effect of future urban expansion in new urban area will be more significant than that in the original urban area (Fig. 7.29, Panel B). The most significant reduction of average monthly precipitation will occur in October with 11.82, 9.23, and 8.14 mm in the period of 2010–2020, 2040–2050, and 2090–2100, respectively. Thereafter, the precipitation in new urban area starts to fall and reaches its minimum (between 2 and 3 mm) in May. More interesting, we also find that the more expanded urban area will weaken drought effect in new urban area. This can be deduced from the fact that the average monthly precipitation decreases in the periods of 2040–2050 and 2090–2100 will be smaller than that in the period of 2010–2020. This can be explained that the enhancement of UHI effect in the Northeast megalopolis will arouse the inflow of humid air from the Atlantic.

To investigate the effects of future urban expansion on average monthly precipitation in nonurban area, we counted the number of pixels with average monthly precipitation changes exceeding ±1 mm (Fig. 7.28, Panel B). The results show that the impacts of future urban expansion on average monthly precipitation in nonurban areas will be larger in summer than in winter. Additionally, the larger the urban area expands, the larger area of which the average monthly precipitation will be affected by urban expansion. For instance, the number of pixels with average monthly precipitation changes exceeding ±1 mm in July will be 35 (covering an area of 8.75×10^4 km^2) in the period of 2090–2100, and 32 (covering an area of 8.00×10^4 km^2), and 24 (covering an area of 6.00×10^4 km^2) in the period of 2040–2050 and 2090–2100, respectively. It implies the area with average monthly precipitation changes exceeding ±1 mm will spread persistently along with the urban expansion.

7.5.3 *Concluding Remarks on the Effects of Urban Expansion in the Northeast Megalopolis, USA*

A simulation-based research on the intension and scope of influences of future urban expansion on regional climate in developed megalopolis was implemented. The average annual and monthly temperature and precipitation change caused by urban expansion from 1993 to 2100 were presented taking the Northeast megalopolis, USA as a case study area. Some conclusions were drawn as follows:

(i) The future urban expansion will result in the increase of the average annual temperature, ranging from 2 to 5 °C in new urban area and decrease in the south of the Northeast megalopolis, ranging from 0.40 to 1.20 °C. The average annual precipitation in the study area will reduce by 5.75, 7.10 and 8.35 mm due to urban expansion in the period of 2010–2020, 2040–2050, and 2090–2100, respectively. This reduction is especially severe in the south region of the Northeast megalopolis.

(ii) The effects of future urban expansion on average monthly temperature will vary from month to month and become more and more obvious in not only original and new urban area but also nonurban area. The warming effect of future urban expansion in original and new urban area will be more significant in summer than in winter, and there will be a cooling effect in winter in original urban area.
(iii) The effects of future urban expansion on average monthly precipitation will be significant in new urban area. The drought effect in new urban area will weaken along with urban expansion. The nonurban areas where influenced by urban expansion on precipitation will be larger in summer than winter and will increase with urban expansion.
(iv) The rules of how urban expansion in the metropolis influences the climate differ from those in a single city. A large-scale study on the impacts of urban expansion on climate helps to understand the integrated effect of combination and interaction of multiple cities and their surroundings. This integrated effect may crucially determine the climate patterns.

7.6 Summary

In this chapter, we have five case studies based upon WRF model from a global perspective, which shows that the method introduced in this book is not only suitable for study in China, but also can be applied to other countries in the world.

In the case study, the impacts of cultivated land reclamation on the future climate change in India were analyzed by forecasting the future cultivated land reclamation and its related changes of energy flux and temperature in summer and winter. The results show that under the future situation of increasing food demand, reclamation of cultivated land in India will lead to a large amount of land conversion. These types of land conversion will overall result in increase of latent heat and decrease of sensible heat flux, which will eventually reduce the regional average temperature. Furthermore, this impact on climate change is seasonally different, i.e., reclamation of cultivated land mainly decreases the temperature in the summer, while increases the temperature in the winter.

In the second case study, the regional temperature variation induced by future boreal deforestation in European Russia was simulated based on future land cover change and WRF model. The results indicated that WRF model has good ability to simulate the temperature change in European Russia. The land cover change in European Russia, which was characterized by the conversion from boreal forests to croplands in the future 100 years, will lead to significant change of the near-surface temperature. Generally, the regional annual temperature will decrease by 0.58 °C in future 100 years. Though the boreal deforestation will reduce the evapotranspiration, the increase of surface albedo caused by the snow masking

will result in cooling effects to some extent and make the near-surface temperature decrease in most seasons except the spring.

The third case study aimed to model the potential climatological variability caused by future tropical deforestation in the Brazilian Amazon over the twenty-first century. The study results show that the forests in the Brazilian Amazon will primarily convert into dryland cropland and pasture in the northwest part and into cropland/woodland mosaic in the southeast part, with 5.12 and 13.11 % of the study area, respectively. These land surface changes will therefore lead to the significant reduction of the sum of sensible heat flux and latent heat flux and precipitation and the increase of the surface temperature. Furthermore, the variability of surface temperature is observed with close link to the deforested areas.

The fourth case study simulated the climatological changes caused by future grassland changes in Mongolia for the years 2010–2020 and 2040–2050. In order to detect the impact on climate change, two experiments were designed in this study: control experiment and simulation experiment. And the simulation results showed that the future grassland degradation will lead to an increasing trend on temperature and a decreasing trend on precipitation in some areas of Mongolia. The result of this study can provide some theoretical and scientific support for the development and strategy plan in Mongolia.

In the last case, some evidences for influences of future urban expansion on regional climate in the Northeast megalopolis, USA, were presented. The model-based analysis shows that future urban expansion will significantly jeopardize the regional climate change. The warming effect of future urban expansion in original and new urban area and drought effects in nonurban area will be more serious in summer than in winter. However, a cooling effect will turn up in original urban area in winter. All these indicate that the future urban expansion in the Northeast megalopolis will be a serious climate signal. In addition, this research further shows that study at the scale of megalopolis helps to understand the integrated effect of combination and interaction of multiple cities and their surroundings, which may crucially determine regional climate pattern and should be highly valued in the future.

References

Roy SB, Avissar R (2002) Impact of land use/land cover change on regional hydrometeorology in Amazonia. J Geophys Res Atmos (1984–2012), 107:LBA 4-1–LBA 4-12

Bala G, Caldeira K, Wickett M, Phillips T, Lobell D, Delire C et al (2007) Combined climate and carbon-cycle effects of large-scale deforestation. Proc Natl Acad Sci 104:6550–6555.

Barger NN, Ojima DS, Belnap J, Shiping W, Yanfen W, Chen Z (2004) Changes in plant functional groups, litter quality, and soil carbon and nitrogen mineralization with sheep grazing in an Inner Mongolian grassland. Rangeland Ecol Manag 57:613–619

Basara JB, Basara HG, Illston BG, Crawford KC (2010) The impact of the urban heat island during an intense heat wave in Oklahoma City. Advances in Meteorology 2010

Bathiany S, Claussen M, Brovkin V, Raddatz T, Gayler V (2010) Combined biogeophysical and biogeochemical effects of large-scale forest cover changes in the MPI earth system model. Biogeosciences 7:1383–1399

Baumann M, Ozdogan M, Kuemmerle T, Wendland,KJ, Esipova E, Radeloff VC (2012) Using the Landsat record to detect forest-cover changes during and after the collapse of the Soviet Union in the temperate zone of European Russia. Remote Sens Environ 124:174–184

Bonan GB (1997) Effects of land use on the climate of the United States. Clim Change 37:449–486

Bonan GB (2008) Forests and climate change: forcings, feedbacks, and the climate benefits of forests. Science 320:1444–1449

Challa VS, Indracanti J, Rabarison MK, Patrick C, Baham JM, Young J et al (2009) A simulation study of mesoscale coastal circulations in Mississippi Gulf coast. Atmos Res 91:9–25

Costa MH, Foley JA (2000) Combined effects of deforestation and doubled atmospheric CO2 concentrations on the climate of Amazonia. J Clim 13:18–34

Deng X, Jiang QO, Zhan J, He S, Lin Y (2010) Simulation on the dynamics of forest area changes in Northeast China. J Geograph Sci 20:495–509

Deng X, Zhao C, Yan H (2013) Systematic modeling of impacts of land use and land cover changes on regional climate: a review. Adv Meteorol 317678:11 doi:10.1155/2013/317678

Duchelle AE, Cromberg M, Gebara MF, Guerra R, Melo T, Larson A et al (2013) Linking forest tenure reform, environmental compliance, and incentives: Lessons from REDD + Initiatives in the Brazilian Amazon. World Development.

Ek ME, Mitchell KE, Lin Y, Rogers E, Grunmann P, Koren V et al (2003) Implementation of Noah land surface model advances in the National Centers for Environmental Prediction operational mesoscale Eta model. J Geophys Res Atmos 1984–2012:108

Ellis E, Pontius R (2007) Land-use and land-cover change. Encyclopedia of Earth. Environmental Information Coalition, National Council for Science and the Environment. Washington, DC: URL: http://www.eoearth.org/article/Landuse_and_land-cover_change.

Feddema JJ, Oleson KW, Bonan GB, Mearns LO, Buja, LE, Meehl GA et al (2005) The importance of land-cover change in simulating future climates. Science 310:1674–1678

Fujino J, Nair R, Kainuma M, Masui T, Matsuoka Y (2006) Multi-gas mitigation analysis on stabilization scenarios using AIM global model. Energy J Multi-Greenhouse Gas Mitig Clim Policy 27:343–354

Gettelman A, Morrison H, Ghan SJ (2008) A new two-moment bulk stratiform cloud microphysics scheme in the community atmosphere model, version 3 (CAM3). Part II: Single-column and global results. J Clim 21:3660–3679

Gottmann J (1964) Megalopolis: the urbanized northeastern seaboard of the United States. MIT Press, Cambridge

Guo X, Fu D, Wang J (2006) Mesoscale convective precipitation system modified by urbanization in Beijing City. Atmos Res 82:112–126

Hansen MC, Stehman SV, Potapov PV (2010) Quantification of global gross forest cover loss. Proc Natl Acad Sci 107:8650–8655

Hijioka Y, Matsuoka Y, Nishimoto H, Masui T, Kainuma M (2008) Global GHG emission scenarios under GHG concentration stabilization targets. J Global Environ Eng 13:97–108

Hong S, Noh Y, Dudhia J (2006) A new vertical diffusion package with an explicit treatment of entrainment processes. Monthly Weather Rev 134:2318–2341

Humphrey C (1978) Pastoral nomadism in Mongolia: the role of herdsmen's cooperatives in the national economy. Dev Change 9:133–160

Hurtt G, Chini LP, Frolking S, Betts R, Feddema J, Fischer G et al (2011) Harmonization of land-use scenarios for the period 1500–2100: 600 years of global gridded annual land-use transitions, wood harvest, and resulting secondary lands. Clim Change 109:117–161

Jin J, Miller NL (2007) Analysis of the impact of snow on daily weather variability in mountainous regions using MM5. J Hydrometeorology 8:245–258

Ke Y, Leung LR, Huang M, Coleman AM, Li H, Wigmosta MS (2012) Development of high resolution land surface parameters for the community land model. Geosci Model Dev 5:1341–1362

Kleerekoper L, van Esch M, Salcedo TB (2012) How to make a city climate-proof, addressing the urban heat island effect. Res Conserv Recycl 64:30–38

Kunzig R (2011) Population 7 billion. Natl Geographic 219:32–63
Lawrence PJ, Chase TN (2010) Investigating the climate impacts of global land cover change in the community climate system model. Int J Climatol 30:2066–2087
Lee X, Goulden ML, Hollinger DY, Barr A, Black TA, Bohrer G et al (2011) Observed increase in local cooling effect of deforestation at higher latitudes. Nature 479:384–387
Lei M, Niyogi D, Kishtawal C, Pielke R Sr, Beltrán-Przekurat A, Nobis T et al (2008) Effect of explicit urban land surface representation on the simulation of the 26 July 2005 heavy rain event over Mumbai, India. Atmos Chem Phys 8: 5975–5995
Lin C-Y, Chen W-C, Liu SC, Liou Y A, Liu G, Lin T (2008) Numerical study of the impact of urbanization on the precipitation over Taiwan. Atmos Environ 42:2934–2947
Lin YL, Farley RD, Orville HD (1983) Bulk parameterization of the snow field in a cloud model. Journal of Climate and Applied Meteorology 22(6):1065–1092
Liu J, Deng X (2011) Influence of different land use on urban microenvironment in Beijing City, China. J Food Agric Environ 9:1005–1011
Malhi Y, Roberts JT, Betts RA, Killeen TJ, Li W, Nobre CA (2008) Climate change, deforestation, and the fate of the Amazon. Science 319:169–172
Mawalagedara R, Oglesby RJ (2012) The climatic effects of deforestation in South and Southeast Asia. In: Dr. Paulo Moutinho (ed) Deforestation Around the World. Available from: http://www.intechopen.com/books/deforestation-around-the-world/the-climatic-effects-of-deforestation-in-south-and-southeast-asia
Negri AJ, Adler RF, Xu L, Surratt J (2004) The impact of Amazonian deforestation on dry season rainfall. J Clim 17:1306–1319
Phillips OL, Aragão LE, Lewis SL, Fisher JB, Lloyd J, López-González G et al (2009) Drought sensitivity of the Amazon rainforest. Science 323:1344–1347
Pielke RA, Marland G, Betts RA, Chase TN, Eastman JL, Niles JO et al (2002) The influence of land-use change and landscape dynamics on the climate system: relevance to climate-change policy beyond the radiative effect of greenhouse gases. Philosophical transactions of the royal society of London. Ser A Math Phys Eng Sci 360:1705–1719
Potapov P, Turubanova S, Hansen MC (2011) Regional-scale boreal forest cover and change mapping using Landsat data composites for European Russia. Remote Sens Environ 115(2):548–561
Ramos da Silva R, Werth D, Avissar R (2008) Regional impacts of future land-cover changes on the Amazon basin wet-season climate. J Clim 21:1153–1170
Schneider N, Eugster W, Schichler B (2004) The impact of historical land-use changes on the near-surface atmospheric conditions on the Swiss Plateau. Earth Interact 8:1–27
Taylor KE, Stouffer RJ, Meehl GA (2012) An overview of CMIP5 and the experiment design. Bull Am Meteorol Soc 93:485–498
Weng Q, Lu D, Schubring J (2004) Estimation of land surface temperature–vegetation abundance relationship for urban heat island studies. Rem Sens Environ 89:467–483
Werth D, Avissar R (2002) The local and global effects of Amazon deforestation. J Geophys Res Atmos (1984–2012) 107:LBA 55-51–LBA 55-58
Yatagai A, Yasunari T (1994) Trends and decadal-scale fluctuations of surface air temperature and precipitation over China and Mongolia during the recent 40 year period (1951–1990) J Meteorol Soc Japan 72:937–957
Zhang MA, Borjigin E, Zhang H (2007) Mongolian nomadic culture and ecological culture: On the ecological reconstruction in the agro-pastoral mosaic zone in Northern China. Ecol Econ 62:19–26
Zhang CL, Chen F, Miao SG, Li QC, Xia XA, Xuan CY (2009) Impacts of urban expansion and future green planting on summer precipitation in the Beijing metropolitan area. J Geophys Res Atmos 1984–2012 114
Хауленбек А (2009) The present situation of desertification Mongolia. Ulaanbaatar. (in Mongolia)

Chapter 8
Concluding Remarks on Improved Data, Upgraded Models and Case Studies

R. B. Singh, Chenchen Shi and Xiangzheng Deng

This chapter explores the advancement in data, models, and application for observing and estimating land use impacts on surface climate, and points out further research needs and priorities, which will provide some references for related studies. The reclassification of time series land cover data can meet the accuracy requirement of climate simulation and can be used as the parameters of dynamical downscaling in regional climate simulation, which enhances the data processing and laid a good foundation for Land Use and Cover Change (LUCC) simulation.

There have been tremendous changes of global land use pattern in the past 50 years, which has enormous influence on global climate change. Quantitative analysis for the impacts of LUCC on surface climate is one of the core scientific issues to understand the influence of human activities on global climate. For instance, the diverse roles of LUCC on precipitation have been documented and sustained rapid land conversions make human-induced disturbances of climate system continue and become even more significant (Pielke et al. 2007). The review paper of Deng et al. (2013a), comprehensively analyzed the primary scientific issues about the impacts of LUCC on regional climate and systematically reviewed the progress in relevant researches. In this chapter, we summarize the major

X. Deng (✉)
Institute of Geographic Sciences and Natural Resources Research,
Chinese Academy of Sciences, Beijing 100101, China
e-mail: dengxz.ccap@igsnrr.ac.cn

X. Deng
Center for Chinese Agricultural Policy, Chinese Academy of Sciences,
Beijing 100101, China

R. B. Singh
Department of Geography, Delhi School of Economics, University of Delhi,
Delhi 110007, India

C. Shi
State Key Laboratory of Water Environment Simulation, School of Environment,
Beijing Normal University, Beijing 100875, China

X. Deng et al. (eds.), *Land Use Impacts on Climate*, Springer Geography

DOI: 10.1007/978-3-642-54876-5_8,

findings of improved data, upgraded models, and case studies in observation and estimation of land use impacts on surface climate.

8.1 Advancement in LUCC Dataset

8.1.1 Overview of the Previous Dataset

LUCC has been recognized as a key component in global environmental change. However, land cover products were applied to most of the climate models until the recent 20 years. These products were initially compiled from maps, ground surveys, and various national statistical sources, which have inherent limitations (Matthews 1983; Olson et al. 1983; Cihlar 2000). In the mid-1990s, global-scale land cover products generated from remote sensing images became available. Various land cover datasets were usually generated from classification and interpretation of remote sensing images, including MSS/TM/ETM+, SPOT, MODIS, and so on, which have been used in numerous climate modeling studies at regional and global scales. Since the 1990s, a series of land use/cover datasets have been produced in many international institutes and countries, such as Global Land Cover Characteristics (GLCC) (Loveland et al. 2000), University of Maryland land cover dataset (UMD) (Hansen and Reed 2000), OGE dataset (Olson 1994a, b). These products were interpreted artificially with computer aids and then verified by systematic field survey. The need of land use/cover dataset with high accuracy for climate simulation has been recognized widely in the climate modeling community (Ge et al. 2007). Previous studies showed that the result of regional precipitation study would be greatly influenced if the accuracy of land cover data is under 80 %, and the result may get progressively worse as the accuracy continues to decrease (Feddema et al. 2005). Therefore, the accuracy of land cover data is of crucial importance to the climate study. For example, in China, large amount of land cover data have been produced in recent years using the remote sensing data (Ran et al. 2012).Unfortunately, neither the overall nor class-specific accuracy of most datasets was able to meet the common requirements of regional climate modeling.

The disagreement and low accuracy among these land cover datasets primarily resulted from the differences in the sensors, spatial resolutions, classification schemes, and algorithms (Herold et al. 2008). Moreover, most of the land cover datasets derived from remote sensing are not 100 % accurate. A new statistical measure was developed to evaluate land cover datasets in land–climate interaction research, which calculates biophysical precision of land cover datasets using 1 km monthly MODIS Leaf Area Index (LAI) product (Ge et al. 2009). Spatial data mining is proposed to produce a higher accuracy land cover map, whose classification system should be compatible with the accepted classification system used in regional climate simulation (Ran et al. 2012; Wu et al. 2013).

8.1.2 Classification of LUCC Data for Climate Models

There are a number of schemes that have been proposed for land cover categorization from regional to global-scale, including the International Geosphere–Biosphere Programme (IGBP)—Data and Information Systems: Land Cover Working Group land cover categorization scheme (Belward and Loveland 1995), a six-class biome categorization, the Simple Biosphere Model scheme (Sellers et al. 1996), and the Federal Geographic Data Committee vegetation characterization and information standards (F. G. D. Committee 1996). Many parameters in land surface model are identified based on land cover types; for instance, time-invariant model variables (e.g., vegetation reflectance, canopy top height, canopy base height, root depth, and leaf respiration factor) in the Simple Biosphere Model 2 (SIB2) (Sellers et al. 1996) and the Common Land Model (CoLM) (Dai et al. 2001). Thus, the specific land cover classification units must not only be discernible (with high accuracy) from remotely sensing image and ancillary data but also be directly related to the physical characteristics of land surface. The IGBP scheme embraces the same philosophy but with modifications to be compatible with existing schemes used by environmental models, to incorporate land use in addition to land cover and to represent mosaics (Belward and Loveland, 1995).

In order to enhance the studies on land use/cover change, data have to be updated to increase the accuracy. Time series land cover datasets have been widely used in numerous climate simulation projects. Most attention has been paid on effects of the accuracy of land cover data on climate simulation. Though there are temporal land use data with accuracy higher than 90 % (Wu et al. 2013), the high-precision land cover data is still absent. Therefore, there is an urgent need to reclassify the LUCC dataset to feed into Global Climate Models (GCMs) and Regional Climate Models (RCMs). For example, in a case study on North China, Wu et al. (2013) overlaid the land cover maps of the IGBP-DIS, GLC (Loveland et al. 2000), University of Maryland Data (UMD) and Data Center for West China (WESTDC), and selected the compatible grids with classification as sample grids. They then combine land cover data with land use data to generate new land cover data of high accuracy for climate simulation. Their study showed that the C4.5 algorithm was suitable for converting land use data to land cover data of IGBP classification. The temporal land cover data produced by their method can meet the accuracy requirement of climate simulation and can be used as the parameters of dynamical downscaling in regional climate simulation, which constitutes a significant improvement in data processing.

8.1.3 Data Resolution and Reliability

Land surface has considerable heterogeneity because of the existence of different land cover types such as bare area, water bodies, urban land, trees, and snow/ice, which vary over small distance. This surface variability not only determines the

microclimate but also affects mesoscale atmospheric circulation (Hartmann 1994; Weaver and Avissar 2001; Yang 2004). The accurate land cover maps are the foundation for land surface, ecological and hydrological modeling, carbon and water cycle studies, and research on global climate change (Sellers et al. 1997). With many land cover products from different sources becoming available for a given region of the Earth, a challenge arises as to which product is optimal for a land–climate modeling study. Traditional classification accuracy assessment is primarily dependent on ground-based surveys or interpretation of high-spatial resolution aerial photos and satellite images. By comparing the classified land cover dataset with the ground-truth data, error metrics can be developed to report the commission and omission errors. Measures of accuracy, such as the Kappa coefficient of agreement, are frequently calculated to express classification accuracy (Congalton 1991; Foody 2002). Therefore, the researcher should take full advantage of geographic knowledge in GIS database to support classification to improve the accuracy of land cover classification.

Accurate representation of land surfaces is an important factor for climate modeling. However, little attention has been paid to the effect of land cover classification accuracy on climate simulations. In reality, land cover accuracy rarely reaches the commonly recommended 85 % target (Ge et al. 2007). The accuracy of land use classification is approximate 73–77 % using decision-tree classification methods and thereby increasing mapping efficiency by 50 % (Homer et al. 2004). In addition, most assessments of classification accuracy were conducted using the same dataset as was used to train the classifier. Therefore, the classified accuracy was overstated. Spatial data mining techniques for land cover classification is also applied. The accuracy of land cover data that is accomplished by different methods could reach 88.62 % (Wu et al. 2013). Inaccurate representation of land cover will lead to differences in simulating sensible heat flux, latent heat flux, and many other variables depending on vegetation and land use parameters. Remote sensing provides accurate representation of Earth's surface at different spatial and temporal scales and is an attractive source for creating high accuracy land cover data. Therefore, it is feasible to take advantage of the existing land cover data from different sources to make a high accuracy land cover data using spatial data mining method. The information fusion strategy is proposed to produce a higher accuracy land cover map of China (Ran et al. 2010), whose classification system should be compatible with the widely accepted classification system used for surface climate simulation.

8.2 Upgraded Models

Studies on LUCC processes are often challenged by the complex nature and unexpected behavior of both human drivers and natural constraints. Therefore, we need a land use change dynamic model to simulate the interdependencies and feedback mechanisms between social, economic, and ecosystem environments.

Land use change emerges from the interactions among various components of the coupled human-landscape system, which then feeds back to the subsequent development of those interactions (Le et al. 2008). Currently, there are a lot of evaluation models to simulate the spatiotemporal process and patterns of land use change (Deng et al. 2013b).

8.2.1 Current Models

8.2.1.1 Empirical Statistical Model

There are numerous empirical statistical models applied to land system dynamics simulation (Verburg et al. 2008; Liu and Deng 2010). The empirical statistical model can provide the information of key driving forces of land use change and reflect the time lag effect of response. Moreover, the data input could be multi-scaled. However, certain deficiencies exist in this kind of model, as the model requires to be driven by the data of exogenous land use change rate and amount. Besides, the conversion rule of land use should be manually set. Therefore, the model could not provide references for other regions except for the study area.

8.2.1.2 Econometric Model

Econometric model is a policy evaluation model based on sustainable utilization of land which can evaluate the influence of policy factors on land use and promote mixed land for sustainable development. For example, European Commission FP6 framework research programme SENSOR "Sustainability Impact Assessment: Tools for Environmental, Social and Economic Effects on Multifunctional Land Use in European Regions" aims to develop tools for ex-ante impact assessment for European policies related to rural land use (Helming et al. 2006). It includes a detailed macroeconometric model called NEMESIS, which models cross-sector impacts, being the major characteristic of this project (Jansson et al. 2008). As it applies a cross-sector approach to land use, it is suitable for large region. The Dynamics of Land System (DLS) model as another representative econometric model can simulate the dynamics of land system at the fine-grid scale through analysis of land use allocation constraints, and simulation of land supply and demand balance. Several case studies show that DLS is able to measure the influence of natural and socioeconomic driving factors and predict the future LUCC, which could provide meaningful decision-making information for land use planning and management (Deng et al. 2010).

8.2.1.3 Agent-Based Model

Since the 1990s, with the rapid development of computational power, agent-based models began to be applied in LUCC research, and agent models for Land Use and Cover Change (ABM/LUCC) studies have been gradually developed (Evans and Kelley 2004). Agent-based model has high flexibility. However, the flexibility of ABM model increases the uncertainty of the model and thus brings the difficulties for model validation. Agent-based model strives to simulate the individual and group behavior together, but the individual decision-making behavior is diverse and complicated. In addition, previous research showed that ABM model is sensitive to the climatic conditions, which gave credit to ABM on modeling the impact of LUCC on climate.

8.2.1.4 Coupled Econometric and ABM Model

The combination of agent-based model and econometric model can simulate complex decision problem of land use in a better way, so as to provide new methods for simulation of land use dynamics.

Coupled econometric and ABM model in the areas of land use will get recognition and application in the future. The coupled model can simulate both individual and group decision behaviors through considering the interaction among the combination of micro and macro decisions at the same time. The integration of econometric and agent-based model combines the process of social and economic factors with land use dynamics. This integrated model can be used not only in the simple scenario simulation of land use but also in complex scenario. These two kinds of models are interconnected and interdependent on each other, which constitute a complex system with hierarchical heterogeneity.

Among recent studies on land use models, Deng et al. (2013b) introduced a land use change dynamic (LUCD) model embedded in regional climate model (RCM). The Agro-Ecological Zone (AEZ) model is supposed as the optimal option for constructing one of the constitute modules. The other module, agent-based module, identifies land use change demand and vegetation change and provides land use change simulation results which are the underlying surfaces needed by RCM. By importing land use simulation results to regional climate modeling, the LUCD is embedded in RCM. The coupled simulation system of LUCD and RCM will be extraordinarily powerful in land surface system simulation. The innovation of these studies lies in that current research could only simulate land cover changes through vegetation change module in RCM and GCM but not the land use changes. However, this study simulated land use dynamics, which is a breakthrough in systematically reporting the land use change and its impact on surface climate.

8.2.2 Scenario Development

Scenario analysis of land use change and dynamic prediction involves many driving factors that affect land use change, which has always been the attention of academia worldwide. Through simulating regional land use change under different scenarios, rational forecasting and evaluation of future land use could be made, which will offer scientific reference for sustainable land use planning and management at regional and national scale.

Climate scenarios are plausible representations of future climate conditions, which can be produced using a variety of approaches, and among which, regional climate models are increasingly popular (Moss et al. 2010). There is a notable increase in interest in regional-scale climate scenarios and projection methods, especially for impact and adaptation assessment (Solomon et al. 2007).

The Intergovernmental Panel on Climate Change (IPCC) has been working on the scenarios of potential future anthropogenic climate change, the underlying driving forces, and the response options. According to IPCC (Kriegler et al. 2010; Nakicenovic et al. 2000), socioeconomic scenarios consist of qualitative narrative descriptions of future trends and quantitative assumptions (also called the storyline) about key socioeconomic variables, and could facilitate the exploration of long-term consequences of anthropogenic climate change and available response options. A reliable database and an appropriate method shall be adopted to facilitate the study of land use impact on surface climate, and the scenario analysis can be adopted to perform macrostructure change. In the study of Xu et al. (2013), three kinds of scenarios were designed based on the socioeconomic development. They simulated land use trends under three different scenarios including baseline scenario and two control scenarios (risk scenario and rapid development mode transformation scenario), and obtained the most suitable scenario to control CO_2 emissions of the three scenarios. Their scenarios excel other scenarios as they compile the IPCC scenarios with the specific situation in the research area. With the scenario analysis, it is possible to provide a theoretical basis for the future land use planning in mitigating the impact of climate change. As the first attempt of systematic analysis of LUCC scenarios and with the dataset produced by their study, their research laid a good foundation for relevant researches.

8.3 Case Studies of Land Use Impacts on Surface Climate

With an improved database and model base, climate model shall be introduced in order to apply this simulation platform to study land use impact on surface climate. Climate change in China has been simulated in recent years by many scholars. The representative methods include Gao et al. simulated climate change in China using the Abdus Salam International Centre for Theoretical Physics (ICTP) Regional Climate Model version 3 (RegCM3) (Gao et al. 2012). The RegCM3 can reproduce

the observed spatial structure of surface air temperature and precipitation well. However, RegCM3 is a hydrostatic model so far, which limits the further increase of its resolution beyond ~10 km (Wu et al. 2012). Wu and Fu (2013) used a linear fitting method to estimate the change of precipitation intensity spectra at different spatial scales in China. Qu et al. (2013) used WRF to explore the impacts of land cover change on the near-surface temperature in a research in Northern China Plain. They tested and verified the ability of WRF to simulate the near-surface temperature in the study area. Notably, LUCC dynamic model and LUCC reclassification were also applied to form a good systematic modeling of LUCC. Coupled with WRF Model, land use impact on climate was well simulated in this study.

Based on the compiled climate model, climate change influence on ecosystem indicators could be further explored. Zhang et al. (2013a, b) first reported the climate impact on grassland. Their study took a macro and mesoscale analysis of the possible changing trends of net primary productivity (NPP) of local grasslands under four RCPs scenarios. The results showed that grassland productivity will be greatly affected by the fluctuations of precipitation and temperature.

With the above-mentioned studies, LUCC and future climatic scenarios simulation in particular areas were conducted. Simulation of LUCC and its climatic effects were integrated through linking the functions of the newly developed models with those of the existing models.

Further, studies related to land use changes associated with climate variations were promoted with the advances in research methods. Deng et al. (2013c) conducted a revisit to the impact of land use changes on human well-being through altering the ecosystem provisioning services. LUCC and climate change exert tremendous influence on ecosystem provisioning services in agriculture, forest and/or grassland ecosystem. In order to tackle the ecosystem provisioning services problems, measures were taken, which increased the input and reduced the outcome, at the same time augmented the health risk, and harming human well-being.

Recently, satellite meteorology products and applications get more and more attention. However, it cannot replace surface measurements. For example, satellite data in the form of GCM needs observed data for model validation and improves the quality of statistical and scientific significances in research methods. Therefore, increasing emphasis should be given to integrate observed and simulated datasets for improving understanding about land use impacts on surface climate.

8.4 Summary

This chapter reviewed the progress of the studies on observing and estimating the impact of land use change on surface climate from the perspective of improved models, enhanced data, and widely expanded applications. The major findings include: The reclassification of time series land cover data can meet the accuracy requirement of climate simulation and can be used as the parameters of dynamical downscaling in regional climate simulation, which enhanced the data processing

and laid a good foundation for LUCC simulation. Land Use Change Dynamics Model compatible with RCMs is a great breakthrough in systematically reporting the changes of land use/cover. Scenarios analysis performed the macrostructure change, which facilitated the study on the impact of land use change on surface climate. Land use change dynamic model and land use reclassification can be applied to form a good systematic modeling of LUCC. Coupled with WRF Model, land use impact on surface climate was well simulated.

Despite the progresses in these studies there are still some research needs, which should be further addressed. For example, LUCC parameters need to be precisely expressed to make sure of the accuracy of simulation. It is necessary to strengthen the observation of land surface processes due to the variations in the impact of land use change on surface climate.

The researches of observing and estimating land use impact on surface climate should mainly focus on two aspects: (i) exploring the climate effects of future LUCC since the current studies have mainly addressed on the past and current LUCC and (ii) improving the prediction of land use changes in the future and assessing its influence on future surface climate.

References

Belward A, Loveland T (1995) The IGBP DIS 1 km land cover project: Remote sensing in action[C]. In: Proceedings of the 21st annual conference of the remote sensing society,.vol 1995, pp 1099–1106. Southampton, UK

Cihlar J (2000) Land cover mapping of large areas from satellites: status and research priorities. Int J Remote Sens 21(6–7):1093–1114

Congalton RG (1991) A review of assessing the accuracy of classifications of remotely sensed data. Remote Sens Environ 37(1):35–46

Dai X, Zeng X, Dickinson R (2001) The Common Land Model (CLM): technical documentation and user's guide. Georgia Institute of Technology, Atlanta

Deng X, Jiang QO, Zhan J, He S, Lin Y (2010) Simulation on the dynamics of forest area changes in Northeast China. J Geog Sci 20(4):495–509

Deng X, Zhao C, Yan H (2013) Systematic modeling of impacts of land use and land cover changes on regional climate: a review. Adv Meteorol 2013 317678:1–11, doi:10.1155/2013/317678

Deng X, Liu J, Lin Y, Shi C (2013) A framework for the land use change dynamics model compatible with RCMs. Adv Meteorol 2013 658941:1–7, doi:10.1155/2013/658941

Deng X, Li Z, Huang J, Shi Q, Li Y (2013) A revisit to the impact of land use changes on the human well-being via altering the ecosystem provisioning services. Adv Meteorol 2013 907367:1–8, doi:10.1155/2013/907367

Evans TP, Kelley H (2004) Multi-scale analysis of a household level agent-based model of landcover change. J Environ Manag 72(1):57–72

F. G. D. Committee (1996) Vegetation Subcommittee. 1997. FGDC vegetation classification and information standards—June, vol 3

Feddema JJ, Oleson KW, Bonan GB, Mearns LO, Buja LE, Meehl GA, Washington WM (2005) The importance of land-cover change in simulating future climates. Science 310(5754):1674–1678

Foody GM (2002) Status of land cover classification accuracy assessment. Remote Sens Environ 80(1):185–201

Gao X, Shi Y, Zhang D, Giorgi F (2012) Climate change in China in the 21st century as simulated by a high resolution regional climate model. Chin Sci Bull 57(10):1188–1195
Ge J, Qi J, Lofgren BM, Moore N, Torbick N, Olson JM (2007) Impacts of land use/cover classification accuracy on regional climate simulations. J Geophys Res Atmos (1984–2012) 112(D5)
Ge J, Torbick N, Qi J (2009) Biophysical evaluation of land-cover products for land-climate modeling. Earth Interact 13(6):1–16
Hansen M, Reed B (2000) A comparison of the IGBP DISCover and University of Maryland 1 km global land cover products. Int J Remote Sens 21(6–7):1365–1373
Hartmann DL (1994) Global physical climatology. Academic press, San Dieg
Helming K, König B, Tscherning K (2006) SENSOR first annual report (public part). Management 30(3):391-405
Herold M, Mayaux P, Woodcock C, Baccini A, Schmullius C (2008) Some challenges in global land cover mapping: An assessment of agreement and accuracy in existing 1 km datasets. Remote Sens Environ 112(5):2538–2556
Homer C, Huang C, Yang L, Wylie B, and Coan M (2004) Development of a 2001 National Landcover Database for the United States. Photogrammetric Engineering and Remote Sensing 70(7):829–840
Jansson T, Bakker M, Boitier B, Fougeyrollas A, Helming J, van Meijl H, Verkerk PJ (2008) Cross sector land use modelling framework [M]. Sustainability impact assessment of land use changes. Springer, Berlin, p 159–180
Kriegler E, O'neill B, Hallegatte S, Kram T, Lempert R, Moss R, Wilbanks T (2010) CIRED working paper DT/WP
Le QB, Park SJ, Vlek PL, Cremers AB (2008) Land-Use Dynamic Simulator (LUDAS): a multi-agent system model for simulating spatio-temporal dynamics of coupled human–landscape system. I. Structure and theoretical specification. Ecol Inform 3(2):135–153
Liu J, Deng X (2010) Progress of the research methodologies on the temporal and spatial process of LUCC. Chin Sci Bull 55(14):1354–1362
Loveland T, Reed B, Brown J, Ohlen D, Zhu Z, Yang L, Merchant J (2000) Development of a global land cover characteristics database and IGBP DISCover from 1 km AVHRR data. Int J Remote Sens 21(6–7):1303–1330
Matthews E (1983) Global vegetation and land use: new high-resolution data bases for climate studies. J Clim Appl Meteorol 22(3):474–487
Moss RH, Edmonds JA, Hibbard KA, Manning MR, Rose SK, van Vuuren DP, Carter TR, Emori S, Kainuma M, Kram T (2010) The next generation of scenarios for climate change research and assessment. Nature 463(7282):747–756
Nakicenovic N, Alcamo J, Davis G, de Vries B, Fenhann J, Gaffin S, Gregory K, Grubler A, Jung TY, Kram T (2000) Pacific Northwest National Laboratory. Environmental Molecular Sciences Laboratory (US), Richland, WA (US)
Olson J (1994) Global ecosystem framework-definitions. USGS EROS Data Center Internal Report, Sioux Falls, SD, vol 37
Olson J (1994) Global ecosystem framework-definitions. USGS EROS Data Center Internal Report, Sioux Falls, SD, vol 39
Olson JS, Watts JA, Allison LJ (1983) Oak Ridge National Lab, TN (USA)
Pielke R, Adegoke J, Beltran-Przekurat A, Hiemstra C, Lin J, Nair U, Niyogi D, Nobis T (2007) An overview of regional land-use and land-cover impacts on rainfall. Tellus Ser B-Chem Phys Meteorol 59(3):587–601
Qu R, Cui X, Yan H, Ma E, Zhan J (2013) Impacts of land cover change on the near-surface temperature in the North China Plain. Adv Meteorol 2013 409302:1–12, doi:10.1155/2013/409302
Ran Y, Li X, Lu L (2010) Evaluation of four remote sensing based land cover products over China. Int J Remote Sens 31(2):391–401
Ran Y, Li X, Lu L, Li Z (2012) Large-scale land cover mapping with the integration of multi-source information based on the Dempster-Shafer theory. Int J Geogr Inf Sci 26(1):169–191

Sellers PJ, Tucker CJ, Collatz GJ, Los SO, Justice CO, Dazlich DA, Randall DA (1996) A revised land surface parameterization (SiB2) for atmospheric GCMs. Part II: the generation of global fields of terrestrial biophysical parameters from satellite data. J Clim 9(4):706–737

Sellers P, Dickinson R, Randall D, Betts A, Hall F, Berry J, Collatz G, Denning A, Mooney H, Nobre C (1997) Modeling the exchanges of energy, water, and carbon between continents and the atmosphere. Science 275(5299):502–509

Solomon S, Qin D, Manning M, Chen Z, Marquis M, Averyt K, Tignor M, Miller H (2007) The physical science basis. Contribution of working group I to the fourth assessment report of the intergovernmental panel on climate change, pp 235–337

Verburg PH, Eickhout B, Van Meijl H (2008) A multi-scale, multi-model approach for analyzing the future dynamics of European land use. Ann Reg Sci 42(1):57–77

Weaver CP, Avissar R (2001) Atmospheric disturbances caused by human modification of the landscape. Bull Am Meteorol Soc 82(2):269–281

Wu F, Fu C (2013) Change of precipitation intensity spectra at different spatial scales under warming conditions. Chin Sci Bull 58(12):1385–1394

Wu J, Gao X, Giorgi F, Chen Z, Yu D (2012) Climate effects of the Three Gorges Reservoir as simulated by a high resolution double nested regional climate model. Quat Int 282:27–36

Wu F, Zhan J, Yan H, Shi C, Huang J (2013) Land cover mapping based on multisource spatial data mining approach for climate simulation: a case study in the farming-pastoral ecotone of North China. Adv Meteorol 2013 520803:1–12, doi:10.1155/2013/520803

Xu Q, Jiang Q, Cao K, Li X, Deng X (2013) Adaptation to climate change: possible trends of land use changes in China. Adv Meteorol 2013 919013:1–12, doi:10.1155/2013/919013

Yang Z-L (2004) Modeling land surface processes in short-term weather and climate studies. World Scientific Series on Meteorology of East Asia

Zhang T, Zhan J, Huang J, Yu R, Shi C (2013) An Agent-based reasoning of impacts of regional climate changes on land use changes in the Three-River Headwaters Region of China. Adv Meteorol

Zhang R, Li Z, Yuan Y, Li Z, Yin F (2013) Analyses on the changes of grazing capacity in the Three-River Headwaters Region of China under various climate change scenarios. Adv Meteorol